Wireless Channel Modelling for Specknet

A DISSERTATION SUBMITTED TO
THE INSTITUTE FOR COMMUNICATIONS AND SIGNAL PROCESSING,
DEPARTMENT OF ELECTRONIC AND ELECTRICAL ENGINEERING,
AND THE COMMITTEE FOR POSTGRADUATE STUDIES
OF THE UNIVERSITY OF STRATHCLYDE
IN PARTIAL FULFILLMENT OF THE REQUIREMENTS
FOR THE DEGREE OF DOCTOR OF PHILOSOPHY

By

Faisal Darbari

Sep 2008

Declaration

I declare that this thesis embodies my own research work and that it is composed by myself. Where appropriate, I have made acknowledgements to the work of others.

Faisal Darbari

Abstract

A wireless sensor network (WSN) consists of spatially distributed autonomous devices using sensors to cooperatively monitor physical or environmental conditions, such as pressure, temperature, sound, vibration or motion at different locations. The development of wireless sensor networks was originally motivated by military applications such as battlefield surveillance. However, wireless sensor networks are now used in many commercial applications, including environment and habitat monitoring, healthcare applications, home automation, and traffic control.

The physical size of these devices is shrinking due to advances in semiconductor technology. The main challenge is to produce low cost and miniature sensor nodes. Energy is the scarcest resource for these nodes as it determines the WSN lifetime. Since these nodes will be deployed close together to form a dense wireless network the received signal to noise ratio at any instant of time not only depends on physical channel (i.e. path loss and fading) but also on various design parameters like CSMA/CA inhibition threshold, polarization, deployment strategy and node density.

This thesis characterises the propagation channel for miniature wireless nodes. A characterization of the short range (<10cm), narrowband, wireless channel, appropriate to a dense network of wireless transceivers operating in the 2.4 GHz ISM band, is presented. Transmission loss measurements have been made in the laboratory at 2.45 GHz and a fading model derived. Aggregate interference due to neighboring carrier-sense-multiple-access (CSMA) nodes has been calculated. The resulting dependence of signal-to-interference ratio (SIR) on node density is presented to allow density dimensioning. Cumulative distributions of SIR have been used to establish performance statistics for example modulation and detection schemes. A simulation model has been developed to characterise the physical link experienced by these networks.

Key words: Wireless Sensor Network (WSN), Signal to Interference Ratio (SIR), Carrier Sense Multiple Access Collision Avoidance (CSMA).

Acknowledgement

Firstly, I wish to thank Professor R. W. Stewart for giving the opportunity for the research degree and the Specknet project for providing funding during the course of my research. I also wish to thanks Dr I. A. Glover for his continual guidance and support during my research work. His overly enthusiasm and integral view on research and his mission for providing high-quality work has made a deep impression on me. I owe him lots of gratitude for having me shown this way of research. He could not even realize how much I have learned from him. Besides of being an excellent supervisor, he is an excellent human being. I am really glad that I have come to get know Ian in my life. I would like to thank both Bob Stewart and Ian Glover who kept an eye on the progress of my work during the course of my degree and was always available when I needed advises.

A number of staff at Strathclyde University has been exceptionally helpful. In particular I would like to thanks technician David McCrindle and Robin Cochrane in Mechanical workshop of electronic and electrical engineering department for their support in design and manufacturing of test bench and timely modification of the measurement equipment. I would like to acknowledge Mr Konstantinos Sasloglou for his contribution on measurement and analysis of surface wave related measurements.

I am very grateful to my colleagues Dr Louise Crockett, Dr Steven Alexander, Mr. Neil MacEwen, Mr. Graham Stephen and Dr Eugen Pfann as with out their presence in the lab the environment would be very desolate. It was a pleasure to work with them.

I would like to express thanks to my family and parents as with out their consistent support and prayer I could have never achieved this task. Finally I would like to thanks my wife Kiran, for her love and patience during the PhD period. She formed part of my vision and taught me the good things that really matter in life. One of the

best experiences that we lived through in this period was the birth of the twins, who provided an additional and joyful dimension to our life.

Abbreviations

AR	Axial Ratio
BER	Bit Error Rate
CSMA/CA	Carrier Sense Multiple Access with Collision Avoidance
CTS	Clear to Send
dBi	Decibels Relative to an Isotropic Antenna
DOI	Degree of Irregularity
DSP	Digital Signal Processing
ENP	Energy Neutral Platform
FSPL	Free Space Path Loss Model
HF	High Frequency
ISM	Industrial, Scientific and Medical
LHCP	Left Hand Circularly Polarised
LF	Low Frequency
LOS	Line of Sight
MAC	Medium Access Control
NLOS	Non Line of Sight
PDF	Probability Density Function
RF	Radio Frequency
RHCP	Right Hand Circularly Polarised
RTS	Request to Send
SIR	Signal to Interference Ratio
SNR	Signal to Noise Ratio
TDMA	Time Division Multiple Access
VHF	Very High Frequency
VLF	Very Low Frequency
WSN	Wireless Sensor Network

Table of Contents

List of Figures

List of Tables

Chapter One

1. Introduction

This thesis is submitted for the fulfilment of the degree of Doctor of Philosophy, which has been carried out at the Institute for Communication and Signal Processing at the University of Strathclyde, Glasgow, United Kingdom. The research has been performed on short wireless links as envisaged by specknet.

1.1 Specknet Project

Speckled Computing offers a radically new concept in information technology that has the potential to revolutionise the way we communicate and exchange information i.e. a system design that encapsulates sensing, processing and wireless networking in a single chip. Speckled Computing [1] is a project being undertaken by five collaborating Scottish universities; Edinburgh, Glasgow, Strathclyde, St. Andrews and Napier. The consortium has a vision of an ad-hoc network of small (1mm×1mm×1mm) computing transceivers scattered, sprayed or otherwise deployed over a variety of surfaces (walls, floors, ceilings, furniture, clothing) at a density depending upon the application. The transceivers are referred to as 'specks'.

The specks will be capable of both sensing and processing data using state-of-the-art transducers and digital signal processing (DSP) technology. Each speck will be autonomous, with its own captive, renewable energy source, and will be capable of wireless communication with other specks. They will have low power consumption and therefore limited range. (The tight constraint on speck power budget is primarily imposed by their small size.) A combination of many specks (nodes) forms a dense wireless ad-hoc network called 'specknet'.

Communication between widely spaced nodes in the specknet will be via a chain of

intermediary nodes. The development of first-generation, narrowband RF, prototype specks, which fit within a 5mm×5mm×5mm cube, is well under way [1], and a channel model is required to inform the design of the physical layer protocols governing communications between them. This research proposes such a model.

Another project being undertaken by the Specknet consortium is the 'Energy Neutral Platform'. The consortium is developing indoor wireless sensors that will approximately be half the credit card sized and can be used in number of indoor applications e.g. location tracking, surveillance, fire detection. These devices are powered using solar cells and in many cases, deployed over wall surfaces. They are designed to have low data rate and are expected to communicate on short paths (< 1 m). Energy neutral wireless nodes will be deployed on planar surfaces e.g. walls, roofs with the intentions to receive maximum energy from the light source (i.e. artificial light or sunlight).

1.2 Motivation

Wireless sensors have the possibility to sense the surrounding world and communicate wirelessly among each other or with mobile devices over a short range. Until now the concept of short range was limited to devices operating in an indoor environment for ranges of the order of few meters e.g. Bluetooth [2] and Zig-bee standards [3] where the main focus was to design high data rate device operating in the ISM band. In resent years the wireless sensor community is moving towards miniaturization and even shorter range devices (< 1 m) [1] [4]. Because of their small size these devices are constrained by the amount of energy they can transmit. They generally will be located very close to flat surfaces and thus the communication between the nodes is not only affected by medium properties (i.e. permittivity and conductivity) but also on physical design parameters (i.e. physical size of the node, antenna height and polarisation).

There is little existing literature on wireless channel modeling for such short ranges (= 10 cm). Most of the work reported being for ranges greater than 1 m. The signal to

noise interference ratio (SNIR) was reported for a moderately dense network with the assumption of perfect synchronization between nodes [5]. This models the network as a noise limited system (ignoring interference from neighbouring nodes). Also the effect of antenna height and polarisation on radio propagation is ignored for short wireless links operating at gigahertz frequencies. Polarisation loss (i.e. due to antenna and/or media) is not considered in existing wireless channel simulators [5] [6].

The research reported here aims to understand the propagation phenomena relevant for devices operating over short distances (< 10 cm) as envisaged by specknet. A rich set of empirical measurements have been carried out. A simulation model is developed to characterise the physical channel for future networks (like specknet) which are decentralized and randomly distributed. The resulting channel parameters have been incorporated in a simulation environment to predict performance.

1.3 Aim and Objectives

The aim of this research is to characterise short wireless links (< 10 cm) and to define a simulation environment that could be used to simulate a wireless links specific to a speck network. The simulation model should encapsulate various design and physical channel parameters experienced by these sensing nodes which are miniature in size and are meant to communicate with small separation distance.

The approach used in this research followed a series of ordered objectives, as follows:

1. Review of the literature on wireless channel models and measurements.

2. Review of existing wireless simulators used for indoor wireless channel modelling.

3. Empirical measurements have to be carried out to investigate the physical channel envisaged by Specknet.

4. Use of empirical measurements in a simulation environment specific to a dense ad-hoc network as envisaged by specknet. The simulation considers various design issues e.g. node density, deployment strategy, CSMA/CA inhibition distance and polarisation.

5. Exploration of surface waves effect in relation to antenna heights and polarisation. Since specks are small and are likely to be located close to surfaces the transmission loss depends on antenna height (defined as perpendicular distance from the surface) and polarisation has been investigated to understand the implication of these parameters on received power.

6. The aggregate polarisation loss due to antenna and medium has been investigated through a simulation model developed for specknet.

1.4 Organisation

The topic organisation in the thesis is summarised by the following diagram.

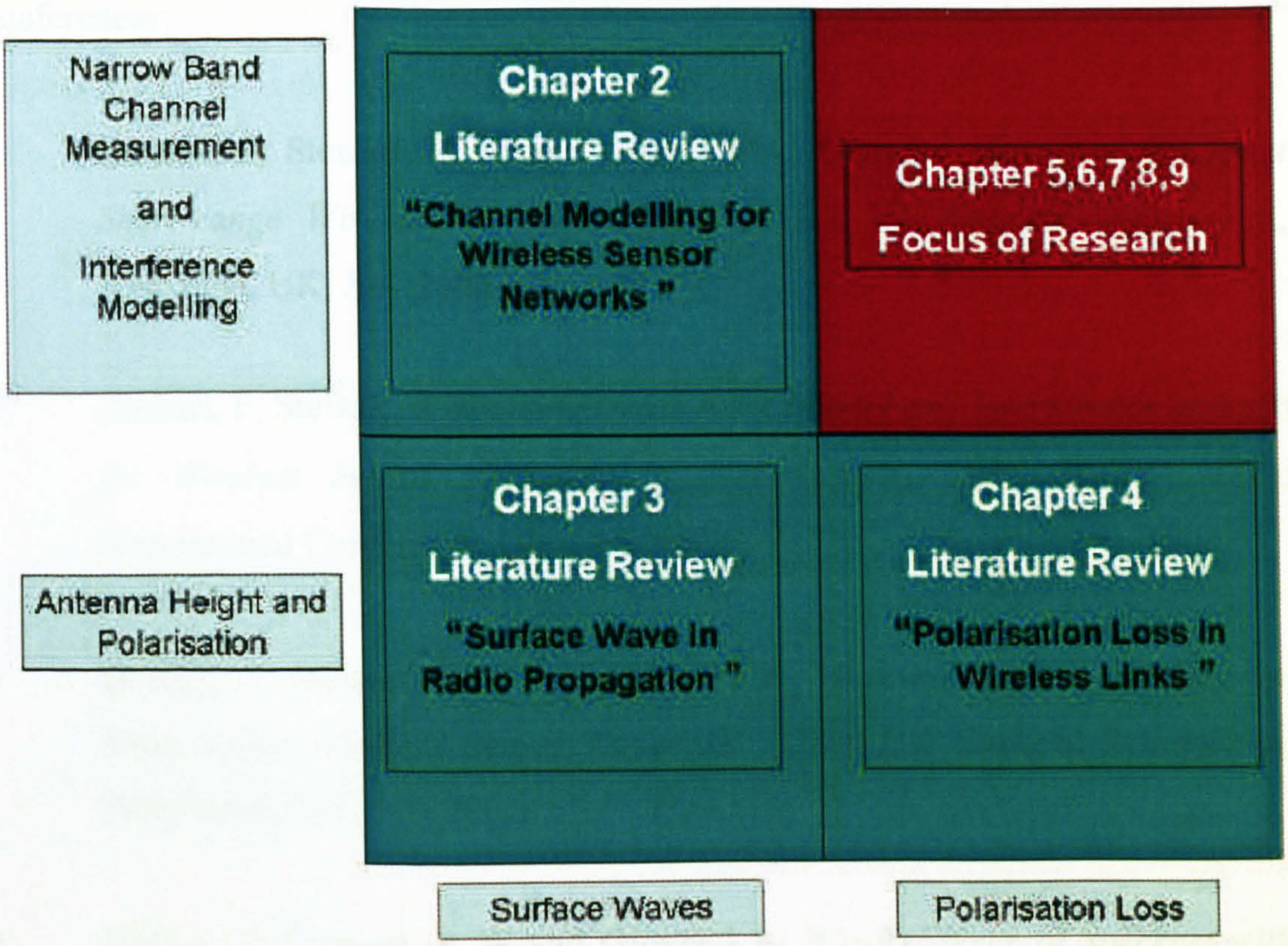

Fig. 1-1 Research methodology

1.5 Publications and Novelty

The principle contributions of the work in the thesis are:

- Propagation measurements for short wireless link (= 10 cm) and provide explanation of the physical phenomenon associated with measured data.

- Design and modelling of a simulation environment for the speck network. With appropriate modification the simulation model can be used to model a dense wireless network.

Part of the work have been published and presented in the following international conferences:

- Darbari, F, Stewart, R W and Glover I A, *"Channel Measurements for a Short range Wireless Sensor Network"*, URSI UK National Symposium, Abingdon, UK, July 2006.

- Darbari, F, Stewart, R W and Glover I A," *Channel and Interference analysis for Wireless Sensor Networks*", Communication, 2007. ICC'07. IEEE International Conference, Glasgow 2007.

- Darbari, F, Stewart, R W and Glover I A, *"Physical Layer Modelling for Short Range Wireless Sensor Networks"*, URSI UK National Symposium, Portsmouth, UK, July 2007.

- Darbari, F, Stewart, R W and Glover I A, *"Co-Existence of Specknet with other Wireless Standards"*, URSI UK National Symposium, Portsmouth, UK, July 2007.

- Darbari, F, Stewart, R W and Glover I A" *Multiple Access Interference in Short Range Wireless Sensors Networks*", IET, International Conference on Wireless, Mobile and Multimedia Networks, Mumbai, India 2008.

- F. Darbari, K. Sasloglou, R.W. Stewart, I. A. Glover and I. Andonovic," *Effect of Antenna Height and Polarisation on Short Wireless links*", Eusipco, 16th European Signal Processing Conference, Lausanne, Switzerland, 2008

- Darbari, F, Stewart, R W and Glover I A." *Narrow Band Short Range Channel Measurements*". The XXIX General Assembly of International Union of Radio Sciences (URSI), Santiago, USA, 2008.

- G. Whyte, Darbari, F, I. McGregor, I. Glover, I. Thayne "Different *Feeding Geometries for Planar Elliptical UWB Dipoles, and the Excitation of Leakage Current*". 38th European Microwave Conference, Netherland, Amsterdam, 2008

1.6 Thesis Structure

Chapter 2 provides a review of wireless channel models. The existing wireless simulation models are discussed. The effect of noise and interference in simulating wireless sensors network has been considered.

Chapter 3 focuses on the effect of antenna height and polarisation on short wireless links. The concept of surface waves has been reviewed for short wireless links.

Chapter 4 reviews polarisation loss in wireless channel. Polarisation loss due to antenna and medium has been discussed in relation to the electrical properties of the medium

Chapter 5 provides details of the measurement campaign and a theoretical explanation of the underlying propagation phenomenon.

Chapter 6 provides a through analysis of interference and the simulation of a specknet using empirical information from the previous chapter.

Chapter 7 addresses the effect of antenna height (above the surface on which specks are located) and polarisation using empirical measurements.

Chapter 8 deals with antenna and media polarisation loss.

Chapter 9 draws together the conclusions of the work and suggests future work.

Chapter Two

2. Channel Modelling for Wireless Sensor Networks

2.1 Wireless Channel Model

The wireless channel places fundamental limitation on the performance of wireless communication system. The electromagnetic waves are diffracted, scattered or reflected as the wave propagates through the medium resulting in a decrease of signal strength with distance. The decay in signal strength with respect to distance i.e. the path loss index broadly depends on the following.

- Frequency of operation
- Environment

Future wireless sensing nodes are miniature in size (i.e. specknet) and are operating close to the ground surface. The presence of the ground has an effect on radio propagation and the following have to be considered:

- Antenna polarisation
- Cross Polarisation (due to medium)
- Electrical properties of the ground (i.e. permittivity, permeability and conductivity)
- Surface wave
- Physical size of the device (affecting. the height of the antenna from the ground)

Several recent empirical studies [7] [8] [9] [10] have been conducted in indoor environments in order to investigate the wireless channel. These studies mostly deal

with devices separated by few meters and the effect of antenna height from the ground is mostly ignored may be due to the large physical size of the sensing device. The effect of placing the sensor near the ground for short wireless links (= 10 cm as envisaged by specknet) has not previously been considered for devices operating in ISM band.

2.1.1 Survey of Channel Model

Path loss and coverage prediction for indoor wireless channel could be deterministic or statistical. In a deterministic approach ray tracing (for example) is used to predict signal strength at various indoor bcations. In ray tracing the possible propagation paths are identified and the amplitude and delay of each relevant path is considered. It requires a rich set of information about the environment stored in a three dimensional data base. The process can be time consuming. In a statistical approach mean signal strength over a range of distance is observed through empirical measurement. The signal may experience fading due to ground wave effects (i.e. reflection or absorption). This approach is used for specknet channel modelling where a rich set of empirical data is gathered for different surface materials and antenna heights. The statistical data is compared with theoretical channel models (i.e. free space, two ray model, log normal model etc) in order to infer the underlying physical phenomenon

Propagation models that estimate mean signal strength are useful in estimating the decay in signal power for arbitrary transmitter and receiver separations. The propagation models that are used to characterise rapid fluctuations of the received signal strength for a given separation between the transmitter and receiver are called fading models [11].

Free space propagation is used to predict received signal strength when the transmitter and receiver have a clear, unobstructed line of sight between them. The free space power predicts that the received power decays as a function of the transmitter and receiver separation raised to power two (i.e. a power law function)

[12]. The free space power received by a receiver antenna which is separated from a radiating transmitting antenna by a distance *d*, is given by Friss free space equation.

$$P_r(d) = \frac{P_t G_t G_r \lambda^2}{(4\pi)^2 d^2} \tag{2.1}$$

where P_t is the transmitted power, *?* is the wavength, $P_r(d)$ is the received power which is a function of transmitter and receiver separation distance and G_t and G_r are the transmit and receive antenna gains. The free space path loss model shows that the received power decays with distance at a rate of 20 dB/decade.

Wireless transmission range is defined in terms of transmission loss (L_T) which represents signal attenuation in decibels. It is the difference (in dB) between the transmit-and-received powers at the antenna. From Equation (2.1), the transmission loss is $P_t / P_r(d)$. L_T in decibels is defined as:

$$L_T(dB) = 10\log_{10}\left(\frac{P_t}{P_r}\right) = -10\log_{10}\left(\frac{G_t G_r \lambda^2}{(4\pi)^2 d^2}\right) \tag{2.2}$$

The equation defined for unity gain antenna is called path loss *Lp*:

$$L_P(dB) = -10\log_{10}\left(\frac{\lambda^2}{(4\pi)^2 d^2}\right) \tag{2.3}$$

Equation (2.3) can be expressed as:

$$L_P(dB) = 20\log_{10}(f_{MHz}) + 20\log_{10}(d) - 28 \tag{2.4}$$

where f_{MHz} is the frequency mega-hertz

The path loss and transmission loss are related by:

$$L_P(dB) = L_T(dB) - G_t - G_r \tag{2.5}$$

The received power is given by:

$$P_r\left(dBm/dBw\right) = P_t\left(dBm/dBw\right) - L_T(dB) \tag{2.6}$$

The Friss free space formula calculates the received power for a distance that is in the far field region of the transmitting antenna. The far field region is:

$$d_f \geq \frac{2D^2}{\lambda} \tag{2.7}$$

where D is the largest physical dimension of the antenna [11].

Propagation models typically use a close in reference distance d_o. The received power $P_r(d)$ for $d > d_o$ is calculated with reference to $P_r(d_o)$ The reference distance should *always be in* the far field of the antenna so that near field effects do not alter the reference path loss. The reference path loss is normally established through field measurements [12].

The received power for an arbitrary distance d (where $d > d_o > d_f$) can be calculated using:

$$P_r(d) = P_r(d_o)\left(\frac{d_o}{d}\right)^2 \tag{2.8}$$

where P_r is the received power at a separation distance d, $P_r(d_o)$ is the reference power calculated at a reference distance d_o such that the reference distance is in the far field region of antenna.

For radio frequency power level in dBm or dBw Equation (2.8) becomes:

$$P_r(d)\left(^{dBm}/_{dBw}\right) = P_r(d_o)\left(^{dBm}/_{dBw}\right) + 20\log_{10}\left(\frac{d_o}{d}\right) \quad (2.9)$$

In indoor wireless channel radio propagation is affected by specific features such as building layout and construction material Propagation is normally classified as line-of- sight (LOS) or non-line-of-sight (NLOS). NLOS or obstructed link depends on the building's internal layout which has wide variety of partitions and obstacles. Partitions in a building structure can be classified as hard or soft partitions [11]. The partitions that can move and do not span to the ceiling are soft while the partition in the actual building structure are the hard. Houses typically use wooden frame partitions (especially in UK) while the offices buildings use soft partitions with metal-reinforced concrete between floors. Partitions and building material vary widely in their physical and electrical properties thus making it difficult to apply generic models for indoor channel. A combination of empirical measurement and generic modelling is often used to characterise the channel for a particular application.

2.2 Interference in Wireless Sensor Networks

Quantification of aggregate interference experienced by a wireless sensing node in a collaborative network is vital for the performance of upper layer protocols. The dominant co-channel interference experienced by a wireless sensing node is likely to be due to the neighbouring nodes or due to other wireless equipment operating in the same frequency band.

The signal-to-interference ratio (SIR) experienced by a wireless sensing node depends on the design of the wireless network. A network can be modelled either as a noise limited system or as interference limited system. Which is appropriate depends on various design issues e.g. network architecture, MAC protocol, choice between synchronised and unsynchronised media access protocols, node density and deployment strategy etc.

Dense wireless sensor networks like Specknet [1] are deployed in the environment to form a collaborative network communicating through a chain of intermediate nodes. Specks have a decentralised random access MAC protocol [13]. This allows nodes to access the channel on demand without any requirement for synchronization. The SIR experienced by a node depends on the number of concurrent communications which depends on the application and node density (ignoring interference from other wireless equipment operating in the same band).

Network architectures for low power wireless sensor networks can be broadly classified as either centralised or decentralised [13]. Centralised wireless system requires a synchronising mechanism between nodes thus restricting the nodes to transmit in allocated spatial slots (i.e. TDMA based system). Co-channel interference is minimal and the network can be classified as noise limited. Decentralised architectures allow nodes to access the channel on-demand resulting in higher co-channel interference. Decentralised wireless networks can thus be modelled as interference limited.

In the following discussion noise limited and interference limited design are considered in order to inform the simulation approach appropriate to a speck network.

2.2.1 Noise Limited Systems

In centralised network architectures a base station provides collision-free operation. A centralised wireless network requires a synchronising mechanism between nodes e.g. TDMA as used by Bluetooth technology [14] [15]. In a centralised wireless network the wireless channel is divided in to time slots. Each time slot is allocated to a user and the user is time synchronised (by the base station) to send data in its allocated time slot. The base station is responsible for coordination between nodes and thus requires more resources (i.e. battery power, control channel allocation etc.). The interference experienced by the receiving node is comparatively less than in a decentralised network. Since co-channel interference is limited ideally not present, it is appropriate to model these networks as noise limited.

In order to simulate a wireless sensor network as a noise limited system following has to be defined:

- Propagation and fading modelling
- Noise floor
- Transitional regions (for noise limited systems)

2.2.1.1 Propagation and Fading Modelling

An essential aspect of wireless channel modelling is to quantify propagation loss which depends on various factors i.e. frequency of operation, operating environment and antenna polarisation etc. Most radio propagation models use a combination of analytical and empirical methods [16]. Fig. 2-1 shows received signal strength using a $1/d^n$ model for different path loss indices, n. The statistical fading variations can be characterised using empirical measurements by taking repeated measurements for a given distance and then calculating the standard deviation of the data. As an example Fig. 2-2 assumes a standard deviation of 2 dB (i.e. P_r(dBm) ± 2 dB) which is independent of distance. (Note however that measurements often show that fading standard deviation is positively correlated with distance).

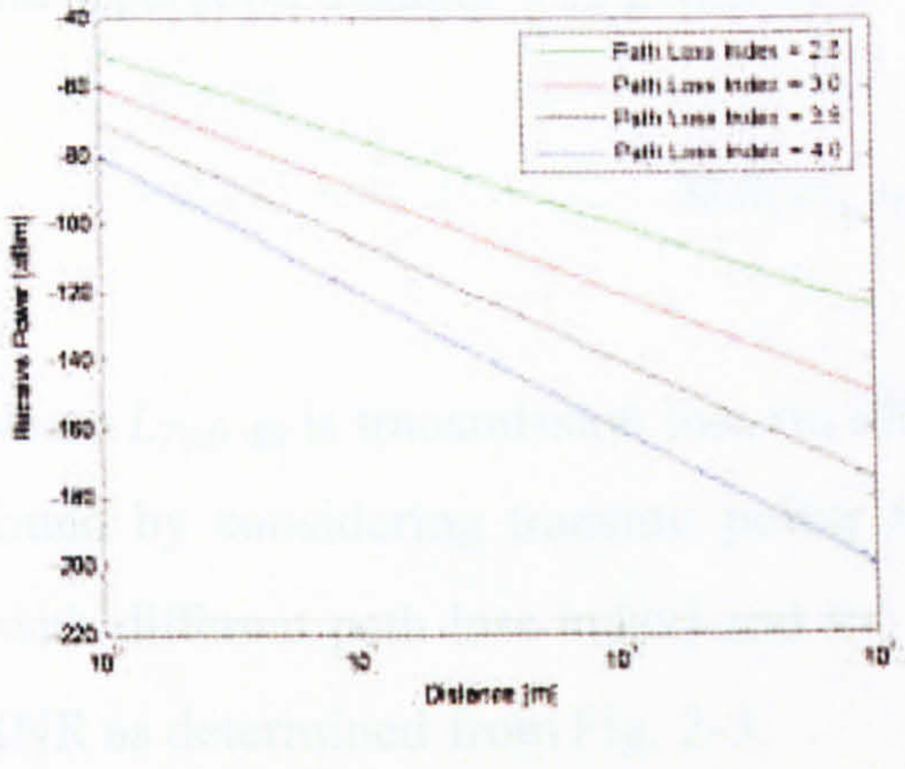

Fig. 2-1 d-n Propagation model (free space)

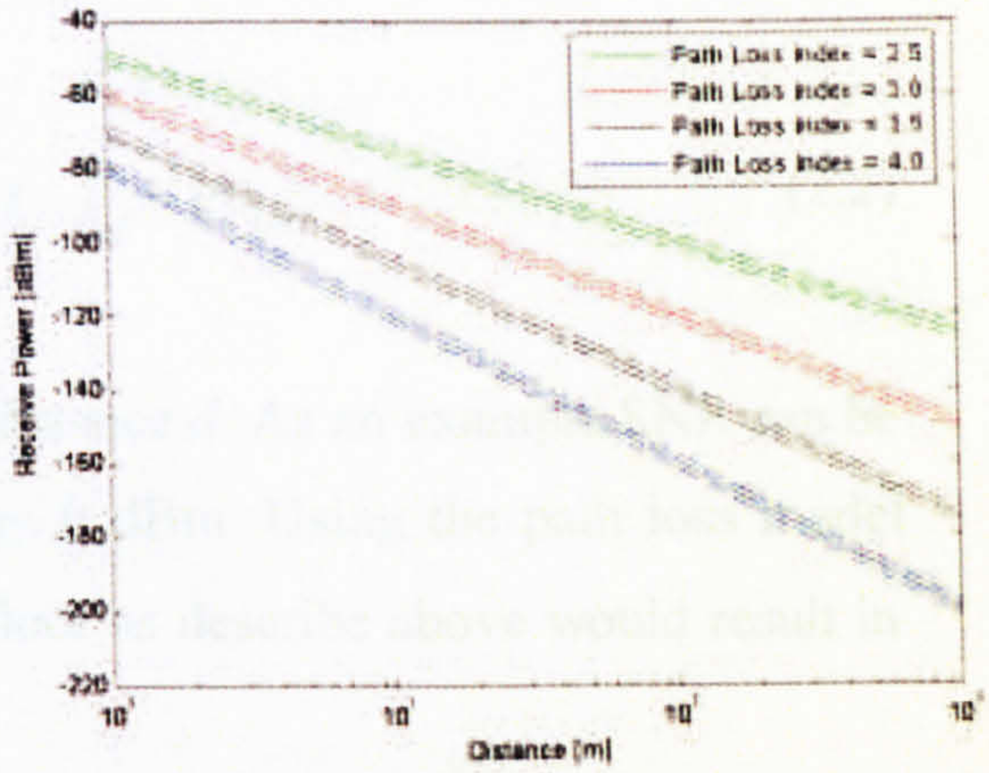

Fig. 2-2 Illustration of propagation model with fading

2.2.1.2 The Noise Floor

Noise floor depends on hardware and the environment. The temperature of the environment influences the thermal noise generated by radio components which increases the noise floor. Noise floor is further affected by interfering signals. Noise floor is usually calculated using [17]

$$P_n = (F + 1) k T_o B \tag{2.1}$$

Where F is the noise figure, k is Boltzmann's constant, T_o a reference temperature of 290k and B is the noise bandwidth. As an example consider the MICA2s mote which uses a Chipcon CC1000 radio [18] has a noise figure of 13 dB and a system noise bandwidth of 30 kHz. Considering an ambient temperature of 300°k (27°C, 75°F) and no interfering signal then the noise floor is -115 dBm [19]. This defines the sensitivity of the wireless system i.e. the minimum possible detectable signal.

The SNR experienced by a wireless sensing node for a given transmitted power P_t and separation distance d is given by

$$SNR(d)_{dB} = P_{(t)_{dB}} - L_{T(d)_{dB}} - P_{(n)_{dB}} \tag{2.2}$$

where $L_{T(d)\ \mathrm{dB}}$ is transmission loss (in dB) at a distance d. As an example SNR can be found by considering transmit power to be say 0 dBm. Using the path loss model (with different path loss index) and the noise floor as describe above would result in SNR as determined from Fig. 2-3.

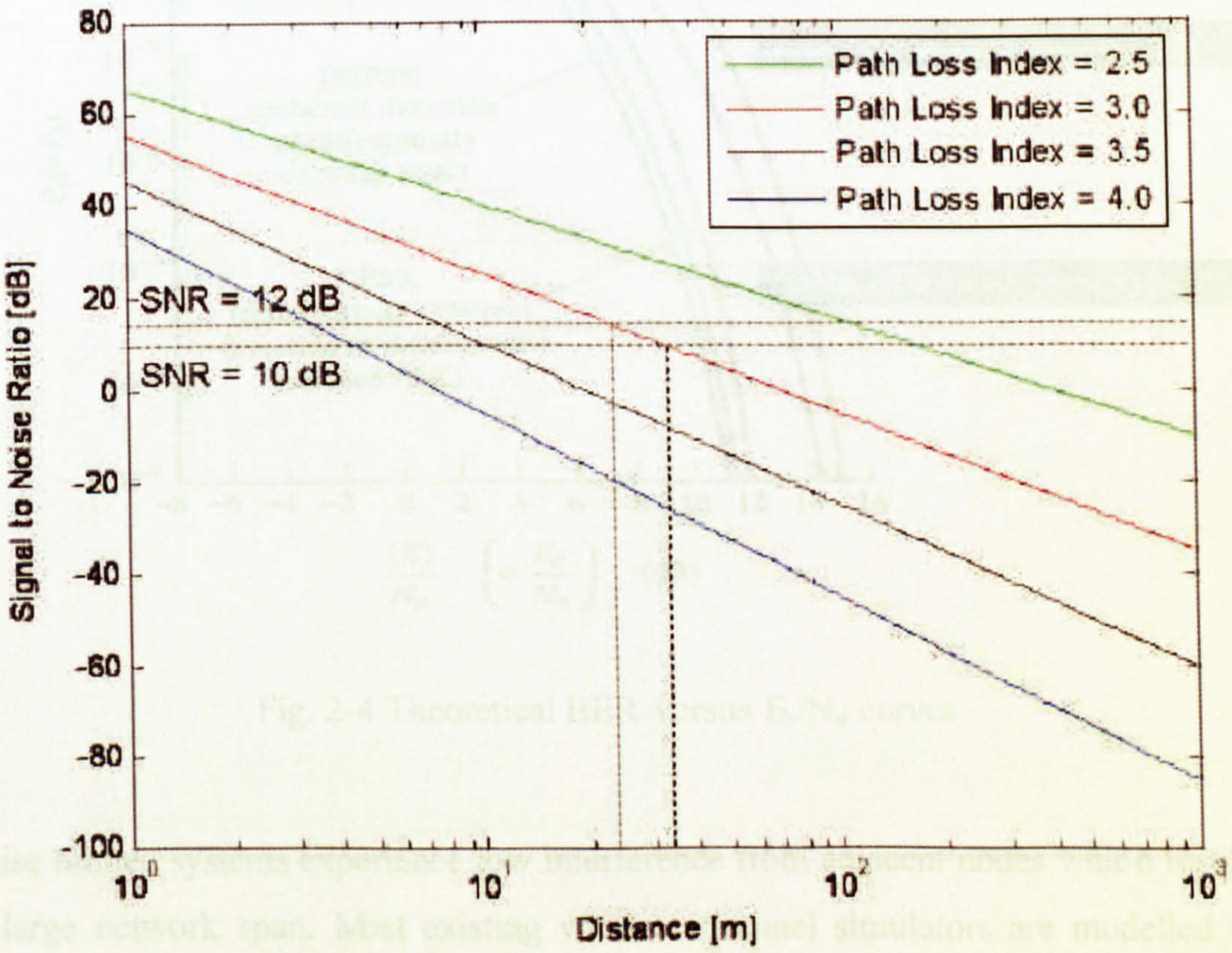

Fig. 2 3 Simple model of SNR as a function of link length

Considering a wireless sensor network deployed in an environment having a path loss index of 3, the corresponding SNR (using (2.2)) as a function of separation distance (ignoring fading) is shown in Fig. 2-3. If the transmitted signal is OOK modulated then the theoretical SNR required for coherent detection is between 10 dB

and 12 dB respectively (for BER between 10^{-2} and 10^{-3}) as in Fig 2-4. The SNR of 10 and 12 dB correspond to the separation distance of 35 m and 25 m as in Fig. 2-3. This suggests that for the environment having a path loss index of 3, the nodes can communicate with reasonable BER to a maximum distance of 35 m.

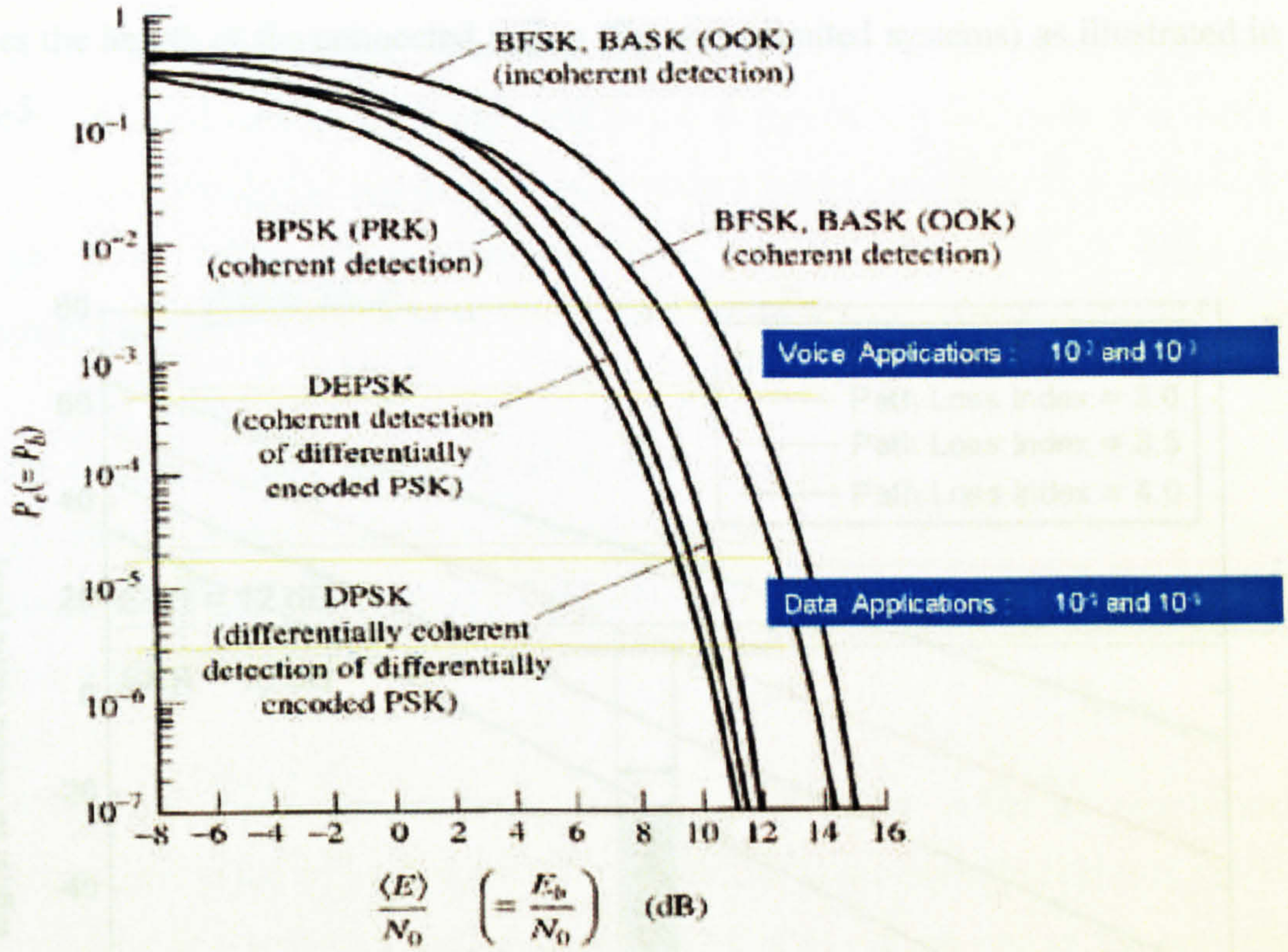

Fig. 2-4 Theoretical BER versus E_b/N_o curves

Noise limited systems experience low interference from adjacent nodes which results in large network span. Most existing wireless channel simulators are modelled as noise limited [17] ignoring interference due to neighbouring nodes.

2.2.1.3 Transitional Regions (for noise limited systems)

Most recent studies of wireless sensor networks defines three distinct regions in wireless links i.e. connected, transitional, and disconnected [20] [21] [22].

The transitional region is generally significant in size and is characterised by higher variance in packet error rate and asymmetric connectivity. Wireless sensor networks are characterised by dense deployments which could result in a large number of links being unreliable because of the existence of the transitional region. The effect of path loss on the transitional region has been explored in detail in [17] which concludes that any increase in path loss index decreases the extent of the transitional region and reduces the length of the connected region (for noise limited systems) as illustrated in Fig. 2-5.

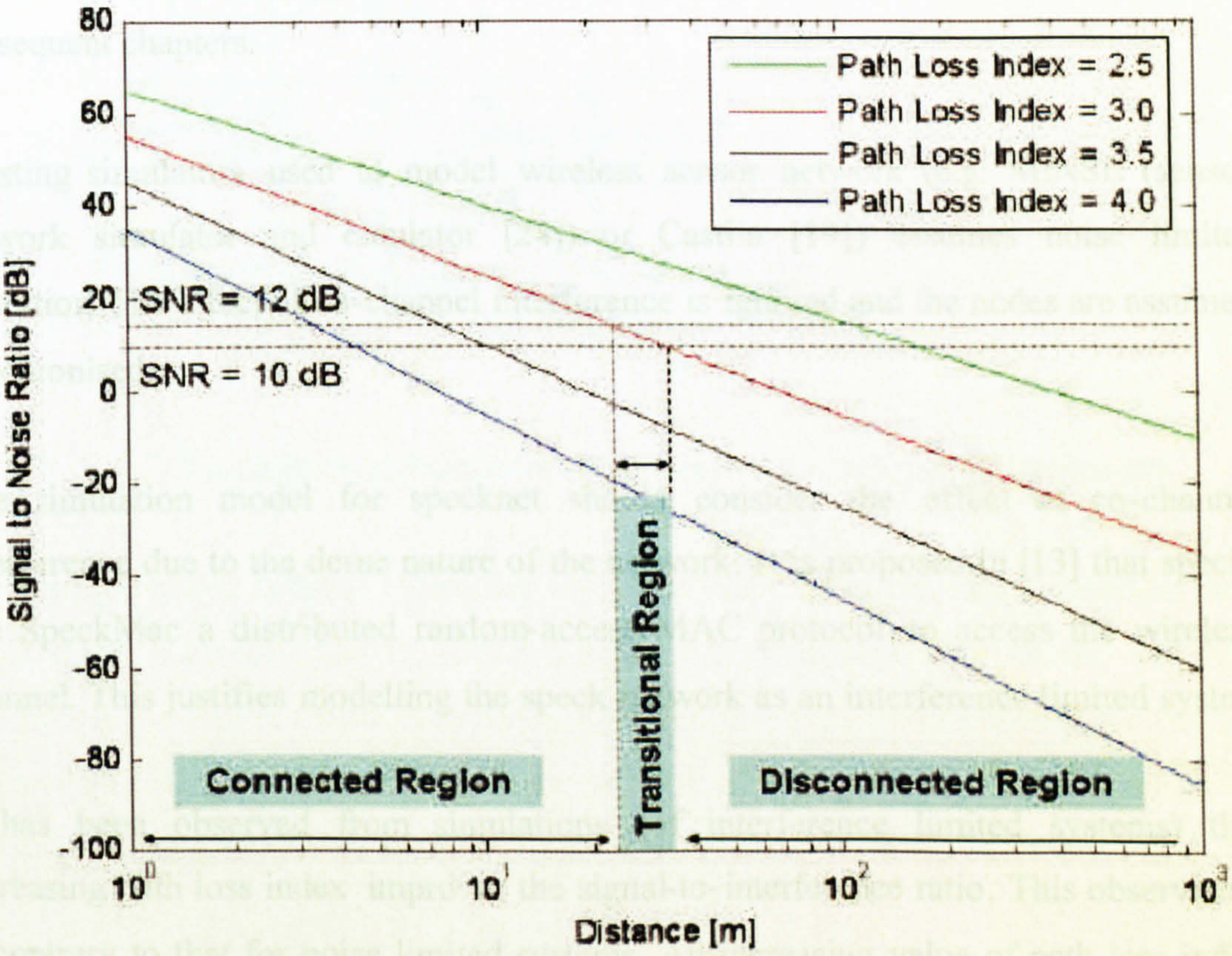

Fig. 2-5 Impact of path loss on transitional region

It is evident from Fig. 2-5 that any increase in path loss shifts the transitional region towards left.

2.2.2 Interference Limited Wireless Systems

Wireless sensor network can be designed to be decentralised networks in which nodes can access the channel randomly. The unsynchronised behaviour of the nodes adds to the aggregate interference thus increasing the overall noise floor. The increased level of interference due to co-channel interference results in reduction in received signal-to-noise ratio. Modelling an interference limited wireless system requires definition of various design and physical parameters i.e. node size, node density, area of simulation and antenna polarisation, media access MAC protocol (i.e. CSMA/CA) etc. [23]. The simulation parameters are considered in detail in subsequent chapters.

Existing simulators used to model wireless sensor network (e.g. SENSE (sensor network simulator and emulator [24]) or Castlia [19]) assumes noise limited operation. The effect of co-channel interference is ignored and the nodes are assumed synchronised.

The simulation model for specknet should consider the effect of co-channel interference due to the dense nature of the network. It is proposed in [13] that specks use SpeckMac a distributed random-access MAC protocol to access the wireless channel. This justifies modelling the speck network as an interference limited system.

It has been observed from simulations (of interference limited systems) that increasing path loss index improves the signal-to-interference ratio. This observation is contrary to that for noise limited systems. An increasing value of path loss index results in improved SIR (Fig. 2-6) due to higher values of propagation loss between interfering and receiving nodes. Fig. 2-6 shows the likely dependence of path loss index on the received SIR.

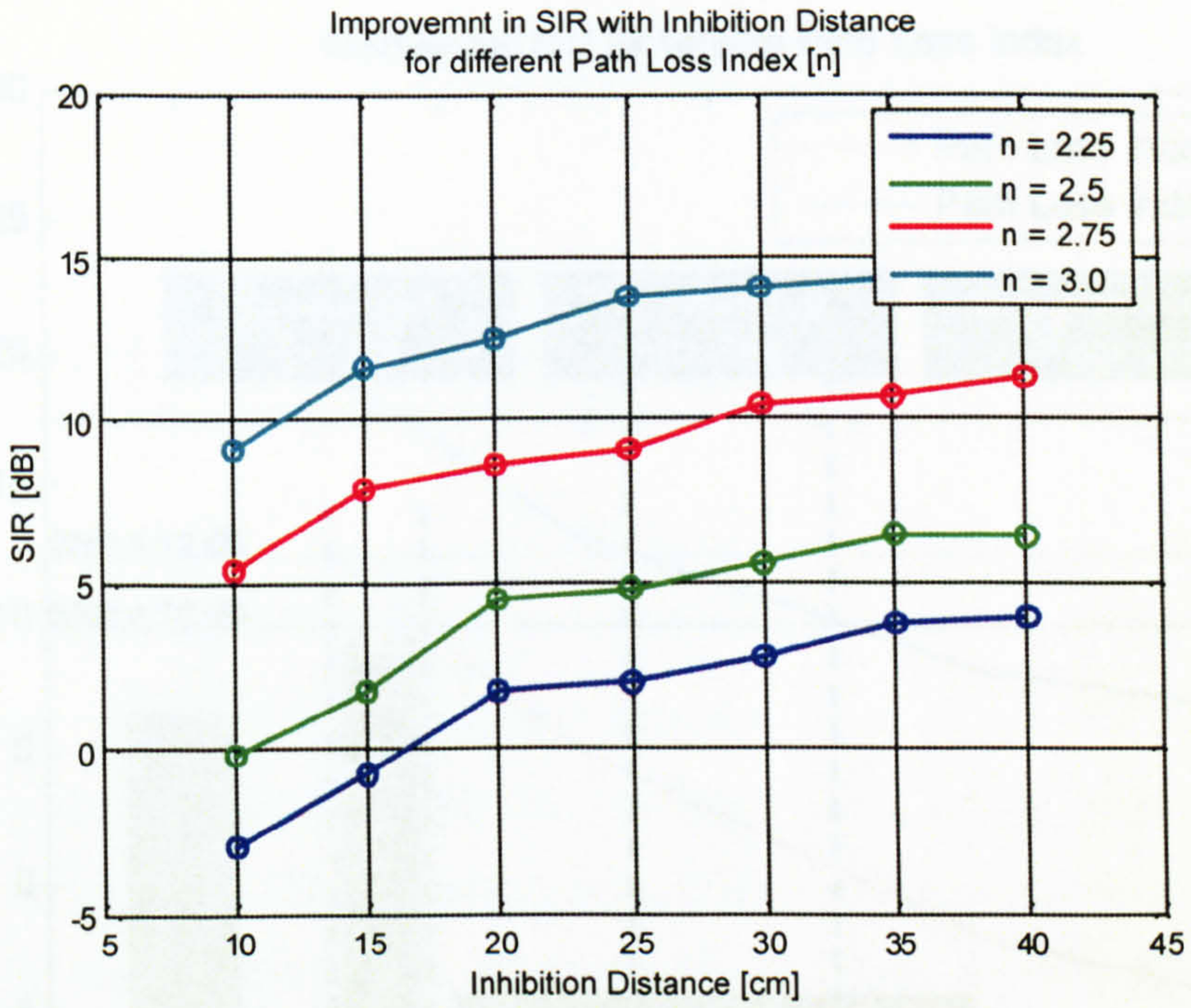

Fig. 2-6 Improvement in SIR with increasing path loss index

2.2.2.1 Transitional Regions (for interference limited systems)

For a noise limited systems increasing path loss index decreases signal-to-noise ratio for a given distance. The transitional regions in this case shift to the left thus decreasing the length of the connected region as in Fig 2-5. For interference limited systems increasing path loss index increase SNR for a given distance and shifting the transitional region to the right as in Fig. 2-7.

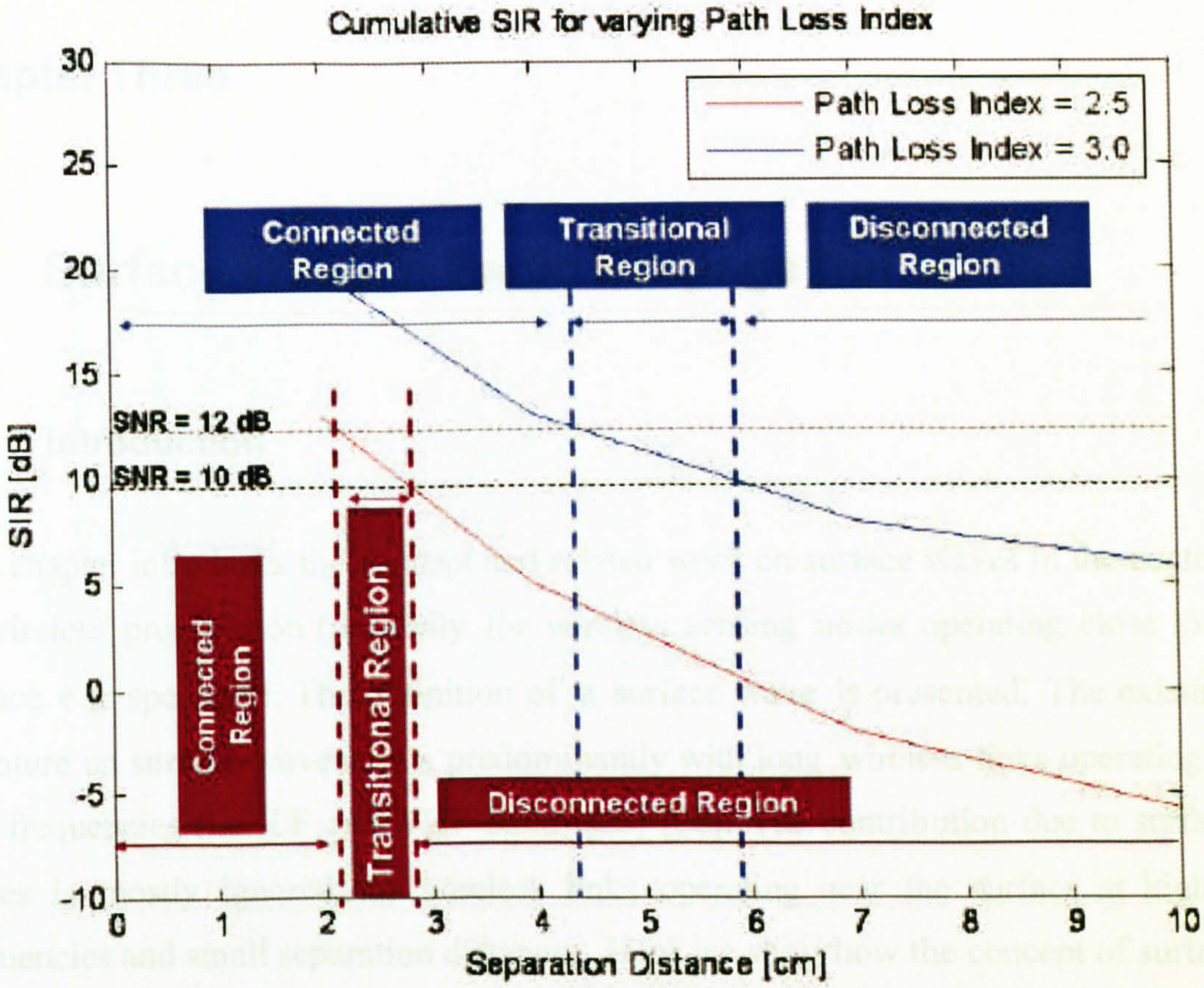

Fig. 2-7 Transitional region for interference limited systems

2.3 Summary

The specknet is a decentralised randomly distributed dense network of autonomous nodes which are meant to communicate at short ranges. The transmission loss is estimated based on statistical modelling of empirical data. The dense network is modelled as interference limited system in order to arrive at signal to interference value likely experienced by a sensing node (in a worst possible case).

Chapter Three

3 Surface Wave in Radio Propagation

3.1 Introduction

This chapter introduces the concept and related work on surface waves in the context of wireless propagation (primarily for wireless sensing nodes operating close to a surface e.g. specknet). The definition of a surface wave is presented. The existing literature on surface waves deals predominantly with long wireless links operating at low frequencies (i.e. LF and VHF band) [25] [26]. The contribution due to surface waves is mostly ignored for wireless links operating near the surface at higher frequencies and small separation distances. Here we show how the concept of surface waves can be used to explain the observed channel characteristic of short wireless links as envisaged by specknet [1].

3.2 Propagation Mechanism

Radio wave propagation between a transmitter and receiver close to the a plane surface can be described in terms of the interference between the free-space field, the field due to re-radiation of energy from the induced surface currents and a surface wave. This is shown schematically in Fig. 3-1.

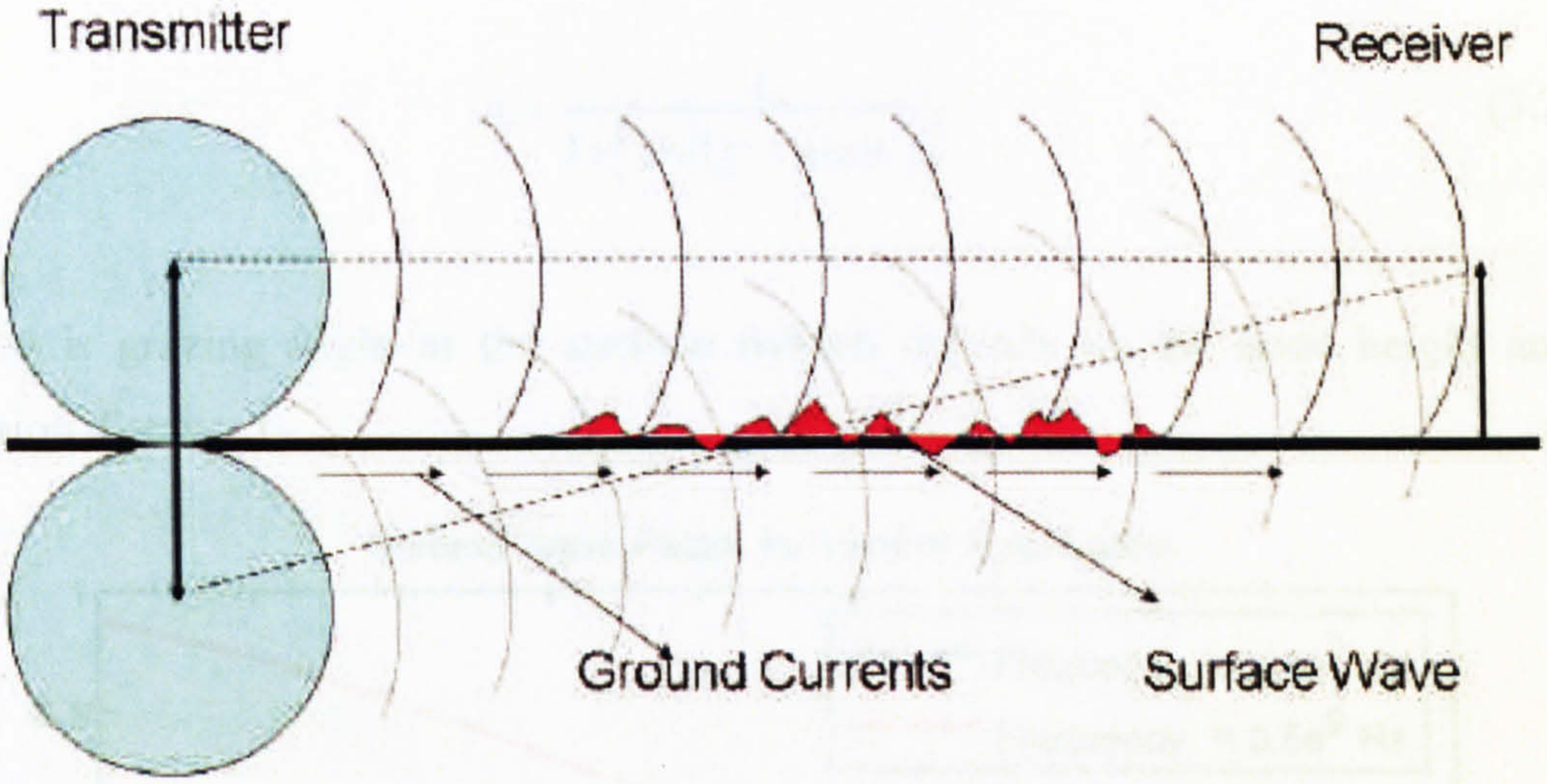

Fig. 3-1 Propagation near a surface

3.3 Transmission Loss for Line of Sight Paths

The presence of the surface modifies the transmission and reception of radio waves [25] [26] [27]. The path loss ratio (L_p) between the received and transmitted power for unity gain antennas [27] is mathematically given by:

$$L_p = \left| \frac{e^{-jkd}}{2kd} \left[F_d + F_r [\Gamma + (1 - \Gamma) A] \right] e^{-j\phi} + \ldots \right]^2 \qquad (3.1)$$

where k is wave number, F_d is the direct (LOS) field strength and F_r is the incident wave field strength which includes amplitude correction for added distance travelled. d is the path length and Γ is the (frequency dependent) plane surface reflection coefficient magnitude which depends on the incident wave polarisation, surface permittivity and conductivity. ϕ is the additional phase delay for the reflected wave.

The remaining component represents a surface wave. A is the (complex) surface-wave factor with a magnitude less than one [27] given by:

$$A = \frac{-1}{1+\left[jkd\left(\Gamma + \sin\theta\right)\right]^2} \tag{3.2}$$

where θ is grazing angle at the surface (which depends on the node height and separation distance).

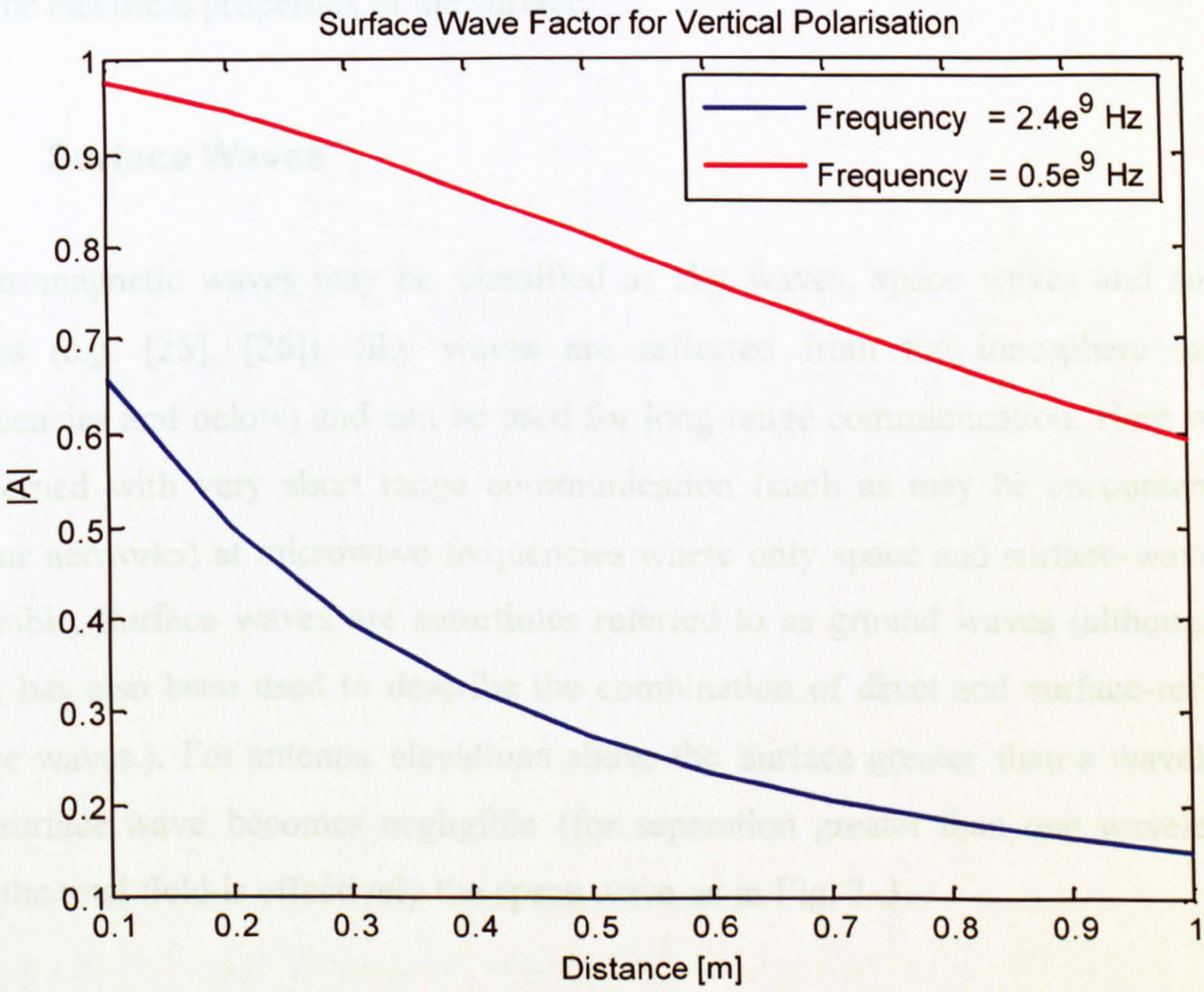

Fig. 3-2 Surface wave factor for increasing distance (node height is 0.65 cm, conductivity is 0.005 S/m, relative dielectric constant is 7.0)

The surface wave factor A introduces an attenuation that is dependent upon distance, antenna height, frequency and the electrical properties of the surface along which the wave travels. For distances within few wavelength from the antenna A has a value greater than 0.25 (for a typical specknet scenario (ENP) i.e. antenna height of 0.65 cm from the ground surface, and separation distances of 50 cm) as in Fig. 3-2. As the

distances approaches zero the value of surface wave factor approaches 1. It has been observed in Fig. 3-2 that the surface contribution decreases with distances.

For the far-field near grazing angles (i.e. low antenna elevations) the reflection coefficient approaches -1 (3.1) (over a smooth surface for both vertical and horizontal polarisation) and the direct and reflected wave component cancel each other thus the received field strength is due to the surface wave component. The contribution due to surface wave is dependent on distances, frequency of operation and the electrical properties of the surface.

3.4 Surface Waves

Electromagnetic waves may be classified as sky waves, space waves and surface waves (e.g. [25], [26]). Sky waves are reflected from the ionosphere (at HF frequencies and below) and can be used for long range communication. Here we are concerned with very short range communication (such as may be encountered in sensor networks) at microwave frequencies where only space and surface-waves are plausible. Surface waves are sometimes referred to as ground waves (although this term has also been used to describe the combination of direct and surface-reflected space waves.). For antenna elevations above the surface greater than a wavelength the surface wave becomes negligible (for separation greater than one wavelength) and the total field is effectively the space wave as in Fig. 3-3.

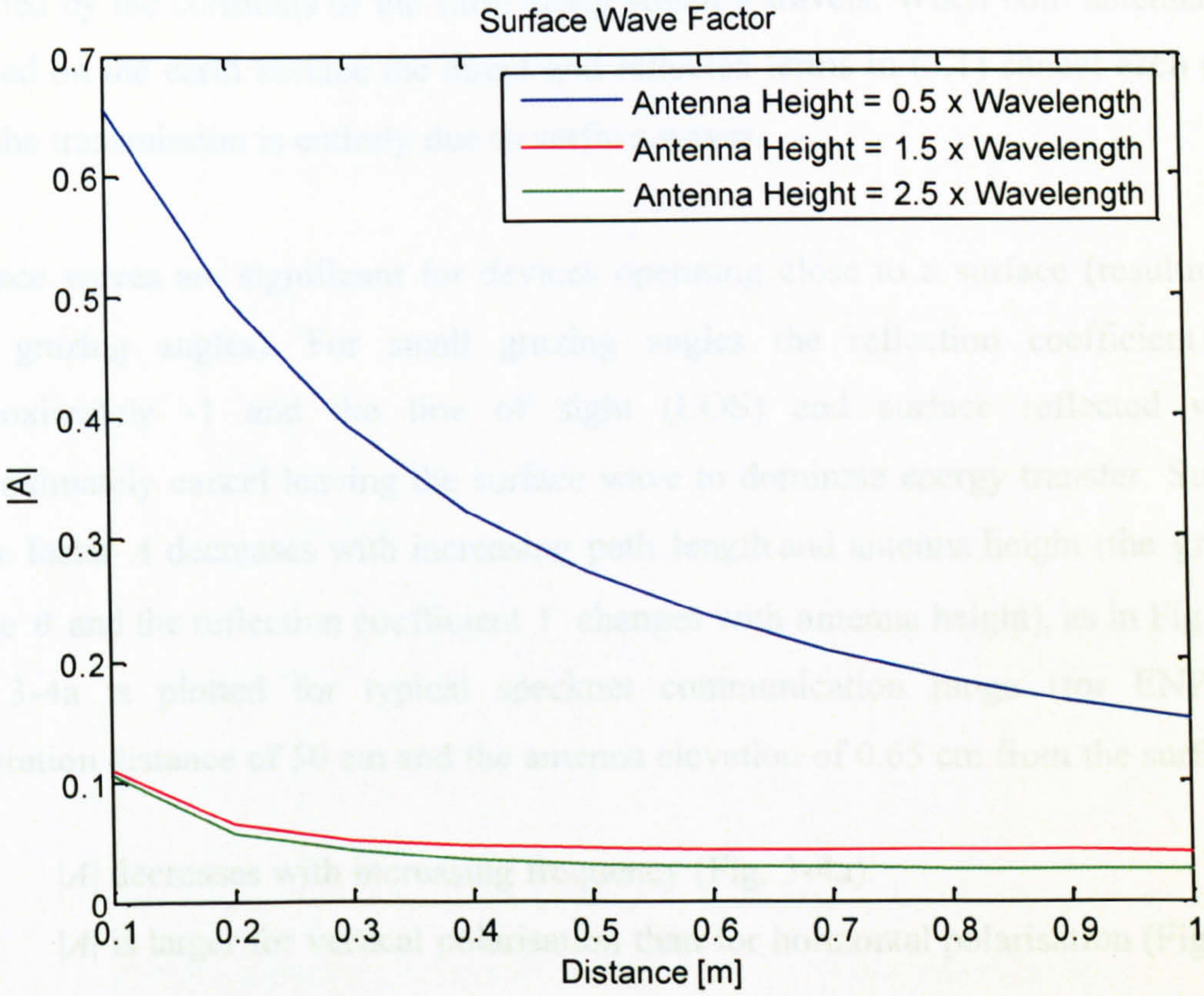

Fig. 3-3 Surface wave factor for increasing antenna height (f = 2.45 GHz)

The concept of a surface wave was proposed in the early 20th century [25] [26]. These waves propagate by interacting with the surface. Since the surface is not a perfect electrical conductor, some of these waves are attenuated rapidly. Attenuation is proportional to the frequency making surface waves mainly useful for LF (30 kHz–300 kHz) and VLF (3 to 30 kHz) frequencies. Surface waves are (at least loosely) bound to the surface over which they propagate.

Space waves travel via the direct line-of-sight path, reflected paths and (sometimes) refracted paths. There are various stages of transition between space waves and surface waves, and in practical wireless communication problems a clear division between the two is often difficult to draw [25].

The surface wave is a wave that is guided along the surface, such as electromagnetic waves is guided by a transmission line. Energy is abstracted from the surface waves to supply the losses in the ground because of this the attenuation of this wave is

affected by the constants of the earth along which it travels. When both antennas are located on the earth surface the direct and reflected terms in (3.1) cancel each other and the transmission is entirely due to surface waves.

Surface waves are significant for devices operating close to a surface (resulting in low grazing angles). For small grazing angles the reflection coefficient Γ is approximately -1 and the line of sight (LOS) and surface reflected waves approximately cancel leaving the surface wave to dominate energy transfer. Surface wave factor A decreases with increasing path length and antenna height (the grazing angle θ and the reflection coefficient Γ changes with antenna height), as in Fig. 3-4a. Fig 3-4a is plotted for typical specknet communication range (for ENP) i.e. separation distance of 50 cm and the antenna elevation of 0.65 cm from the surface.

- $|A|$ decreases with increasing frequency (Fig. 3-4a).
- $|A|$ is larger for vertical polarisation than for horizontal polarisation (Fig. 3-4a)
- $|A|$ decreases with increasing antenna height for vertical polarisation and is small and approximately constant for horizontal polarisation (Fig. 3-4b).
- $|A|$ increases with increasing surface permittivity for vertical polarisation and is small with increasing permittivity for horizontal polarisation (Fig. 3-4c).
- $|A|$ increases with increasing surface conductivity for vertical polarisation and is small with increasing conductivity for horizontal polarisation (Fig. 3-4d).

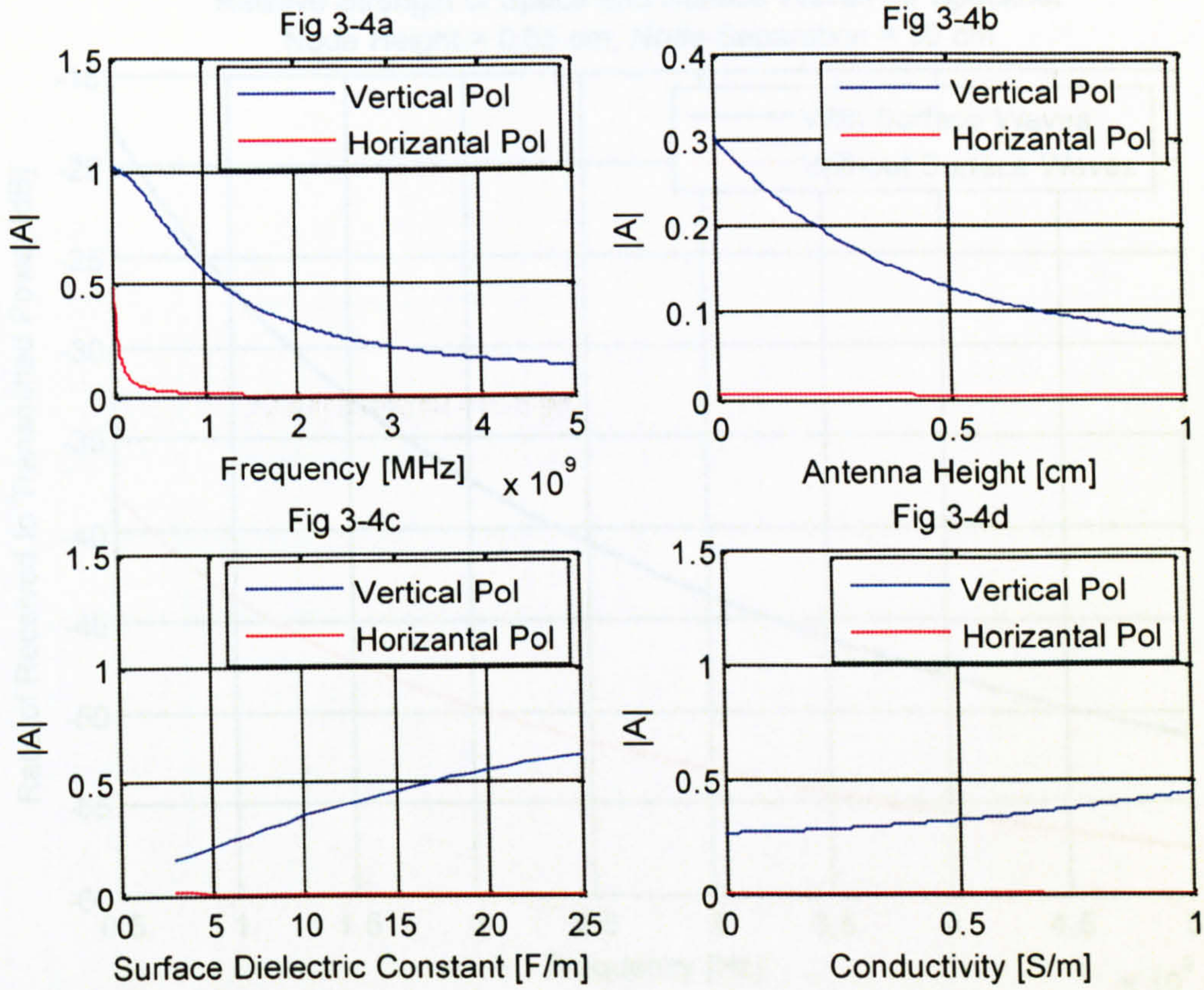

Fig. 3-4 Variation of surface wave factor magnitude ($e_r = 7$, $s = 0.005$ S/m and $f =$ 2.45 GHz)

3.5 Importance of Surface Wave for Specknet

Transceiver nodes in future, densely-packed, wireless sensor networks (e.g. specknet [1]) will be small and are expected to be deployed close to surface features (e.g. walls, floors, ceilings etc.). For node elevation above the surface measured in millimetres it seems is possible that surface-wave propagation will be significant. In addition to link geometry (antenna heights and link length) and surface character (permittivity, conductivity, roughness) polarisation might also affect the proportion of power carried by a surface-wave. Fig. 3-5 and Fig 3-6 shows the relative strength of space and surface waves for typical specknet scenario for ENP. Fig. 3-7 shows the relative strength of space and surface wave on a logarithmic scale.

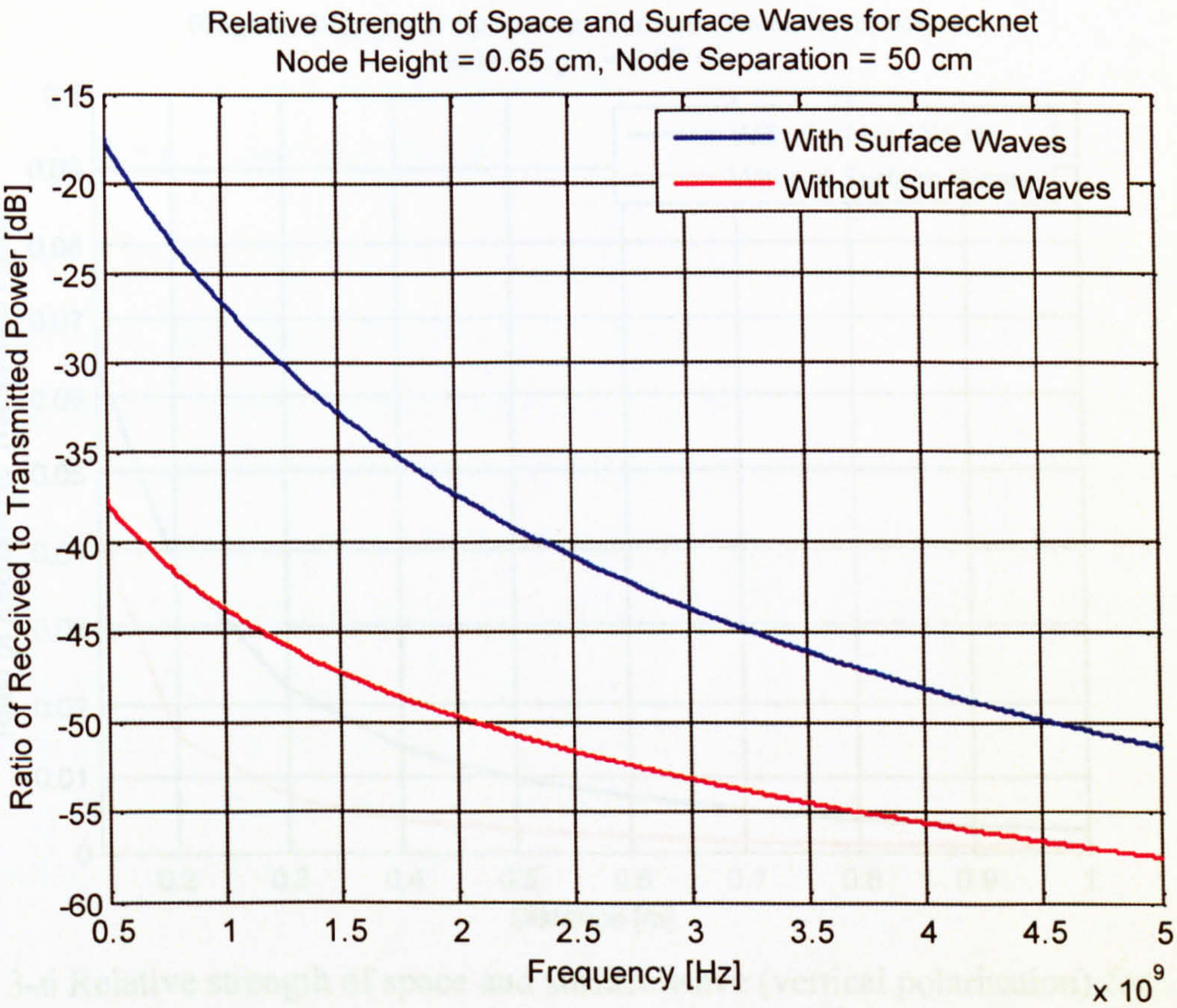

Fig. 3-5 Relative strength of space and surface wave (vertical polarisation) for increasing frequency

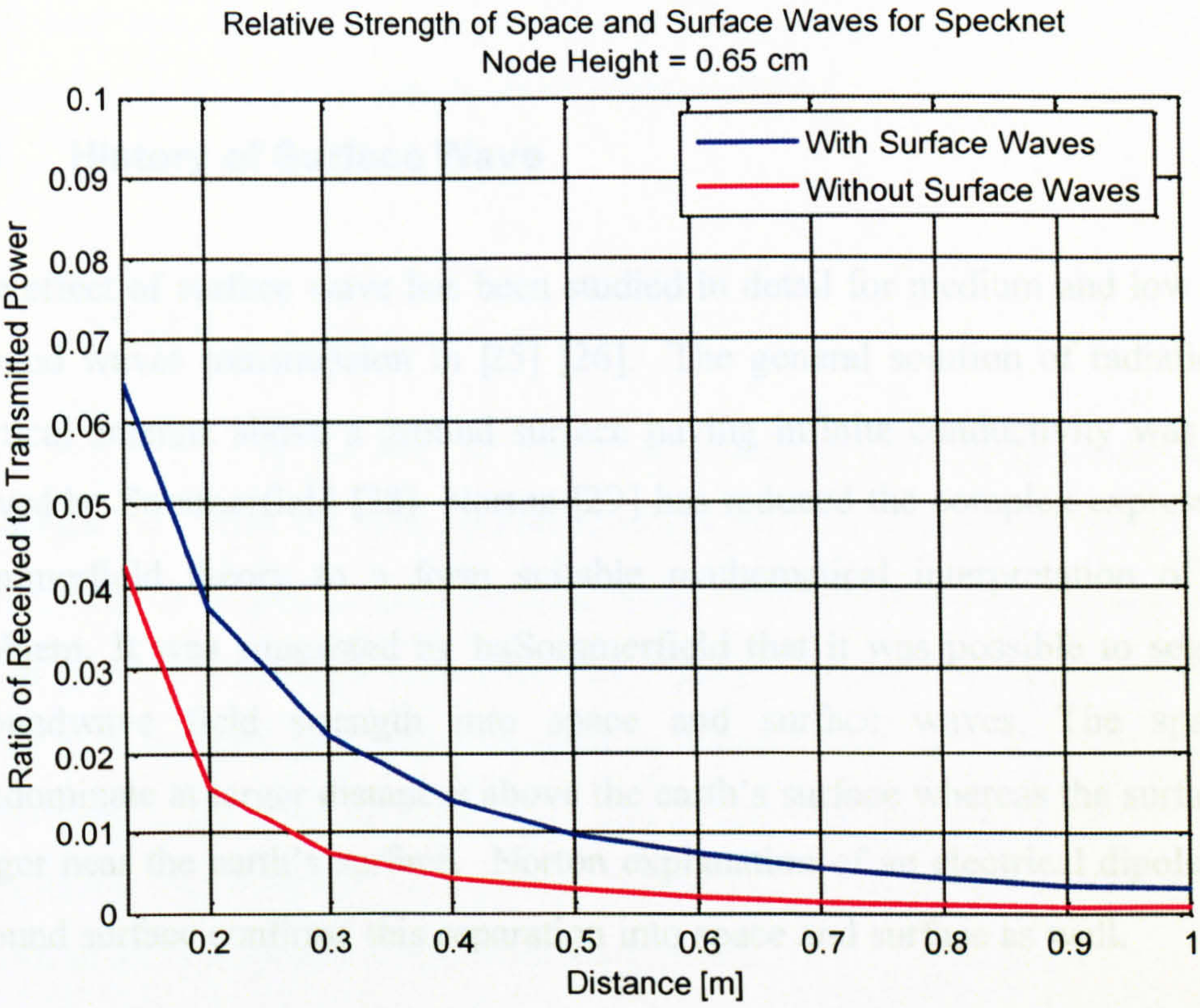

Fig. 3-6 Relative strength of space and surface wave (vertical polarisation) for increasing node separation

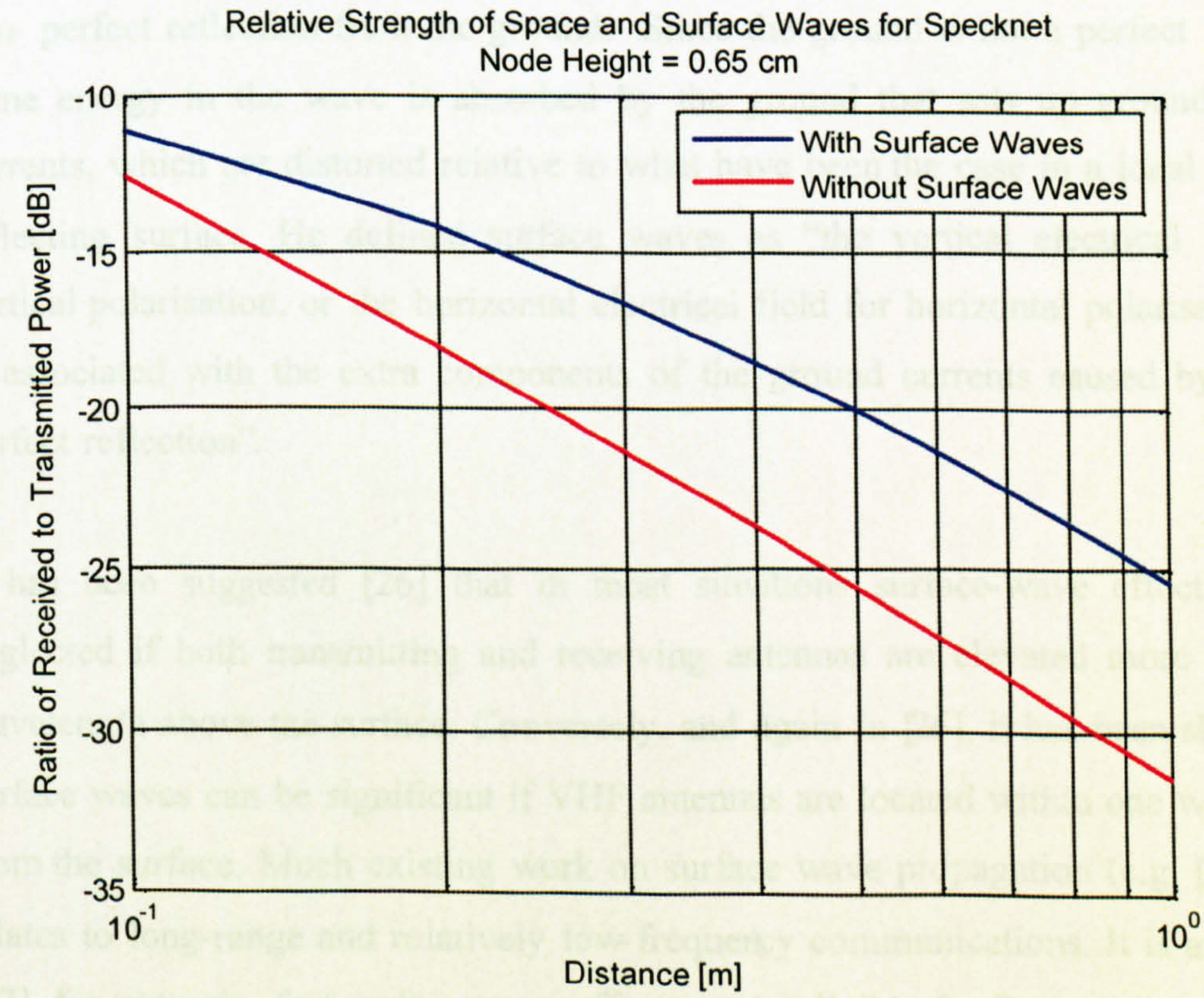

Fig. 3-7 Relative strength of space and surface wave (vertical polarisation) for increasing node separation

3.6 History of Surface Wave

The effect of surface wave has been studied in detail for medium and low frequency ground waves transmission in [25] [26]. The general solution of radiation from a vertical antenna above a ground surface having infinite conductivity was originally solved by Sommerfield [28]. Norton [29] has reduced the complex expression of the Sommerfield theory to a form suitable mathematical interpretation of the same problem. It was suggested by baSommerfield that it was possible to segregate the groundwave field strength into space and surface waves. The space waves predominate at larger distances above the earth's surface whereas the surface wave is larger near the earth's surface. Norton explanation of an electrical dipole above the ground surface confirms this separation into space and surface as well.

Bullington [26] analysed the effect of groundwave for both LOS and beyond horizon transmission. It was suggested by Bullington that the surface wave effect is due to non- perfect reflection from the ground. Since the ground is not a perfect reflector, some energy in the wave is absorbed by the ground that sets up ground surface currents, which are distorted relative to what have been the case in a ideal perfectly reflecting surface. He defined surface waves as "the vertical electrical field for vertical polarisation, or the horizontal electrical field for horizontal polarisation, that is associated with the extra components of the ground currents caused by lack of perfect reflection".

It has been suggested [26] that in most situations surface-wave effects can be neglected if both transmitting and receiving antennas are elevated more than one wavelength above the surface. Conversely, and again in [26], it has been shown that surface waves can be significant if VHF antennas are located within one wavelength from the surface. Much existing work on surface wave propagation (e.g. [25], [26]) relates to long-range and relatively low-frequency communications. It is asserted in [27], for example, that surface wave effects are negligible for frequencies above 100

MHz and can be ignored for horizontal and vertical polarisations provided the accuracies of the order of few decibels are acceptable.

3.7 Summary

The presence of a surface in close proximity to the communicating devices potentially modifies the propagation mechanisms. The concept of surface wave has been explored in great details for long range communication (in LF and VHF band) and is ignored in existing indoor wireless channel models [30]. Since future wireless nodes may be small and deployed close to a surface the surface waves may be quite significant. It has been observed [31] that surface are significant for short links and significant improvement in received power can be achieved if the antennas are placed at an appropriate height from the ground.

Chapter 4

4 Polarisation Loss in Wireless Links

4.1 Introduction

In a typical wireless communication (fixed or portable) system a linearly polarised antenna is used at the base station and the end user. The antenna at the user's end may be oriented such that they are not physical aligned with the base station. The misalignment of antenna polarisation results in polarisation loss.

Multipath reflection is a common phenomenon in wireless links, where a multitude of reflected signals arrives at the receiver after reflection from the ground or scattering objects. The reflected signal may undergo a polarisation change depending on the physical orientation of the reflecting obstruction. This suggest that even if a communication system is equipped with identical transmit and receive antennas having same polarisation sense and axial ratio, the incident wave on the receiving antenna have become cross-polarised thus resulting in polarisation mismatch loss.

To transfer maximum power between transmit and receive antenna (ignoring any cross-polarisation loss due to medium), both antennas must have the same spatial orientation, polarisation sense and axial ratio [32].

4.2 Antenna Polarisation

The polarisation of a wave transmitted from an antenna is defined by the motion of the tip of the instantaneous electric field vector with time at a fixed point in space [33]. In general electromagnetic waves are elliptically polarised. The electric field can be decomposed into two orthogonal linear components (with different phase and

magnitude) horizontal component E_H and vertical component E_V, Fig 4-1. The total electric field E, is the vector sum of E_H and E_V [32].

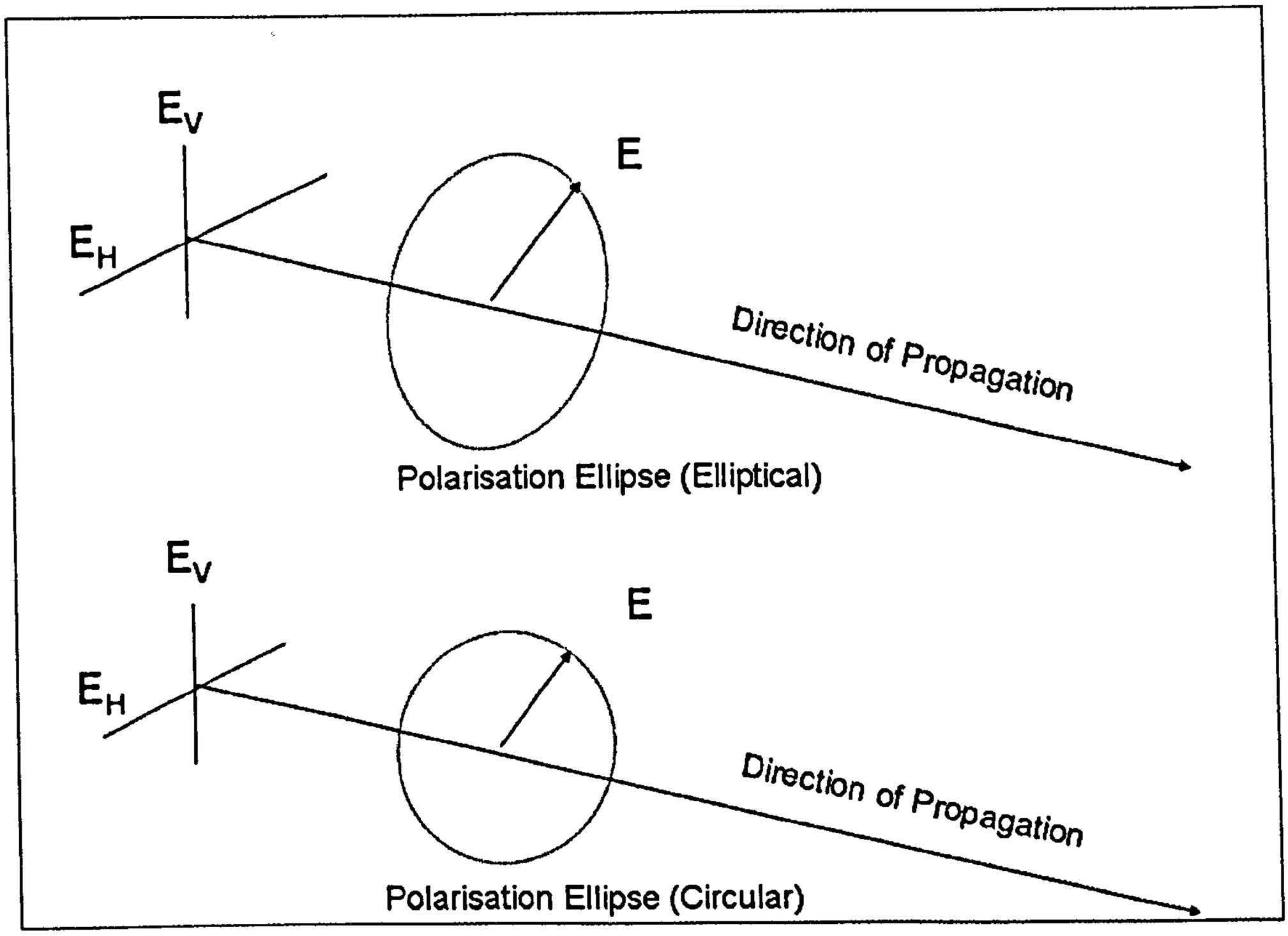

Fig. 4-1 Polarisation state of a wave

Elliptically polarised waves can also be resolved in to two circular polarisations. In a circularly polarized wave, the electrical field vector with constant magnitude complete one revolution during one period of the wave. If the rotation is clockwise looking in the direction of propagation, the sense is said to be hand leading to right-hand circular polarisation (RHCP). If the rotation is anti-counter clockwise, the sense is said to be left hand leading to left hand circularly polarisation (LHCP). The two linearly polarised components of a circular polarised wave have equal amplitude and are in phase quadrature. A linearly polarised wave from an antenna may be composed of single electric field component (either vertical or horizontal as in Fig. 4-2) or the combination of two with a phase difference 0^o.

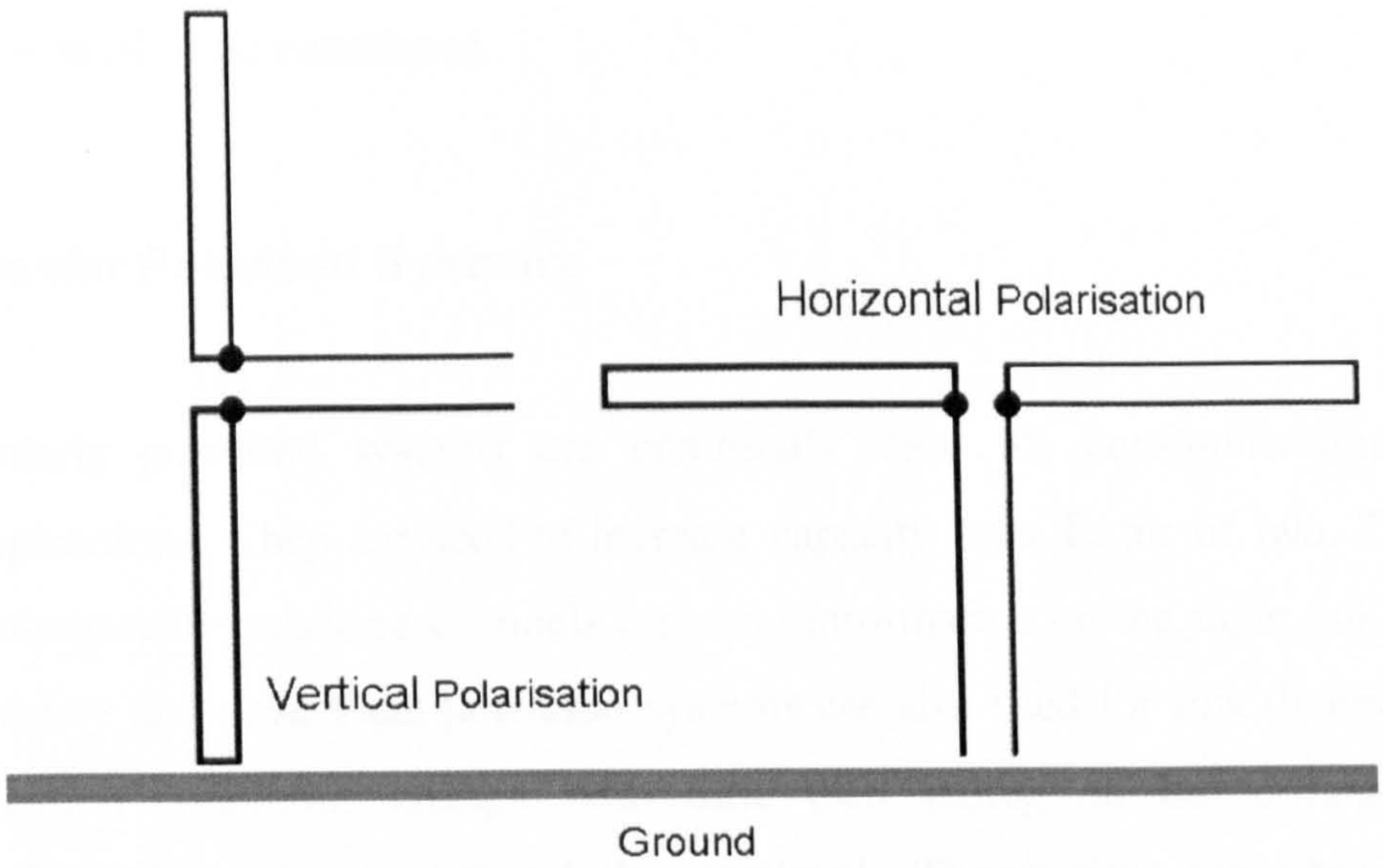

Fig. 4-2 Linearly polarised wave

An antenna is said to be horizontally polarized when its electric field is parallel to the ground. Vertically polarized antennas nominally have their electric field perpendicular to the ground (e.g. Fig. 4-2). If the transmitted electric field is from a linear polarised antenna that is vertically polarised and is received by an antenna having horizontal polarisation then the polarisation mismatch loss is maximum. In a linearly polarized system, a polarisation misalignment of 45^{o} will degrade the signal by 3 dB and if the antennas are misaligned by 90^{o} the attenuation is infinity in theory and can be more than 20 dB [32]) in practice. In a wireless sensor network where the sensing nodes are randomly deployed and could have any arbitrary (random) orientation, linear polarisation is not the best solution.

The polarisation of an ideally circularly polarised antenna radiation is unchanged with changes in antenna orientation. Note, however, that an ideally circularly polarised antenna (in all θ,ϕ) directions may be difficult to realise in practice. For

randomly oriented nodes circular polarisation may therefore be advantageous. In practice cross-polarisation occurring during propagation between transmitter and receiver may need to be considered.

4.3 Circular Polarised Systems

Dual circularly polarised systems are commonly used for communication and sensing applications. They are used to increase capacity by a factor of two. This is because orthogonally polarised channels can send information on the same link at the same frequency and time. Dual polarised systems are also used for link diversity. If the propagation conditions change with time then fading on the orthogonally polarised channel is often less than fully correlated. The receiver can choose the strongest channel i.e. either vertical or horizontal polarised channel. This phenomenon is called polarisation diversity.

Wireless sensor networks could be designed as dual polarised in order to achieve link diversity and capacity improvement. Sensing nodes in future are likely to be deployed randomly (in both location and orientation) over surfaces. This could result in random orientation of specks with respect to each other. To ensure that the link between any two nodes is polarisation matched it is proposed that the specks should use circularly polarised antennas.

4.4 Polarisation Loss in Wireless Channel

The polarisation mismatch in a wireless channel is the result of two effects (i) polarisation mismatch between transmit and receive antennas and (ii) polarisation change due to the medium (commonly referred as cross polarisation).

The polarisation mismatch loss due to the antennas depends on two factors (i) the physical design of the antenna (i.e. the axial ratio and tilt angle as a function of θ,ϕ and (ii) the orientation of the antennas with respect of each other (i.e. the value of

θ,ϕ for transmit and receive antenna). In a fixed circularly polarised system (e.g. a satellite link) the polarisation loss due to the alignment of antenna can be minimized by judicially aligning both transmit and receive antenna's bore-sight axes. The alignment loss can also be minimized by a good antenna design i.e. in a pure circular polarised antenna the loss due to the miss alignment of antenna major axis is negligible (neglecting any cross-polarisation due to medium).

The polarisation loss due to the medium depends on a number of physical and design parameters i.e. the size of the sensor, link length (that affects the grazing angle), frequency of operation and the electrical properties of the medium (i.e. permittivity, permeability and conductivity). A cross-polarising medium will change incident circular polarised wave into an elliptical polarised wave, a fraction of the power being coupled into the cross-polarised component. The polarisation loss then depends on the axial ratio of the incident wave on the circular polarised receiving antenna.

4.5 Existing Wireless Channel Models

Polarisation loss in wireless channels has been mostly considered for long links (e.g. satellite systems) [34] [35] [36]. For short wireless links polarisation loss has been mostly ignored in existing wireless simulators (e.g. Castlia [37] [38]).

It has been proposed in the subsequent study (chapter 8) that the polarisation loss should be considered if the accuracies of the order few decibels are required in link budget.

4.6 Summary

Future wireless sensing nodes will be small and will be deployed randomly and close to the ground or other surfaces. The polarisation loss experienced by a wireless node is affected by antenna design (e.g. axial ratio and tile angle) and the alignment of major axis of the transmit and receive antennas. Also the presence of the ground cross polarises the reflected wave thus changing the ellipticity of the received wave.

Chapter 5

5. Channel Modelling for Specknet

5.1 Introduction

A characterization of the short range (<10cm) narrowband wireless channel, appropriate to a dense network of wireless transceivers operating in the 2.4 GHz ISM band, is presented. Transmission loss measurements have been made in the laboratory using rectaxial antennas at 2.45 GHz and a fading model derived.

Since specks are small and will be operating at short wireless ranges (≈ 10 cm) a channel model is required to inform the design of the physical layer protocols governing communications between them. This chapter proposes such a model. The model is generic in nature and could, with appropriate selection of parameters, be applied to other, similar, short-range wireless networks operating in the 2.45 GHz ISM band.

5.2 Proposed Channel Model

A broadband channel model is required only when the delay spread of the channel is a significant fraction of the symbol duration. The proposed specknet symbol rate is 200 kbaud [39] corresponding to a symbol period of 5μs. Multiple propagation paths with relative delay greater than approximately 0.5μs might therefore result in sufficient pulse spreading to cause inter-symbol interference (ISI). An excess delay of 0.5μs corresponds to maximum excess path length of 150 m. The ratio of transmission loss for a 10 cm path - assumed to be the maximum line-of-sight (LOS) link length - and a 150 m path (arising from a lossless plane reflection in otherwise free space) is 63.5 dB as in Fig. 5-1. This suggests that paths with delay sufficient to

cause ISI will result in negligible received power. The channel can therefore be modelled as narrowband and subject only to flat fading [40].

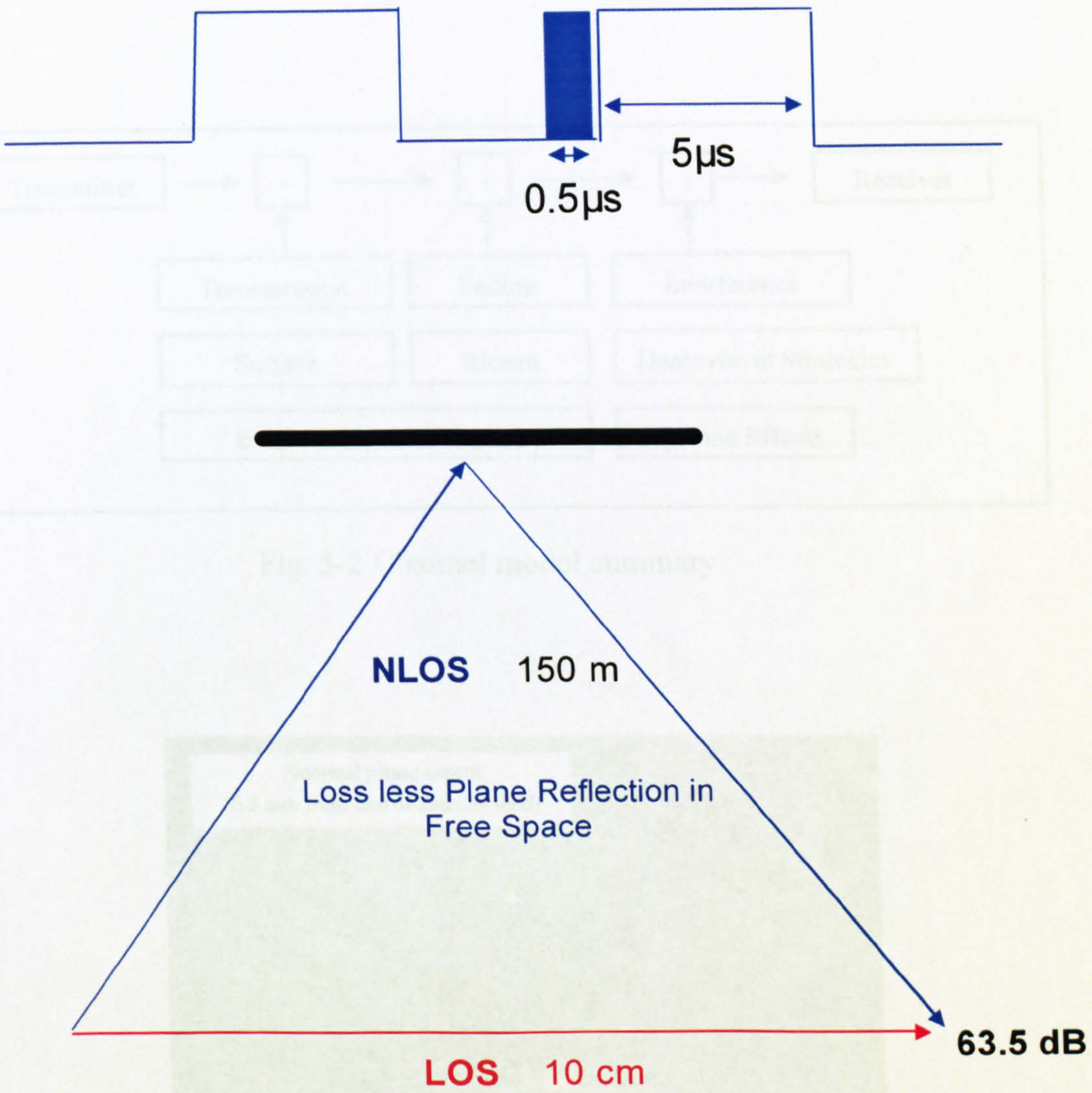

Fig. 5-1 Specknet data rate with corresponding delay path

Fig. 5-2 is a block diagram representation of such a channel. The dependence of path loss on distance has been established, empirically, from propagation measurements made over two different plane surfaces. The fading model adopted is a best-fit Ricean distribution derived from many independent measurements for several (constant) path lengths. The noise and interference due to the neighbouring nodes depends on the deployment of these nodes, i.e. on their spatial distribution, antenna

patterns and orientation. The effect of interference due to neighbouring nodes has been considered in Chapter 6.

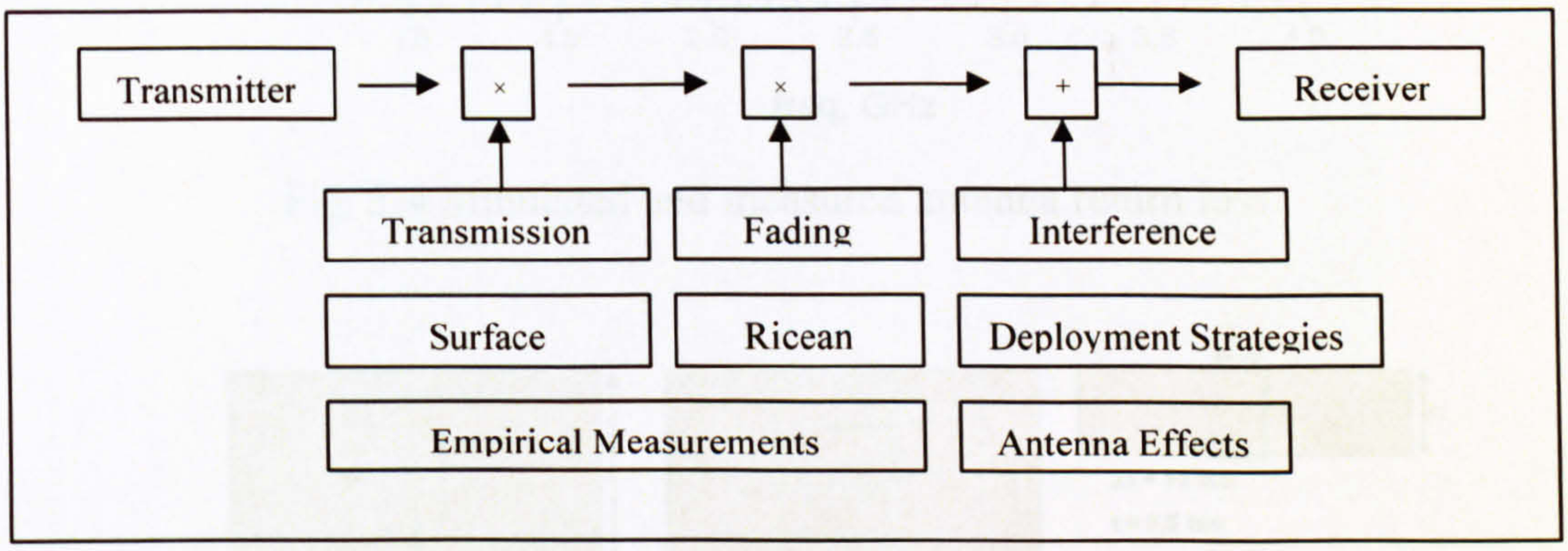

Fig. 5-2 Channel model summary

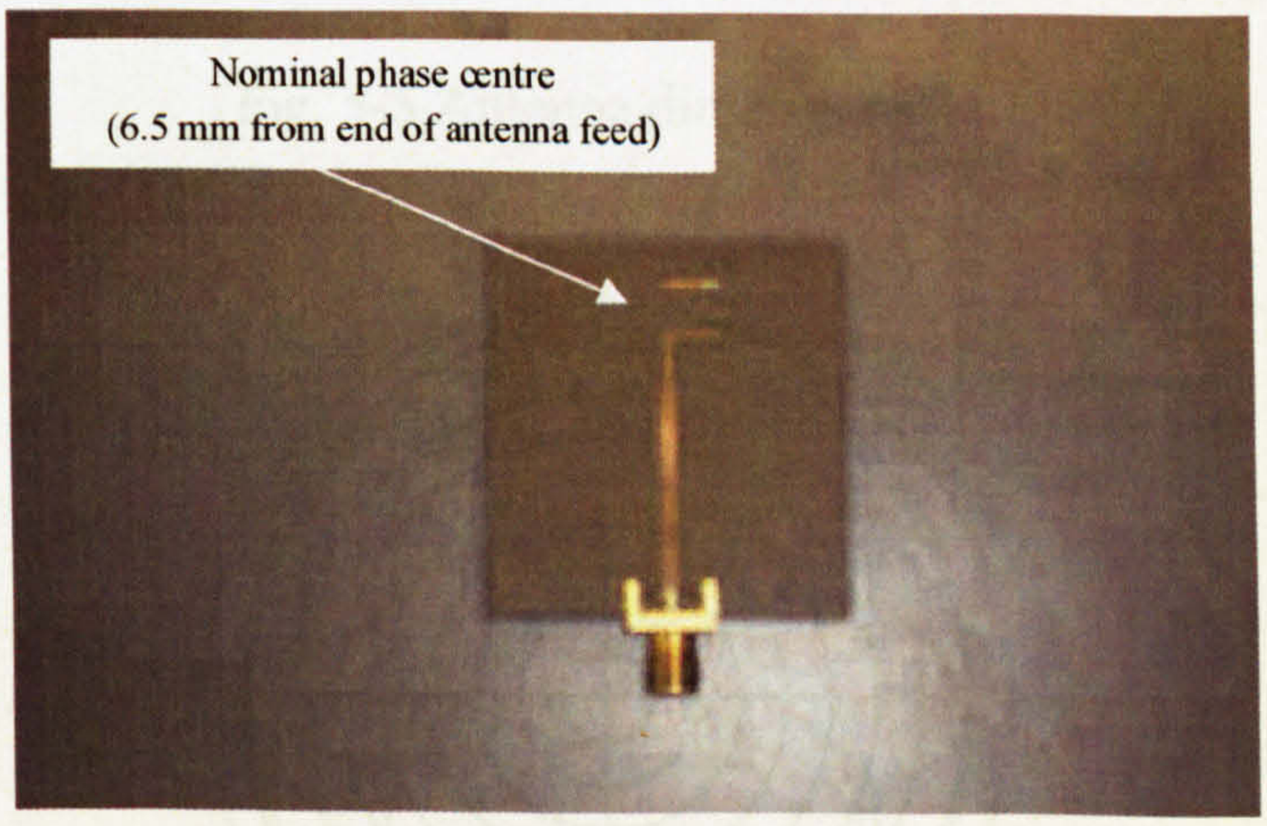

Fig. 5-3 Rectaxial antenna

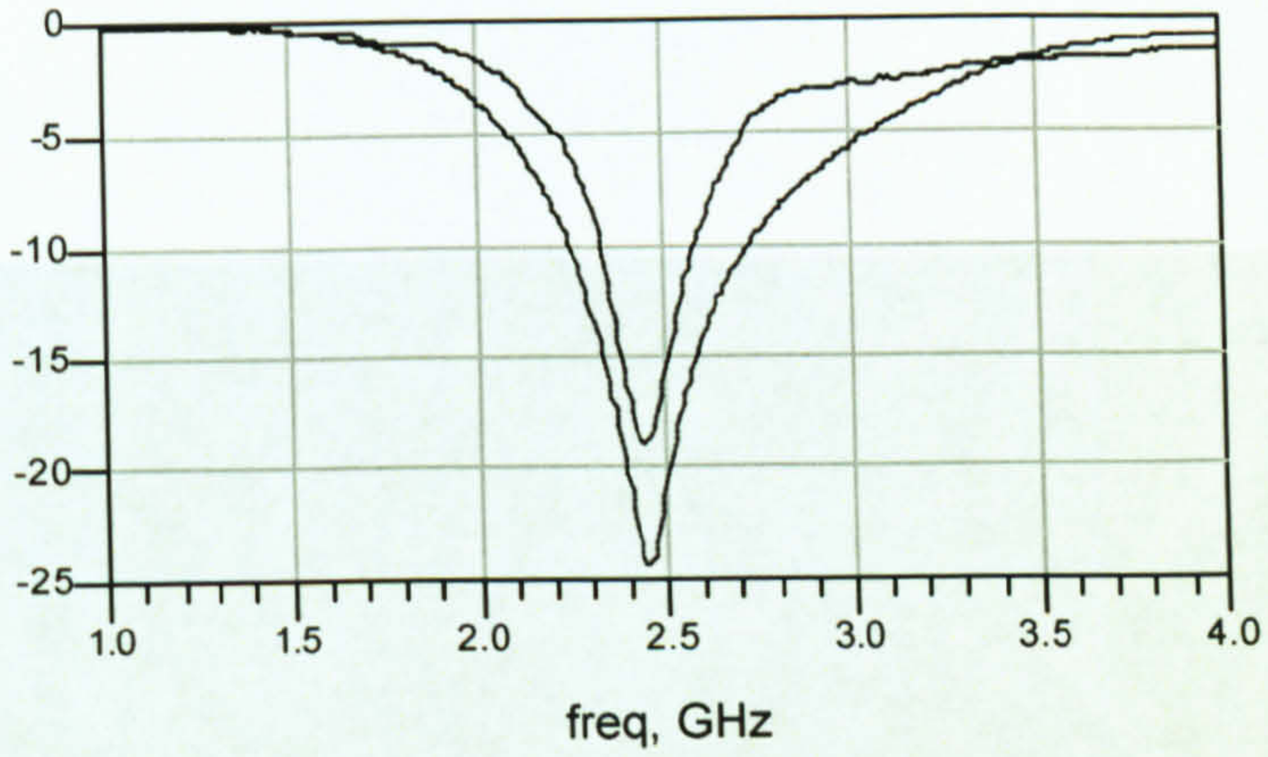

Fig. 5-4 Simulated and measured antenna return loss

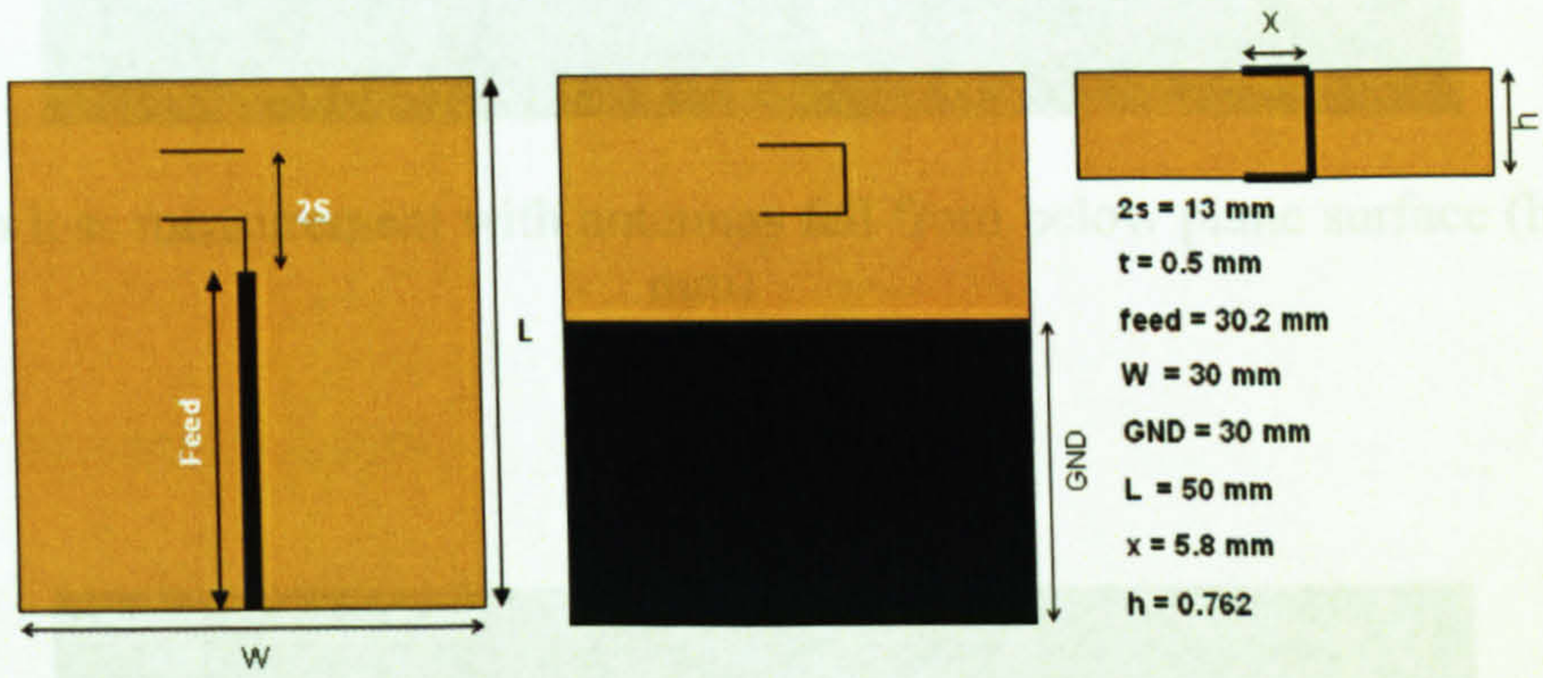

Fig. 5-5 Antenna dimensions

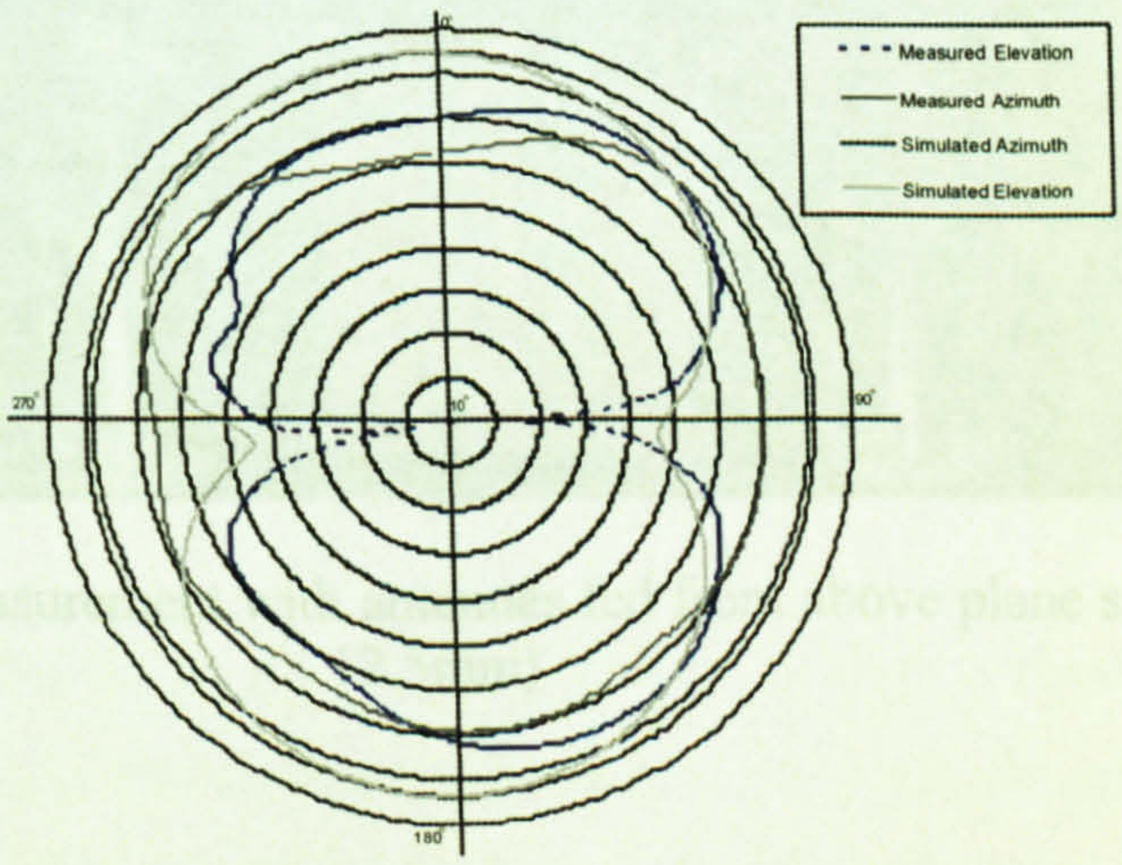

Fig. 5-6 Simulated and measured radiation patterns

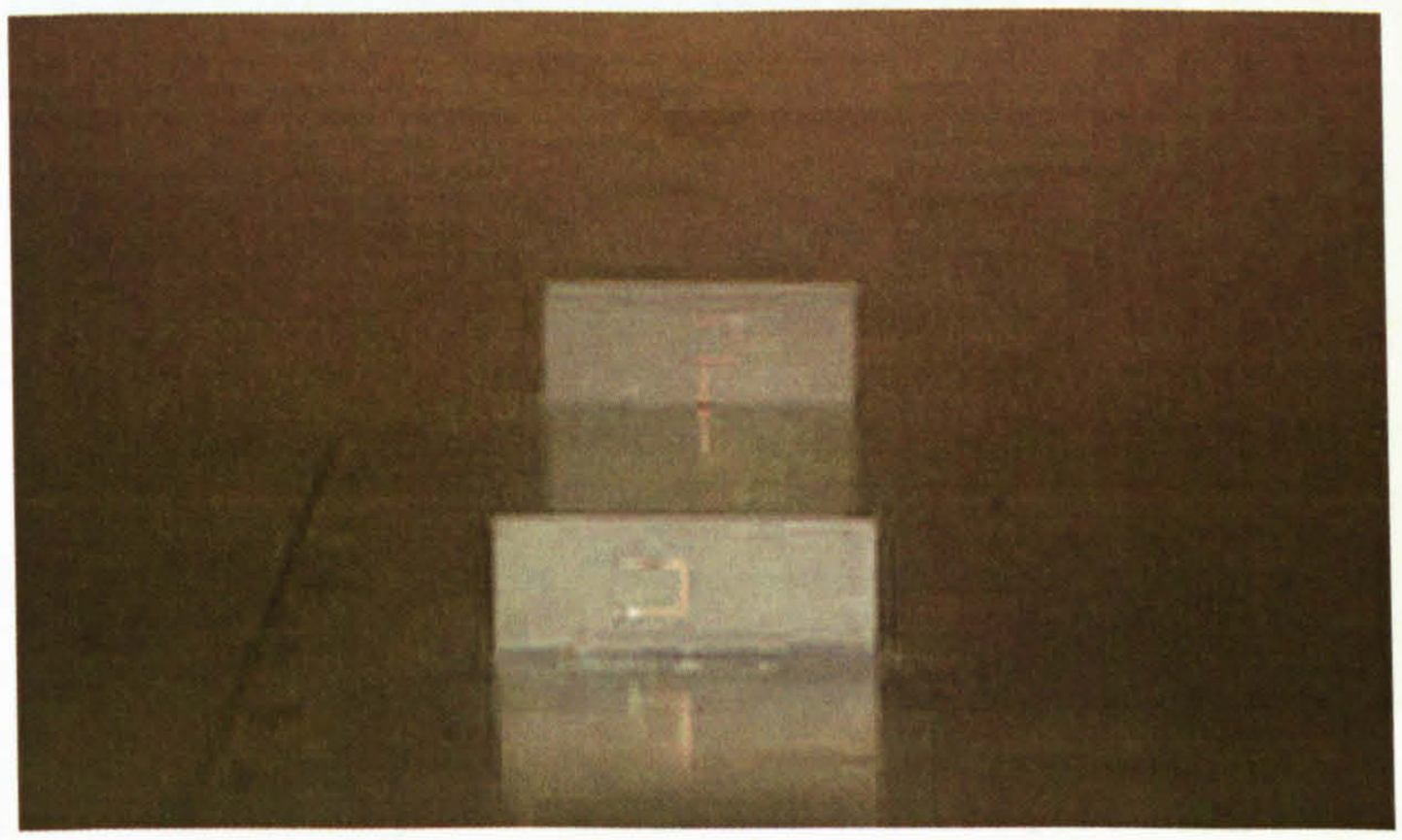

Fig. 5-7 Path loss measurement with antennas fed from below plane surface (h = 6.5 mm)

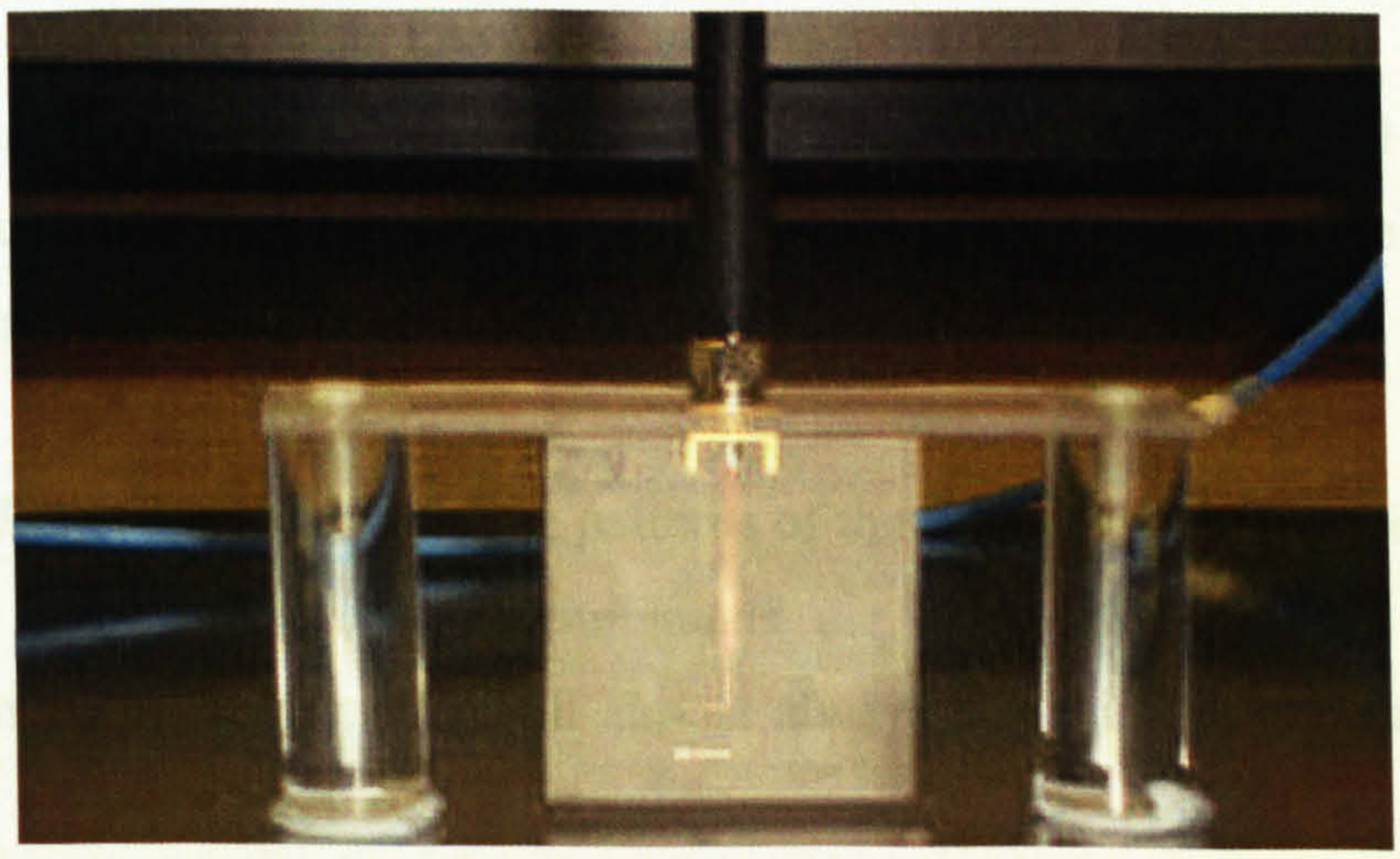

Fig. 5-8 Path loss measurement with antennas fed from above plane surface (h = 12.5mm)

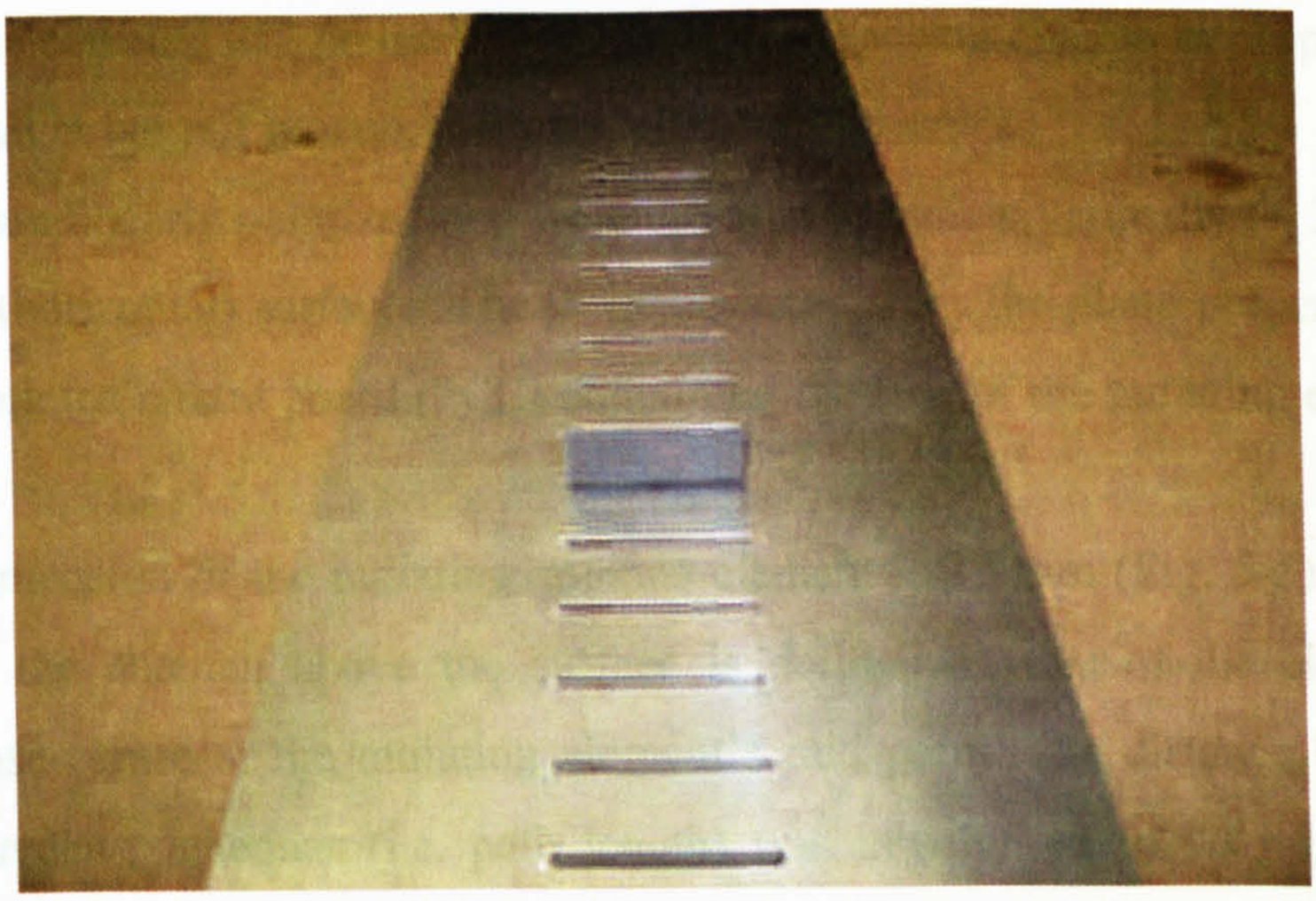

Fig. 5-9 Aluminium plane surface with reduced (155 mm) width

5.2.1 Transmission Loss

Measurements of transmission loss have been made at 2.45 GHz using a pair of identical rectaxial antennas [41], Fig. 5-3. The transmitted signal was an unmodulated carrier. The return loss of the antenna, measured using a network analyzer, is better than 15 dB between 2.40 and 2.50 GHz, Fig. 5-4.

The physical dimensions and radiation patterns of the antennas are shown in Fig. 5-5 and 5-6. All transmission loss measurements are line-of-sight (LOS) since the deployment and density of specks will almost always result in this condition being satisfied.

A test-bench was constructed to make measurements over two plane surfaces. A good conductor (surface A) was represented by a 1m×1m×1mm aluminium sheet. A poor conductor (surface B) was represented by a 1m×1m×10mm medium density fibre (MDF) sheet. (MDF is a building material made from wood fibre and resin.) Slots (3mm× 40mm) were cut into both surfaces allowing the antennas to be fed from below, Fig. 5-7. (The slots were necessary in order to locate the antennas phase centre sufficient close to the surface. This does mean, however, that any longitudinal

currents surface currents will be interrupted with a consequent change in propagation fields. It is thought but not proven, that this effect will be small.)
The antennas are linearly polarized and were oriented to radiate vertically (± 2°) with respect to the (horizontal) surface. The 0^o is measured from the plane perpendicular to that of the printed circuit board (PCB) containing the feed of the radiating element.

The largest dimension of the radiating antenna element is 13 mm (Fig. 5-5) and the height (h) of the antenna above the surface is defined as that of the element's (nominal) phase-centre at the radiating element's mid-point. The distance between transmit and receive antennas (i.e. path length) was initially set to 20 mm, i.e. at (approximately) the radian sphere radius. (The conventional calculation of far-field distance for this antenna is 2.8 mm but since the antenna is electrically small this estimate is erroneous.) The antenna heights were set to 6.5 mm putting the conventionally-calculated farthest point of constructive interference at a range of 1.3 mm from the transmitting antenna. (Being inside the radian sphere this calculation is, like the previous far-field calculation, not really appropriate. It conclusively excludes, however, the possibility of conventional interference fringes.) Path length was then increased in steps of 20 mm up to a maximum distance of 300 mm (2.5 wavelengths) and received power recorded at each step. Path length, antenna heights and power were measured with accuracies better than ±1 mm, ±0.5 mm and ±1 nW, respectively.

A second series of measurements was made with the antenna height increased to 12.5 mm. (A third series of measurements was made with transmit and receive antennas at a height of 12.5 mm but fed from above the surface rather than from below it, Fig. 5-8.)

Transmission loss (L) was plotted in decibels against link length (R) on a logarithmic scale (e.g. Fig. 5-10). The data is well-represented by a three-segment piecewise-linear curve of the form given in Equation (5.1) where K is a constant, R_1 is the first break point (and the path-length for which $L = K$), R_2 is the second break point (and the path-length for which $L = K+10n_2\log_{10}(R_2/R_1)$) and n_i is the path-loss index determining the slope of the ith curve-segment. Figs. 5-10 – 5-17 show the experimental data and resulting segmented curves.

Table 5-1 contains the corresponding values of K, R_1, R_2 and n_i. The middle-segment line (corresponding to n_2) is a minimum mean square error (MMSE) fit. The first- and last-segment lines (corresponding to n_1 and n_3) are determined subjectively since there are generally too few data points to justify a more objective MMSE calculation (the validity of establishing a linear curve segment on only two points as is the case for segment 1 and 2 could be questioned. It is noted, however that (i) each point represents the mean of five spatially independent measurements and (ii) the relative gradient of the segments 1 and 2 are similar in all Fig. 5-10 through Fig. 5-17. Our interpretation is that this represents convincing evidence that the fitted curves reflect genuine physical phenomenon).

The piecewise linear nature of the transmission loss versus distance curves appears to reflect the underlying data, i.e. the data points reflect underlying linear segments rather than a single smooth curve to which an arbitrary number of straight line segments have been fit. This is suggestive of three distinct propagation mechanisms, each of which dominates at different distance ranges.

An objection might be raised, however, to fitting a linear segment to the two data points representing shortest path length. The generic point here could be expressed by the question 'can two points be used to infer a trend?' It is clear that two points in isolation on a graph cannot be used to infer the curvature or, strictly, even the continuity of an underlying function. In this case there are compelling physical arguments for the continuity of the field strength-distance relationship. (It is physically implausible for the relationship to be otherwise.) Furthermore, since the free-space field due to a dipole is the sum of inverse power laws ($1/r^3$ for the quasi-static field, $1/r^2$ for the induction field and $1/r$ for the radiation field) and since the field due to surface waves also decays as an inverse power law (with decay index dependent on surface ohmic losses), then we argue that it is likely that the relationship at all distances is given by a power law, thus justifying the use of straight lines for each piecewise linear segment. (If this argument is found unconvincing then, in the absence of any evidence to the contrary, a least complexity

argument favours the assumption of a straight line fit; if there is no evidence for either positive or negative curvature then zero curvature is surely the most rational assumption.)

A residual uncertainty remains, however, in that (accepting either of the above arguments) a choice must be made as to the breakpoint between the first and second linear segments. The breakpoint here has been chosen (perhaps arbitrarily) to coincide with the second data point. This has the effect of maximising the gradient of the first segment. (Choosing the break point somewhere between the first two points obviously extends the length of the second line segment and reduces the gradient of the first line segment. Strictly speaking then, it can be argued that the gradient of this first segment can only be determined as lying between zero and the value that has been adopted. (The author is grateful to one of his examiners for pointing this out.)

$$L_{(dB)} = \begin{cases} k + 10n_1 \log_{10}\left(\frac{R}{R_1}\right), & \text{for } R \leq R_1 \\ k + 10n_2 \log_{10}\left(\frac{R}{R_1}\right), & \text{for } R_1 \leq R \leq R_2 \\ k + 10n_2 \log_{10}\left(\frac{R_2}{R_1}\right) + 10n_3 \log_{10}\left(\frac{R}{R_2}\right), & \text{for } R \geq R_2 \end{cases} \qquad (5.1)$$

,

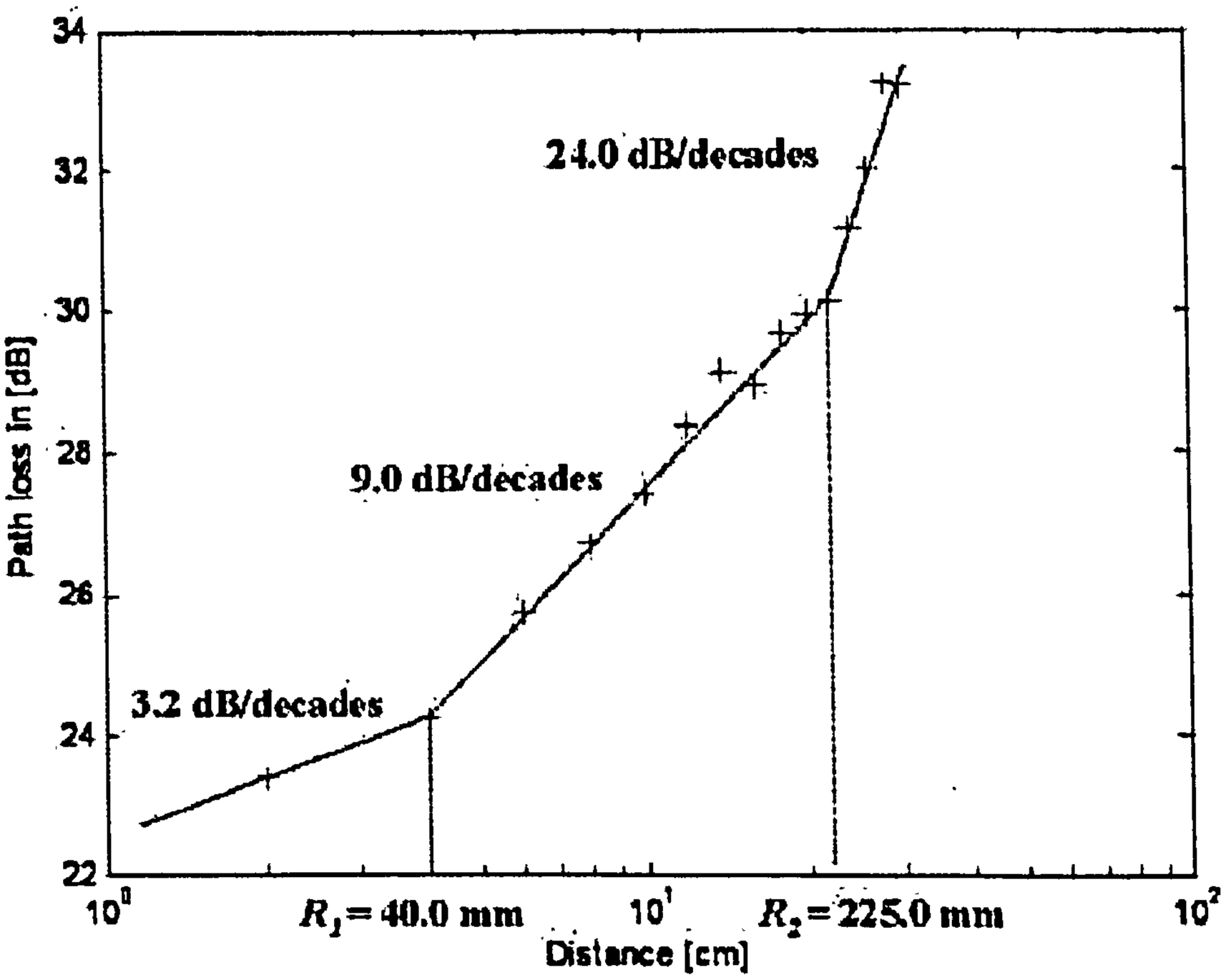

Fig. 5-10 Transmission losses (aluminium surface, 1m×1m×1mm, h = 6.5 mm)

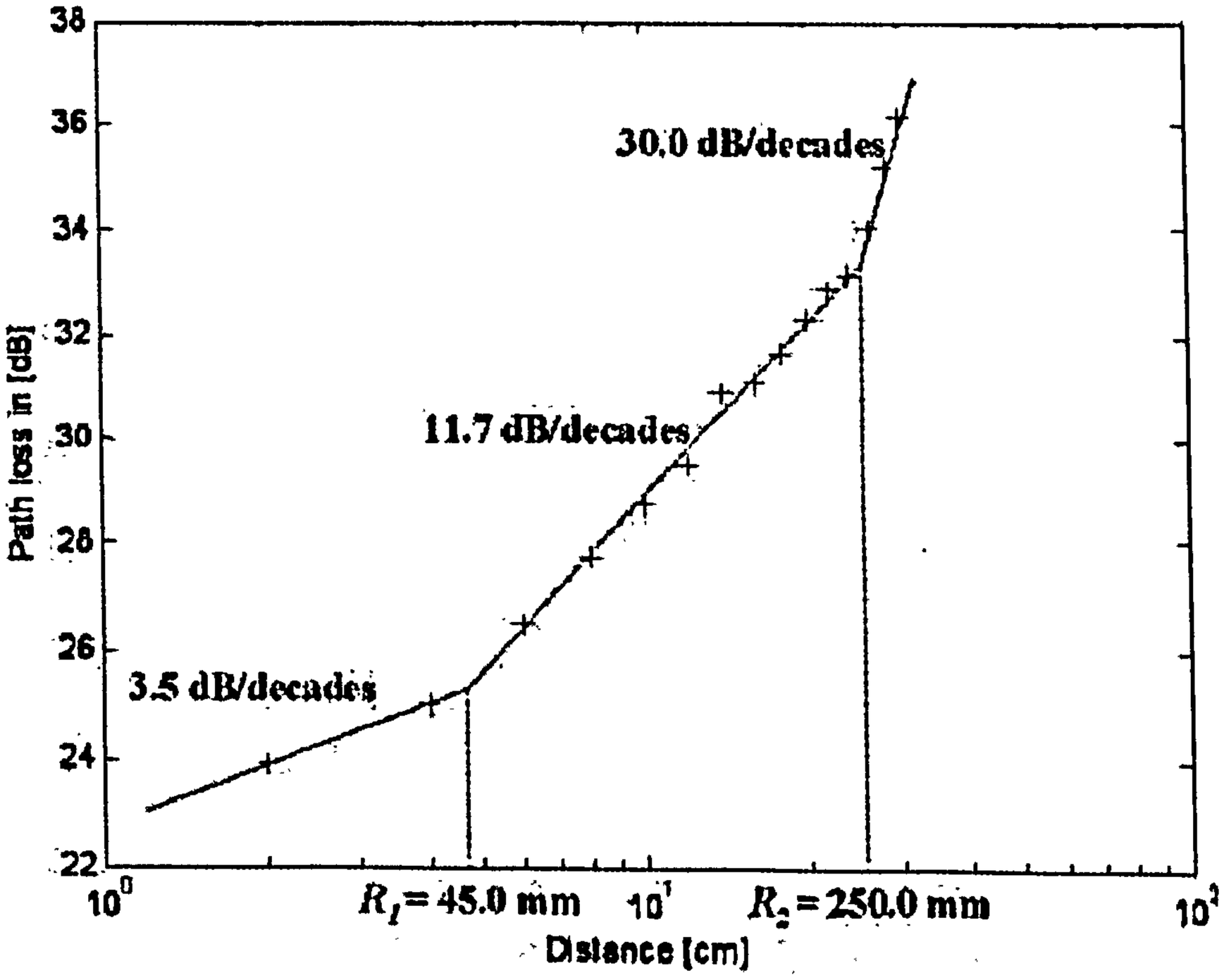

Fig. 5-11 Transmission loss (aluminium surface, 1m×1m×1mm, h = 12.5 mm)

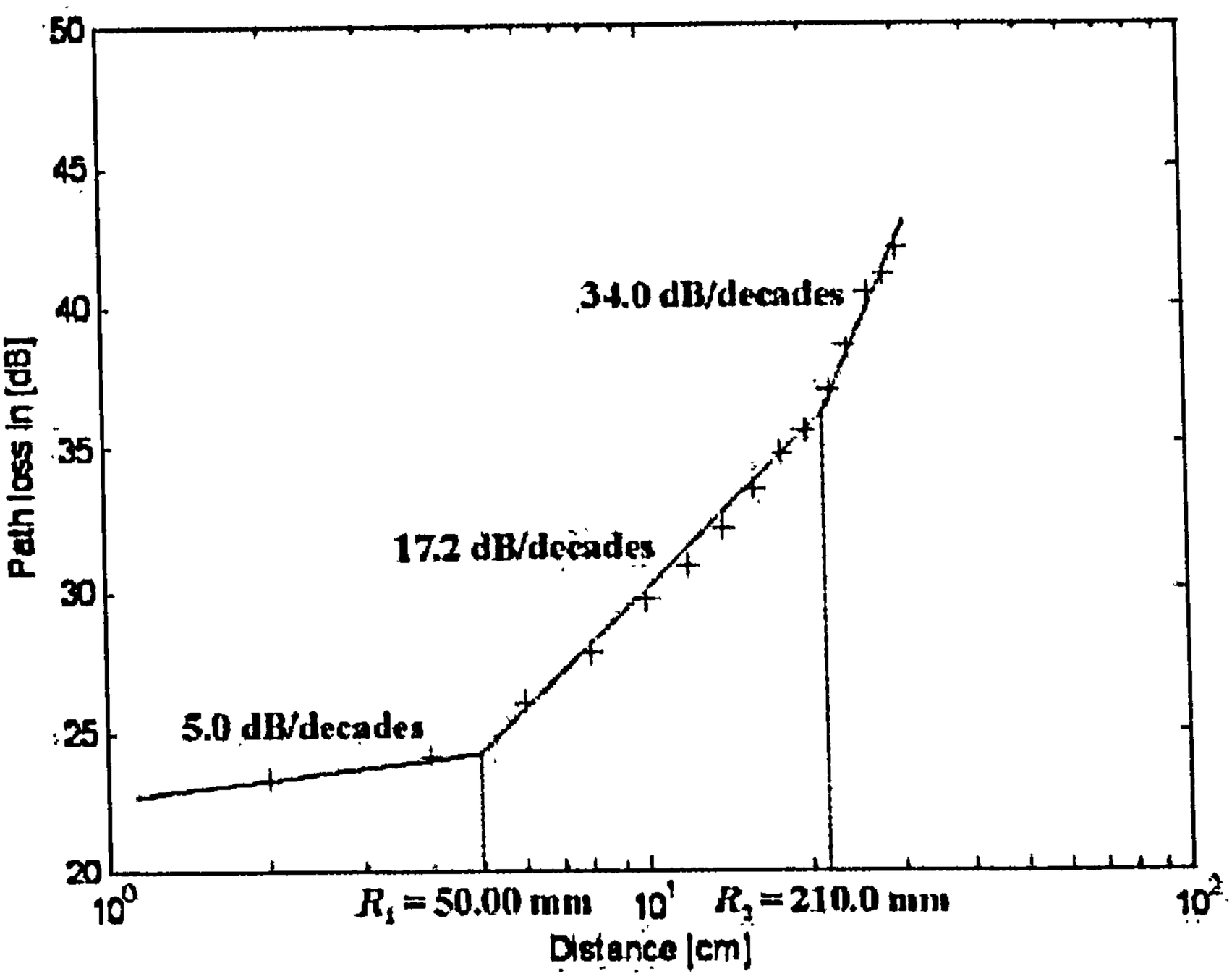

Fig. 5-12 Transmission loss versus distance (MDF surface, 1m×1m×10mm, h = 6.5 mm)

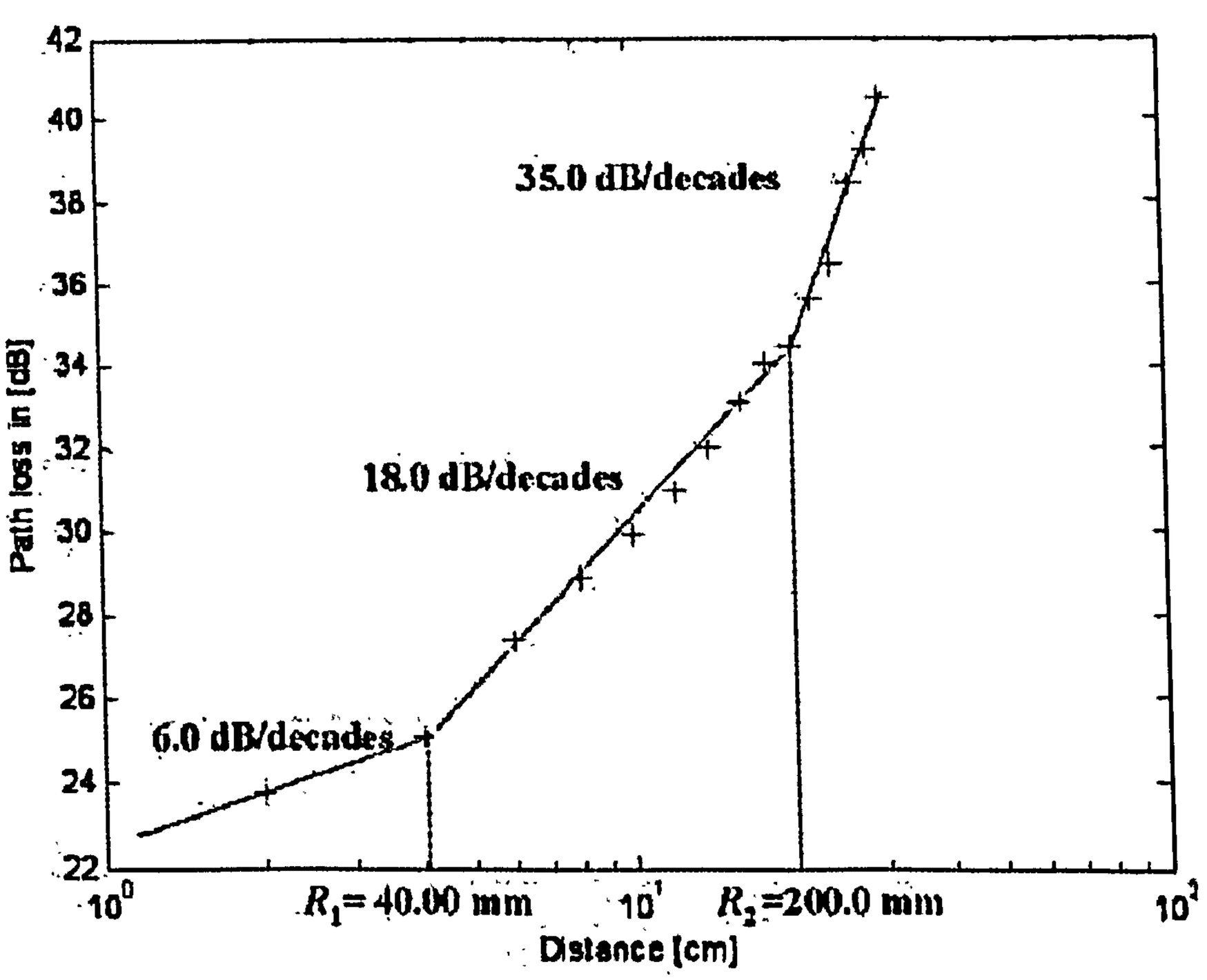

Fig. 5-13 Transmission loss versus distance (MDF surface, 1m×1m×10mm, h =12.5 mm)

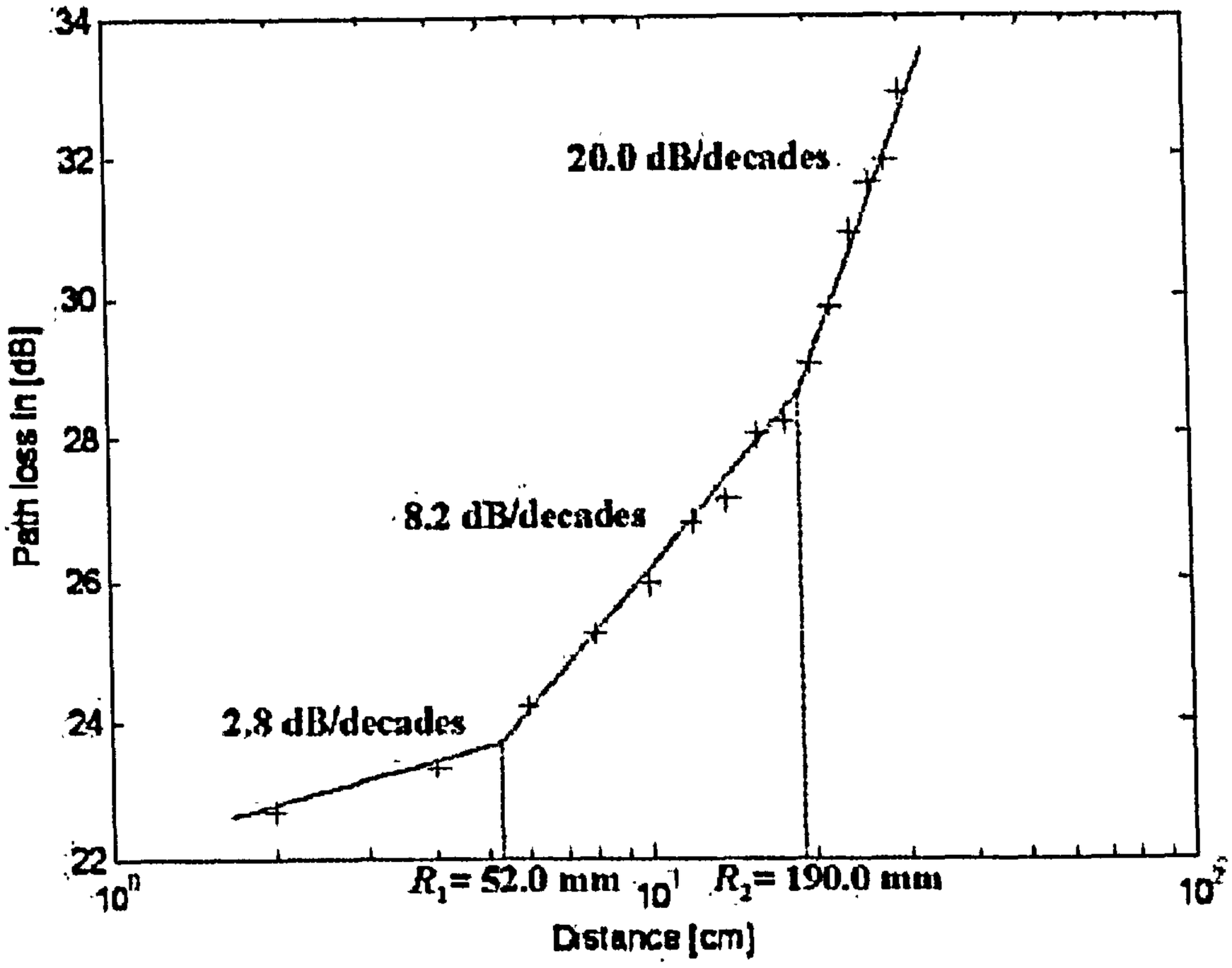

Fig. 5-14 Transmission loss versus (aluminium surface, 1m×0.155m×1mm, h = 6.5 mm)

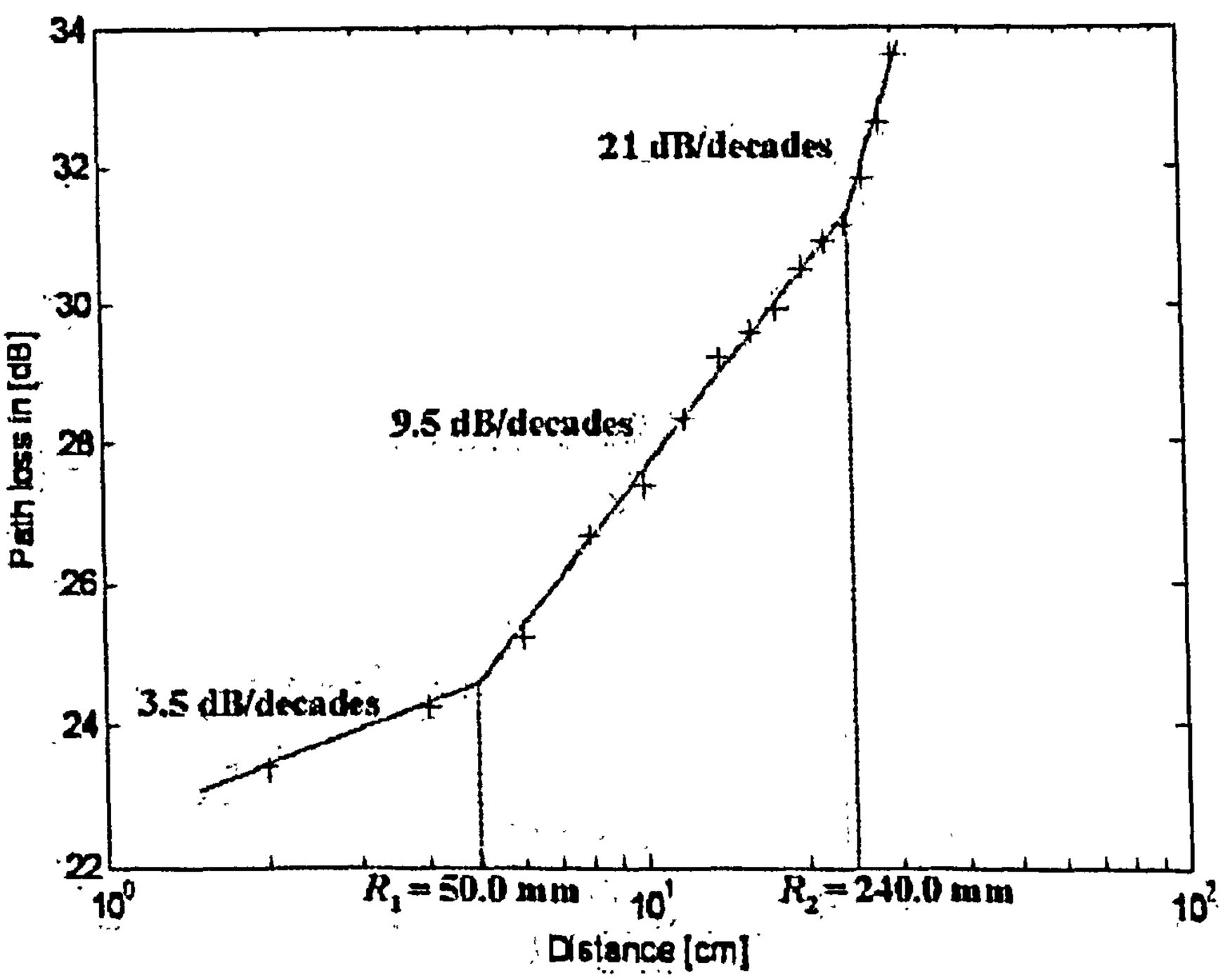

Fig. 5-15 Transmission loss (aluminium surface, 1m×0.155m×1mm, h = 12.5 mm)

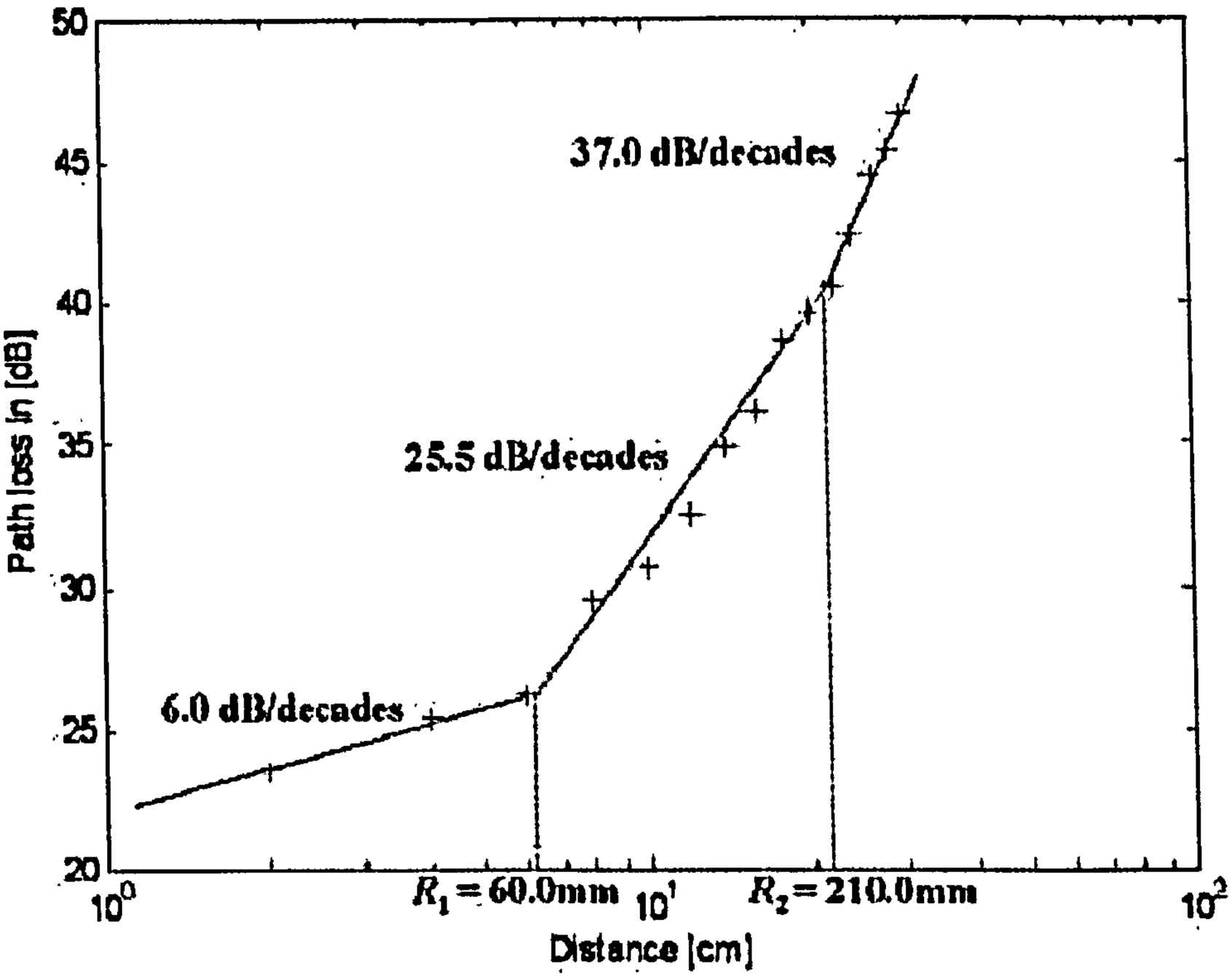

Fig. 5-16 Transmission loss verses distance with antennas fed from above (aluminium surface, 1m×1m×1mm, h = 12.5mm)

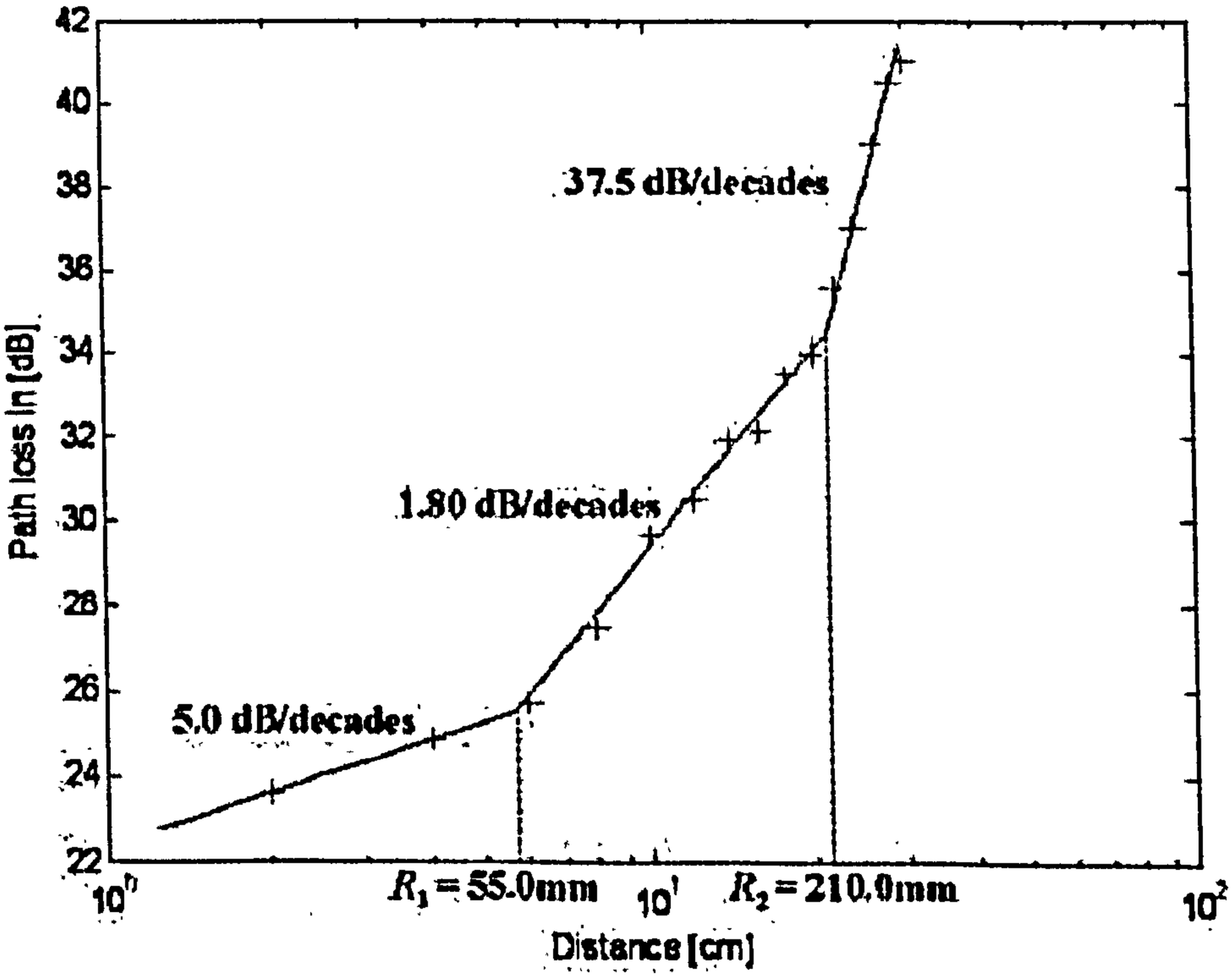

Fig. 5-17 Transmission loss versus distance with antennas fed from above (MDF surface, 1m× 1m×10mm, h = 12.5mm)

Material	h (mm)	K (dB)	n_1	n_2	n_3	R_1 (mm)	R_2 (mm)
Al	6.5	24.26	0.32	0.90	2.4	40.0	225.0
Al	12.5	24.80	0.35	1.17	3.0	45.0	250.0
MDF	6.5	24.30	0.50	1.72	3.4	50.0	210.0
MDF	12.5	25.10	0.60	1.80	3.5	40.0	200.0

Table 5-1 Intercept and path loss indices (Surface a and b, dimension 1m × 1m)

Material	h (mm)	K (dB)	n_1	n_2	n_3	R_1 (mm)	R_2 (mm)
Al	6.5	23.4	0.28	0.82	2.0	52.0	190.0
Al	12.5	24.2	0.35	0.95	2.1	50.0	240.0

Table 5-2 Intercept and path loss indices (Surface c, dimensions 1m×155mm)

Material	H (mm)	K (dB)	n_1	n_2	n_3	R_1 (mm)	R_2 (mm)
Al	12.5	25.9	0.60	2.55	3.70	60.0	210.0
MDF	12.5	24.9	0.50	1.80	3.75	55.0	210.0

Table 5-3 Intercept and path loss indices (Surface a and b, dimensions 1m×1m)

The following is inferred from the empirical analysis:

1. The generally low values of n_1 are thought to be due to non-radiating near-field coupling between transmit and receive antennas. (Since the antennas are identical a spacing of twice the radian sphere radius is required to ensure negligible coupling between quasi-static fields.)

2. The values of n_2, intermediate between those of n_1 and n_3, are close to unity for the aluminum surface and close to 2.0 for the MDF surface suggesting significantly different modes or mechanisms of propagation. At least two (not necessarily independent) mechanisms can be proposed. Firstly, it is possible that near-field coupling between the electrically small antenna and the surface results in a composite radiating structure that is no longer electrically small. In this case we would expect a significant radiating near-field region extending beyond the radian sphere. In the case of the MDF surface, for example, if a fraction of the field were coupled to the surface then this fraction (in its radiating near-field) might be expected to decay with an index close to 2. The field fraction not coupled to the surface (in its far-field) would decay with a free-space index close to unity. The overall field strength decay index might therefore be expected to be between 1 and 2 and the power density decay index between 2 and 4. Secondly, it is possible that near-field coupling between antenna and surface launches a surface wave which dominates in the intermediate region (between R_1 and R_2). Coupling may be especially close, and the surface wave correspondingly large, when the antenna, or its feed, intersects the surface slot forming what is effectively a single turn current transformer. A power density decay index close to unity is consistent with a dominant surface wave since spreading loss in this case would tend to be constrained to two dimensions. An increasing value of n_2 with increasing antenna height above the surface is also consistent with a surface wave interpretation; a decrease in coupling resulting in a decrease in the relative strength of the surface wave.

The nodes in future wireless sensor networks may be small. In [1], for example, the objective is to contain a node within a 1mm cube. If such nodes are deployed on conducting surfaces and the interpretation relating to surface wave propagation is correct then low path loss indices will be common.

In order to test the surface wave hypothesis the 1m×1m aluminum square surface was reduced to a thin strip (1m×155mm) to form surface C and the measurements were repeated. The hypothesis predicts a surface wave propagating via the reduced conducting area would be subject to a further reduction in the value of n due to constraining spreading to less than two dimensions. The measurement results (Fig. 5-14 and 5-15) summarized in Table 5-2, show that path loss index is reduced by 43% irrespective of h *(*for antenna heights of 12.5 mm*)*.

To minimize coupling between antennas and surface the measurements for h = 12.5mm were repeated but with the radiating elements inverted and fed from above, Figure 5-8. The results are shown in Fig. 5-15 and 5-16 for 1m×1m aluminum and MDF surfaces respectively. Table 5-3 shows the resulting model parameters.

The path loss index in the intermediate region for the MDF surface remains almost unchanged suggesting that coupling between surface and antenna is modest. The corresponding path loss index for the aluminum surface rises significantly (from 1.17 to 2.55). This is consistent with a reduction in surface wave amplitude which may be due to the removal of feed leakage fields from the proximity of the surface

5.2.2 Fading

An empirical fading model has been derived by making many independent measurements for each transmitter-receiver path length as in Fig. 5-8. The test-bench was displaced by at least one wavelength between measurements. The fading distribution of the measured data was compared against theoretical distribution (i.e. Ricean and Rayleigh) using quartiles technique [42]. The data set is divided into quartiles and if the samples do come from the same distribution, even if one

distribution is shifted and re-scaled from the other (different location and scale parameters), the plot will be linear.

Fig. 5-18 shows the measured fading distributions of received signal for a range of path lengths as compared to a Ricean process with a k-factor of 10. In Ricean fading a dominant component is present. The dominant component could be a line of sight component or the combination of line of sight plus the reflected component. Following observation are made regarding Fig. 5-18.

1. The observation below the upper quartile i.e. q (0.75) follow a linear line (for the theoretical Ricean distribution) as shown in Fig. 5-19.

2. The observation greater than upper quartile i.e. q (0.75) as in Fig. 5-19, shows slight increase in amplitude but the data remains almost linear, which confirms the data to be Ricean distributed.

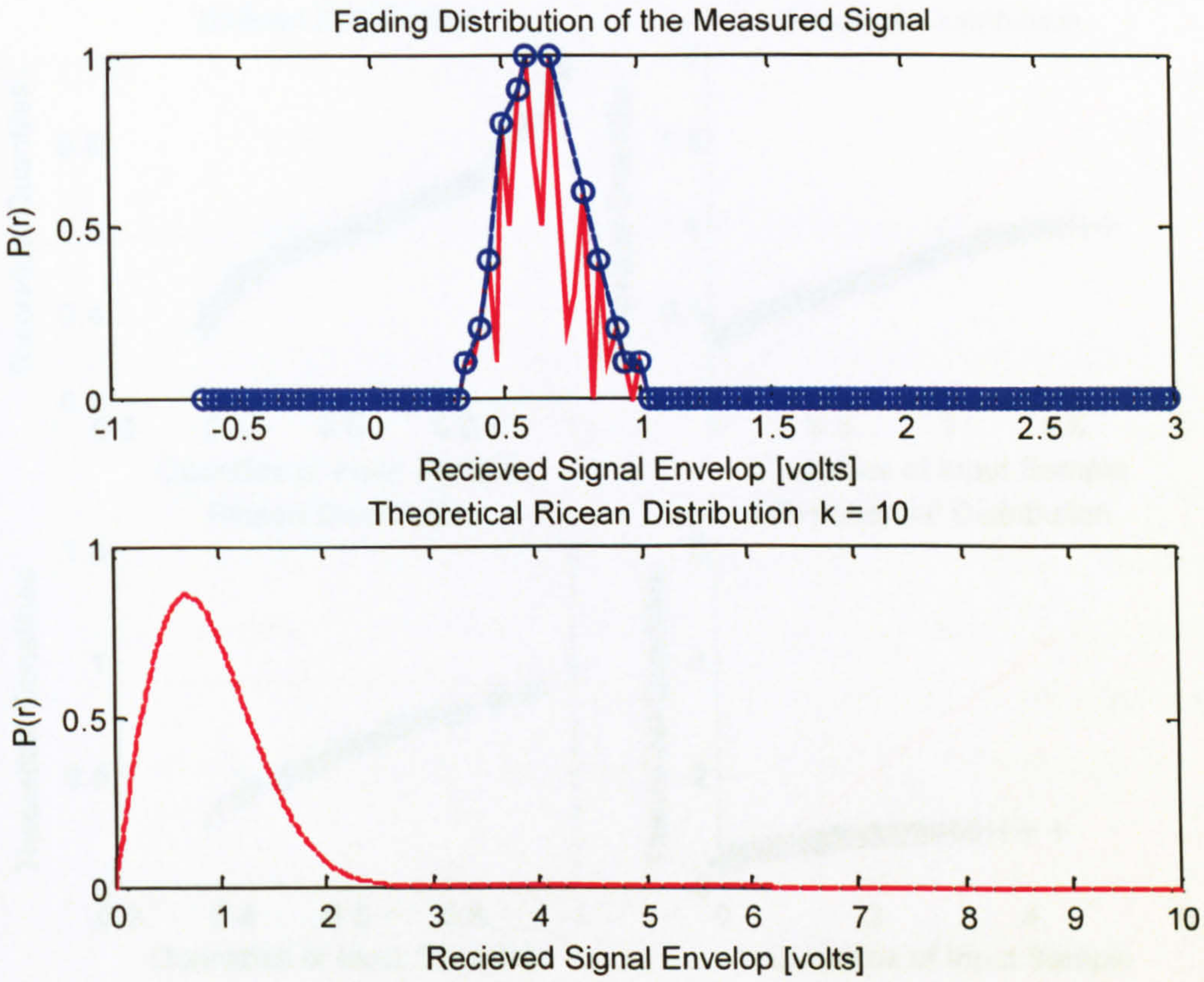

Fig. 5-18 Fading distribution of measured data

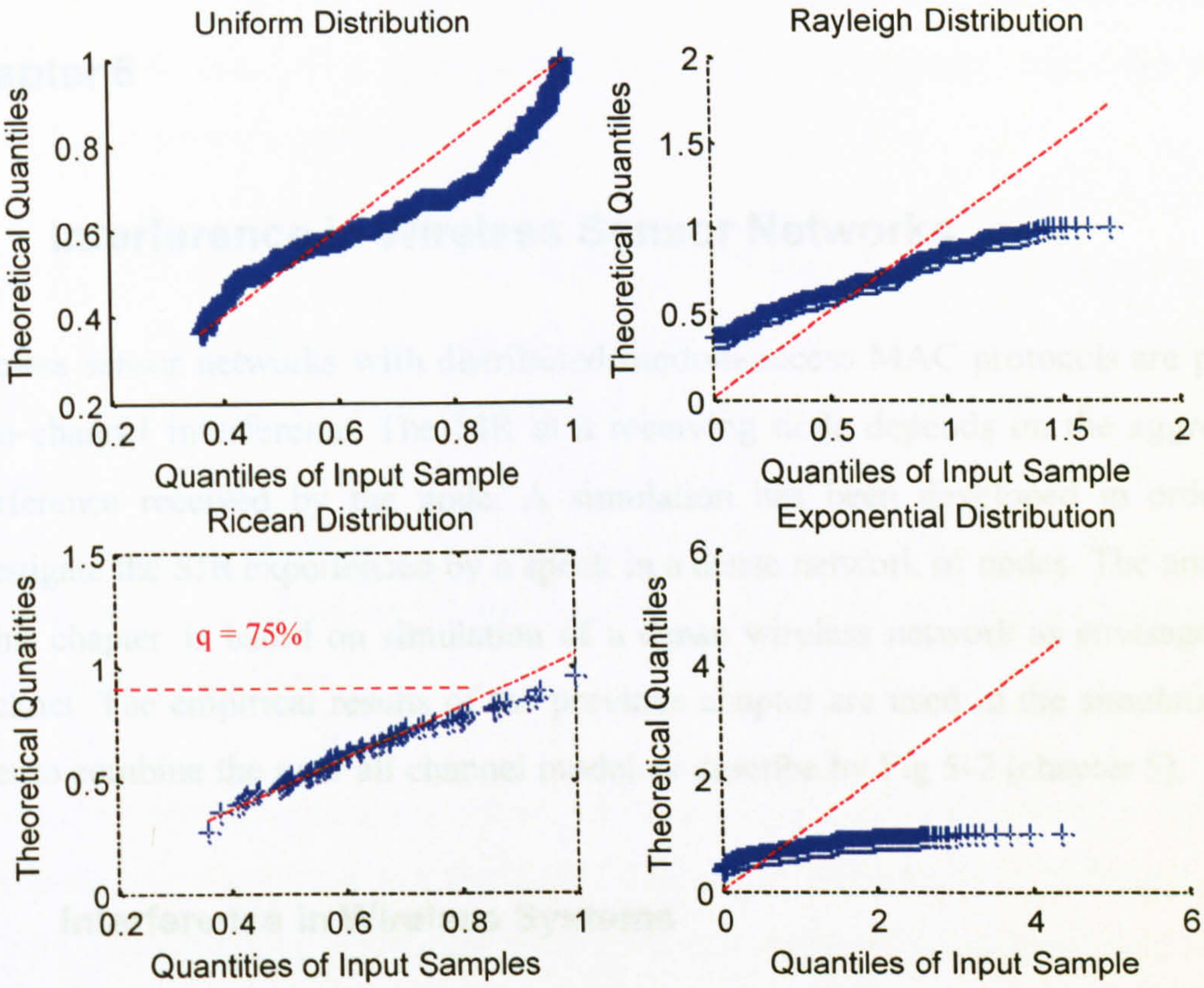

Fig. 5-19 Quantile-Quantile plots of measured data (blue) with different distributions.

5.3 Summary

Wireless channel parameters (i.e. path loss and fading) for wireless sensing nodes that are likely to be placed closed to the ground have been estimated. Empirical measurements are used to define a model which is used in chapter 6 for the estimation of signal to interference ratio experienced by a node in a dense wireless network as envisaged by specknet. The study relates path loss index for different antenna height and separation distance. It is concluded that for short wireless links path loss index is affected by antenna height possibly explained by the presence of a surface wave.

Chapter 6

6. Interference in Wireless Sensor Networks

Wireless sensor networks with distributed random-access MAC protocols are prone to co-channel interference. The SIR at a receiving node depends on the aggregate interference received by the node. A simulation has been developed in order to investigate the SIR experienced by a speck in a dense network of nodes. The analysis in this chapter is based on simulation of a dense wireless network as envisaged by specknet. The empirical results of the previous chapter are used in the simulation in order to combine the over all channel model as describe by Fig 5-2 (chapter 5).

6.2 Interference in Wireless Systems

Asynchronous sensor networks typically use carrier-sense-multiple-access/collision-avoidance (CSMA/CA) as the medium access control (MAC) protocol. The resulting level of interference experienced by a receiving node depends on three factors. These are: (i) inhibition distance, (ii) antenna characteristics (including polarization) and (iii) node deployment strategy (i.e. the process by which the spatial distribution, and orientation, of transceivers is established). Each of these factors is addressed below.

6.1.1 Inhibition Distance

CSMA/CA is simple to implement (not requiring synchronization between nodes), power efficient and cost effective. Such networks can be characterized by an inhibition distance, i.e. the radius of a nominal circle within which a transmitting node inhibits the transmission of any contending nodes. (In practice, of course, the inhibition region is unlikely to be precisely circular (for larger indoor ranges) since transmission losses will not generally be azimuth independent.) Nodes possess a received signal level threshold which, if exceeded during medium sensing, results in

transmission back-off. The larger the inhibition distance (i.e. the lower the threshold), the greater is the number of neighbouring nodes that will be inhibited and the less is the aggregate interfering power.

CSMA/CA based networks can be defined by two radii. The communication radius (R_c) is the maximum range between communicating nodes in the absence of interference. It is dependent on the signal to noise ratio. The inhibition radius (R_{Ih}), is defined as the range (centred on a transmitting node) within which a second node is inhibited from transmitting. These radii can be defined at the physical layer as a received power threshold depending upon the application, network traffic and the surrounding environment.

CSMA/CA communication is prone to radio irregularity which is a common phenomenon in wireless sensor networks. It results in irregularity in radio range thus resulting in packet loss in different directions. The variance in the signal path loss (in 360° azimuth plane) is one of the major reasons of anisotropy or radio irregularity. The radio irregularity is caused by devices and the propagation medium.

It has been pointed out in several empirical studies [43] [44] [45] conducted using the Berkeley mote platform that radio range varies significantly with directions. The variance in signal path loss is the one of the major cause of radio irregularity. During the course of signal propagation the radio waves are reflected, diffracted and scattered due to the medium. The medium is normally different in different directions resulting in anistropic pattern around the node in most environments.

To simulate an interference limited CSMA/CA system it is necessary to take into account both the anisotropic properties of the propagation model and the characteristic properties of the sensors used. The value of R_c and R_{Ih} depends on these two properties. It has been pointed out in [46] that the radio irregularity depends on both the device and the propagation medium. Device properties include the antenna used i.e. gain, radiation pattern (directional or omni-directional radiation

pattern) and polarisation. The medium properties include propagation loss, interference and noise in the environment.

In order to justify the use of an isotropic assumption (i.e. R_c and R_{Ih} circular) in CSMA/CA the radio irregularity model (RIM) is used as defined by [46]. The RIM model defines the irregularity of the radio pattern using the parameter DOI (degree of irregularity). DOI is defined as the "maximum transmission loss percentage variation per unit degree change in the direction of radio propagation". Fig. 6-1 illustrate the DOI parameter if there is no azimuth range variation then DOI = 0. There is no range variation and the communication range is a sphere. Any increase in DOI value results in irregular communication range with respect to azimuth.

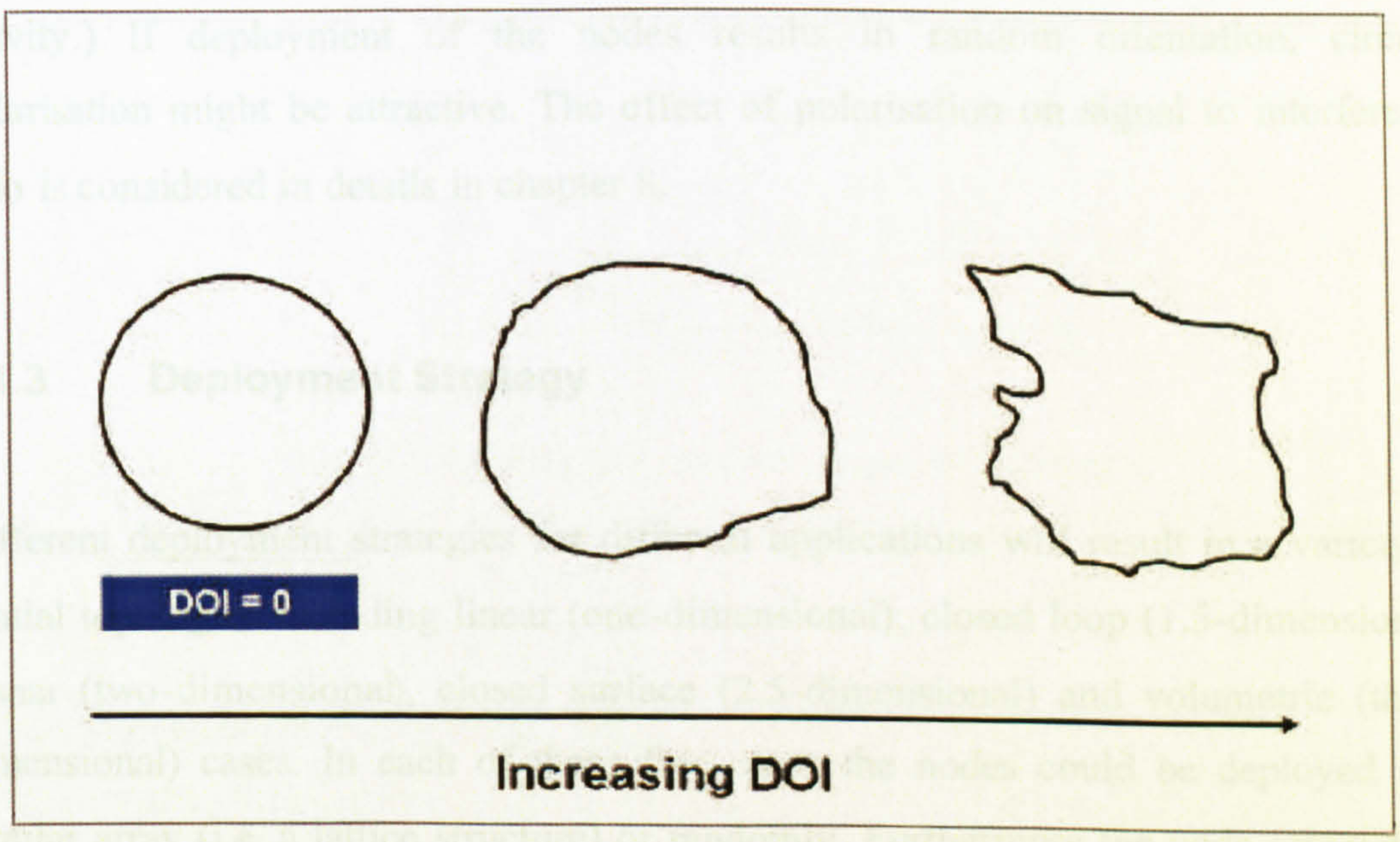

Fig. 6-1 Degree of irregularity

Detailed set of experiment using different motes were conducted in [46] which suggest DOI values close to zero for radios equipped with less powerful transmitter or smaller antennas. Low power would result in fewer multipaths due to weak reflections from the surrounding objects.

6.1.2 Antenna Characteristics

Antennas play a significant role in determining interference. Network nodes will, typically, be randomly distributed. Received power from a specific interfering node depends on both transmitting and receiving antenna radiation patterns. This includes polarization characteristics (since any mismatch between transmit and receive antennas will result in additional transmission loss).

Omni-directional antennas would maximize potential connectivity between nodes and linear polarization would be attractive if the deployment mechanism could ensure orientation perpendicular to the deployment surface. (We will refer to this as vertical polarization irrespective of the orientation of the surface with respect to gravity.) If deployment of the nodes results in random orientation, circular polarisation might be attractive. The effect of polarisation on signal to interference ratio is considered in details in chapter 8.

6.1.3 Deployment Strategy

Different deployment strategies for different applications will result in a variety of spatial topologies including linear (one-dimensional), closed loop (1.5-dimensional), planar (two-dimensional), closed surface (2.5-dimensional) and volumetric (three-dimensional) cases. In each of these five cases the nodes could be deployed in a regular array (i.e. a lattice structure) or randomly. Furthermore the node orientations may be aligned or random. (The potential advantage of circular polarization in the context of randomly oriented antennas has already been pointed out although, if propagation is close to a plane surface, significant ellipticisation may result, even if the antenna were polarization pure in free space.) The expected SIR experienced by any node will depend on the deployment strategy. A linear network (Fig. 6-2), for example, will suffer less interference for a given mean distance between adjacent nodes than a planar network (Fig. 6-3).

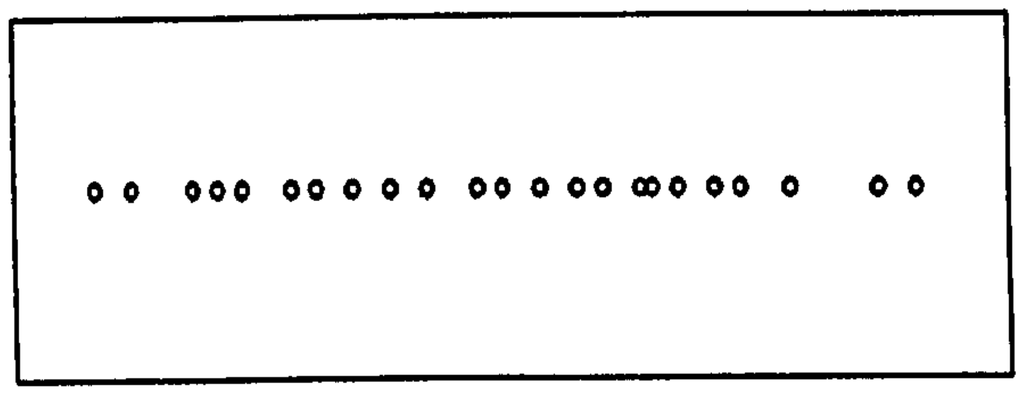

Fig. 6-2 Random linear deployment

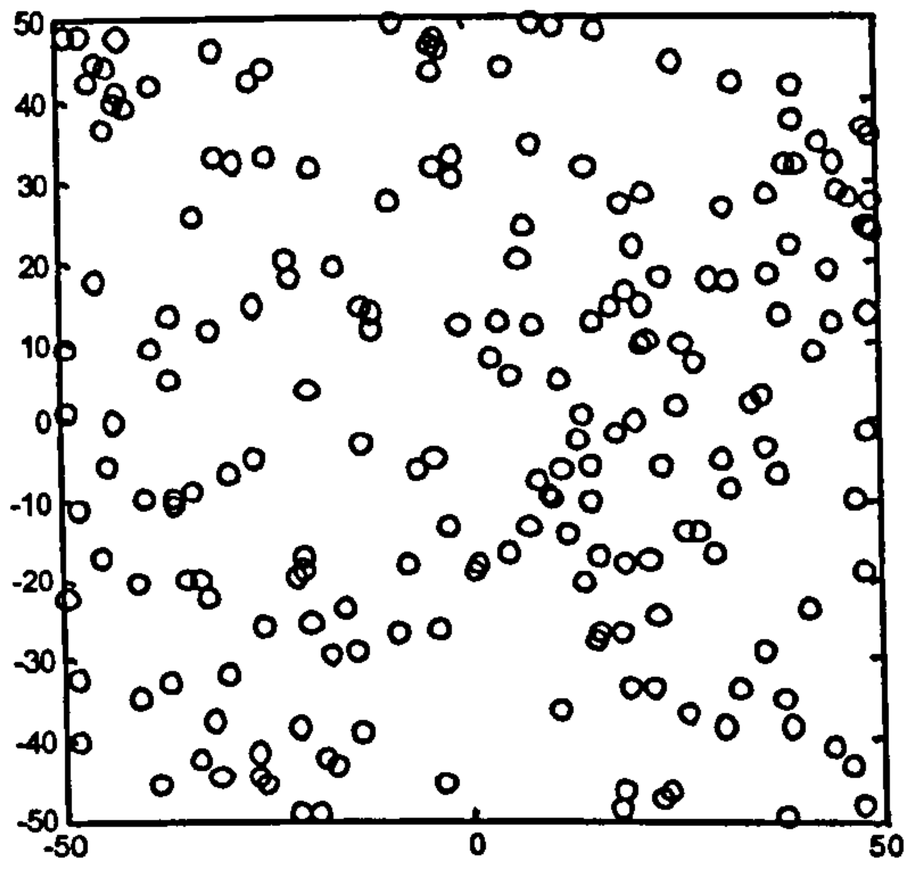

Fig. 6-3 Regular and random planar deployment

6.2 Simulation to Quantify SIR

Simulations to establish expected SIR have been performed based on two-dimensional random deployment with the parameters shown in Table 6-1.

Inhibition distance (R_{Ih}) [cm]	10, 15, 20, 25, 30, 35, 40
Simulation space	200 cm x 200 cm
Mean speck density [/m^2]	200
Deployment	2-D, Poisson distributed
MAC protocol	CSMA/CA
Antenna	Dipole
Polarization	Vertical
Path loss model	As in Chapter 5

Table 6-1 Interference simulation parameters

The simulation has been carried out for two different cases i.e. (i) when the communication radius is equal to the inhibition radius i.e. ($R_c = R_{Ih}$) and (ii) the communicating radius (R_c) is fixed at 10 cm and the inhibition distance R_{Ih} is increased from 10 cm to 20 cm in steps of 5 cm. This is achieved by incorporating RTS and CTS interchange at each node. The two set of simulations are discussed in detail below.

6.2.1 Communication Radius Equal to Inhibition Distance ($R_c = R_{Ih}$)

A receiving speck is chosen near the centre of the simulation space and the (desired) transmitting speck is chosen randomly from all those within range. (Range in this context is inhibition distance which has been varied between 10 cm and 40 cm in steps of 5 cm.) An interfering speck is then chosen randomly from all those not lying within the CSMA inhibition distance of the speck already transmitting. This process is repeated with new interfering specks being chosen from those not within the inhibition distance of any speck already transmitting (Fig. 6-4) until no more specks are available (Fig. 6-5 keeping $R_c = R_{Ih}$). The result is a worst possible case of interference. The interference power at the receiving speck is calculated using the path loss model described in chapter 5 for an MDF surface (Fig. 5-12). The aggregated interference experienced by the receiving speck is given by (6.1). Specks

are assumed to radiate as vertically polarized dipoles and both transmit and receive antenna gains are assumed to be 0 dBi (allowing for miscellaneous losses).

$$I = \sum_{k=1}^{N} G_{TK} I_k \tag{6.1}$$

where G_{TK} is the gain of the transmitting antenna, I_K is the total interference power due to neighbouring specks. The SIR is calculated using (6.2)

$$SIR = \frac{P_T - L}{I} \tag{6.2}$$

where P_T - L is the power received by the speck.

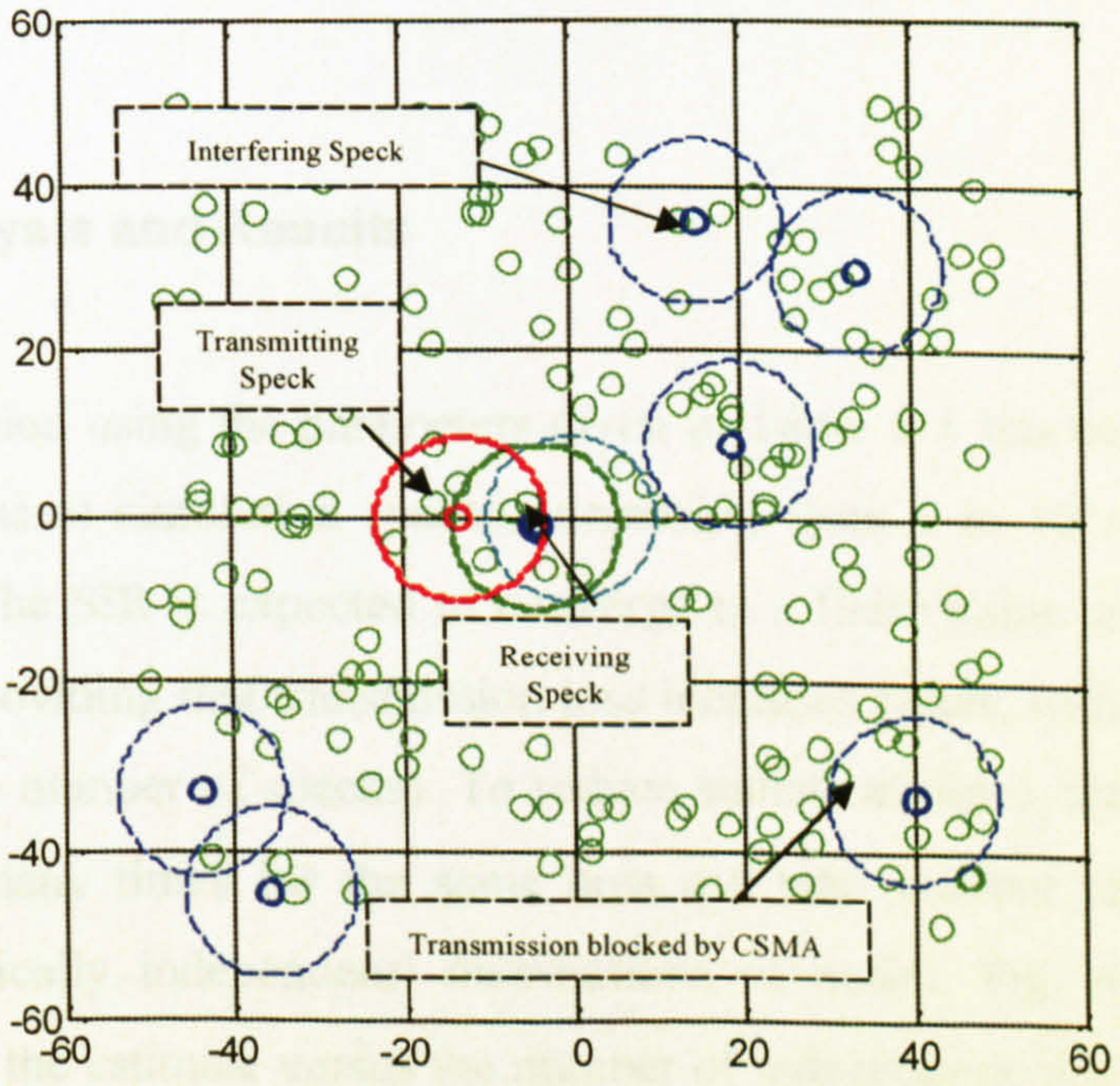

Fig. 6-4 Illustration of inhibition regions for vertically polarized specks

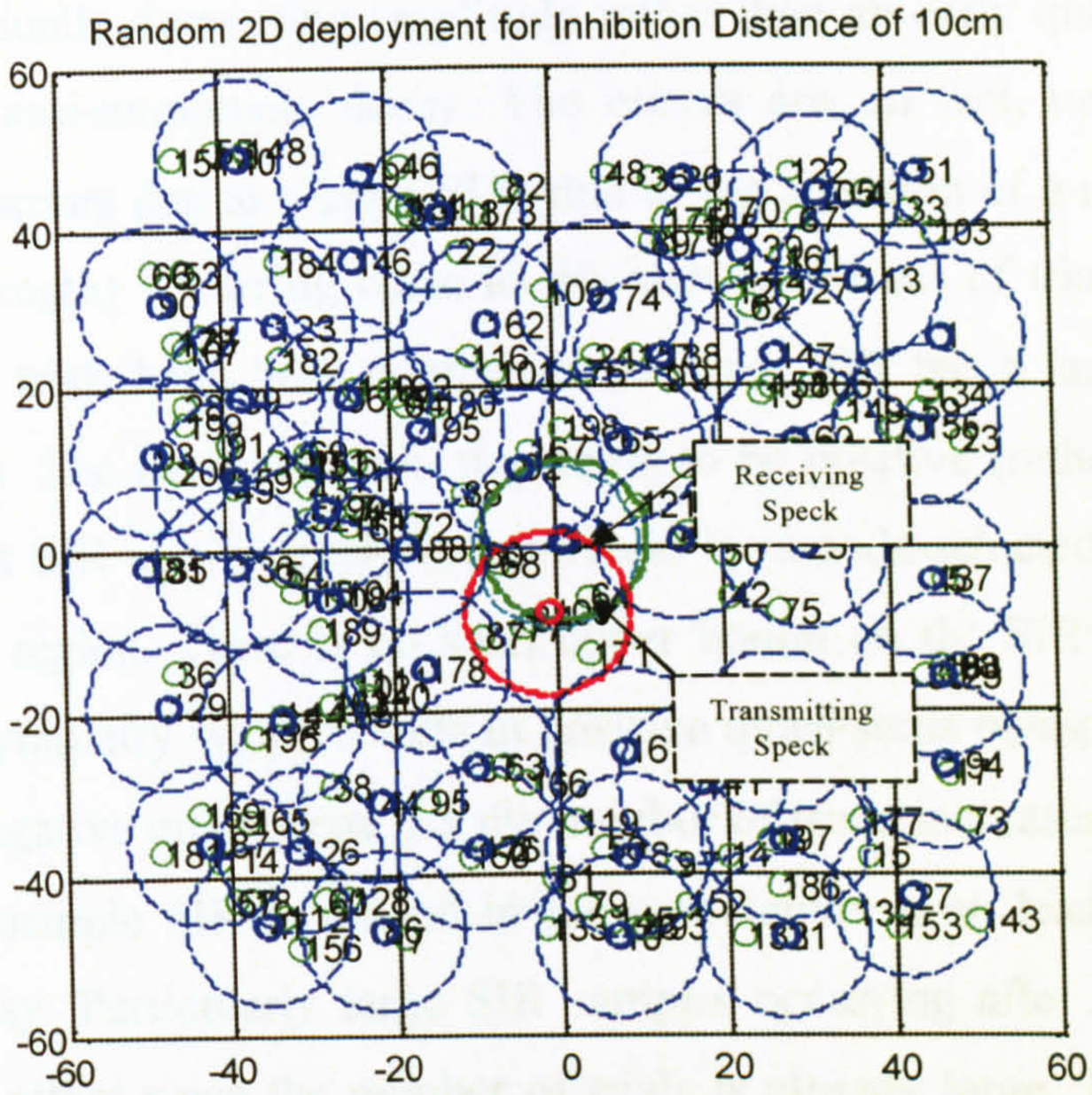

Fig. 6-5 Transmitting specks and interference regions for random two-dimensional deployment, vertical polarization and an inhibition distance of 10 cm ($R_c = R_{Ih}$).

6.2.2 Analysis and Results

The SIR calculation using the parameters given in Table 6-1 has been repeated for a selection of (square) simulation spaces, increasing from 1 to 10 m^2 (with constant node density). The SIR is expected to converge to a finite value as the deployment area increases providing that transmission loss increases faster, with increasing range, than area (or the number of specks). To reduce statistical noise each simulation has been repeated many times for the same area and total number of nodes but with different (statistically independent) distributions of nodes. Fig. 6-6 illustrates the improvement of the estimate versus the number of independent simulations. Table 6-2 shows the results. This table, together with Fig. 6-6, suggests that a space 200 cm x 200 cm gives a result close to (i.e. within the statistical noise of) that for an infinite plane.

The behaviour of the curves in Fig. 6-6 requires some comment. Superficially it might be expected that the curves would display (statistically) symmetrical random

variations of gradually decreasing amplitude rather than an early quasi-step increase followed by a quasi-monotonic decay. The curves are, in fact, unsurprising. The initial large rise occurs due to a large SIR (due to the selection of a node resulting in very short link length) occurring close to the start of the set of trials. Since only a small number of trials have been completed the large SIR has a large effect on the cumulative mean. The resultant quasi-step tends to be positive (rather than negative) since the smallest SIR is effectively lower-bound by a node selected at the boundary of the inhibition region. There is no such upper bound on the SIR resulting from a trial. It is this asymmetry which results in positive quasi-steps being apparently more common than negative quasi-steps. As the number of trials increases the effect of the unusually large sample SIR is diluted in the cumulative mean leading to the quasi-exponential decay. Particularly large SIR samples occurring after many trials have little noticeable effect since the number of trials is already large. The apparent (i.e. noticeable) exponential-like feature therefore appears only once.

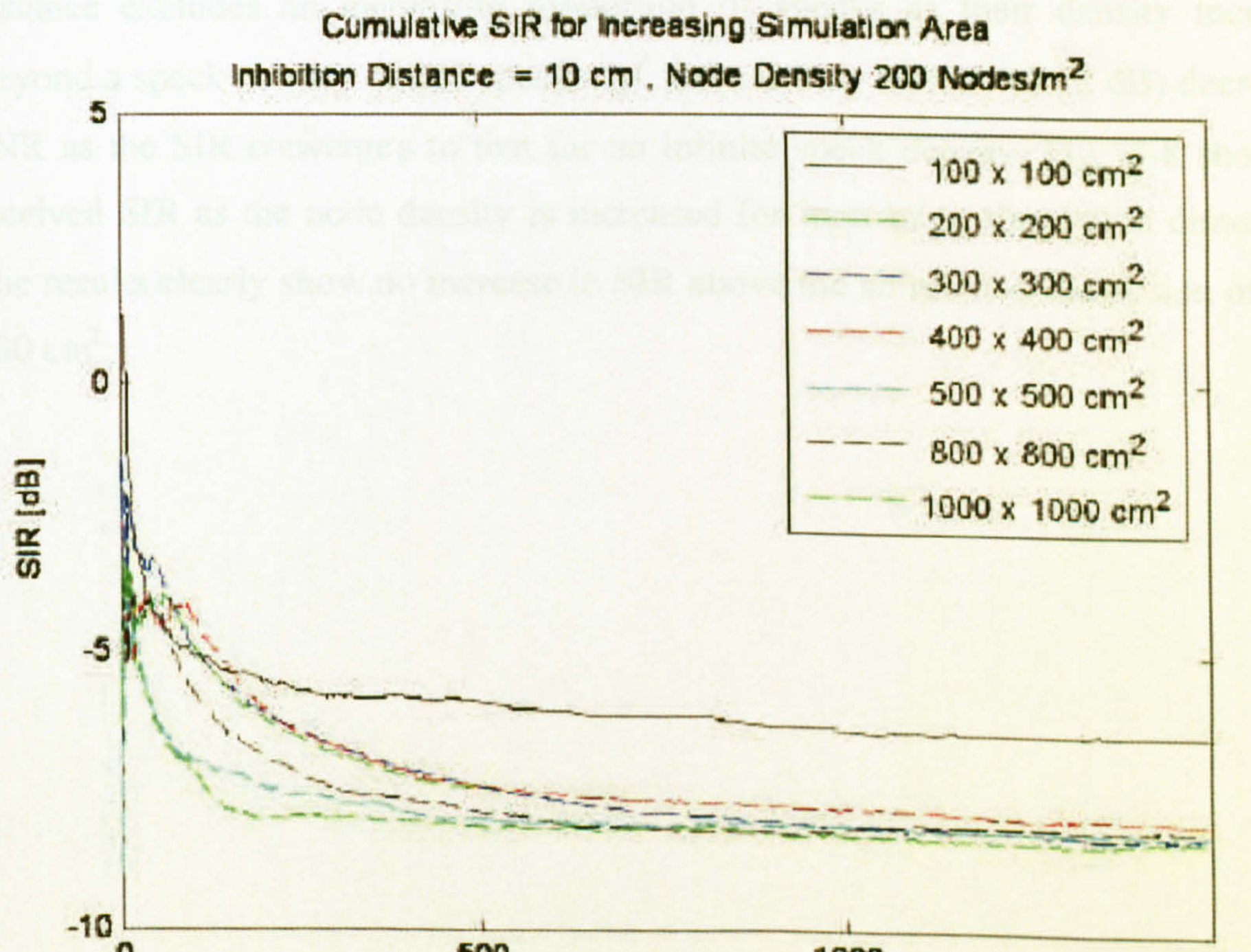

Fig. 6-6 Mean SIR versus number of trials. (Parameter is simulation area.) Inhibition distance (R_{Ih}) 10 cm, node density 200 nodes/m^2.

Simulation area [cm^2]	**SIR** [dB]	**SIR increment** [dB]
100 × 100	-6.46	NA
200 × 200	-8.30	-1.84
300 × 300	-8.28	-0.02
400 × 400	-8.04	-0.24
500 × 500	-8.27	+0.23
800 × 800	-8.20	-0.07
1000 × 1000	-8.25	+0.05

Table 6-2 SIR for increasing area (constant node density)

Fig. 6-7 shows the simulation results for different node densities (in cm^2). Increasing node density results in a decrease of SIR. This is because a constant inhibition distance excludes an increasing proportion of specks as their density increases. Beyond a speck density of 200 specks /m^2 there is only a small (0.22 dB) decrease in SNR as the SIR converges to that for an infinite speck density. Fig. 6-8 shows the received SIR as the node density is increased for increasing simulation dimensions. The results clearly show no increase in SIR above the simulation dimension of 200 × 200 cm^2.

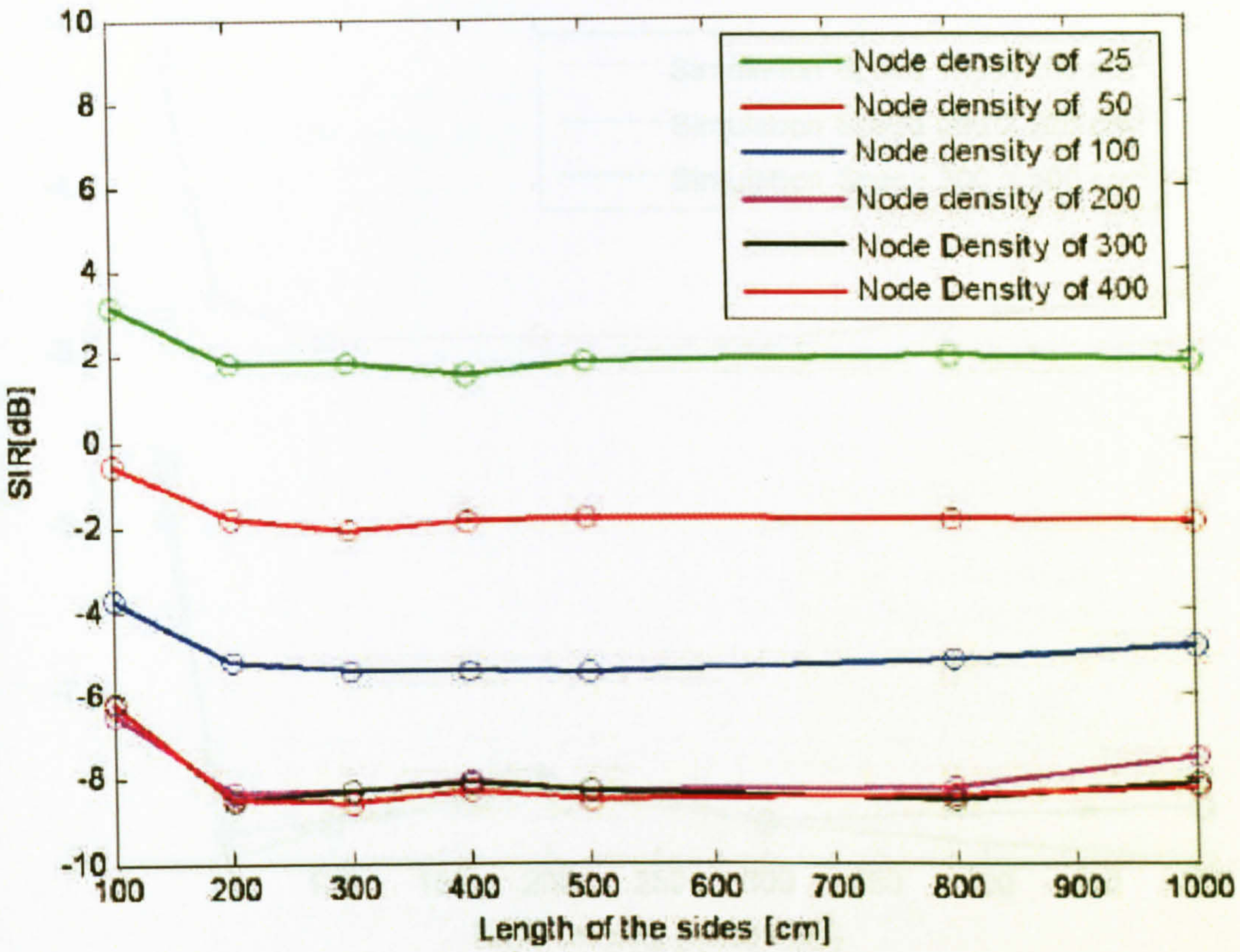

Fig. 6-7 SIR versus simulation area for different node densities

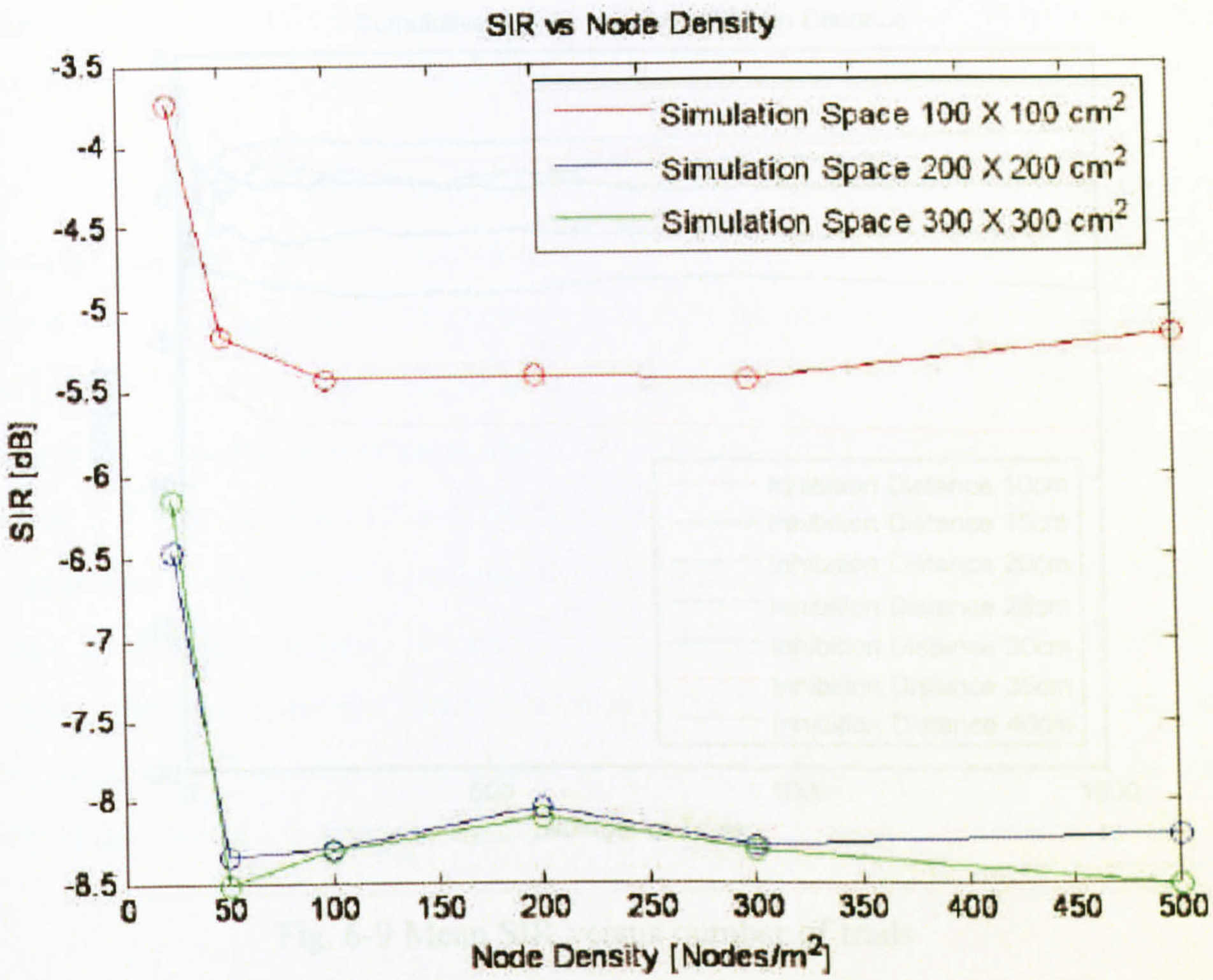

Fig. 6-8 SIR versus node density in different simulation space

Figs. 6-9 shows mean SIR versus number of trials for a range of inhibition distances (R_{Ih}) from 10 cm to 40 cm (i.e. $R_c = R_{Ih}$), using the path loss model of chapter 5 and the simulation parameters of Table 6-1. The simulation is based on antennas placed at a height of 6.5 mm above the MDF surface (Fig 5-12), as in Table 5-1.

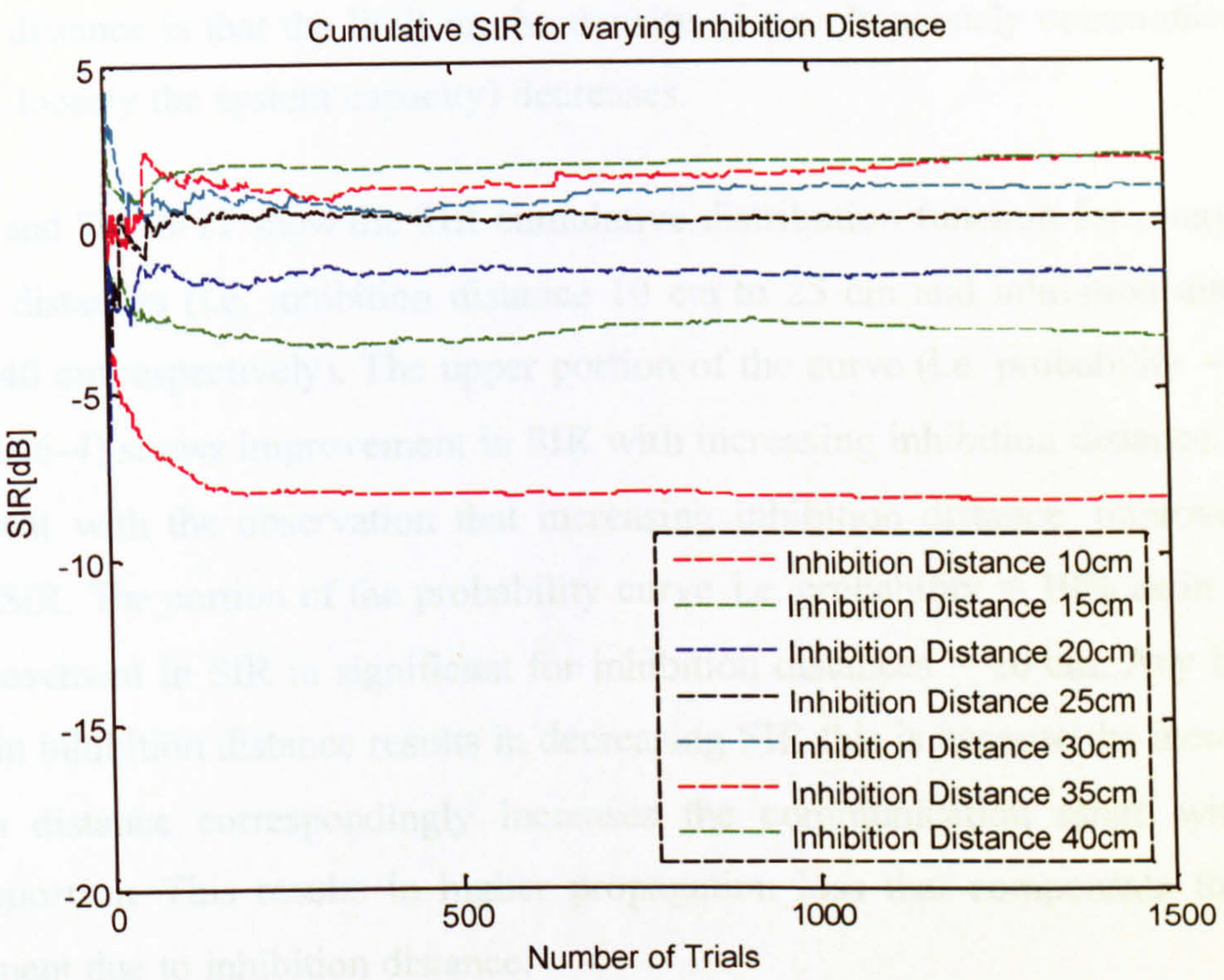

Fig. 6-9 Mean SIR versus number of trials

Inhibition Distance (R_{Ih}) [cm]	**SIR** [dB]	**Improvement in SIR with respect to the inhibition distance** [dB]
10	-8.33	NA
15	-3.44	4.89
20	-1.46	1.98
25	+0.23	1.23
30	+1.08	0.85
35	+1.99	0.91
40	+2.11	0.12

Table 6-3 SIR for increasing inhibition distance

SIR improvement is significant for inhibition distance (R_{Ih}) changes from 10 cm to 15 cm, and from 15 cm to 20 cm (Table 6-3). Further increases in inhibition distance (R_{Ih}) result in diminishing SIR returns. The diminishing returns behaviour of the curves in Fig. 6-9 suggests that the simulation space is sufficiently large to reflect the SIR variation expected for an infinite plane of nodes. The disadvantage of increasing

inhibition distance is that the limit on the density of simultaneously communicating nodes (i.e. loosely the system capacity) decreases.

Fig. 6-10 and Fig. 6-11 show the SIR cumulative distribution function for a range of inhibition distances (i.e. inhibition distance 10 cm to 25 cm and inhibition distance 30 cm to 40 cm respectively). The upper portion of the curve (i.e. probability = 90% as in Table 6-4) shows improvement in SIR with increasing inhibition distance. This is consistent with the observation that increasing inhibition distance improves the received SIR. The portion of the probability curve i.e. probability = 10% as in Table 6-4, improvement in SIR in significant for inhibition distances = 20 cm. Any further increase in inhibition distance results in decreasing SIR this is because the increasing inhibition distance correspondingly increases the communication range with the same proportion. This results in higher propagation loss that compensate for any improvement due to inhibition distance.

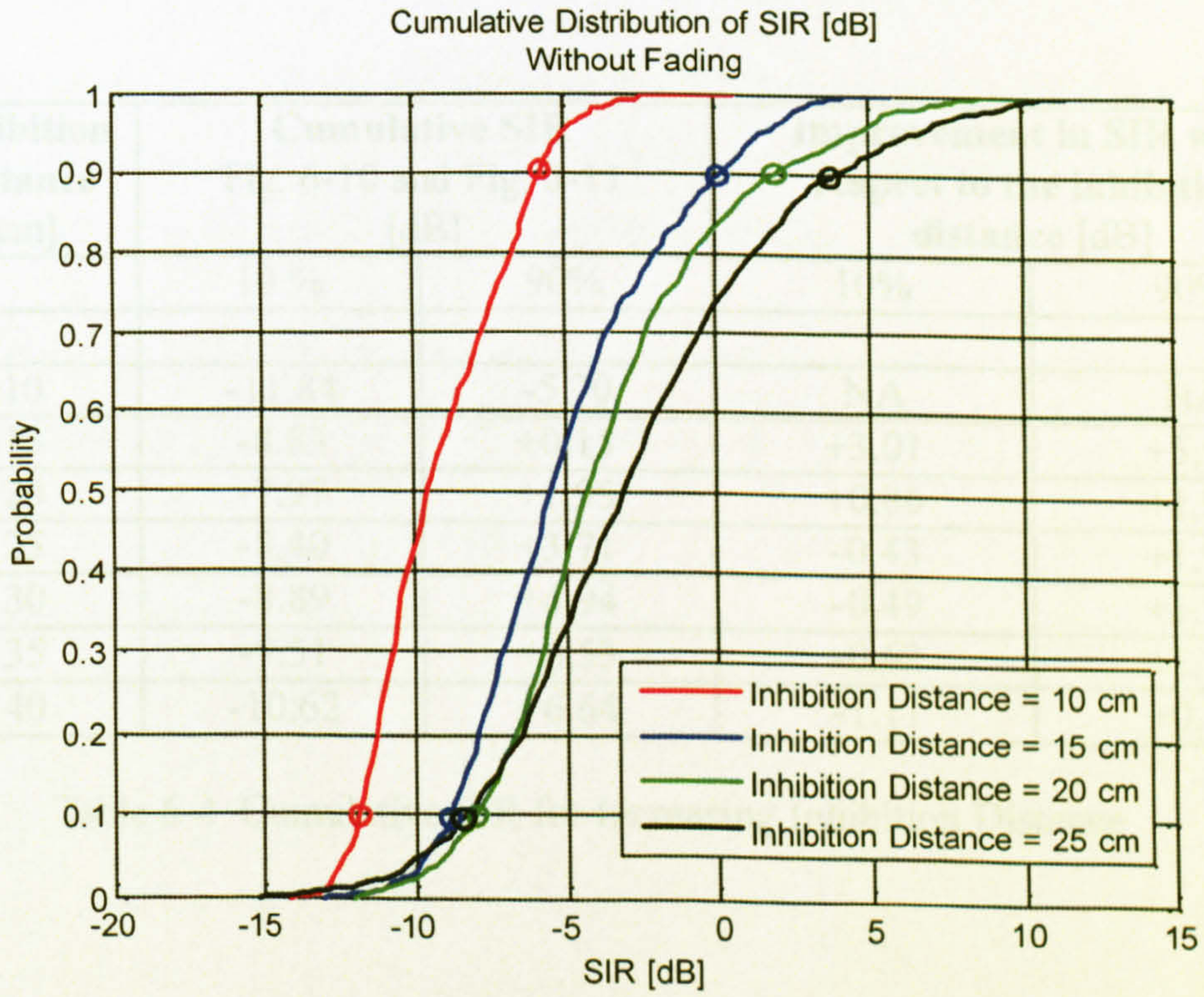

Fig. 6-10 Cumulative distribution of SIR (without fading) ($R_c = R_{Ih}$)

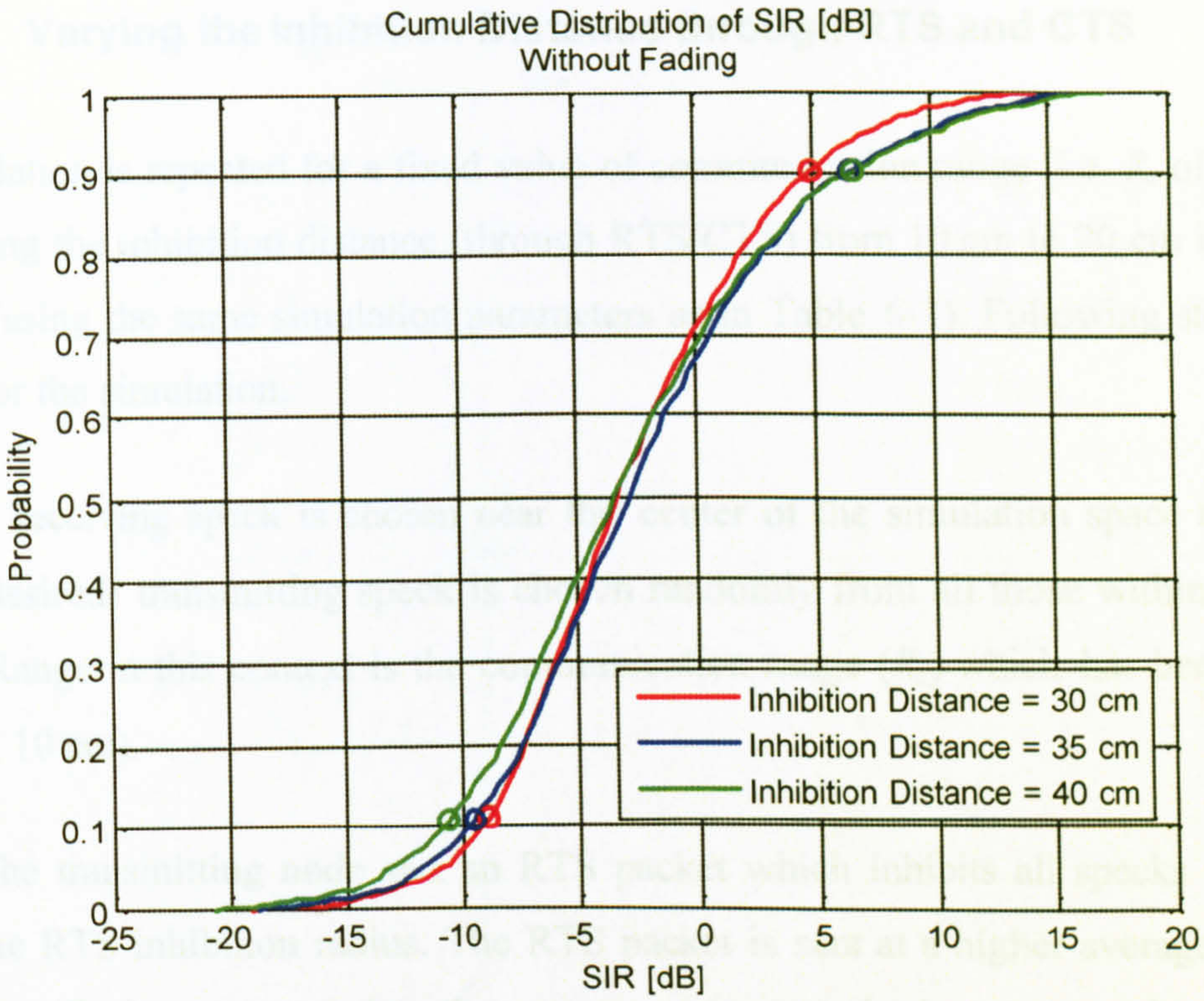

Fig. 6-11 Cumulative distribution of SIR (without fading) ($R_c = R_{lh}$)

Inhibition Distance [cm]	**Cumulative SIR** Fig. 6-10 and Fig. 6-11 [dB]		**Improvement in SIR with respect to the inhibition distance** [dB]	
	10 %	90%	10%	90%
10	-11.84	-5.70	NA	NA
15	-8.83	+0.15	+3.01	+5.55
20	-7.97	+1.95	+0.86	+1.80
25	-8.40	+3.71	-0.43	+1.76
30	-8.89	+4.94	-0.49	+1.23
35	-9.51	+6.53	-0.62	+1.59
40	-10.62	+6.64	-1.11	+0.11

Table 6-4 Cumulative SIR for Increasing Inhibition Distance

6.2.3 Varying the Inhibition Distance through RTS and CTS

The simulation is repeated for a fixed value of communication range (i.e. R_c of 10 cm) and varying the inhibition distance (through RTS/CTS) from 10 cm to 20 cm in steps of 5 cm (using the same simulation parameters as in Table 6-1). Following steps are defined for the simulation.

1. A receiving speck is chosen near the center of the simulation space and the (desired) transmitting speck is chosen randomly from all those within range. (Range in this context is the communication range (R_c) which has been fixed at 10 cm).

2. The transmitting node sent an RTS packet which inhibits all specks with in the RTS inhibition radius. The RTS packet is sent at a higher average power (say P_{Ih}) as compared to the average power required to communicate at 10 cm range (say $P_{Optimum}$). It is noted that $P_{Ih} > P_{Optimum}$, for the RTS packet.

3. The receiving node on reception of the RTS packet sent a CTS packet (it is assumed that CTS packet is sent with the same power as P_{Ih}). This should inhibit all nodes within the CTS inhibition radius.

4. After RTS and CTS interchange the transmit and receive node communicate at a reduced power level i.e. $P_{Optimum}$ as in Fig. 6-12 below.

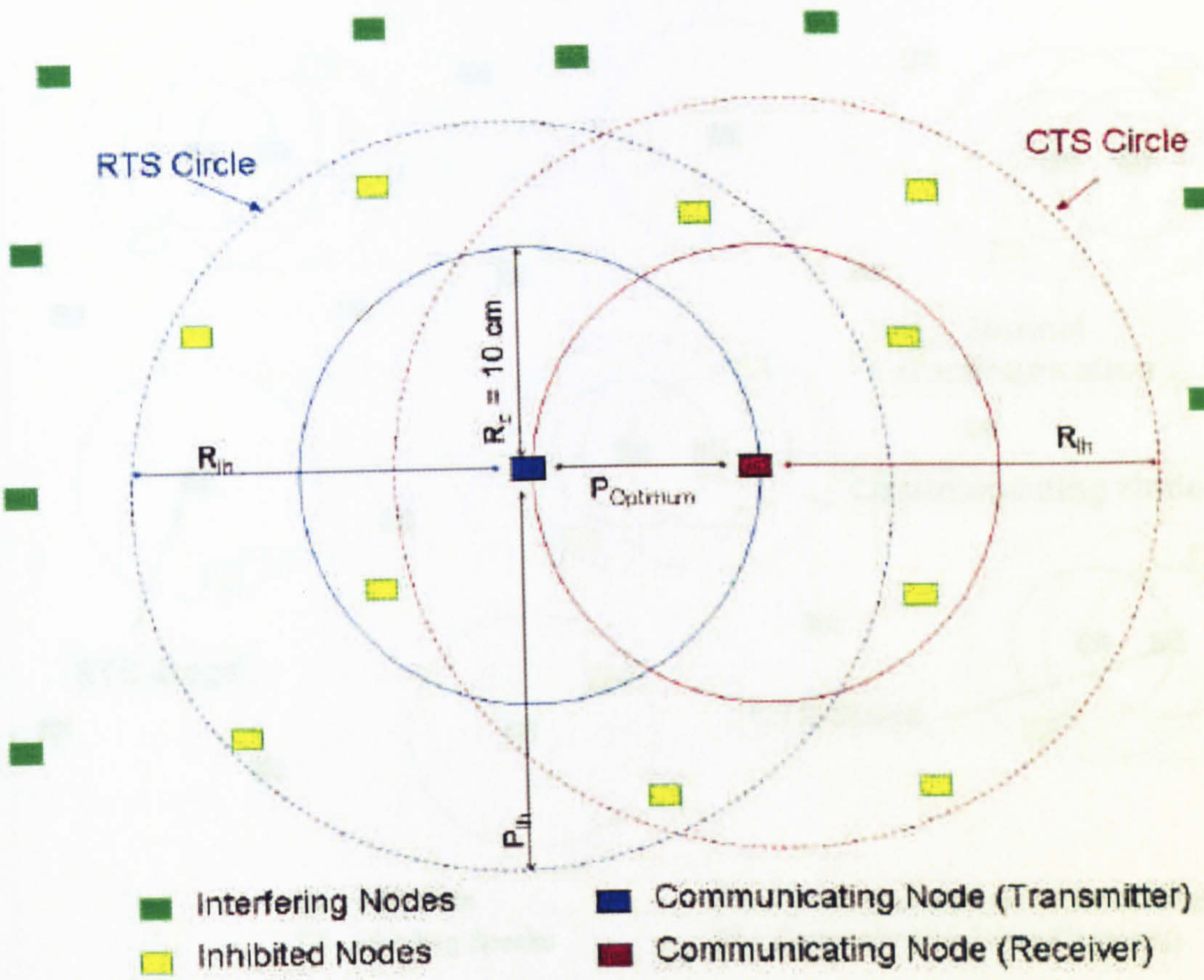

Fig. 6-12 RTS and CTS mechanism for the communicating nodes.

5. An interfering speck is then chosen randomly from all those not lying within the CSMA inhibition distance of the speck already transmitting. The interfering node at any instant of time could be in three different states i.e. the interfering node could be in a state where it is sending (i) an RTS packet (ii) a CTS packet or a (iii) normal data packet. In all three cases the appropriate power levels (as in Table 6-5) are considered to estimate the aggregate SIR. This process is repeated with new interfering specks being chosen from those not within the inhibition distance of any speck already transmitting until no more specks are available. Fig. 6-13 shows the simulation space with RTS and CTS mechanism.

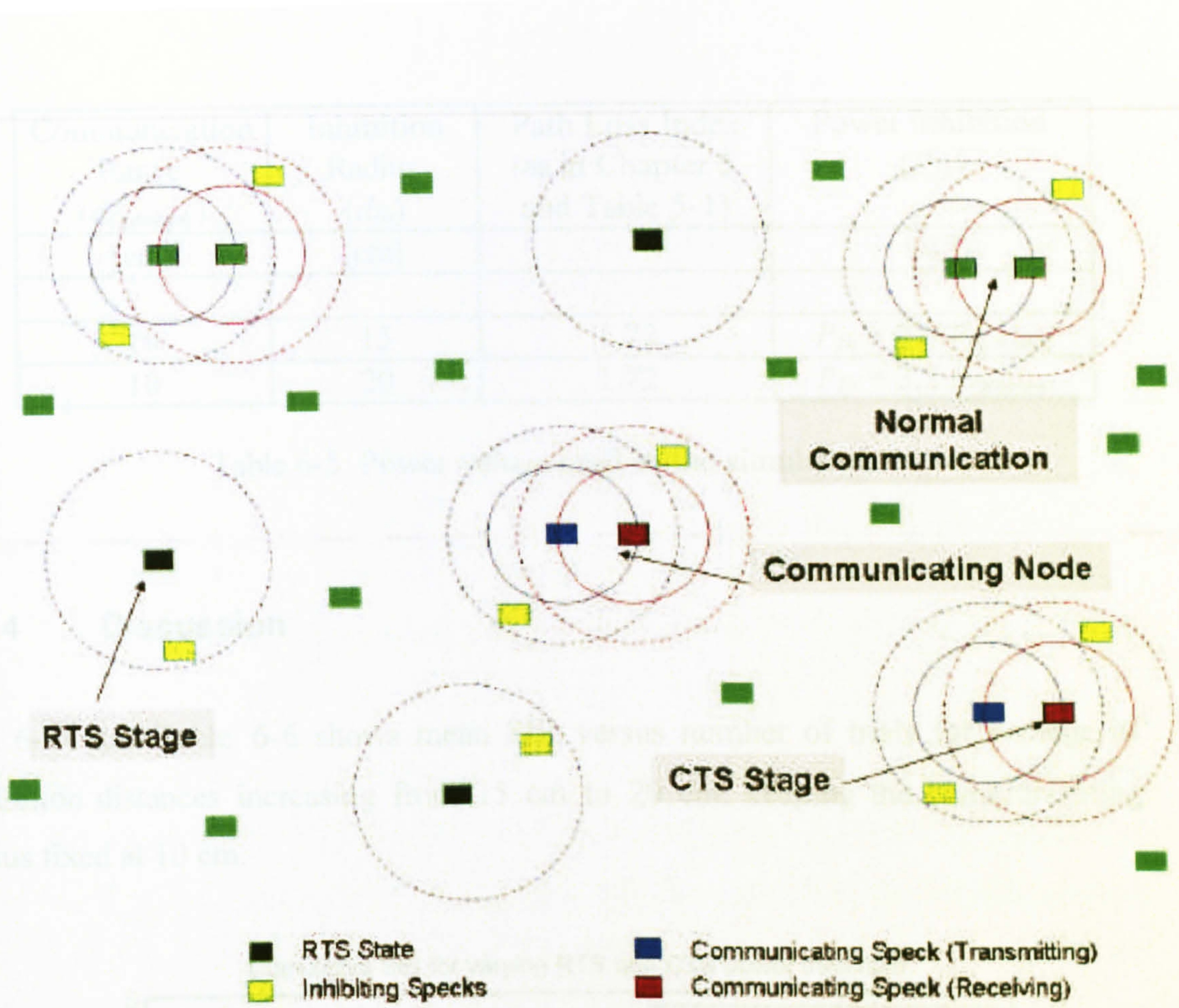

Fig. 6-13 Transmitting specks and interference regions for random two-dimensional deployment, vertical polarization (with RTS and CTS mechanism).

To estimate P_{Ih} in terms of $P_{Optimum}$ equation (6.3) is used with the appropriate value of path loss index based on antennas placed at a height of 6.5mm above the MDF surface (Fig 5-12), as in Table 5-1. The inhibition power corresponding to each state of the specks is represented by:

$$P_{Ih} = P_{Optimum}\left(\frac{d_{Inhibition}}{d_{Optimum}}\right)^{n} \tag{6.3}$$

Table 6-5 shows the power used in the simulation

Communication Range ($d_{Optimum}$)	Inhibition Radius (d_{Ih})	Path Loss Index (as in Chapter 5 and Table 5-1)	Power Inhibition (P_{Ih})
[cm]	[cm]		[W]
10	15	1.72	$P_{Ih} = 2.0\ P_{Optimum}$
10	20	1.72	$P_{Ih} = 3.2\ P_{Optimum}$

Table 6-5 Power values used in the simulation

6.2.4 Discussion

Fig. 6-14 and Table 6-6 shows mean SIR versus number of trials for a range of inhibition distances increasing from 15 cm to 20 cm, keeping the communicating radius fixed at 10 cm.

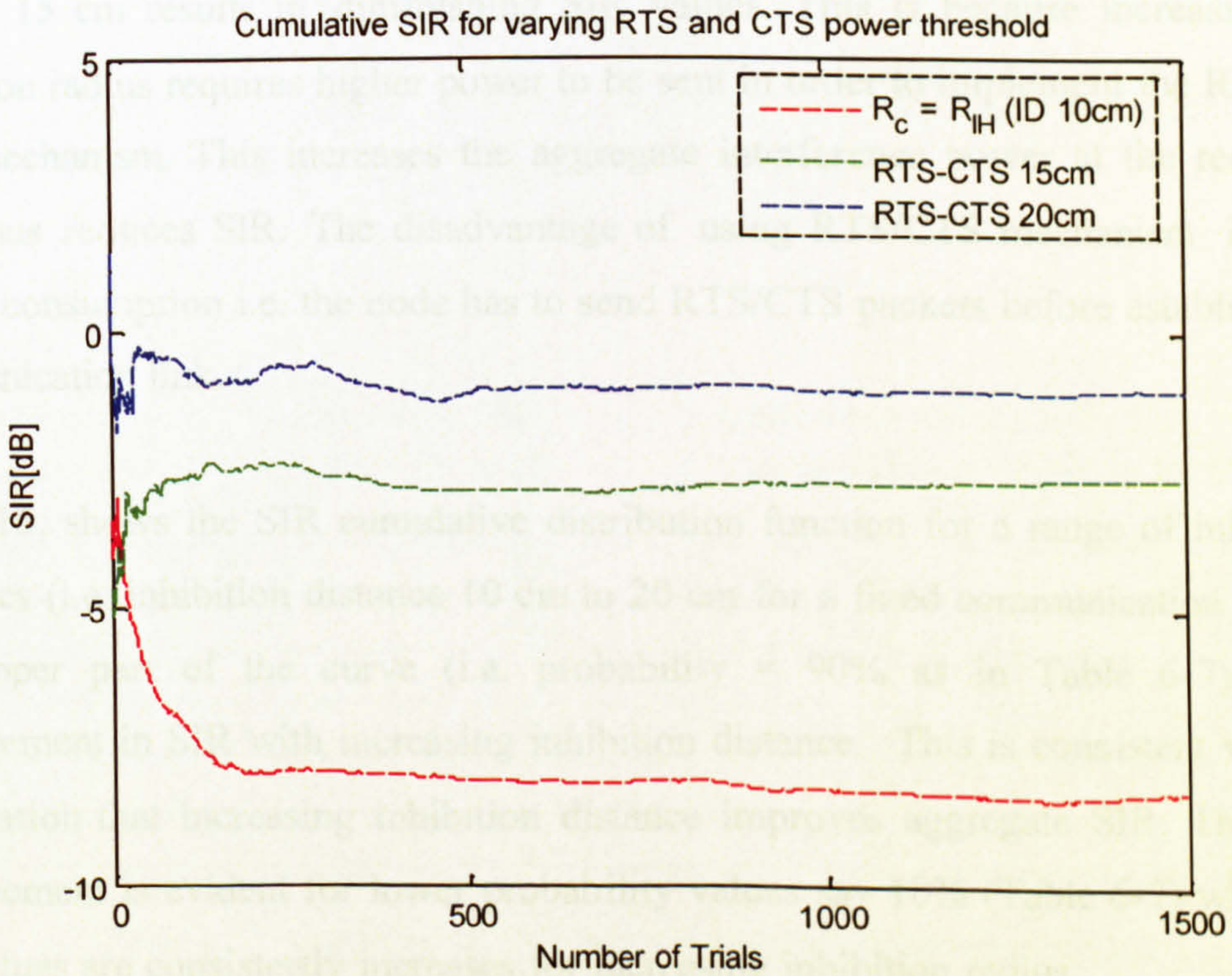

Fig. 6-14 Mean SIR versus number of trials

Inhibition Distance R_{Ih}	**SIR**	**Improvement in SIR with respect to the inhibition distance of 10 cm** (i.e. $P_{Ih} = P_{Optimum}$)
[cm]	[dB]	[dB]
10	-8.32	NA ($P_{Ih} = P_{Optimum}$)
15	-2.65	5.67 ($P_{Ih} = 2.2P_{Optimum}$)
20	-1.05	7.27 ($P_{Ih} = 3.2P_{Optimum}$)

Table 6-6 SIR for increasing inhibition distance (R_c fixed at 10 cm)

The result (in Table 6-6) represents a worst possible case of interference. Table 6-6 shows the improvement in SIR achieved by incorporating an RTS/CTS mechanism in the MAC protocol. It is observed in Table 6-6 that increasing the inhibition radius beyond 15 cm results in diminishing SIR values. This is because increasing the inhibition radius requires higher power to be sent in order to implement the RTS and CTS mechanism. This increases the aggregate interference power at the receiving node thus reduces SIR. The disadvantage of using RTS/CTS mechanism is more energy consumption i.e. the node has to send RTS/CTS packets before establishing a communication link.

Fig. 6-15, shows the SIR cumulative distribution function for a range of inhibition distances (i.e. inhibition distance 10 cm to 20 cm for a fixed communication radius). The upper part of the curve (i.e. probability = 90% as in Table 6-7) shows improvement in SIR with increasing inhibition distance. This is consistent with the observation that increasing inhibition distance improves aggregate SIR. The same improvement is evident for lower probability values say 10% (Table 6-7) where the SIR values are consistently increases for increasing inhibition radius.

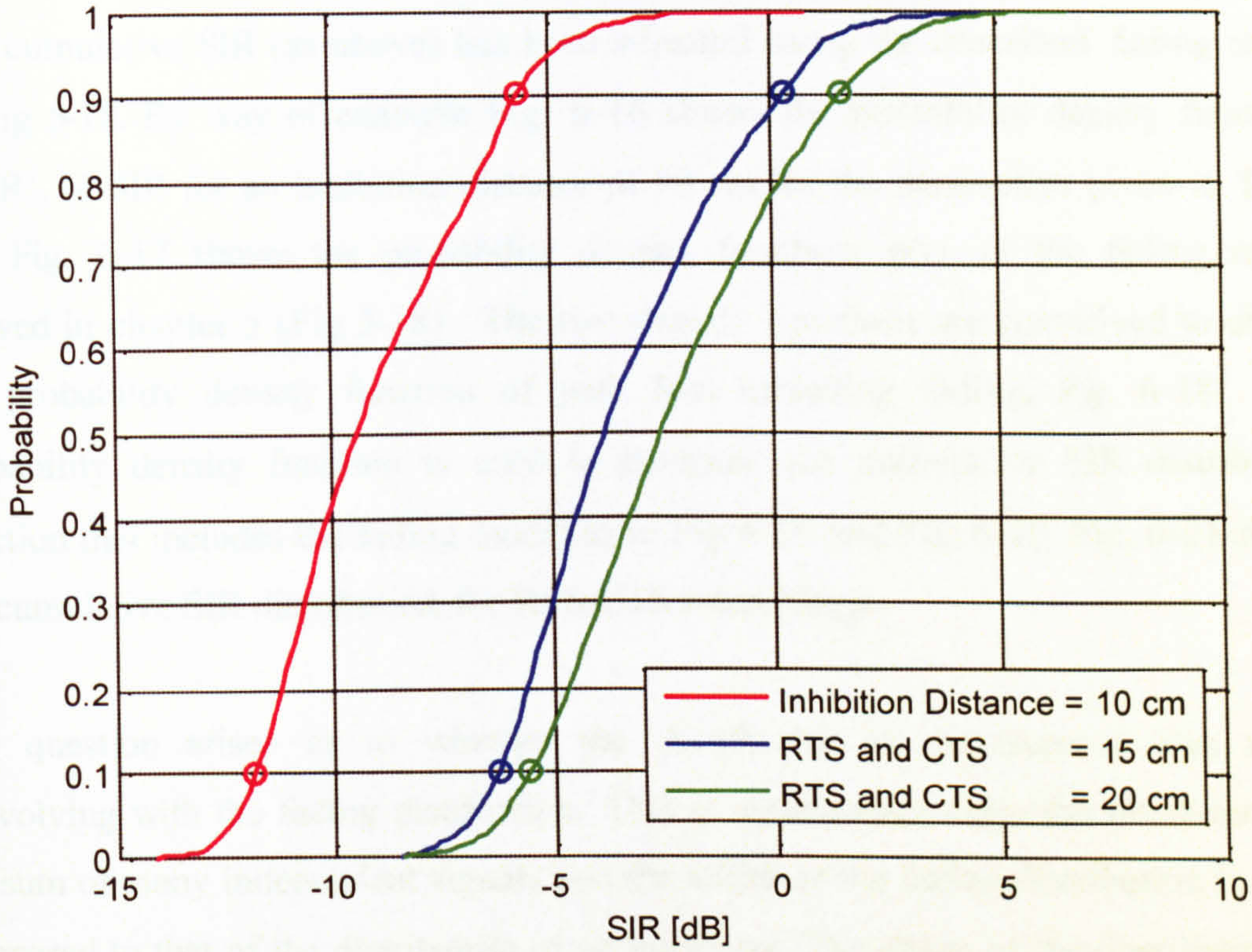

Fig. 6-15 Cumulative distribution of SIR (without fading). Keeping R_c fixed at 10 cm and varying the inhibition distance (R_{Ih}) from 15 to 25 cm.

Inhibition Distance	**Cumulative SIR** in [dB] Fig. 6-15		**Improvement in SIR with respect to inhibition distance at 10 cm**	
	10 %	90%	10%	90%
[cm]	[dB]	[dB]	[dB]	[dB]
10	-11.84	-5.70	NA	NA
15	-6.28	+0.32	+5.56	+5.38
20	-5.56	+1.58	+6.28	+7.28

Table 6-7 Cumulative SIR for increasing inhibition distance

6.3 Statistical Analysis of Channel Parameters

The cumulative SIR (as above) has been adjusted using the described fading model in Fig 5-18. By way of example Fig. 6-16 shows the probability density function, p(SIR), of SIR for an inhibition distance of 10 cm for the parameters given in Table 6-1. Fig. 6-17 shows the probability density function, p(r), of the fading model derived in chapter 5 (Fig 5-18). The two density functions are convolved to obtain the probability density function of path loss including fading, Fig. 6-18. The probability density function is used to compute the cumulative SIR distribution function that includes the fading model as in Fig 6-19 and Fig. 6-20. Fig. 6-21 shows the cumulative SIR distribution for RTS/CTS interchange.

The question arises as to whether the distribution of interference also needs convolving with the fading distribution. This is unnecessary since the interference is the sum of many independent signals and the width of the fading distribution is small compared to that of the distribution of an interferer. The shape of the distribution for each interferer is therefore changed but the increase in its width is small. The aggregate interference, however, remains Gaussianly distributed as a result of the central limit theorem irrespective of whether convolution of individual interferer PDFs with the fading PDF has been undertaken. (This is in contrast to the signal where the central limit theorem cannot be applied and the shape of the distribution is thus changed by fading.)

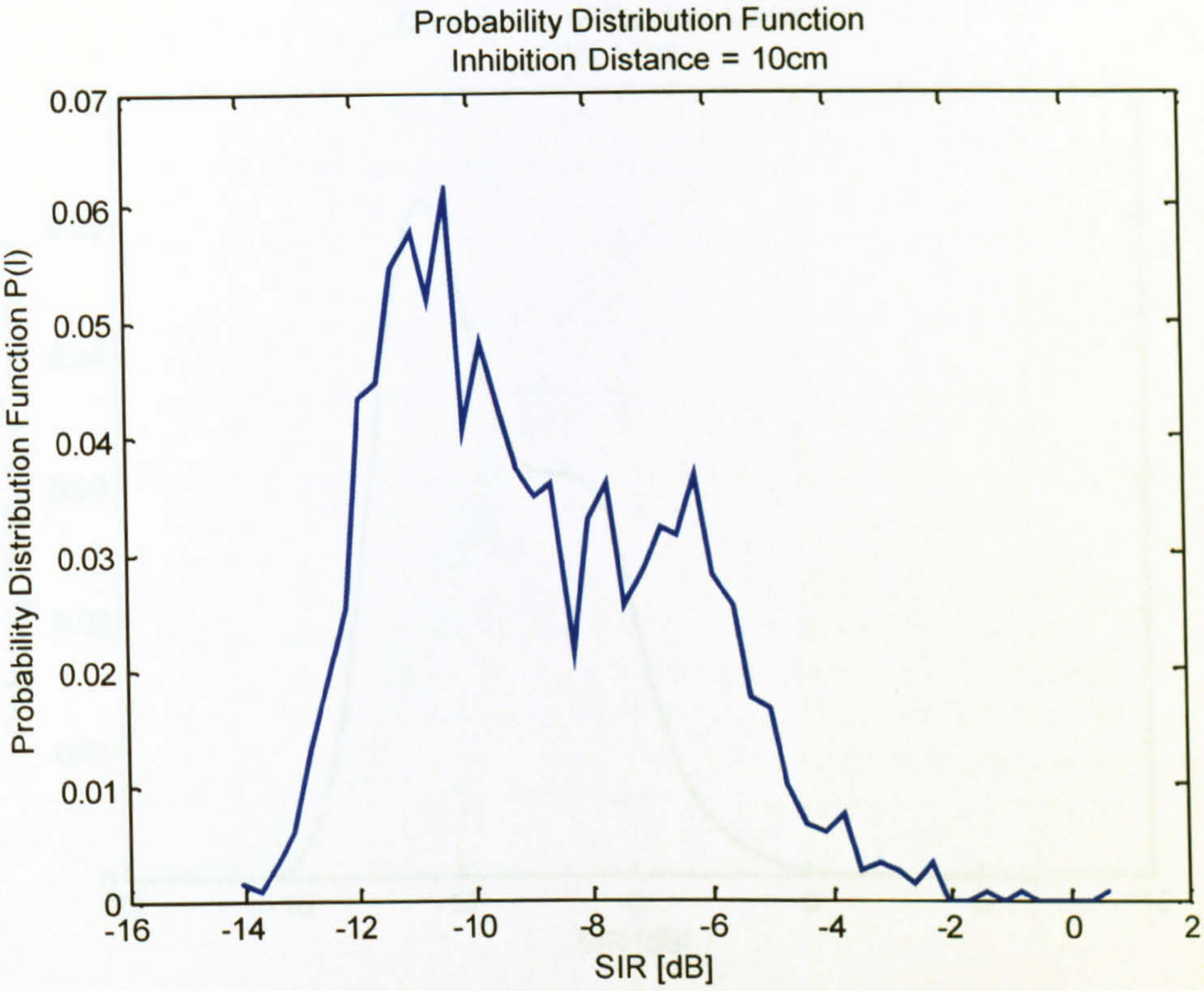

Fig. 6-16 Probability distribution of the SIR [dB]

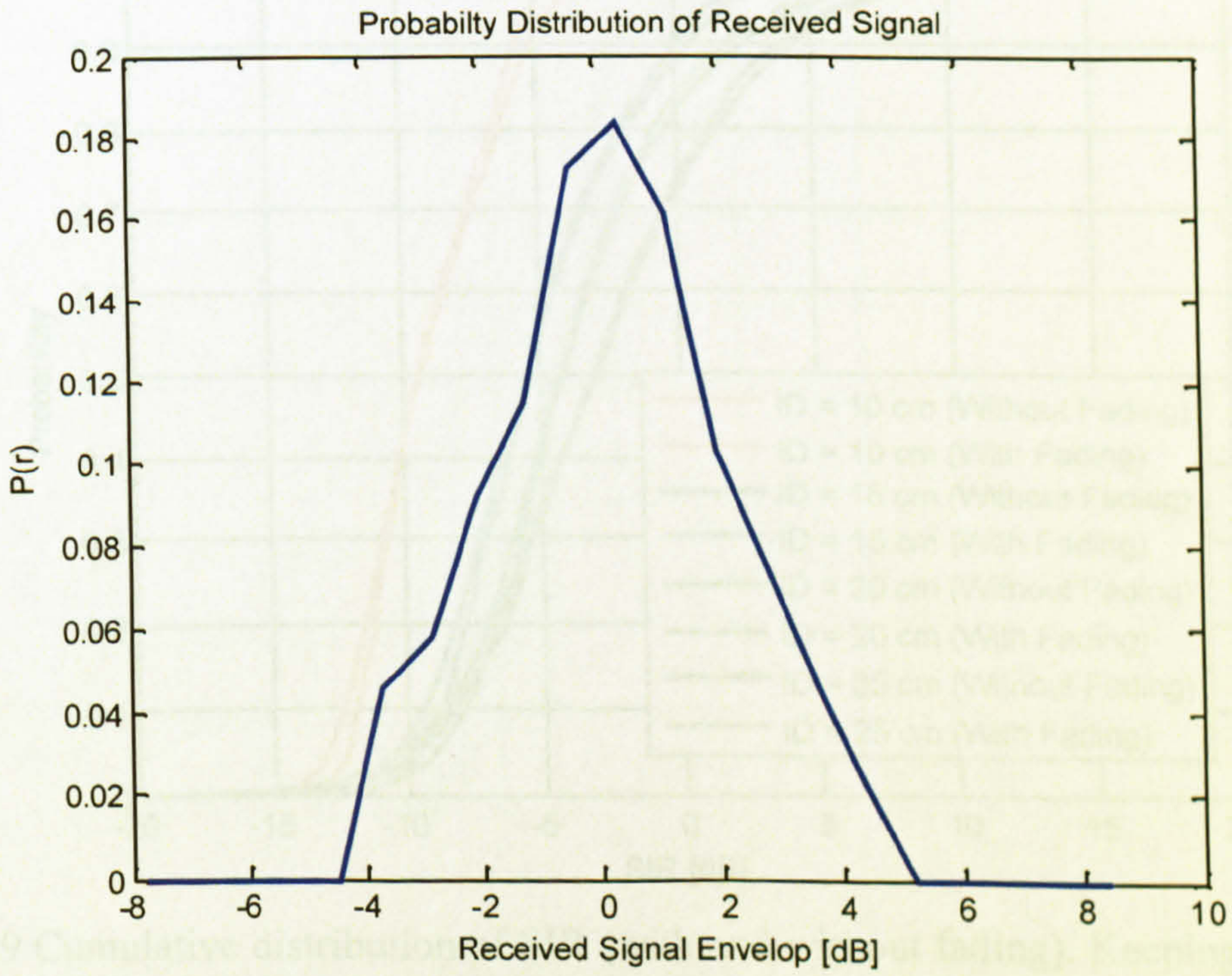

Fig. 6-17 Probability distribution of fading model

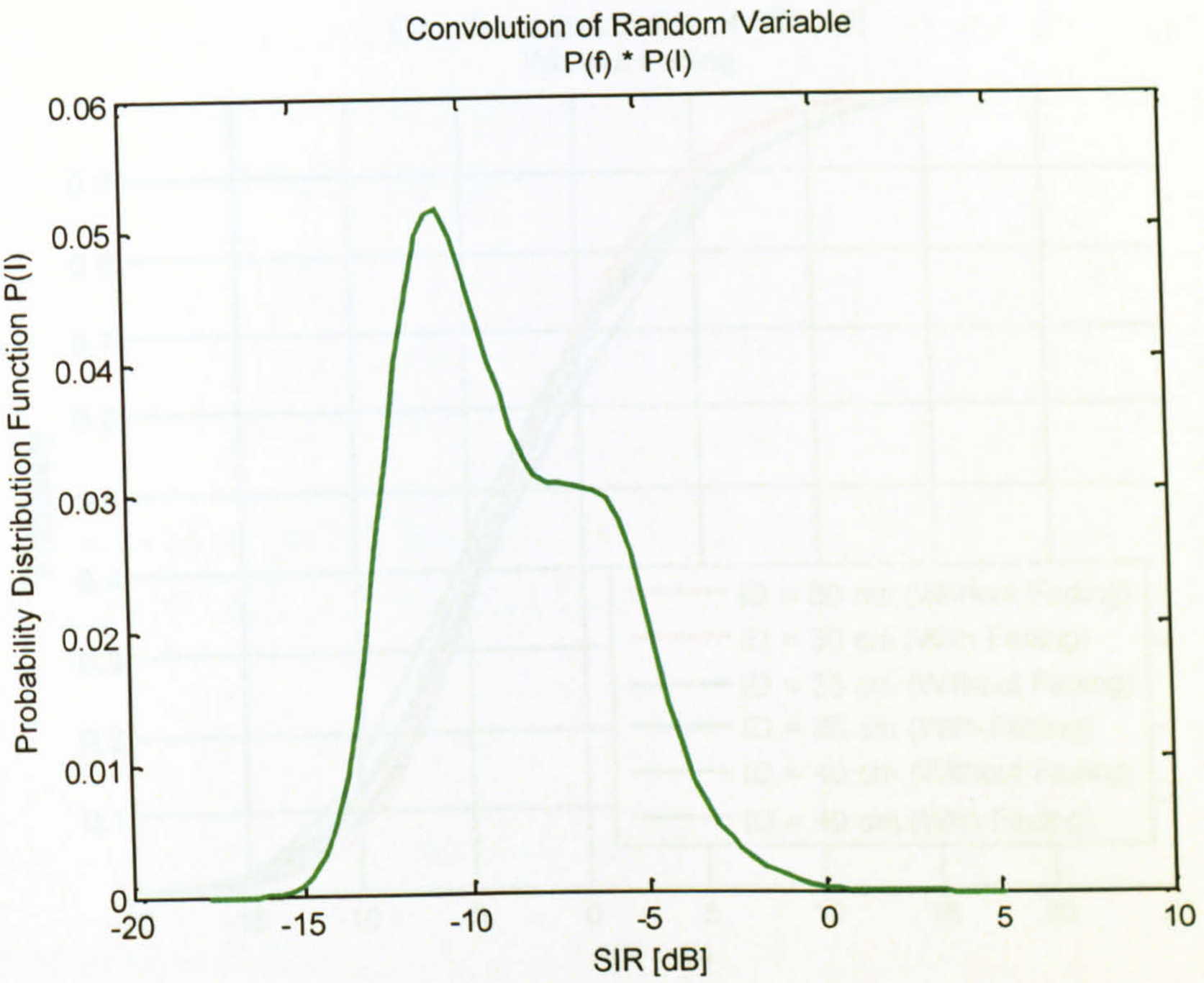

Fig. 6-18 Probability distribution of SIR including the fading model.

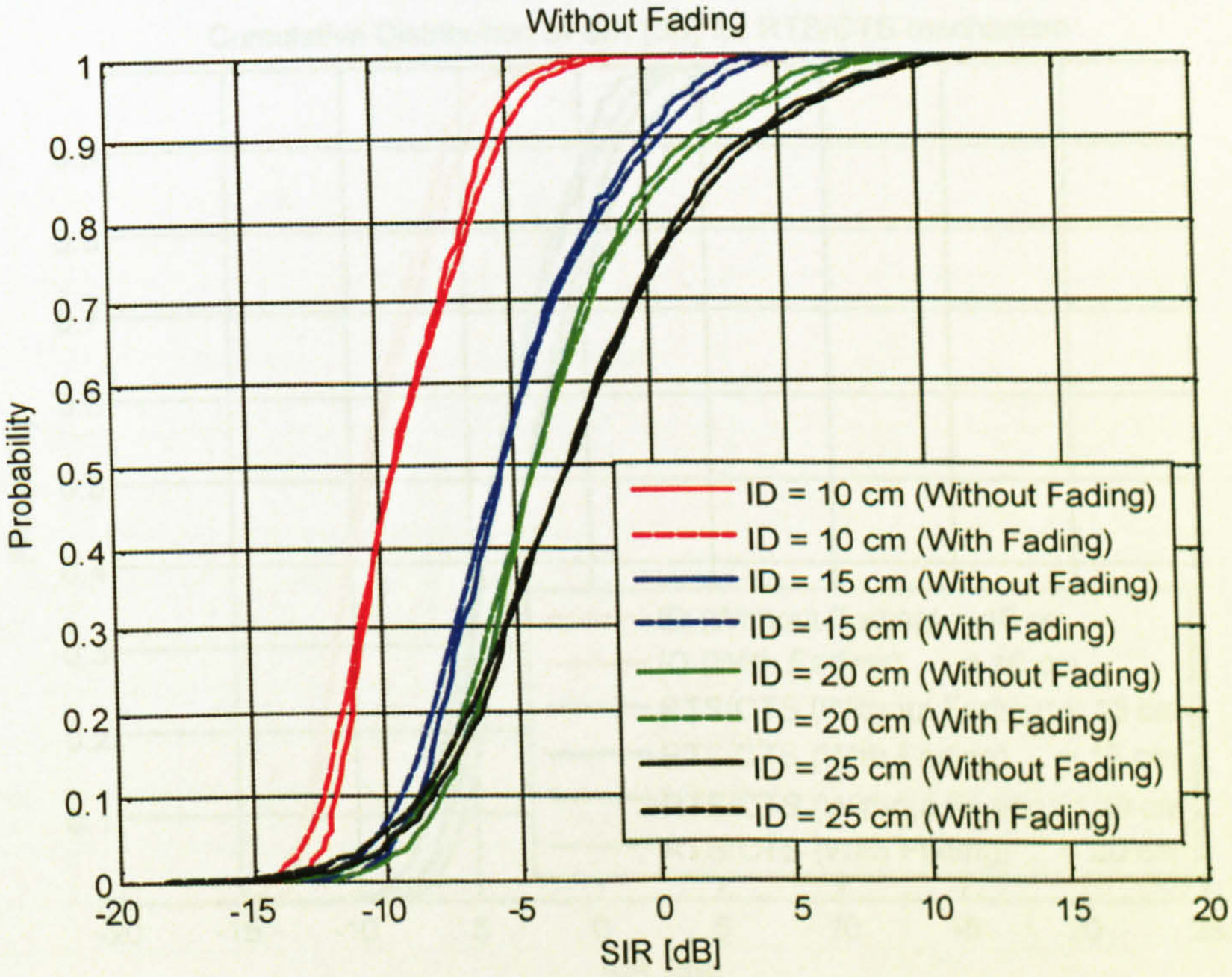

Fig. 6-19 Cumulative distribution of SIR (with and without fading). Keeping R_c fixed at 10 cm and varying the inhibition distance (R_{Ih})

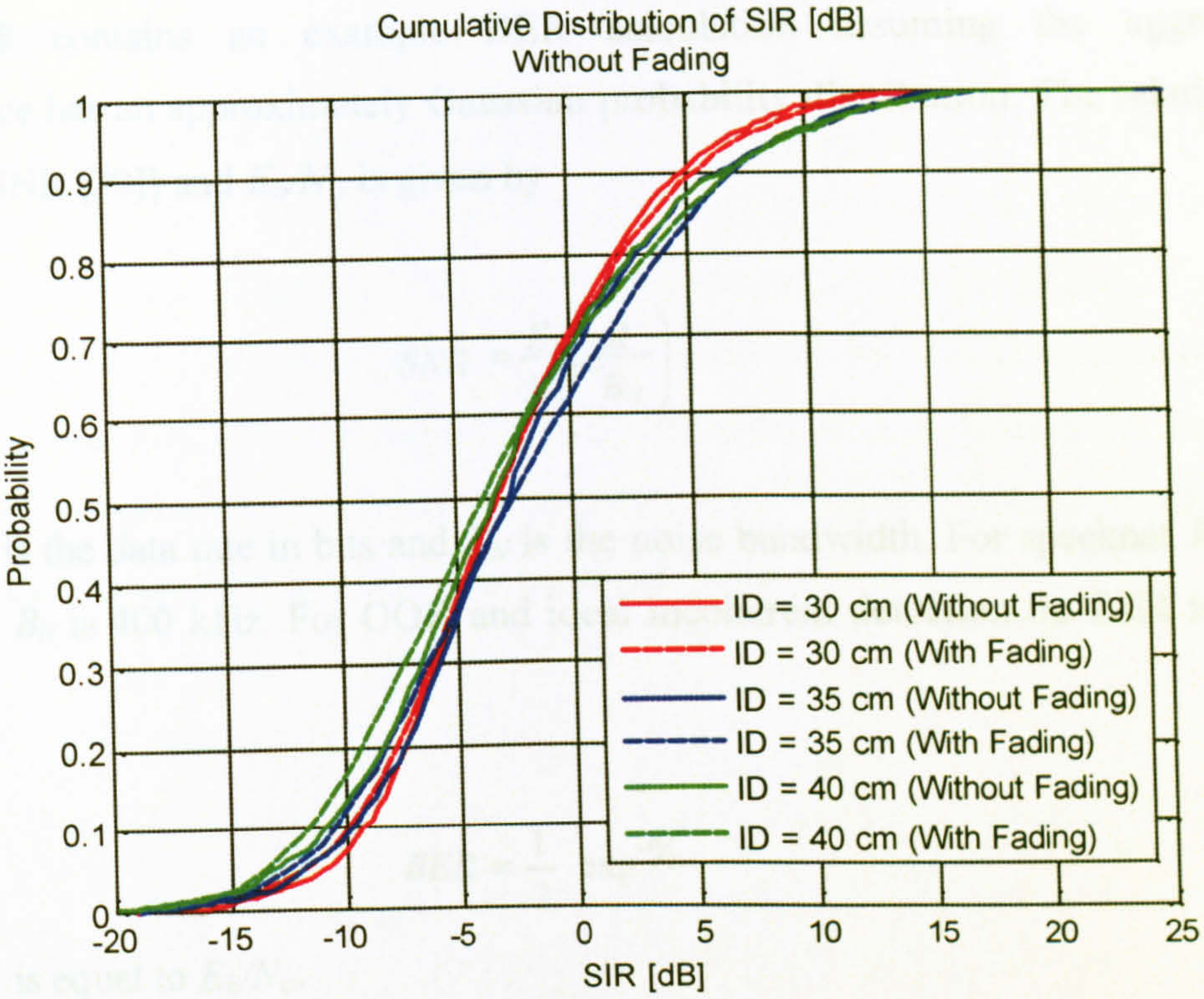

Fig. 6-20 Cumulative distribution of SIR (with and without fading). Keeping R_c fixed at 10 cm and varying the inhibition distance (R_{Ih})

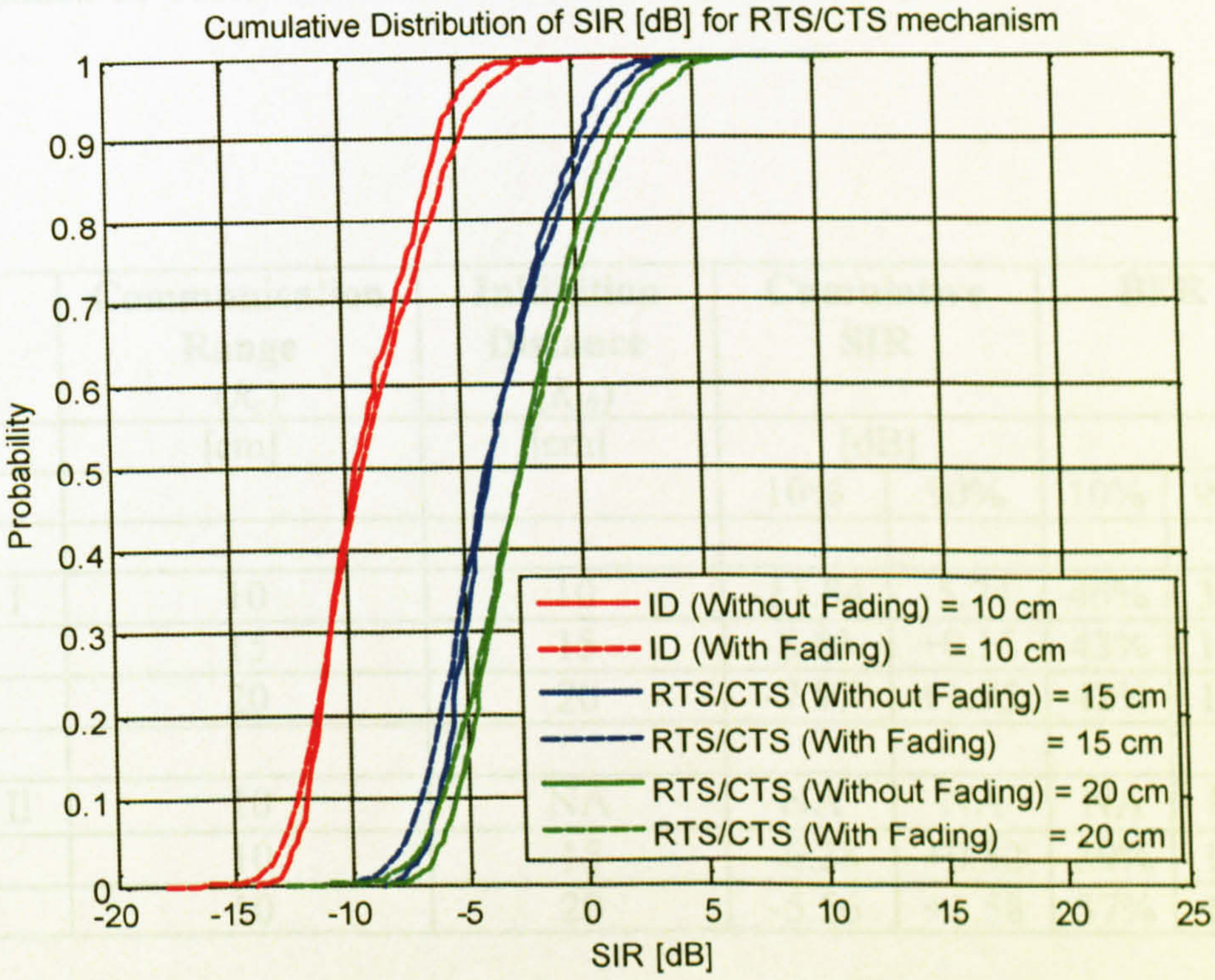

Fig. 6-21 Cumulative distribution of SIR (with and witho ut fading). Keeping R_c fixed at 10 cm and varying the inhibition distance (R_{Ih}) with RTS/CTS interchange.

Table 6-8 contains an example BER calculation assuming the aggregated interference has an approximately Gaussian probability distribution. The relationship between SNR [30]] and E_b/N_o is given by

$$SNR = \frac{E_b}{N_o}\left(\frac{R}{B_N}\right) \qquad \text{.....(6.5)}$$

Where R is the data rate in bits and B_N is the noise bandwidth. For specknet $R = 200$ kbps and B_N is 400 kHz. For OOK and ideal incoherent detection the BER is given by (6.6)

$$BER = \frac{1}{2}\ \exp^{-\alpha/2} \qquad (6.6)$$

Where α is equal to E_b/N_o.

The calculation in Table 6-8 illustrates the likely sensitivity of BER to inhibition distance.

	Communication Range (R_c)	**Inhibition Distance** (R_{Ih})	**Cumulative SIR**		**BER**	
	[cm]	[cm]	[dB]			
			10%	90%	10%	90%
Case I	10	10	-11.84	-5.74	46%	38%
	15	15	-8.83	+0.15	43%	17%
	20	20	-7.97	+1.95	42%	10%
Case II	10	NA	NA	NA	NA	NA
	10	15	-6.28	+0.32	39%	17%
	10	20	-5.56	+1.58	37%	11%

Table 6-8 Link budget calculation for BER (OOK Modulation)

6.4 Summary

The study links wireless channel characteristic (i.e. path loss and fading) and CSMA inhibition distance to (worst case) expected SIR. Two cases of CSMA are considered i.e. with and without RTS/CTS. The interference simulation proposed can be used to simulate any unsynchronised wireless sensor network by defining the path loss model, node density etc. The model predicts the SIR of a node in a decentralised dense wireless network. The model is generic and with appropriate modification could be used to simulate any wireless sensor network.

Chapter 7

7. Effect of Antenna Height and Polarisation on Short Wireless Links

7.1 Introduction

A characterization of the short range (< 100 cm) narrowband wireless channel is presented, appropriate to a dense network of wireless transceivers operating in the 2.4 GHz ISM band. Transmission loss measurements have been made in vertical and horizontal polarisations using rectaxial antennas for a range of antenna heights and separation distances. A preliminary interpretation of the results suggests that surface wave propagation may be significant for short wireless links such as might be used in sensor network applications.

7.2 Review of Existing Propagation Models

Many simulation models (e.g. Castlia [17], Avrora [47]) have been proposed to predict radio link transmission loss but these invariably have been developed for applications typified by macro-, micro-, and pico-cellular systems with path lengths greatly in excess of those being considered here. The effect of antenna heights and polarization has not been considered in these wireless channel simulators.

The propagation models used to describe indoor wireless channels can be broadly divided into free-space (Friss), the two-ray (plane-Earth) and shadowing varieties, the latter two incorporating fading due to multipath propagation. The free-space model may be adequate if line-of-sight (LOS) propagation is dominant (i.e. if multipath from environment boundaries and clutter is weak.). The path loss then

increases with distance at a rate of 6dB/octave. In a radio environment the free space path loss model (FSPL) is expressed in decibels [48] and is given by:

$$FPSL(dB) = 20\log_{10}(d) + 20\log_{10}(f) + 32.44 \qquad (7\text{-}1)$$

where f in units of MHz and d in kilometers.

The two-ray model is a more realistic if a second ray (typically reflected from a single plane surface) is significant. For path length greater than the farthest range of constructive interference, the path loss then increases with distance at a rate of 12 dB/octave. The two ray model in decibels [48] is given by the following equation.

$$P_r(dB) = P_t(dB) + 40\log_{10}(d) - 20\log_{10}(h_t) - 20\log_{10}(h_r) \qquad (7.2)$$

where d is the separation between the transmitter and receiver, h_t and h_r are the transmit and receive antenna height.

The shadowing model [3] is more complicated and considers fading effects caused by multipath mainly due to fast fading as given below.

$$P_r(dB) = PL(d) + X_\sigma = PL(d_o) + 10n\log(\frac{d}{d_o}) + X_\sigma \qquad (7.3)$$

where X_s is a zero mean Gaussian distributed random variable (in dB) with standard deviation s (in dB). Although with short ranges (as envisaged by specknet) flat fading is expected [49].

For a relatively simple indoor communication link it is common to assume free-space propagation for ranges less than d_c and two-ray propagation for ranges greater than d_c, e.g. [50]. The received power falls off with distance raised to the fourth power, or a rate of 40 dB/decades (after the cross over distance). The break-point, (d_c,), often referred to as the crossover distance, is typically given by:

$$d_c = \frac{4\pi h_t h_r}{\lambda} \tag{7.4}$$

where h_t and h_r are transmit and receive antenna heights above the plane surface, respectively, and λ is wavelength.

7.3 Methodology

The effect of antenna height has been investigated using a pair of identical rectaxial antennas [41]. An Agilent E4438C ESG vector signal generator was used as a source to generate a 2.45 GHz unmodulated carrier with a power of 0 dBm. Received power was measured using an Agilent E4440A spectrum analyzer. The measurements were carried on a plane, horizontal, surface (Fig. 7-1) of laminated chipboard (thickness, length and width 2.5 cm, 180 cm and 160 cm respectively).

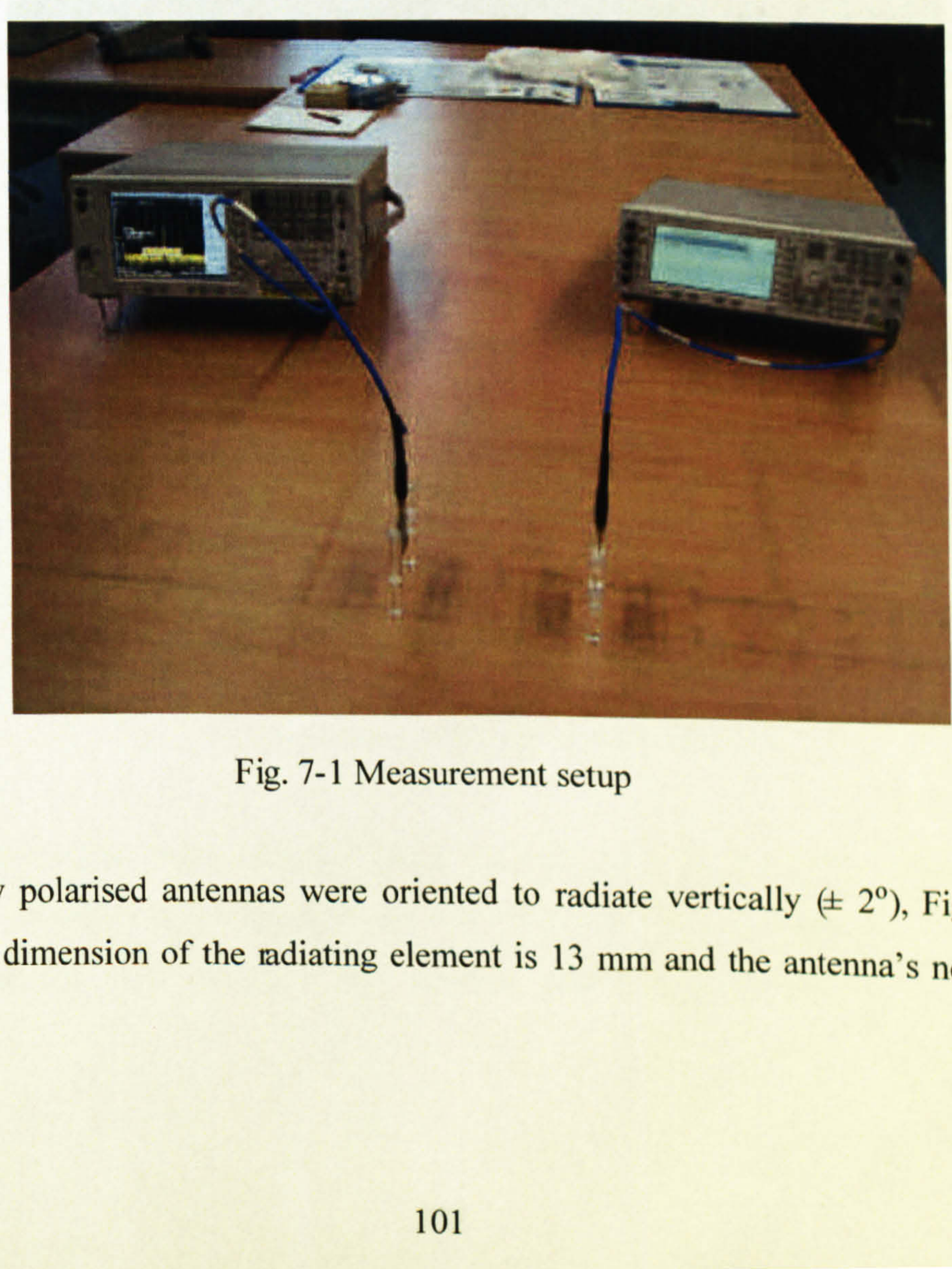

Fig. 7-1 Measurement setup

The linearly polarised antennas were oriented to radiate vertically (± 2°), Fig. 7-2. The largest dimension of the radiating element is 13 mm and the antenna's nominal

phase-centre is assumed to be located at this element's mid point. The height (h) of the antenna

above the surface is defined as that of the nominal phase centre, Fig. 7-3. The distance between transmit and receive antennas was set to 10 cm with the antenna fed from above.

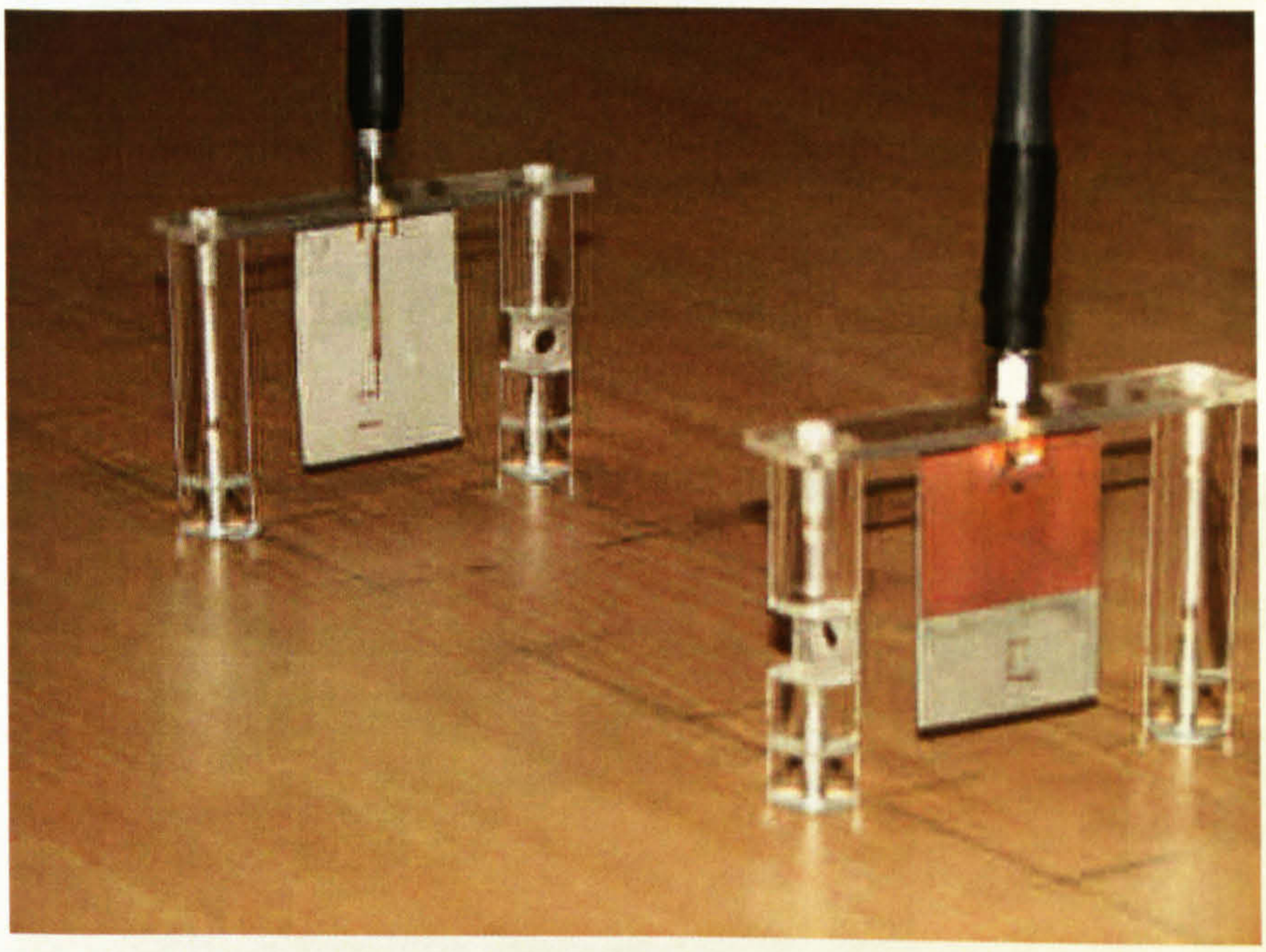

Fig. 7-2 Vertically polarised measurements

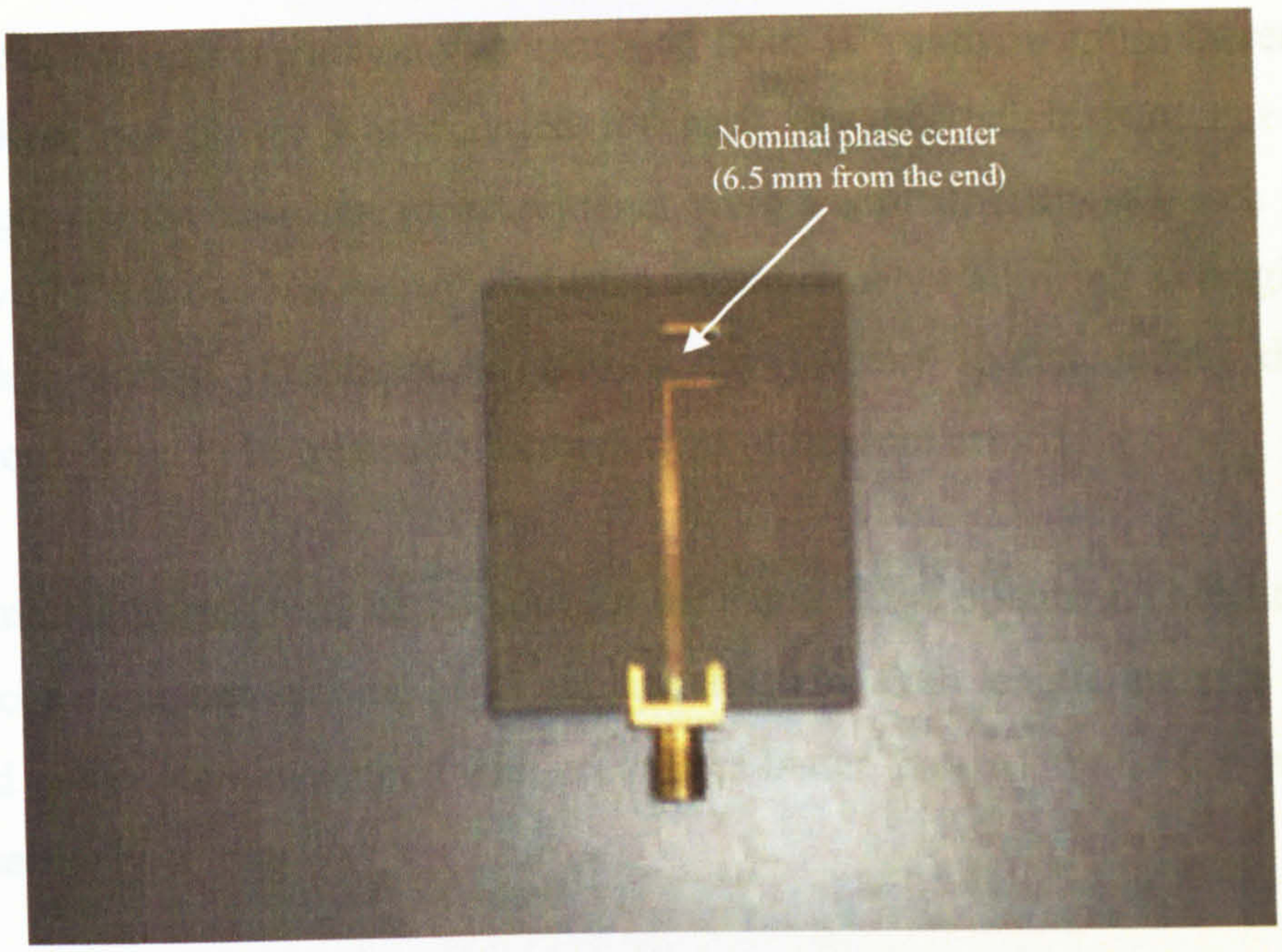

Fig. 7-3 Rectaxial Antenna

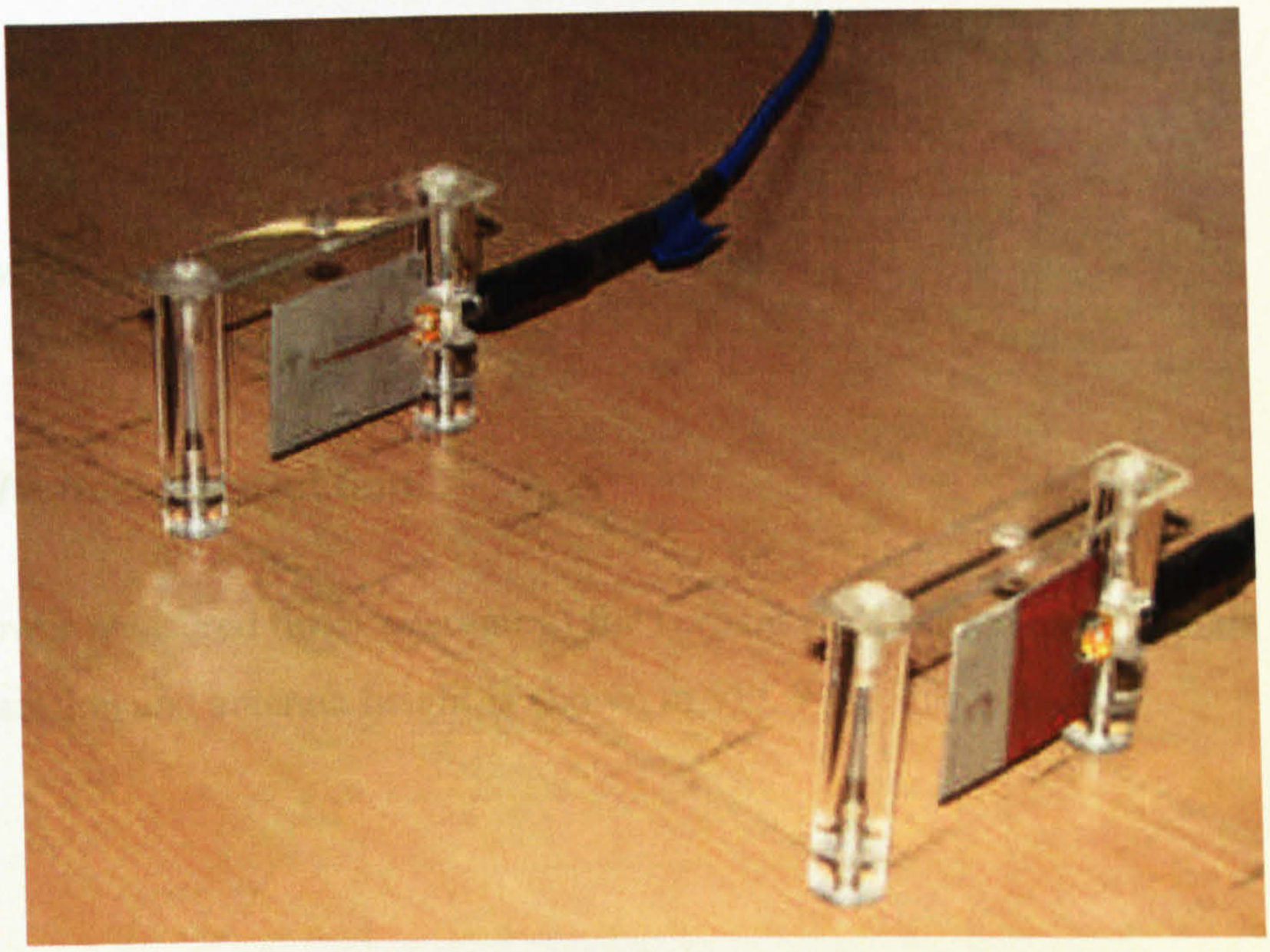

Fig. 7-4 Horizontally polarised measurements

The antenna heights were increased from 0.65 cm to 5.65 cm (since the antenna nominal phase center is 6.5 cm from the end as in Fig. 7-2), in increments of 1 cm. (The heights of both transmit and receive antennas were the same for all

measurements.) Antenna separation was increased from 10 cm to 50 cm in increments of 10 cm. Received power was recorded for each distance-height pair. For each distance-height combination ten measurements were recorded, the test-bench being displaced by at least one wavelength between measurements allowing averaging to reduce random errors. (Displacement allows any (weak) spatial fading due to multipath propagation to be treated as a component of random error.)

Additional measurements were carried out for the same range of antenna heights with transmits-receive antenna spacing of 75 cm and 100 cm. Path length, antenna height and received power were measured with accuracies better than ±1 mm, ±0.5 mm and ±1 nW, respectively.

The above procedure was then repeated with antennas oriented to radiate horizontally (± 2°) as in Fig. 7-4.

7.4 Results

The results of the measurements are summarised below.

7.4.1 Vertical Polarisation

Received power measured (after averaging) for vertical polarisation as a function of antenna separation and antenna height is shown in Fig. 7-5

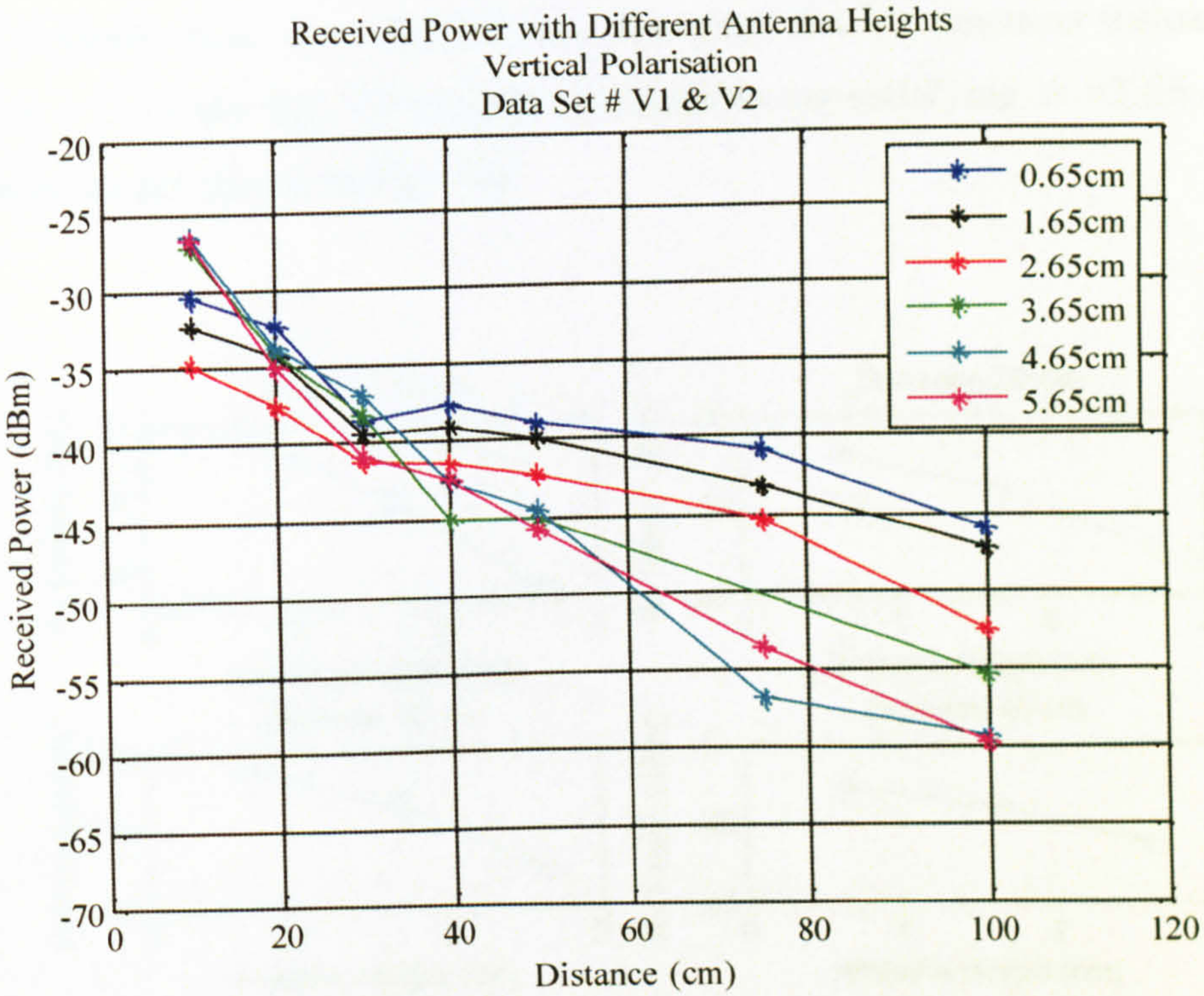

Fig. 7-5 Received power for vertically polarised antennas (total data)

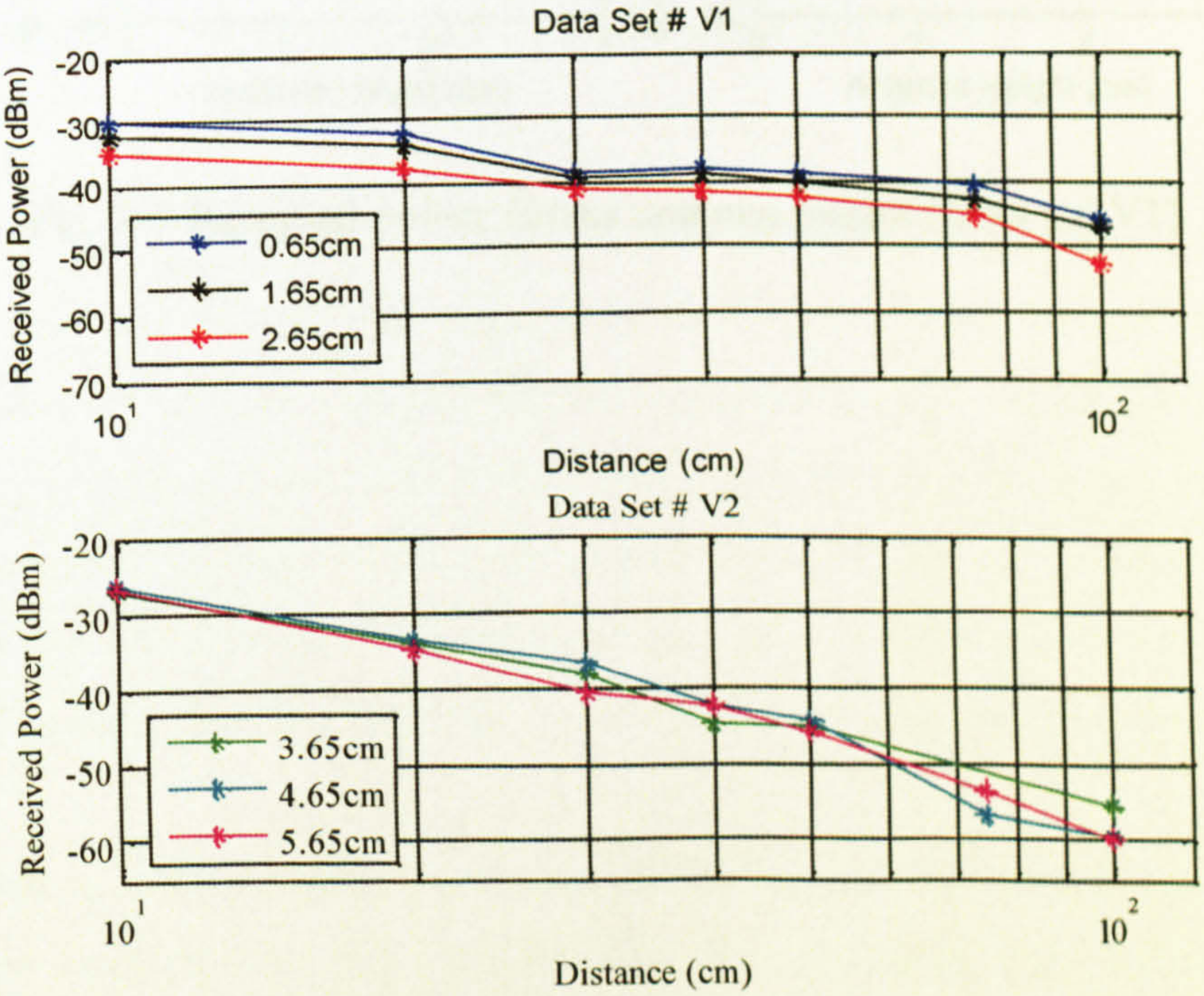

Fig. 7-6 Received power versus antenna separation and height for vertical polarisation (Data separated in to sets V1and V2 on the basis of antenna height dependence)

The measurements have been divided into two sets. Set V1 contains measurements satisfying h = 2.65 cm. Set V2 contains measurements satisfying h =3.65 cm. The data for each set are shown in Fig. 7-6.

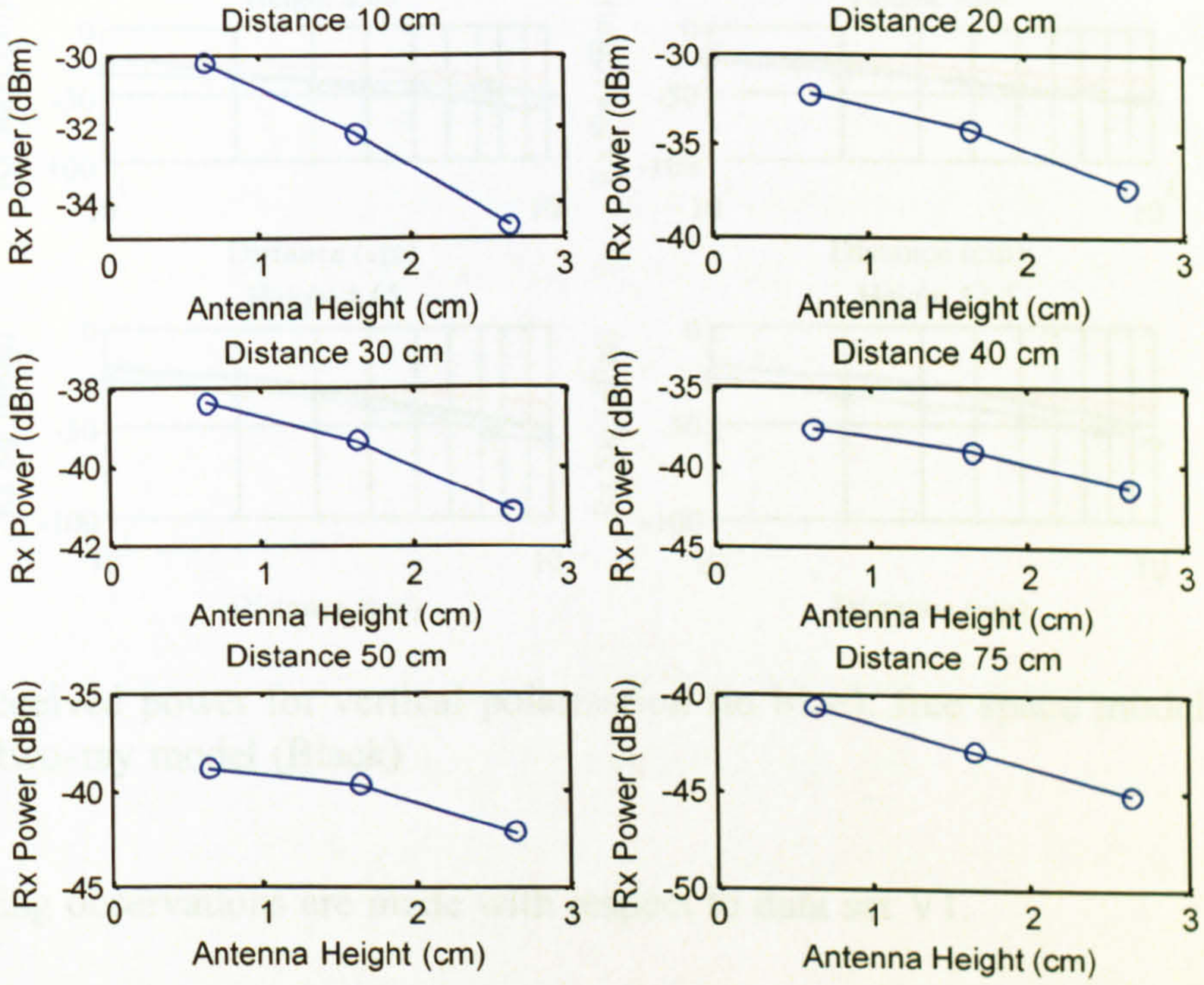

Fig. 7-7 Received power versus antenna height (Data set V1)

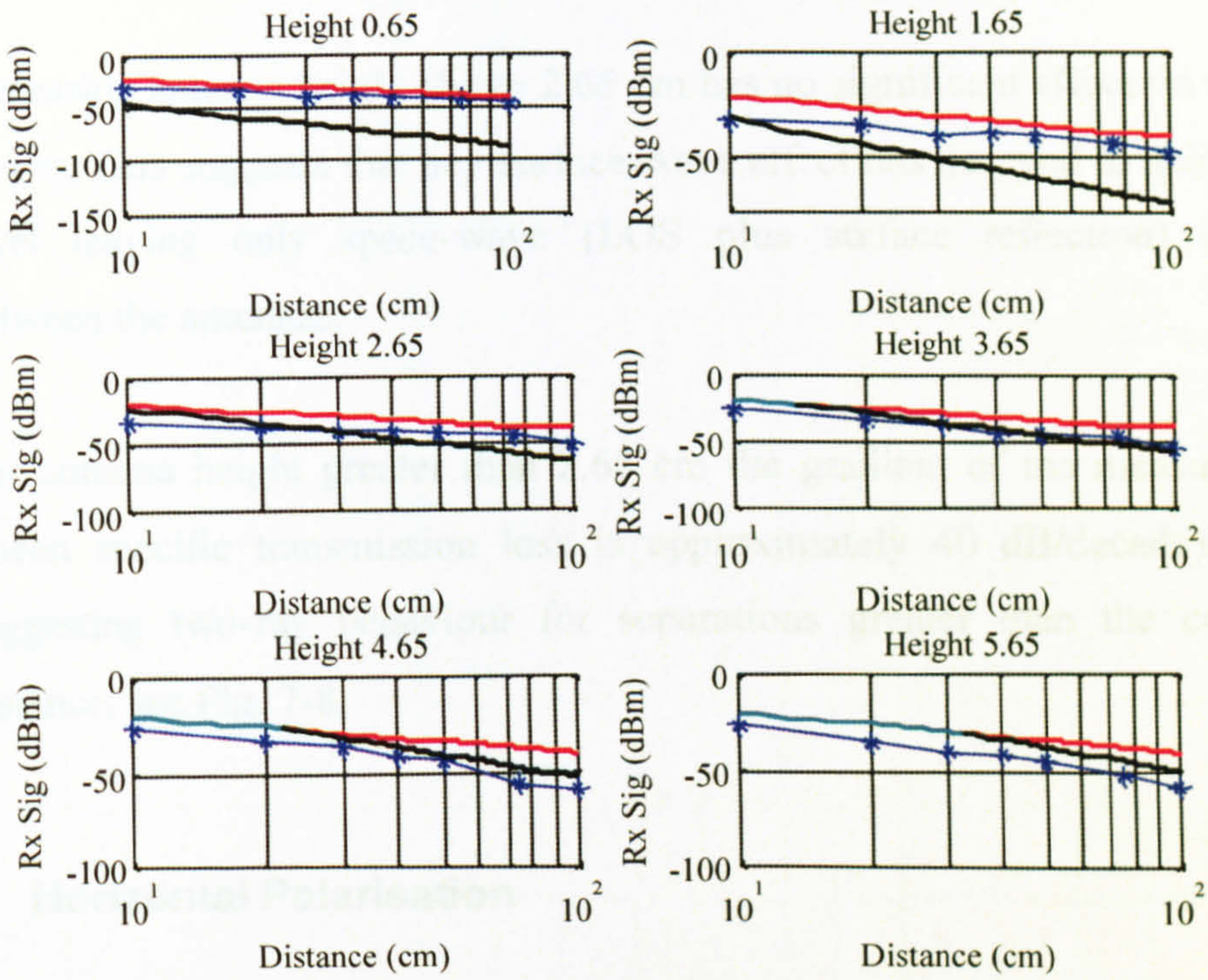

Fig. 7-8 Received power for vertical polarisation (in blue), free space model (in red and cyan), two-ray model (Black)

The following observations are made with respect to data set V1.

1. Received power decreases with increasing antenna height, see also Fig. 7-7. (A decrease in antenna height from 2.65 cm to 1.65 cm yields a power increase, averaged over all antenna separations, of 2.02 dB. A decrease in height from 1.65 cm to 0.65 cm yields a further improvement of 2.63 dB.) This might be explained by a dominant surface-wave component of coupling between the antennas which gets weaker as the antennas move farther from the surface. This interpretation is consistent with Fig. 3-4(b) (Chapter 3).

2. Mean specific transmission loss is 17.5 dB/decade between 10cm and 100cm. This suggests that for data set V1, the measured data follows, at least approximately, a free space law, i.e. 20 dB/decade, see Fig. 7-8.

The following observation is made with respect to data set V2.

1. Increasing antenna height above 2.65 cm has no significant effect on received power. This suggests that any surface-wave effect has decayed to a negligible level leaving only space-wave (LOS plus surface reflection) coupling between the antennas.

2. For antenna height greater than 2.65 cm the gradient of the measured data (mean specific transmission loss is approximately 40 dB/decade), further suggesting two-ray behaviour for separations greater than the cross-over distance, see Fig. 7-8.

7.4.2 Horizontal Polarisation

Received power measured (after averaging) for horizontal polarisation as a function of antenna separation and antenna height is shown in Fig. 7-9.

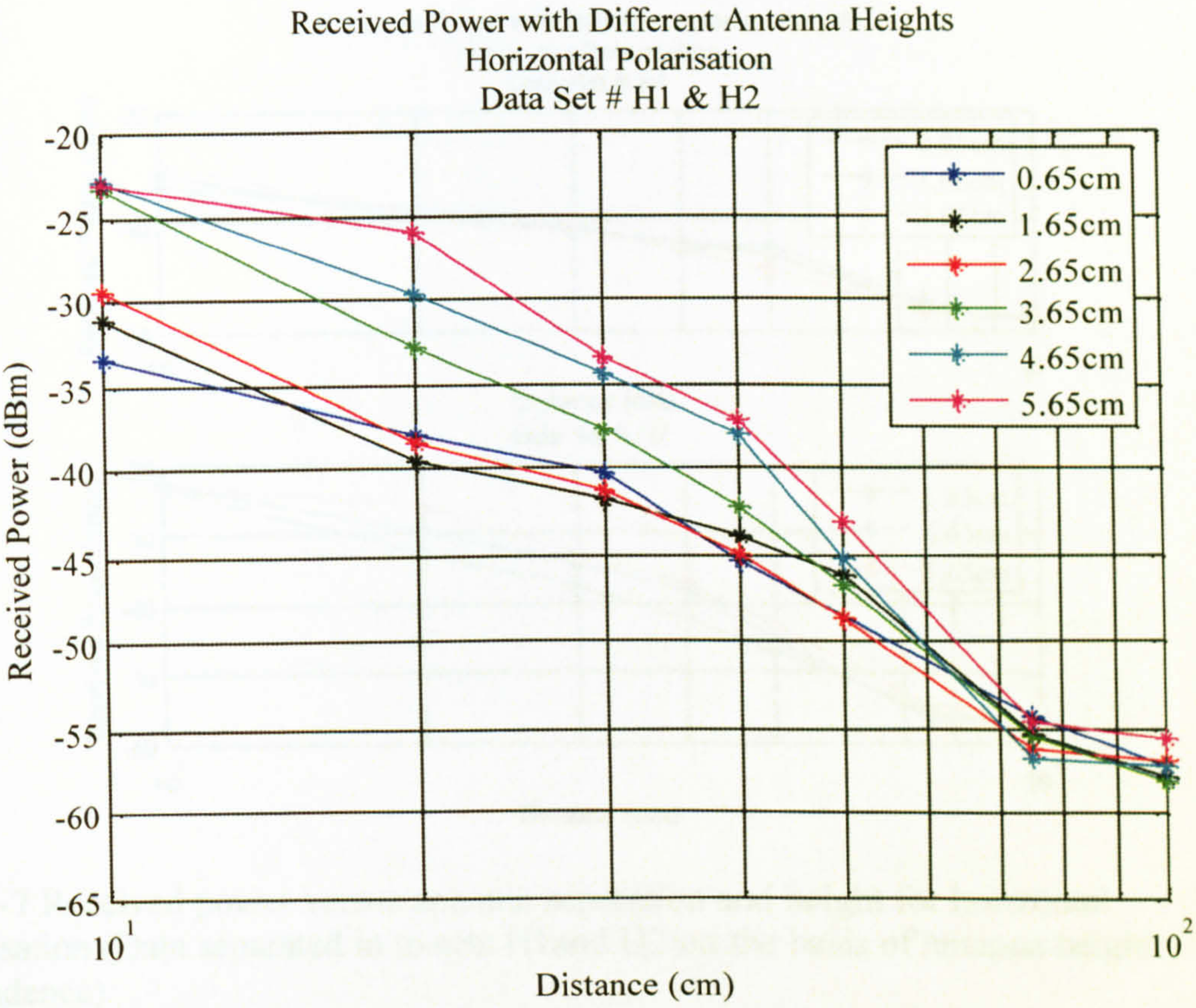

Fig. 7-9 Received power for horizontally polarised antennas (total data)

The measurements have been divided into two sets. Set H1 contains measurements satisfying $h = 2.65$ cm. Set H2 contains measurements satisfying 3.65 cm = h. The data for each set are shown in Fig. 7-10.

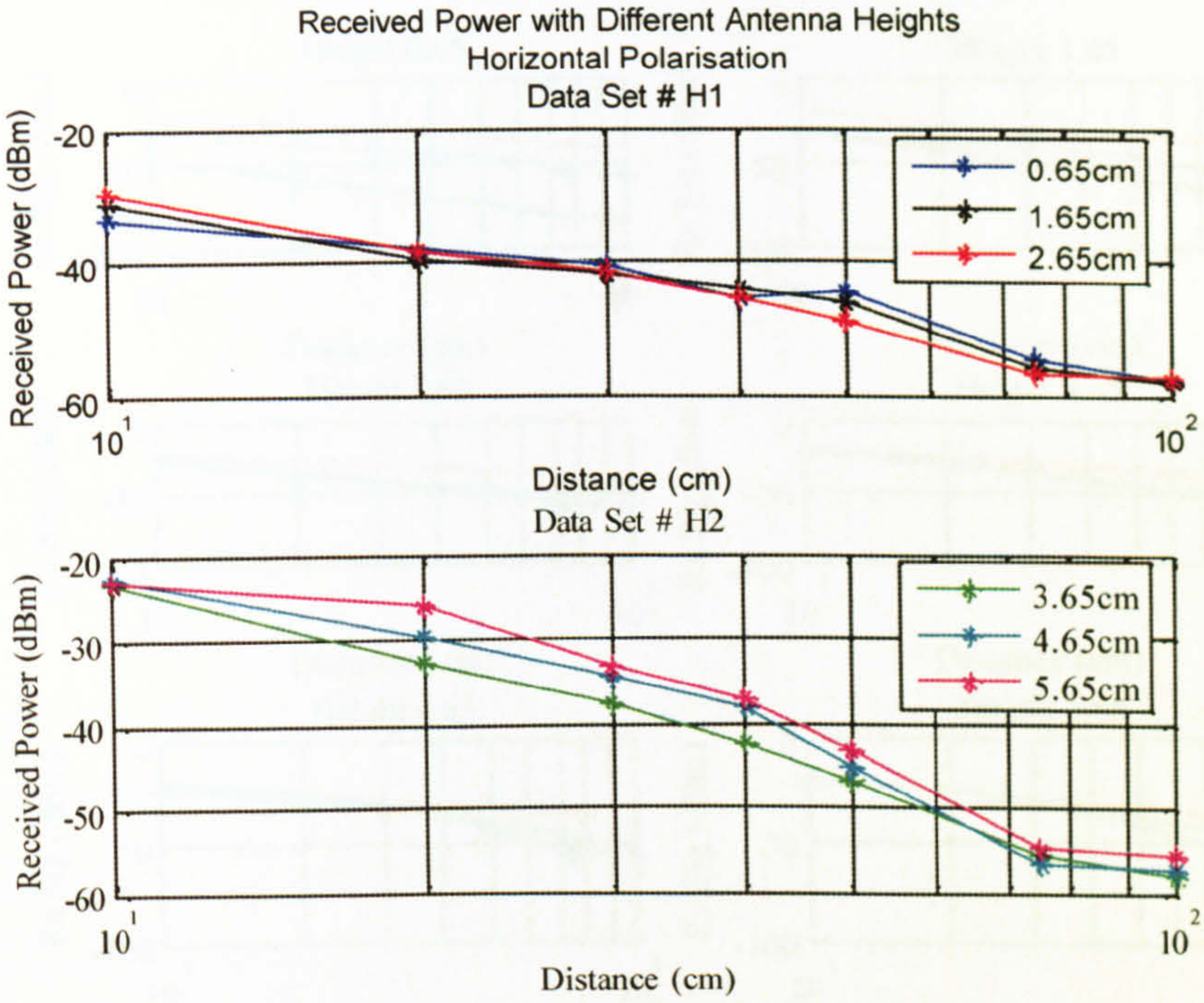

Fig. 7-7 Received power versus antenna separation and height for horizontal polarisation (Data separated in to sets H1and H2 on the basis of antenna height dependence)

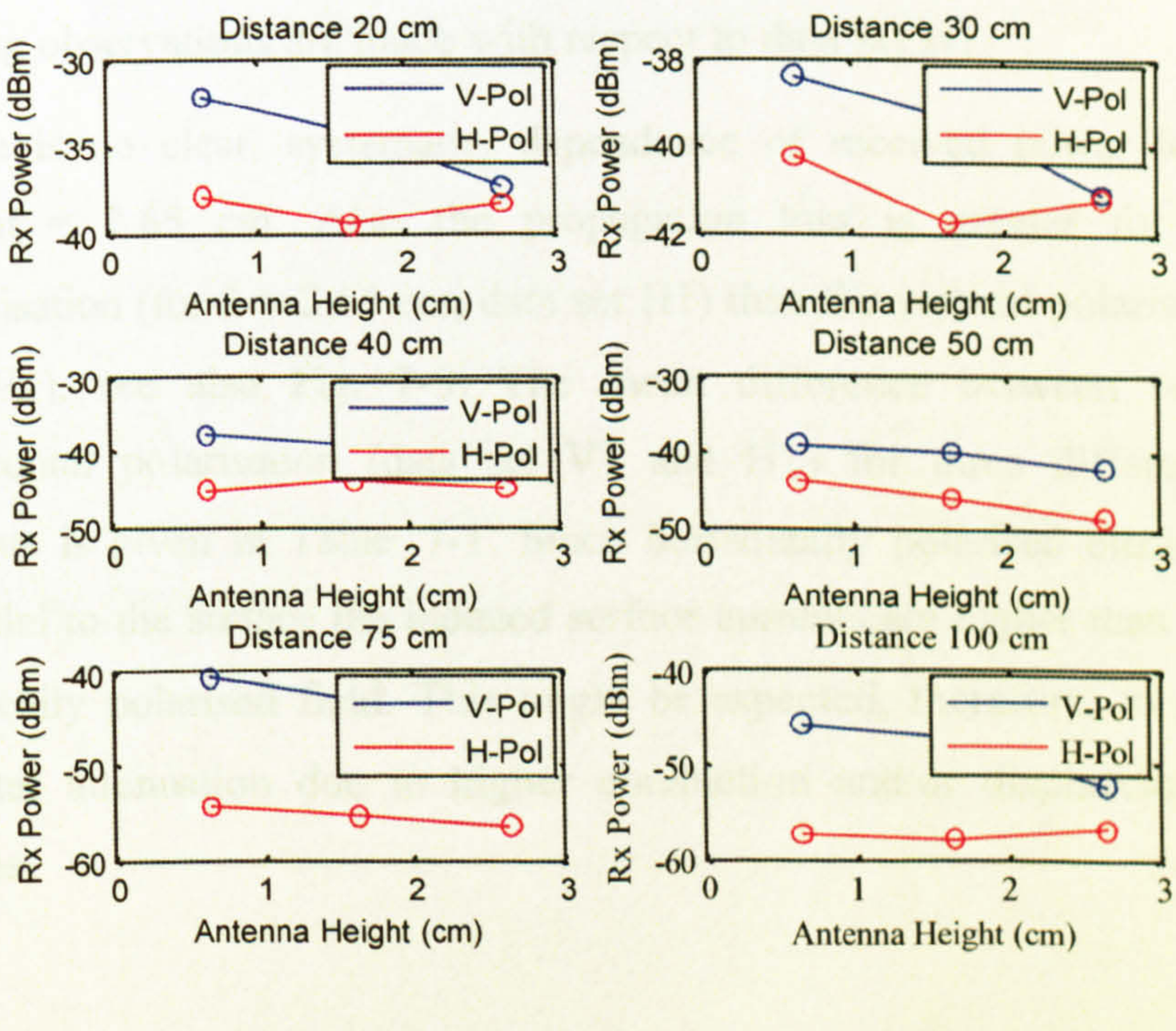

Fig. 7-8 Received power for vertical and horizontal polarisation (date set V1 and H1).

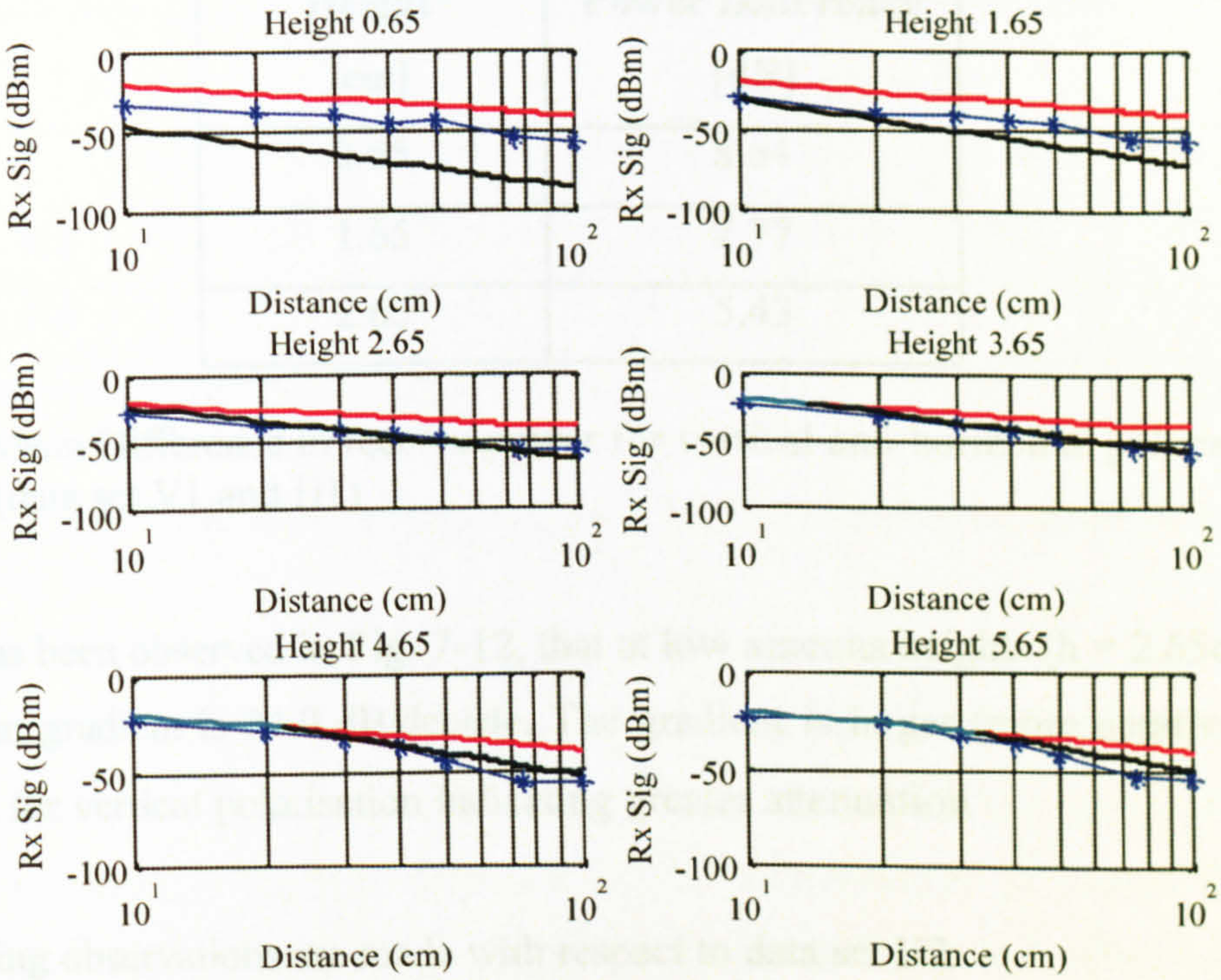

Fig. 7-9 Measured powers for horizontal polarisation (in blue), free space model (in red and cyan), Two Ray model (Black)

The following observations are made with respect to data set H1.

1. There is no clear, systematic, dependence of received power for antenna height = 2.65 cm. Also the propagation loss is greater for horizontal polarisation (for h = 2.65 cm, data set H1) than for vertical polarisation (data set V1), see also Fig. 7-9. The mean difference between vertical and horizontal polarisation (data set V1 and H1) for three different antenna heights is given in Table 7-1. Since horizontally polarised electric field is parallel to the surface the induced surface currents are higher than those for a vertically polarised field. This might be expected, therefore, to give rise to greater attenuation due to higher conduction and/or displacement current losses.

Height [cm]	Power Difference [dB]
0.65	8.64
1.65	7.77
2.65	5.43

Table 7-1 Mean Difference in receive power for vertical and horizontal polarisation (data set V1 and H1)

2. It has been observed in Fig. 7-12, that at low antenna heights (h = 2.65cm) the mean gradient is 24.0 dB/decade. The gradient is larger (more negative) than that for vertical polarisation indicating greater attenuation.

The following observations are made with respect to data set H2.

The losses generally increase as transmit and receive antenna heights are reduced until height = 3.65cm. (This is not true for the shortest path length, i.e. 10cm.)

1. For antenna heights = 2.65cm, the gradient for separations greater than the cross-over distance (42.0 dB/decade) suggests a two-ray model.

2. Received power averaged over antenna height is less for data set H1 than for data set H2. This suggests an increasing propagation loss with decreasing height for horizontal polarisation as in Table 7-2.

Data Set	Average Received Relative Power [dB]					
	10 cm	20 cm	30 cm	40 cm	50 cm	100 cm
H1	-30.9	-38.3	-41.2	-44.6	-45.8	-57.3
H2	-23.0	-28.5	-30.6	-38.5	-44.7	-56.9
Difference	7.9	9.8	10.2	6.1	1.2	0.4

Table 7-2 Average difference in receive power for horizontal polarisation (Data set H1 and H2)

3. The spread of received power for various antenna heights decreases with increasing antenna separation (Table 7-3). This may reflect the diminishing surface-wave effect with distance. If this interpretation is correct then for antenna separations greater than 50 cm, the surface-wave effect could be neglected, see Fig. 7-10.

Antenna Height [cm]	Separation Distance [cm]	Standard Deviation [dB]
0-5	10	4.67
0-5	20	5.49
0-5	30	3.61
0-5	40	3.57
0-5	50	1.98
0-5	75	0.92
0-5	100	0.87

Table 7-3 Standard deviation for horizontal measurement

4. The average received power for data set V2 and H2 indicates that as the antenna heights is increased (for antenna heights > 2.65 cm) the received power is larger (less losses) for horizontal polarization as compared to

vertical polarization as in Table 7-4 (The observation is constituent with [51]) The average difference in received power is quite significant for separation distances less than 50 cm.

Data Set	Average Received Relative Power [dB]					
	10cm	20 cm	30 cm	40 cm	50 cm	100 cm
V2	-26.5	-34.1	-38.2	-43.1	-45.1	-57.8
H2	-23.0	-28.5	-30.6	-38.5	-44.7	-56.9
Difference [dB]	3.5	5.6	7.6	4.6	0.4	0.9

Table 7-4 Average difference in receive power for vertical and horizontal polarisation (Data set V2 and H2)

7.5 Summary

The study has related transmission loss to antenna height and polarisation for short wireless links as envisaged in sensor networks. Since wireless sensor nodes in future are small and are likely to be deployed close to surfaces, significant improvement in received power can be achieved by appropriate selection of antenna height. It has been revealed that Vertical polarisation results in smaller transmission loss than horizontal polarisation for short wireless links and when the antenna height is small (< 2.65cm). For greater antenna heights (> 2.65 cm) and smaller node separation horizontal polarisation results in smaller transmission loss than vertical polarisation.

Chapter 8

8. Polarisation Considerations

A study of polarisation considerations for short wireless links is presented. The study divided in to two parts. The first part deals with polarisation loss due to mismatch between transmit and receive antennas. The second part deals with polarisation loss due to a cross-polarising medium.

8.1 Polarisation Loss due to Antennas

The polarisation of the field propagating away from a transmitting antenna in a particular direction depends, in general, on the direction of propagation. The polarisation between a pair of antennas in free space depends on the polarisation states of the antennas in the directions defined by the line-of-sight (LOS) path connecting them.

In case of Specknet the nodes are randomly deployed (in orientation as well as location). This results in a random polarisation state in the LOS direction (Of course the polarisation pdf may be tightly concentrated around the nominal design polarisation of the antenna.) Each polarisation state corresponds to a unique combination of axial ratio and tilt angle. This pair of parameters can be used to calculate the antenna polarisation mismatch loss. The polarisation state of a node can therefore be modelled as a random variable whose value could be based either on an idealised model of the polarisation pattern of the antenna or on the measured polarisation pattern of a real antenna representative of those that are likely to be used by sensor network transceivers. In order to quantify the expected polarisation mismatch loss for Specknet the second approach has been used. A commercially available patch antenna is assumed and interpolated measurements of the antenna's

measured (but incomplete) polarisation characteristics used in the simulations described in the following section.

8.1.1 Polarisation Loss Model

The proposed model is based on a commercially available ceramic patch antenna [52]. Fig. 8-1 shows the vertically and horizontally polarised patterns for three mutually orthogonal plane cuts through the three dimensional radiation pattern. The patterns are measured at frequencies of 2.4 GHz (red), 2.44 GHz (green) and 2.485 GHz (blue). The simulations that follow are for a narrowband signal at a frequency 2.44 GHz.

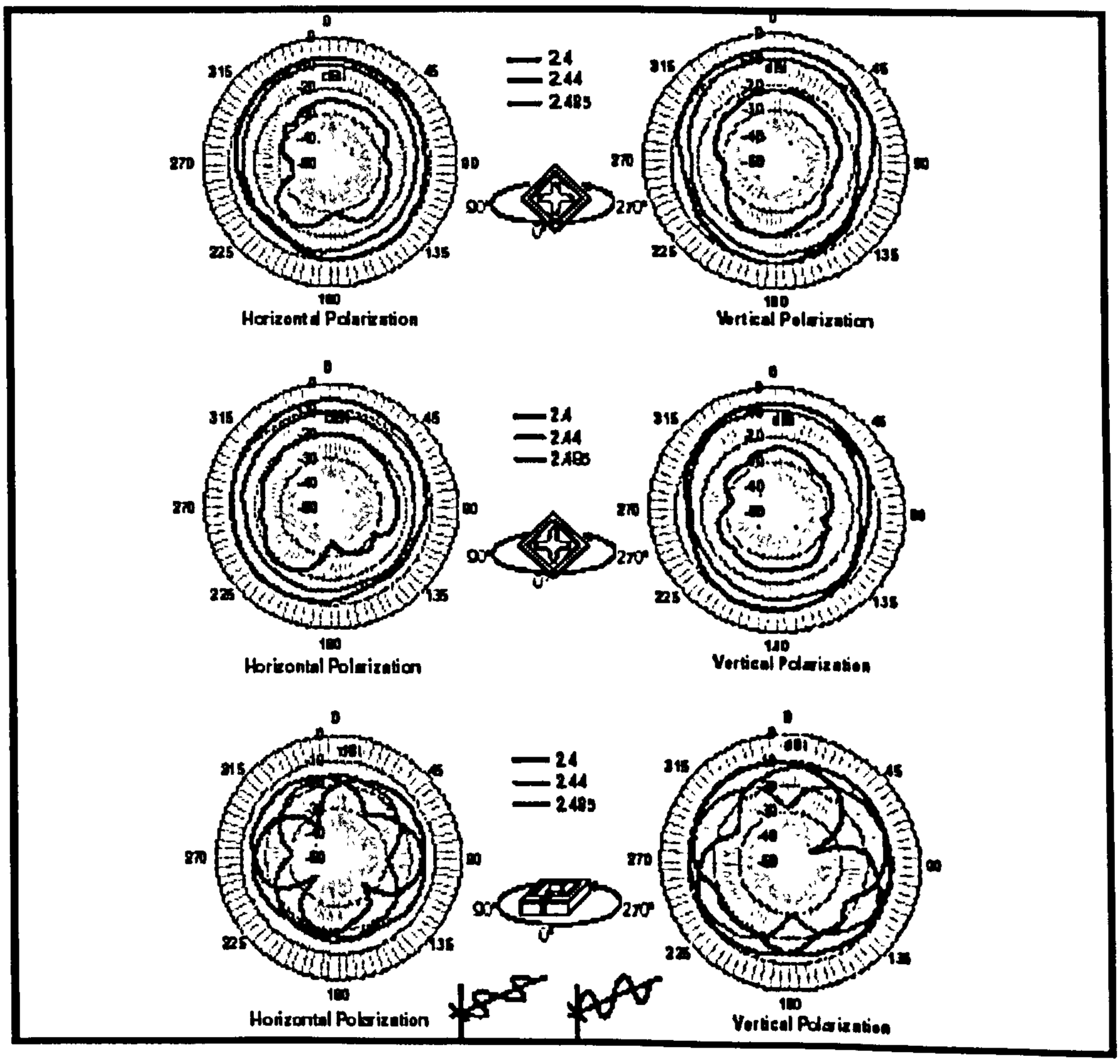

Fig. 8-1 Measured radiation patterns of practical antenna for three different antenna

measured (but incomplete) polarisation characteristics used in the simulations described in the following section.

8.1.1 Polarisation Loss Model

The proposed model is based on a commercially available ceramic patch antenna [52]. Fig. 8-1 shows the vertically and horizontally polarised patterns for three mutually orthogonal plane cuts through the three dimensional radiation pattern. The patterns are measured at frequencies of 2.4 GHz (red), 2.44 GHz (green) and 2.485 GHz (blue). The simulations that follow are for a narrowband signal at a frequency 2.44 GHz.

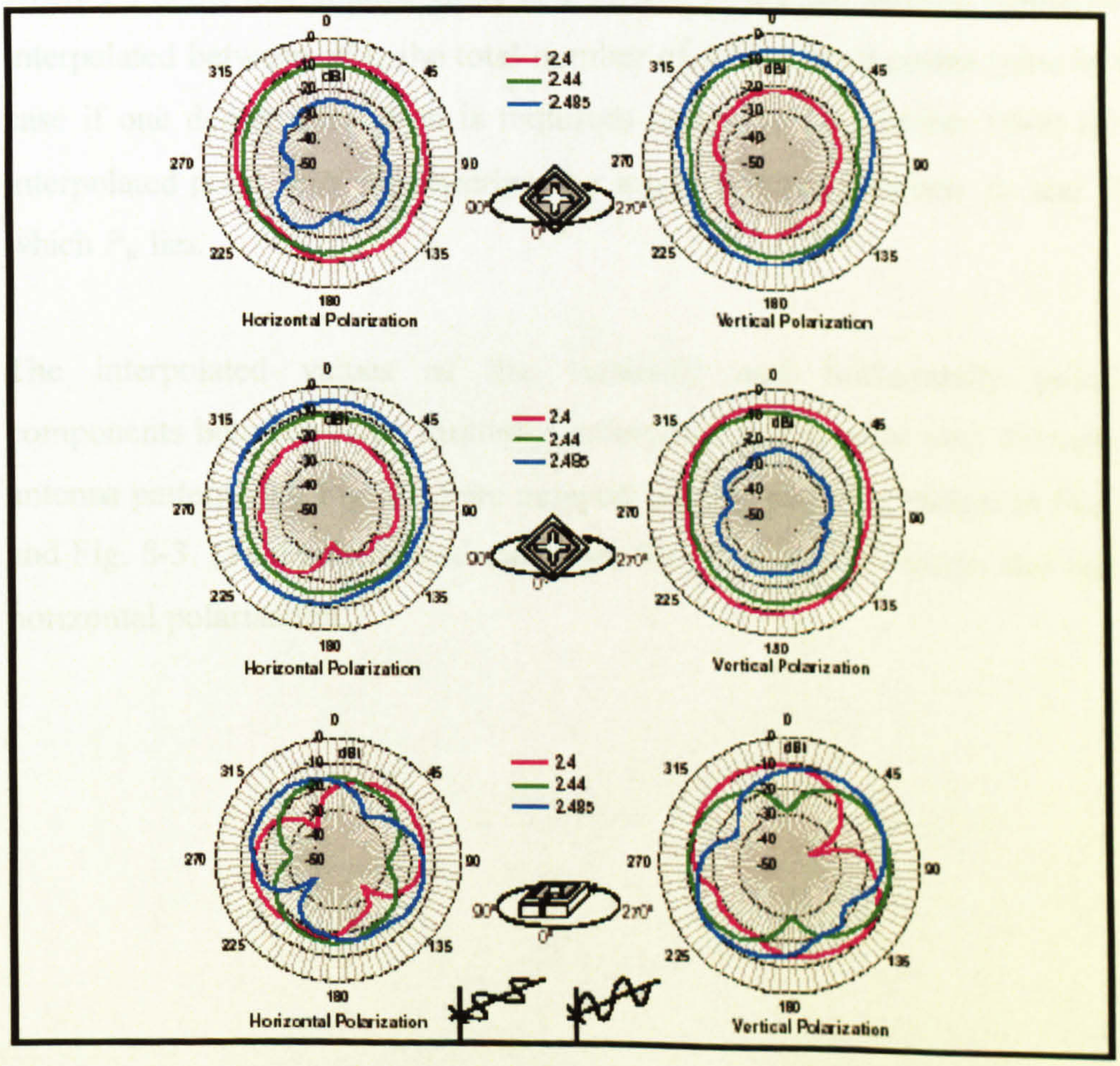

Fig. 8-1 Measured radiation patterns of practical antenna for three different antenna

The following steps are used to arrive at a polarisation model.

1. An antenna definition text file is created which holds the gain values (in decibels) for the antenna at 10° intervals for both vertical and horizontal polarised component. The gain values are normalised to the maximum gain.

2. Linear interpolation is used to estimate the gain between sample points generating vertically and horizontally polarised component with 1° resolution. The interpolation formula used is:

$$P_u = P_o + \frac{n_i}{N}\left(P_i - P_o\right) \tag{8.1}$$

where P_u is the interpolated value and P_o and P_i are the sample points being interpolated between, N is the total number of interpolated points (nine in this case if one degree resolution is required) and n_i is the number (0-9) of the interpolated point, n/N representing the angle fraction between P_o and P_i at which P_u lies.

3. The interpolated values of the vertically and horizontally polarised components between three mutually orthogonal great circle cuts through the antenna pattern (see Fig. 8-1) are mapped onto a sphere as shown in Fig. 8-2 and Fig. 8-3. (Two spheres are used, one for vertical polarisation and one for horizontal polarisation.)

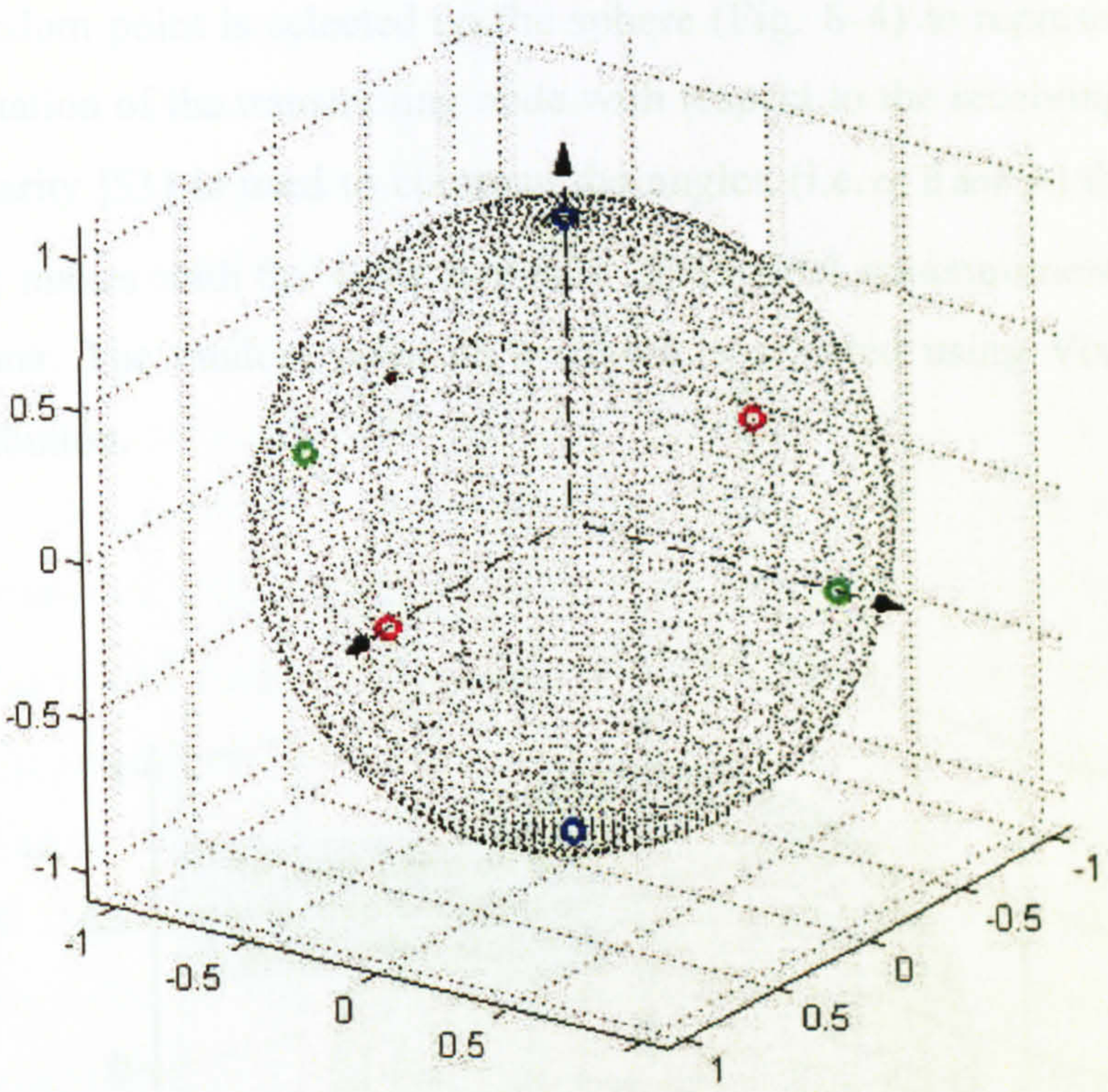

Fig. 8-2 Sphere centred on antenna

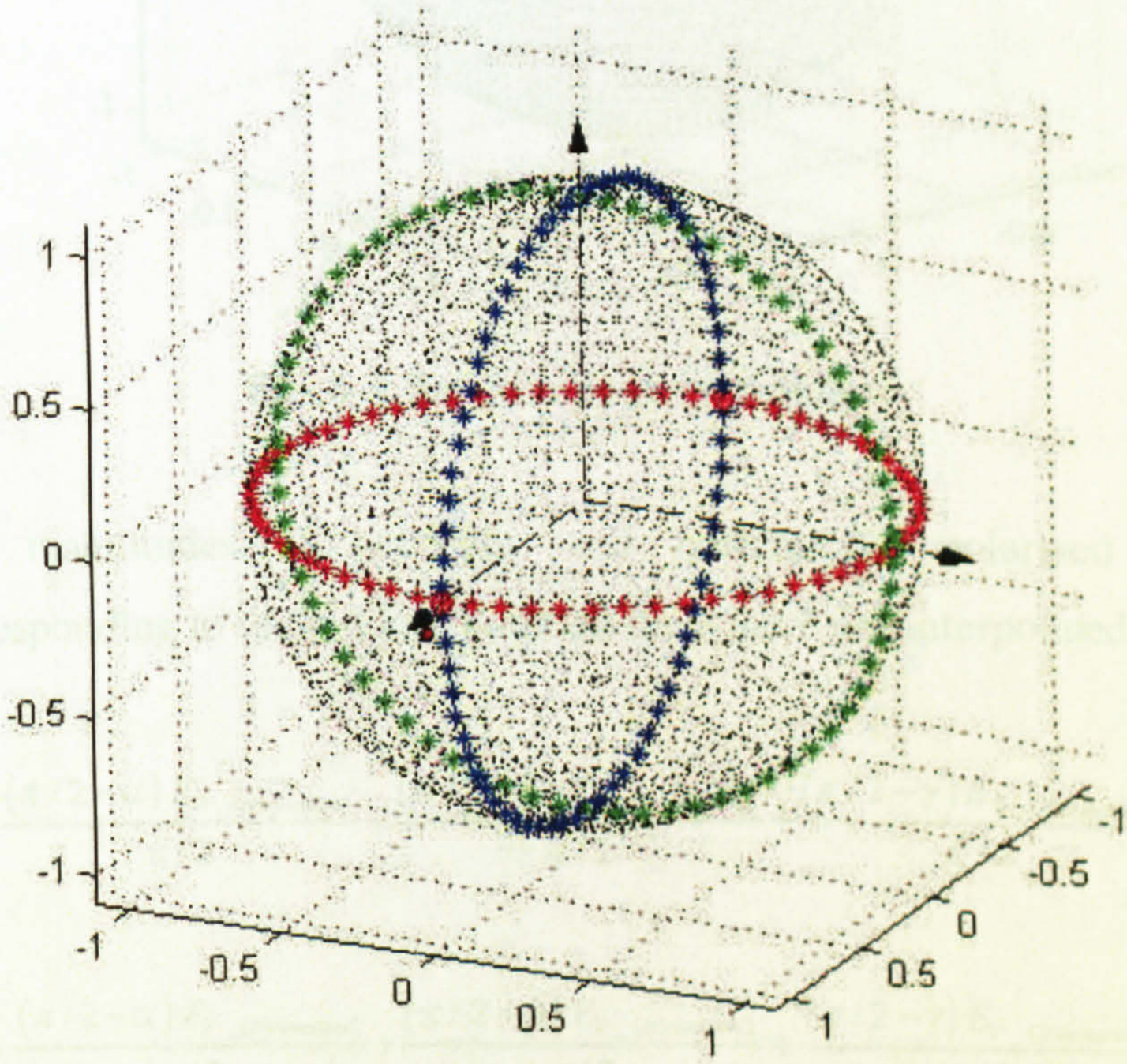

Fig. 8-3 Measured vertical polarised component mapped on to sphere (blue, green, red represent orthogonal measurement cuts)

4. A random point is selected on the sphere (Fig. 8-4) to represent the random orientation of the transmitting node with respect to the receiving node. Cosine similarity [53] is used to compute the angles (i.e. α, ß and γ) that the random point makes with the three mutually orthogonal measurement planes of the antenna. The random point on a sphere is selected using Von Mises-Fisher distribution.

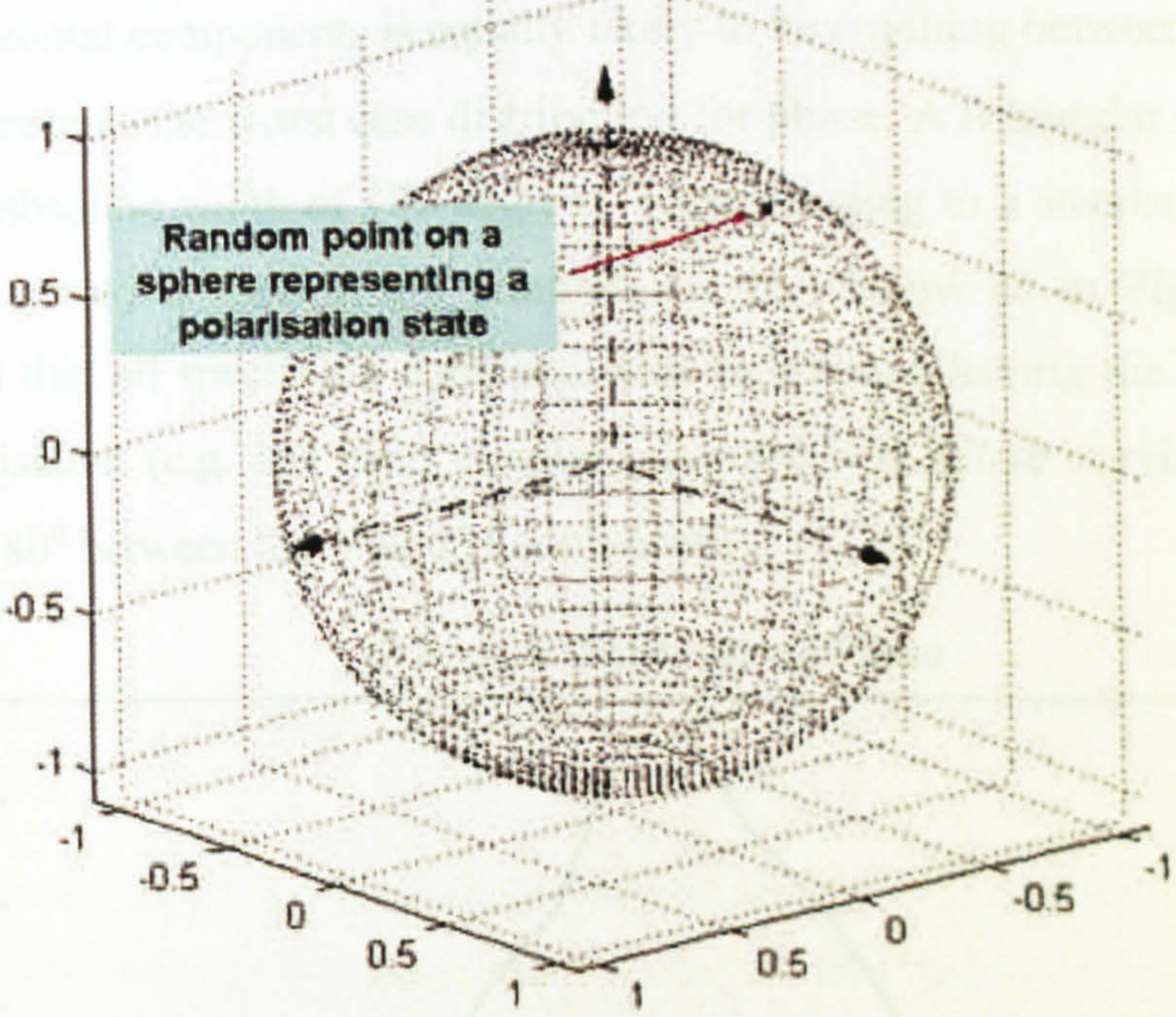

Fig. 8-4 Random point on a sphere

5. The magnitudes of vertically and horizontally polarised components corresponding to the random point on the sphere are interpolated using:

$$E_H = \frac{(\pi/2-\alpha)\,E_{H\_Orientation1}}{\pi/2} + \frac{(\pi/2-\beta)\,E_{H\_Orientation2}}{\pi/2} + \frac{(\pi/2-\gamma)\,E_{H\_Orientation3}}{\pi/2} \qquad (8.2)$$

$$E_V = \frac{(\pi/2-\alpha)\,E_{V\_Orientation1}}{\pi/2} + \frac{(\pi/2-\beta)\,E_{V\_Orientation2}}{\pi/2} + \frac{(\pi/2-\gamma)\,E_{V\_Orientation3}}{\pi/2} \qquad (8.3)$$

6. Pure circular polarisation is the result of equal magnitude of vertical and horizontal polarised components oscillating in phase quadrature. Since the

measured patterns do not give the phase difference between V and H components a value is selected randomly. Two distribution functions are proposed for the phase difference random variable. These are: (i) a triangular distribution and (ii) a uniform distribution. The triangular distribution with peak value at ±90 degree phase difference will, for example, represent a better (circularly polarised) antenna than a uniform distribution. (Better, in this context, refers to the polarisation purity of the antenna over all 4π steradians of solid angle.) A uniform pdf, where the phase between vertical and horizontal components is equally likely to be anything between -180° and 180° represents the worst case distribution for phase. A triangular distribution with an absolute width of 180 degrees (corresponding to a standard deviation of 40 degrees) is used in the simulations that follow as in Fig. 8-5. It is assumed that all specks are equipped with an antenna having the same sense of polarisation (e.g. left hand circular polarised with phase varying between 0° and 180° between the V and H component).

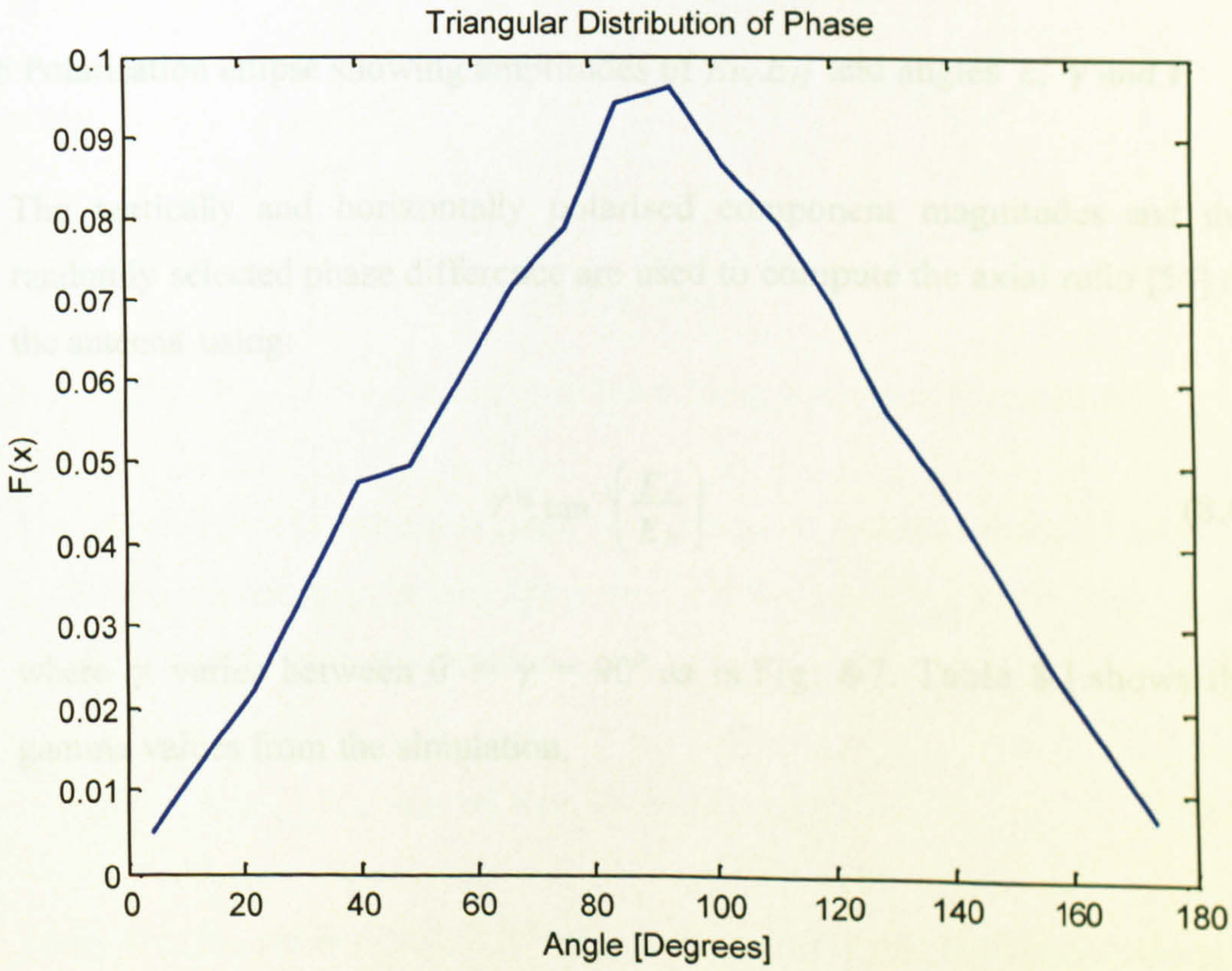

Fig. 8-5 Triangular phase distribution

Gamma values from the simulation	
Mean	58.6°
Standard Deviation	14.8°

Table 8-1 Gamma values

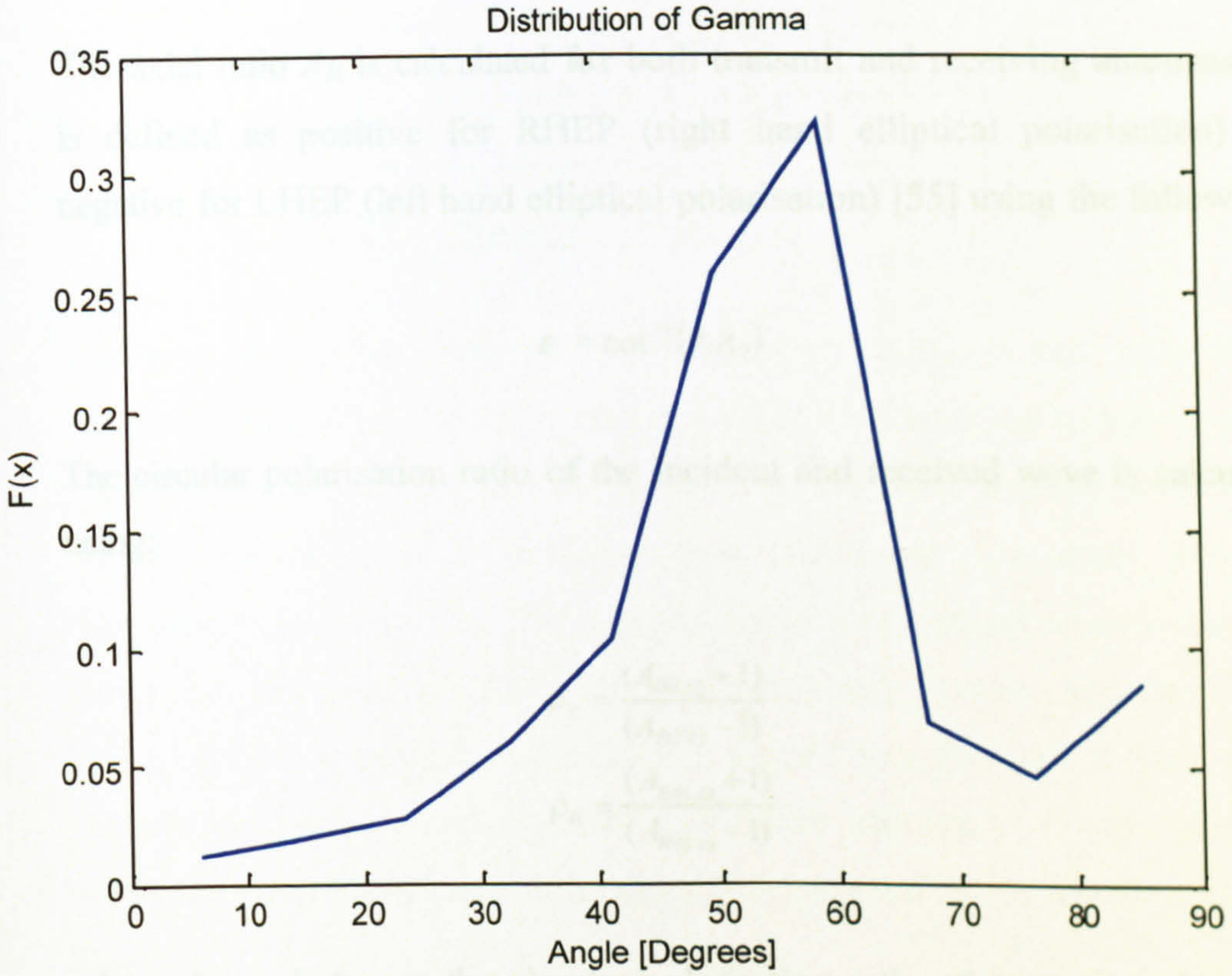

Fig. 8-7 Gamma values calculated using the simulation model.

The ellipticity ε is calculated using (8.5) where ε varies between 0° and 45° for left hand circular polarised antennas (LHCP), Table 8-2.shows the ellipticity values from the simulation.

$$\sin 2\varepsilon = \sin 2\gamma \sin \delta \tag{8.5}$$

where d is the phase difference between the vertical and horizontal polarised component.

Ellipticity values from the simulation	
Mean	20.6°
Standard Deviation	9.8°

Table 8-2 Ellipticity values

The axial ratio A_R is calculated for both transmit and receiving antennas and is defined as positive for RHEP (right hand elliptical polarisation) and negative for LHEP (left hand elliptical polarisation) [55] using the following:

$$\varepsilon = \cot^{-1}(\pm A_R) \tag{8.6}$$

8. The circular polarisation ratio of the incident and received wave is calculated using:

$$\rho_T = \frac{(A_{R(Tx)}+1)}{(A_{R(Tx)}-1)}$$
$$\rho_R = \frac{(A_{R(Rx)}+1)}{(A_{R(Rx)}-1)} \tag{8.7}$$

where ρ_T and ρ_R are the circular polarisation ratio of transmit and receive antenna (ignoring any polarisation due to medium). $A_{R(Tx)}$ and $A_{R(Rx)}$ are the axial ratio corresponding to transmit and receive antennas [55].

9. In order to transfer maximum energy or power between transmit and receive antenna, both antennas must have the same polarisation sense, the same tilt angle and the same axial ratio (along the line connecting them). The random selection of an orientation angle on a sphere (step 4) takes account of both random orientation and relative spatial positions of the nodes. The tilt angle (τ) is defined as the angle of the polarisation ellipse major axis relative to the x axis as in Fig. 8-6. The tilt angle is given by the following equation [56] varies between $0 = \tau = 180^{o}$.

$$\tan 2\tau = \tan 2\gamma \cos \delta \tag{8.8}$$

Table 8-3.shows the tilt angle values from the simulation.

Tilt angle	
Mean	90.6°
Standard Deviation	73.8°

Table 8-3 Tilt angle

10. The polarisation loss between communicating specks is zero only if the relative tilt angle (i.e. the difference in tilt angle between the transmitting and receiving specks) is zero and the axial ratios are equal and the direction of rotation (i.e. polarisation handedness) are the same. The worst case (i.e. maximum polarisation loss for a given pair of axial ratios) occurs when the major axes are perpendicular. The polarisation loss between any two specks varies between maximum and minimum value (for a fixed axial ratio) as the antenna is rotated about its bore-sight. The extremes of minimum and maximum polarisation loss for a given pair of axial ratios are illustrated in Fig. 8-8.

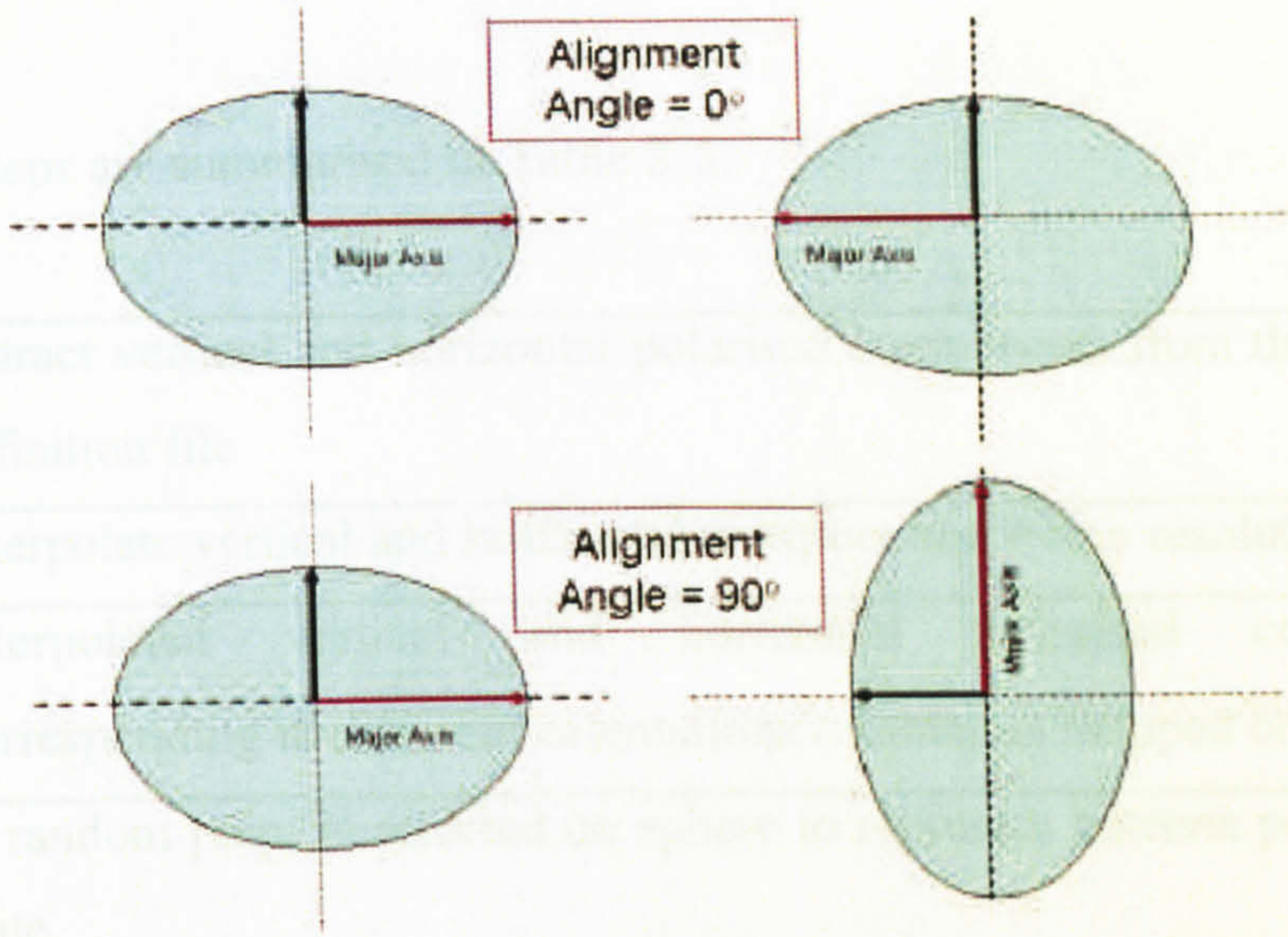

Fig. 8-8 The polarisation mismatch loss between two nodes for any angular alignment of major axis of the polarisation ellipse is given by [55]:

Table 8-4 shows the difference in tilt angle.

Difference in tilt angle	
Mean	29.7°
Standard Deviation	17.9°

Table 8-4 Difference in tilt angle

The difference in tilt angle between two specks varies between 0° and 90°.

11. The polarisation mismatch loss for any angular alignment θ_d between major axis of the polarisation ellipse can be calculated using [55]:

$$L_{pol} = 10\log_{10}\left[\frac{1+\rho_{(Tx)}\rho_{(Rx)}+2\rho_{(Tx)}\rho_{(Rx)}\cos(2\theta_d)}{(1+\rho_{(Tx)}{}^2)(1+\rho_{(Rx)}{}^2)}\right] \tag{8.9}$$

where θ_d is calculated as in step 10.

The simulation steps are summarised in Table 8-5.

Step 1	Extract vertical and horizontal polarised components from the antenna definition file
Step 2	Interpolate vertical and horizontal component for fine resolution
Step 3	Interpolated vertical and horizontal polarised components corresponding to different orientations of antenna mapped onto sphere
Step 4	A random point is selected on sphere to represent antenna polarization state.
Step 5	Vertical and horizontal polarised components (for the random point on a sphere) are interpolated.
Step 6	Phase difference between vertical and horizontal polarised components is selected randomly using a triangular distribution function
Step 7	Axial ratio is calculated.
Step 8	The circular polarisation ratio of the incident and received wave is calculated.
Step 9	The tilt angle (τ) for each antenna is calculated. The relative tilt angle (θ_d) between transmit and receiver specks major axis is calculated
Step 10	Polarization loss is calculated.

Table 8-5 Simulation steps

8.1.2 Simulation and Results

The simulation is written in Matlab. It assumes two-dimensional random deployment of nodes with independent uniform pdfs for x- and y-components of location vector

and θ, ϕ orientation angles.

The simulation steps 1 through 8 are repeated for both transmit and receive nodes. The polarisation loss (steps 9 and 10) is calculated for each trial (representing one instance of a transmitter-receiver link). Propagation losses other than those due to polarization mismatch are ignored.

Table 8-6 shows the results of mean polarization loss versus number of trials for the simulation parameters shown in Table 8-5. The mean polarisation loss converges to 1.14 dB after 2000 trails. Statistics of the simulation results are shown in Table 8-6.

Statistical Parameters (through simulation)	**Values** [dB]
Maximum polarisation loss	10.31
Minimum polarisation loss	0.005
Sample mean	1.14
Sample standard deviation	0.96

Table 8-6 Simulation Results (Triangular distribution of phase)

Fig. 8-9 shows the cumulative distribution function (CDF) of the polarisation loss. It shows that for 10% of links the polarization loss is greater than 2.2 dB.

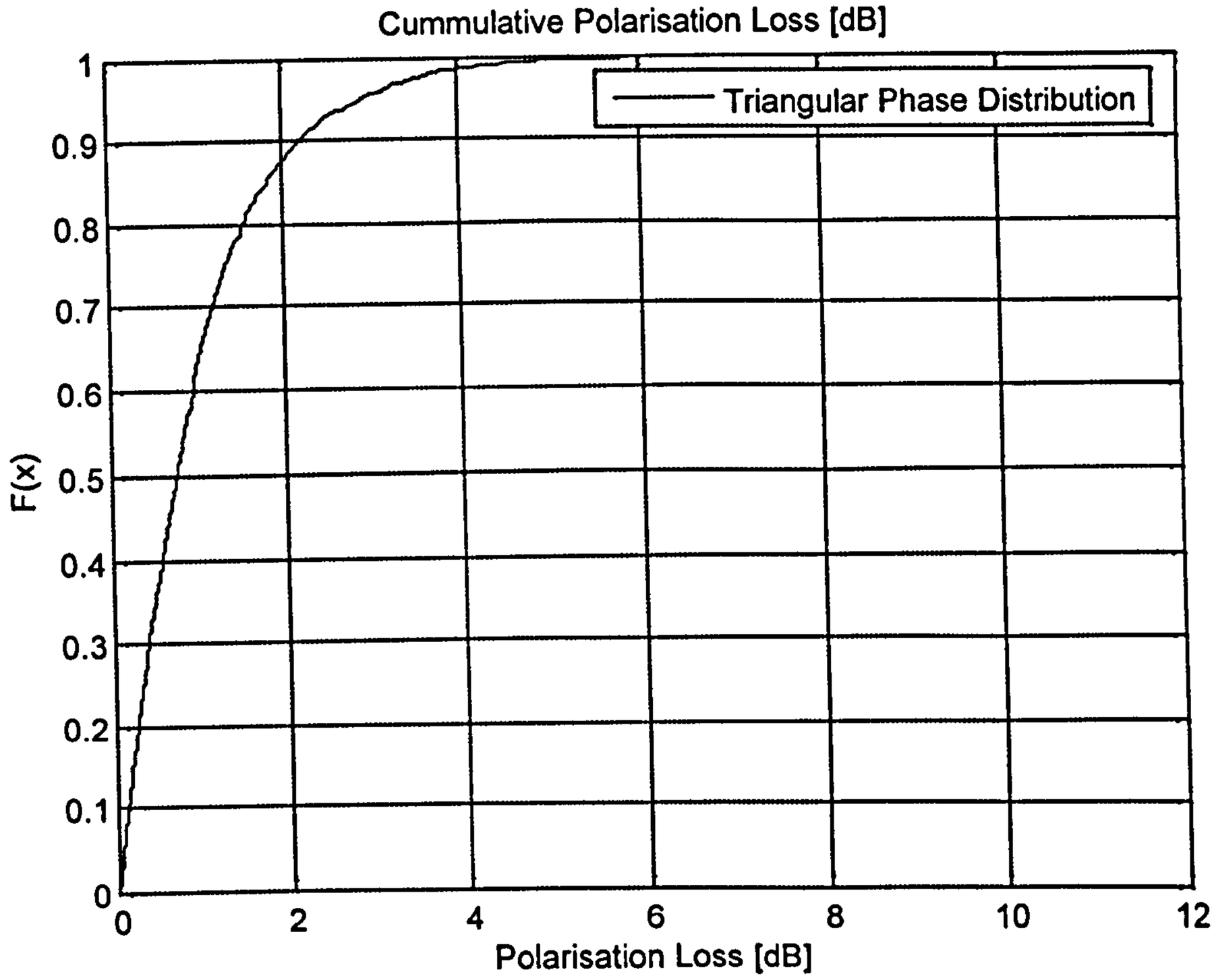

Fig. 8-9 CDF of polarisation loss (assuming a triangular pdf for phase difference between V and H components)

8.1.3 Polarisation Loss due to Uniformly Distributed Phase

The simulation has been repeated for a phase between V and H components that is uniformly distributed with a mean and standard deviation of 88.80° and 59.95° respectively. Table 8-7 shows the results of mean polarization loss (i.e. triangular and uniformly distributed phase) versus number of trials for the simulation parameters shown in Table 8-5. The mean polarisation loss converges to 2.42 dB after 2000 trails. Statistics of the simulation results are shown in Table 8-7.

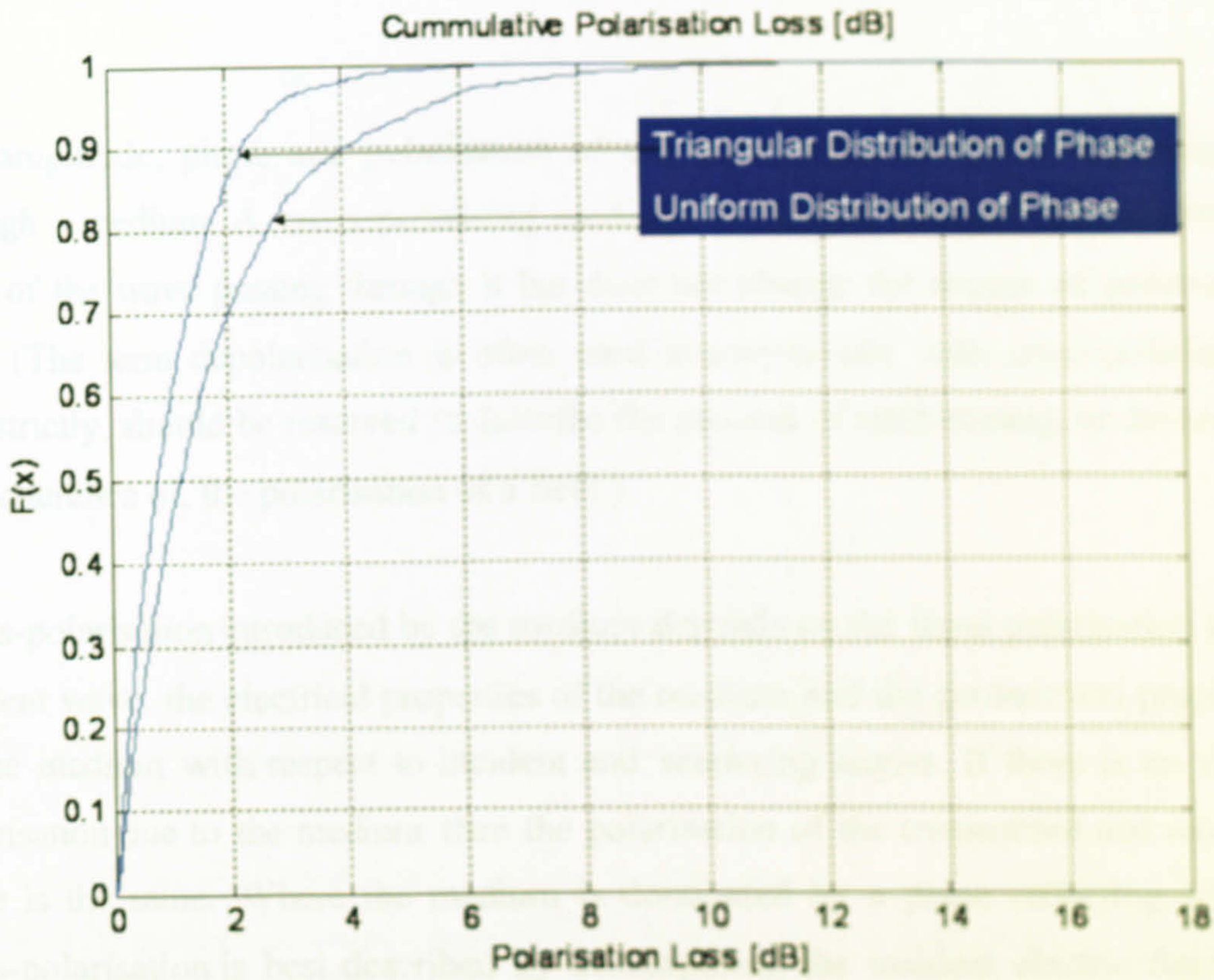

Fig. 8-10 Shows the cumulative distribution of the two cases. It shows that 10% of the time the polarization loss is greater than 4.1 dB.

Statistical Parameters (through simulation)	**Values** [dB]	**Difference from Table 8-6** [dB]
Maximum polarisation loss	16.12	5.81
Minimum polarisation loss	0.011	0.006
Sample mean	2.42	1.38
Sample standard deviation	1.83	0.87

Table 8-7 Simulation Results (for uniform distribution of phase)

8.2 Polarisation Loss due to Medium

The amplitude, phase and polarisation of the wave may change as it propagates through a medium. A cross-polarising medium is one that changes the polarisation state of the wave passing through it but does not change the degree of polarisation [56]. (The term depolarisation is often used synonymously with cross-polarisation but, strictly, should be reserved to describe the process of randomising, or decreasing the coherence of, the polarisation of a field.)

Cross-polarisation introduced by the medium depends on the input polarisation of the incident wave, the electrical properties of the medium and the geometrical properties of the medium with respect to incident and scattering angles. If there is no cross-polarisation due to the medium then the polarisation of the transmitted and received wave is the same. Where the medium is dominated by a plane reflecting surface cross-polarisation is best described by decomposing the incident electric field into parallel $E_{\parallel}$ and perpendicular $E_{\perp}$ components [56] with respect to plane of incidence. The reflection coefficients for these two components are generally different and depend on the grazing angle of the incident field wavenumber vector and the permittivity, conductivity and permeability of the medium. The polarisation of the reflected field will be changed if either the magnitudes or phases of the reflection coefficients are different. The reflection coefficients for infinite plane surfaces are given by the Fresnel equations.

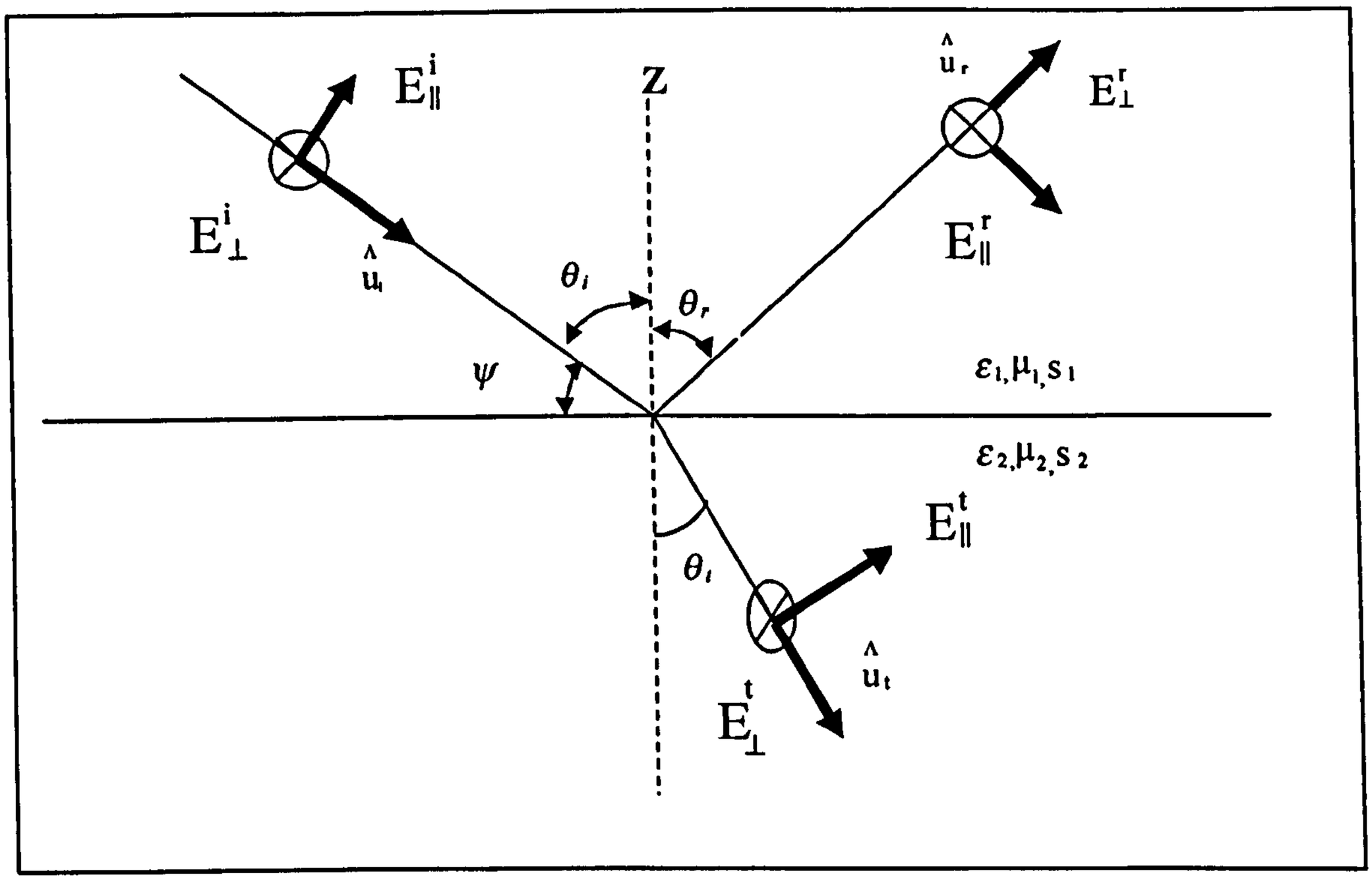

Fig. 8-11 Interface between transmits and receive wave incident on a medium of different electrical properties

8.2.1 Fresnel Equations

The incident and reflected wave in Fig. 8-11 is decomposed into parallel and perpendicular components [57]. The Fresnel reflection and transmission coefficients for each component are defined by:

$$\Gamma_{\parallel} = \frac{E_{\parallel}^{r}}{E_{\parallel}^{i}} \tag{8.10}$$

$$\Gamma_{\perp} = \frac{E_{\perp}^{r}}{E_{\perp}^{i}} \tag{8.11}$$

$$T_{\parallel} = \frac{E_{\parallel}^{t}}{E_{\parallel}^{i}} \tag{8.12}$$

$$T_{\perp} = \frac{E_{\perp}^{t}}{E_{\perp}^{i}} \tag{8.13}$$

where

$\Gamma_{\parallel}$ $\Gamma_{\perp}$ are the parallel and perpendicular reflection coefficients,

$T_{\|}$ $T_{\perp}$ are the parallel and perpendicular transmission coefficients,

$E'_{\|}$ $E_{\perp}{}'$ are the parallel and perpendicular components of the incident wave,

$E''_{\|}$ $E_{\perp}{}''$ are the parallel and perpendicular components of the reflected wave,

$E'_{\|}$ $E_{\perp}{}'$ are the parallel and perpendicular components of the wave transmitted into the reflecting medium.

The Fresnel reflection and transmission coefficient are complex quantities and represent the magnitude and phase change of the incident wave at the interface. The Fresnel coefficient depends on the incident reflected and refracted angles at the interface as in Fig. 8-16. Expressions for the reflection and transmission coefficient, derived by applying the electromagnetic boundary condition as in [58], are:

$$\Gamma_{\|} = \frac{\eta_2 \cos\theta_t - \eta_1 \cos\theta_i}{\eta_2 \cos\theta_t + \eta_1 \cos\theta_i} \tag{8.14}$$

$$T_{\|} = \frac{2\eta_2 \cos\theta_i}{\eta_2 \cos\theta_t + \eta_1 \cos\theta_i} \tag{8.15}$$

$$\Gamma_{\perp_1} = \frac{\eta_2 \cos\theta_i - \eta_1 \cos\theta_t}{\eta_2 \cos\theta_i + \eta_1 \cos\theta_t} \tag{8.16}$$

$$T_{\perp\|} = \frac{2\eta_2 \cos\theta_i}{\eta_2 \cos\theta_i + \eta_1 \cos\theta_t} \tag{8.17}$$

where η_1 and η_2 are the intrinsic impedances of the media as in Fig. 8-16. θ_i and θ_t are the incident and reflected angles as in Fig. 8-16. The intrinsic impendence η for any medium is given by:

$$\eta = \sqrt{\frac{j\omega\mu}{\sigma + j\omega\varepsilon}} \tag{8.18}$$

where σ and μ is the conductivity and permeability of the medium.

Two extreme cases are identified for cross-polarising mediums [57]:

1. The mediums are identical then the interface has no effect (in fact there is no interface) i.e. there is no reflection and the incident wave is transmitted unaltered (i.e. $\Gamma_{\|} = \Gamma_{\perp} = 0$ and $T_{\|} = T_{\|} = 1$).

2. Reflection from a perfect plane conductor ($\sigma = \alpha$, $\eta = 0$) $\Gamma_{\|} = \Gamma_{\perp} = -1$ and $T_{\|} = T_{\|} = 0$. In this case the reflected electric field changes phase by 180 degrees on reflection.

If the media are dielectric and non-magnetic (i.e. $\mu_2 = \mu_1 = \mu_0$,) then the Fresnel reflection and transmission coefficients [60] are given by:

$$\Gamma_{\|} = \frac{\cos\theta_i - \frac{\varepsilon_1}{\varepsilon_2}\sqrt{\frac{\varepsilon_2}{\varepsilon_1} - \sin^2\theta_i}}{\cos\theta_i + \frac{\varepsilon_1}{\varepsilon_2}\sqrt{\frac{\varepsilon_2}{\varepsilon_1} - \sin^2\theta_i}} \tag{8.19}$$

$$T_{\|} = \frac{2\cos\theta_i}{\cos\theta_i + \frac{\varepsilon_1}{\varepsilon_2}\sqrt{\frac{\varepsilon_2}{\varepsilon_1} - \sin^2\theta_i}} \tag{8.20}$$

$$\Gamma_{\perp} = \frac{\cos\theta_i - \sqrt{\frac{\varepsilon_2}{\varepsilon_1} - \sin^2\theta_i}}{\cos\theta_i + \sqrt{\frac{\varepsilon_2}{\varepsilon_1} - \sin^2\theta_i}} \tag{8.21}$$

$$T_{\perp} = \frac{2\cos\theta_i}{\cos\theta_i + \sqrt{\frac{\varepsilon_2}{\varepsilon_1} - \sin^2\theta_i}} \tag{8.22}$$

where ε_1 and ε_2 are the permittivities of the medium as in Fig. 8-16. For a lossy medium the permittivities in (8.19, 8.20, 8.21 and 8.22) are complex. The permittivity of a general lossy medium is given:

$$\varepsilon_c = \varepsilon - j\frac{\sigma}{\omega} \tag{8.23}$$

where ε_c is the complex permittivity of a medium.

Fig. 8.12 and Fig. 8.13 show the parallel and perpendicular Fresnel reflection coefficients at 2.45 GHz for two different surfaces [59] as shown in Table 8-8. Fig. 8-14 and Fig. 8-15 show the associated phase. The conductivity s of a typically medium is between 0.005 S/m and may range from 0.0001 to as much as 0.03 S/m [60].

Surface	**Conductivity** *s [S/m]*	**Dielectric constant** ε_r
Wood (dry)	0.005	2 - 6
Wood (wet)	0.005	10-30

Table 8-8 Material Properties

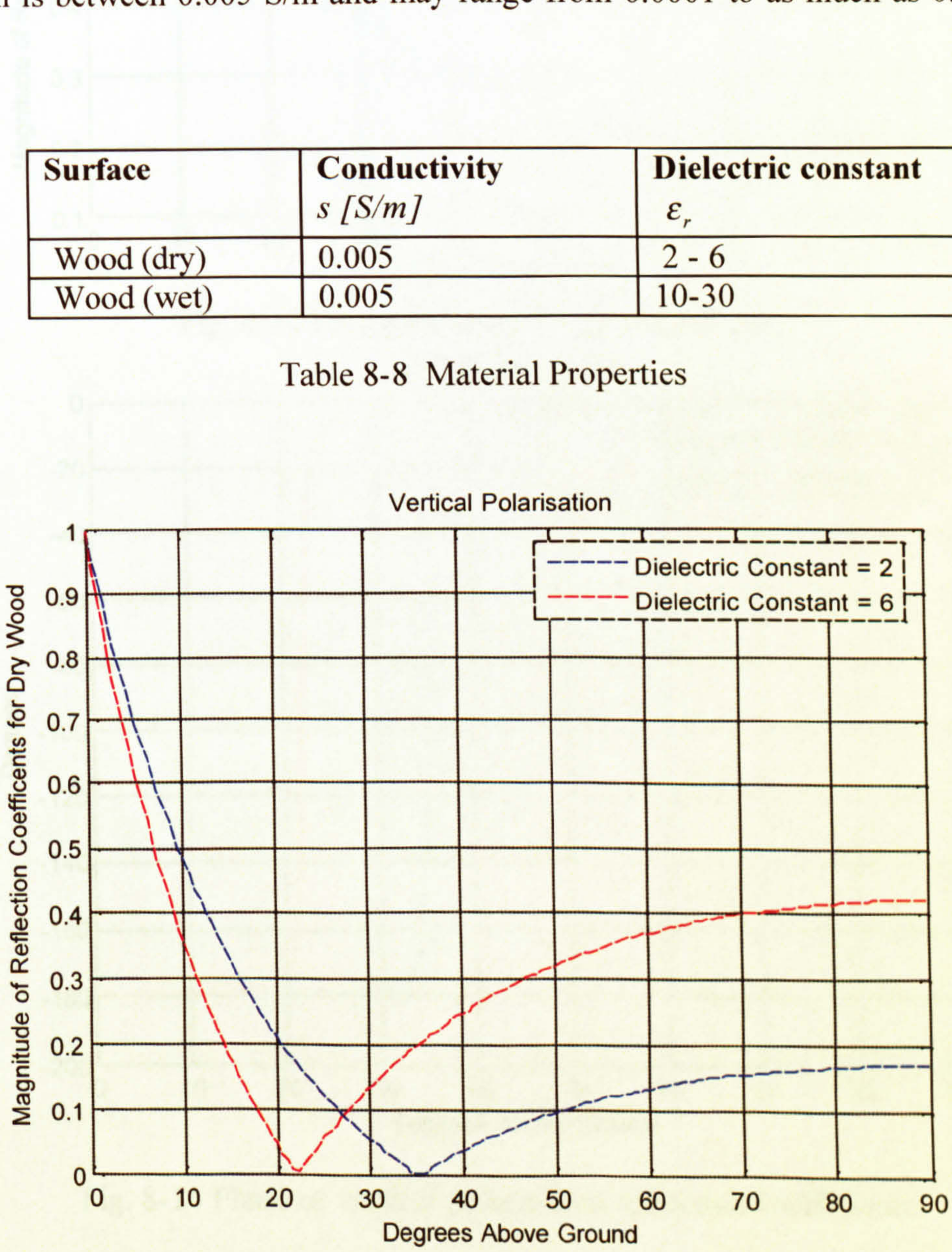

Fig. 8-12 Parallel reflection coefficient

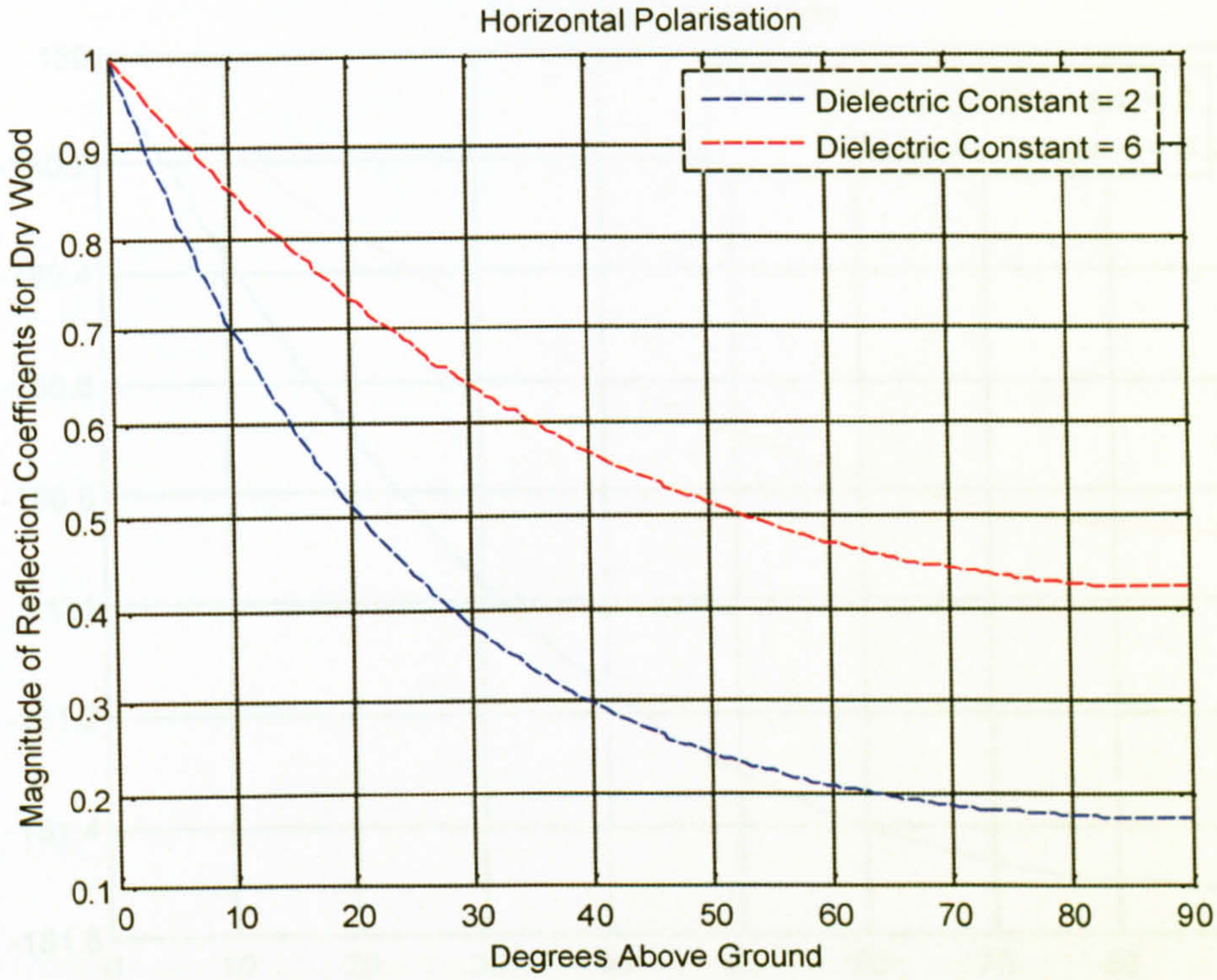

Fig. 8-13 Perpendicular reflection coefficient

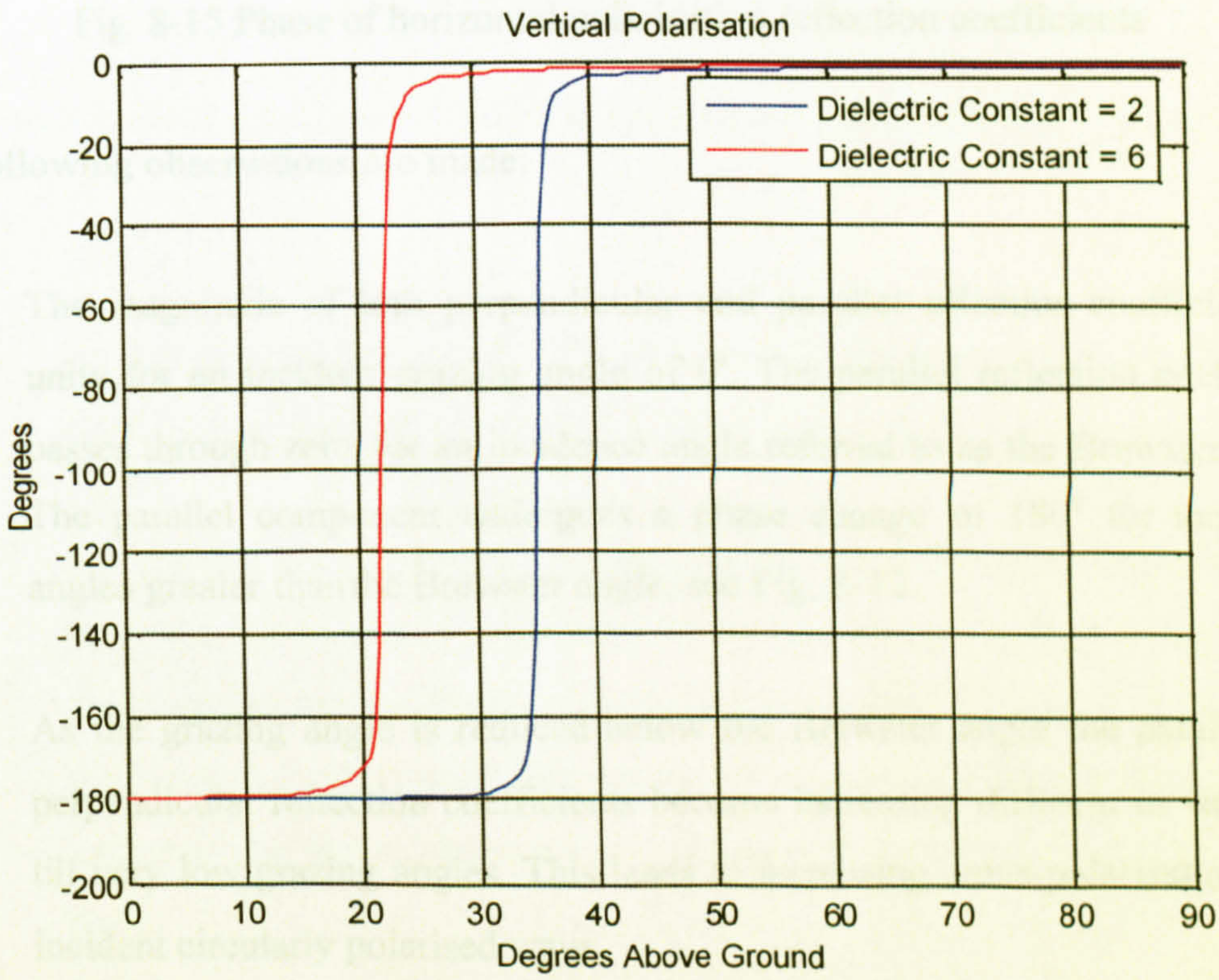

Fig. 8-14 Phase of vertical polarisation reflection coefficients

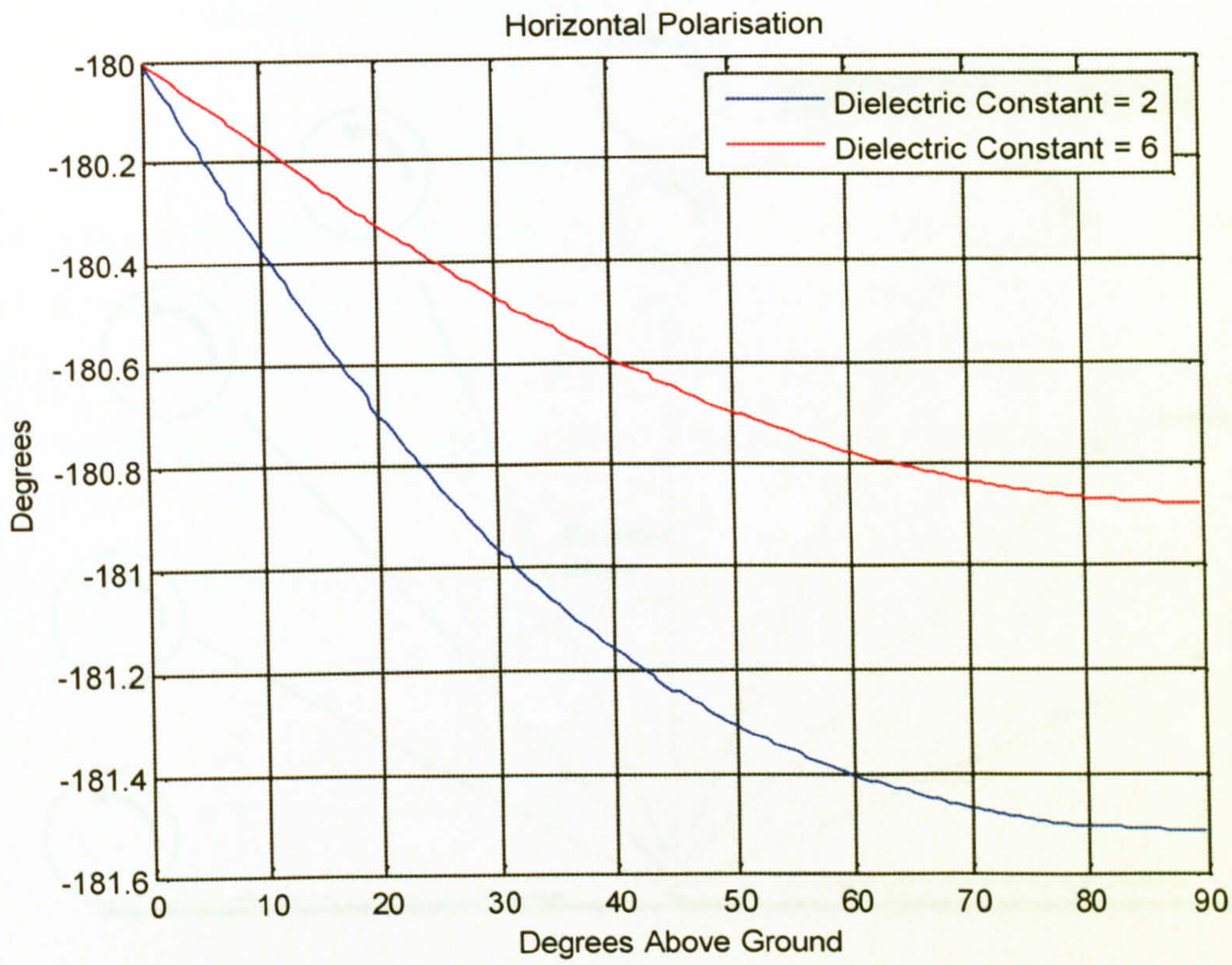

Fig. 8-15 Phase of horizontal polarisation reflection coefficients

The following observations are made:

1. The magnitude of both perpendicular and parallel reflection coefficients is unity for an incident grazing angle of 0^o. The parallel reflection coefficient passes through zero for an incidence angle referred to as the Brewster angle. The parallel component undergoes a phase change of 180^o for incidence angles greater than the Brewster angle, see Fig. 8-12.

2. As the grazing angle is reduced below the Brewster angle the parallel and perpendicular reflection coefficients become increasing different in value (up till very low grazing angles. This leads to increasing cross-polarisation of an incident circularly polarised wave.

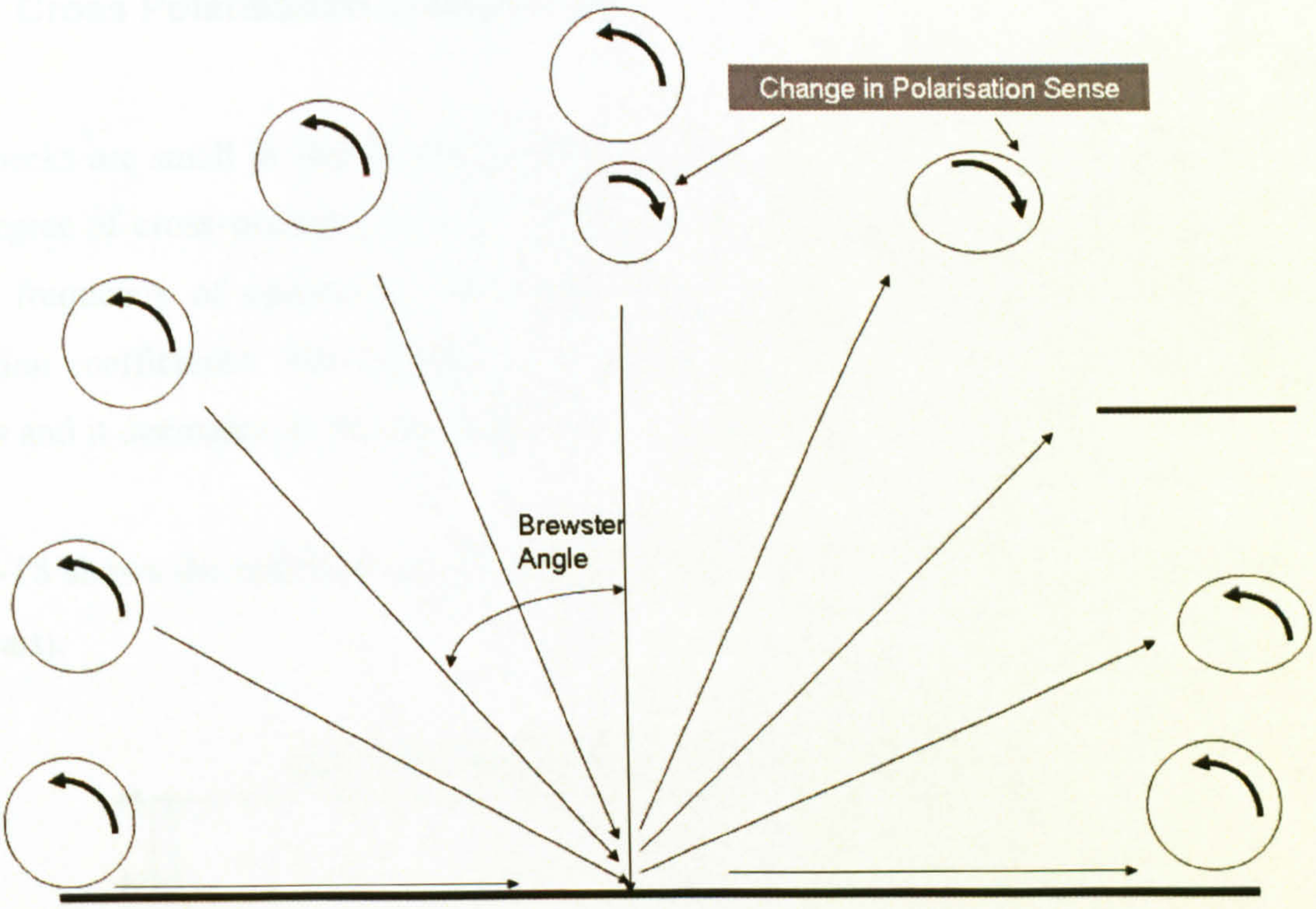

Fig. 8-16 Schematic illustration of circularly polarised wave reflected from a plane surface

3. For normal incidence angles greater than the Brewster angle the reflected wave polarisation sense is reversed, see Fig. 8-16 [60].

4. For grazing angle less than Brewster angle the reflected wave elliptically polarised but is of the same sense as the incident circular polarised wave. Since specks are small and are required to communicate over short ranges the incident grazing angle will always be less than the Brewster angle. This indicates that the reflected wave will have the same sense as the incident wave.

8.2.2 Cross Polarisation in Specknet

The specks are small in size (5 mm^3) and are typically deployed over plane surfaces. The degree of cross-polarisation of a reflected wave depends on the incident grazing angle, frequency of operation, electrical properties of the surface via the Fresnel reflection coefficients. The incident grazing angle depends on the dimension of the specks and it decreases as the separation between specks increases (see Fig. 8-17).

Fig. 8-18 shows the reflected ray for a grazing angle of 5.7° (i.e. when specks are 10 cm apart).

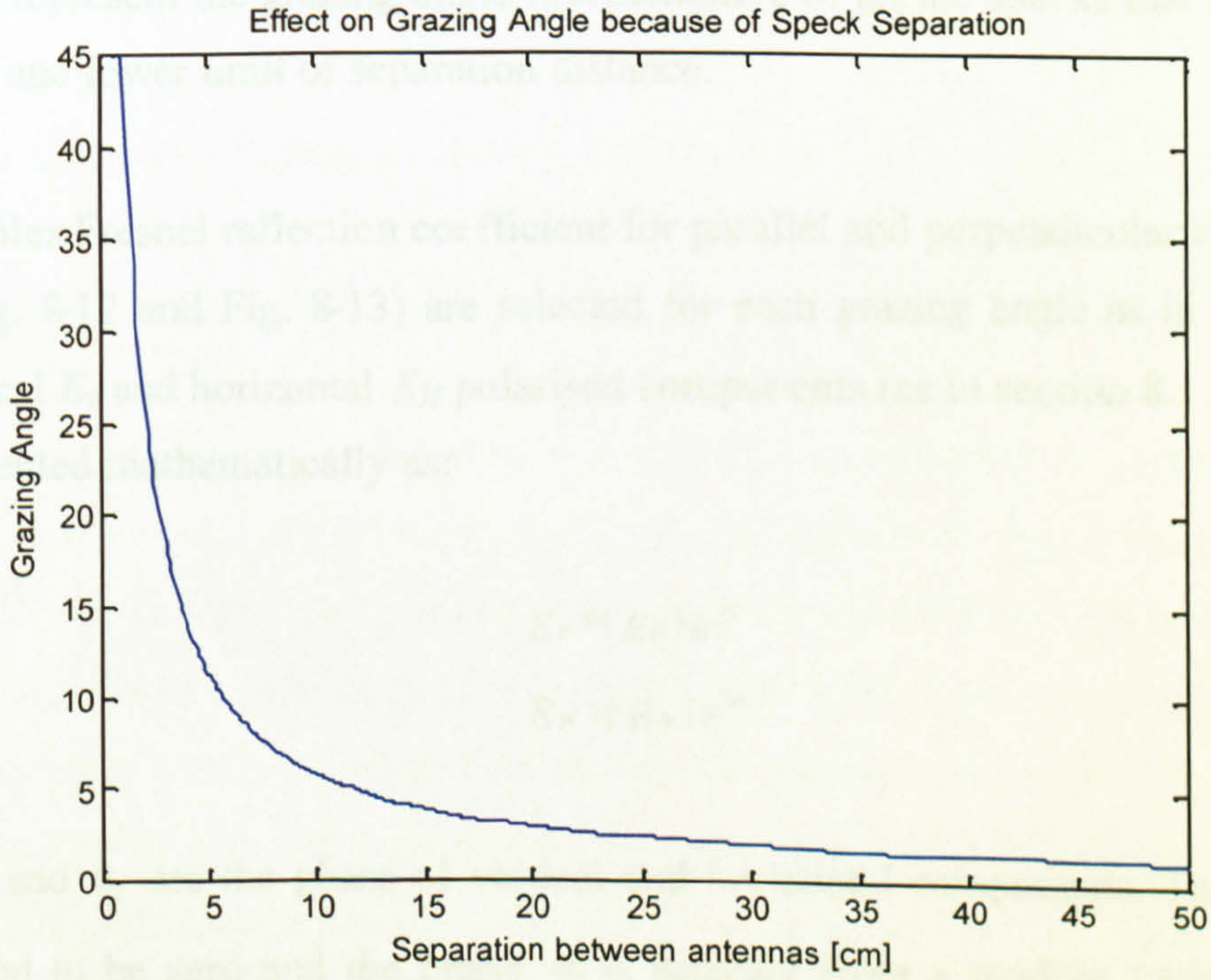

Fig. 8-17 Effect of separation distance on grazing angle

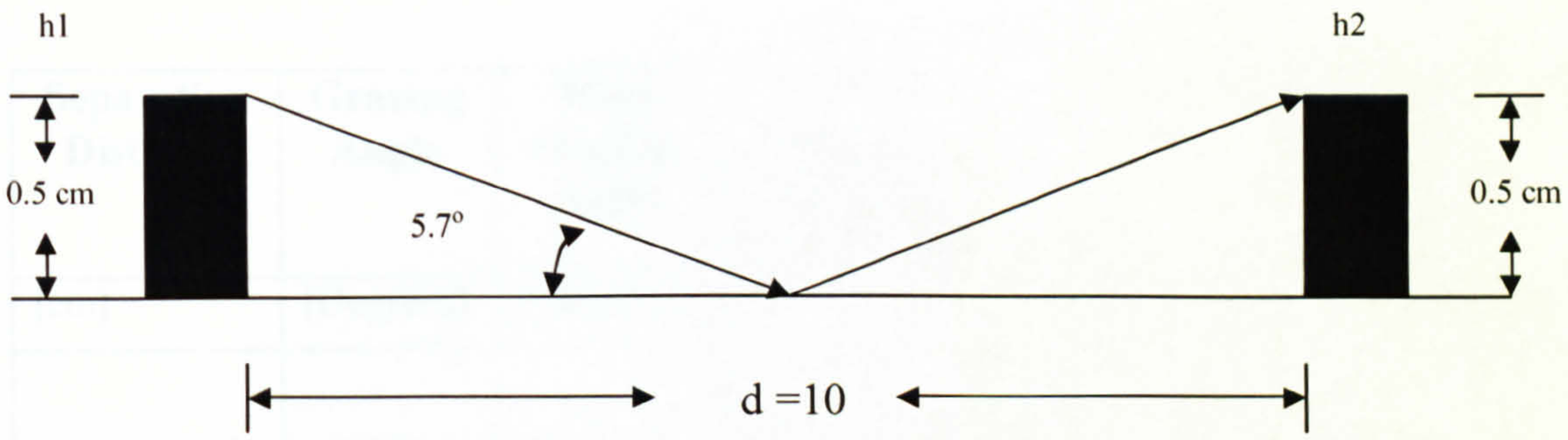

Fig. 8-18 Grazing angle for specks separated by 10 cm

Table 8-4 shows the maximum and minimum grazing angle for different separation distances between nodes. The mean value (as in Table 8-4) of grazing angle is chosen to represent the grazing angle representative of all the specks that fall with in the upper and lower limit of separation distance.

The complex Fresnel reflection coefficient for parallel and perpendicular components (as in Fig. 8-12 and Fig. 8-13) are selected for each grazing angle as in Table 8-9. The vertical E_v and horizontal E_H polarised components (as in section 8.1 above) can be represented mathematically as:

$$E_V = |E_V| e^{j\phi_1} \tag{8.24}$$

$$E_H = |E_H| e^{j\phi_2} \tag{8.25}$$

where ϕ_1 and ϕ_2 are the phase of vertical and horizontal components. The phase ϕ_1 is assumed to be zero and the phase ϕ_2 is selected from a random variable with a triangular or uniform distribution function (δ in the simulation above). The vertically and horizontally polarised components are multiplied by the respective complex reflection coefficient as given by:

$$E_V = E_V \Gamma_V \tag{8.26}$$

$$E_H = E_H \Gamma_H \tag{8.27}$$

The simulation (in section 8.1) is repeated for separation distances as in Table 8-9.

Separation Distance	Grazing Angle	Mean Grazing Angle	Fresnel Reflection Coefficient Magnitude		Polarisation Loss [dB]		
[cm]	[Degrees]	[Degrees]	$E_{\parallel}$	$E_{\perp}$	NLOS	LOS	Difference
					ρ_{NLOS}	ρ_{LOS}	
5	11.3	11.3	0.31	0.84	3.49	2.48	1.01
20 – 25	2.8 - 2.2	2.50	0.78	0.96	3.35	2.48	0.87
45 – 50	1.2 - 1.1	1.15	0.90	0.97	2.77	2.48	0.29

Table 8-9 Polarisation loss due to depolarising medium

8.2.3 Results and Observations

The following has been observed

1. Since the specks are small (= 5mm^3) and are required to communicate for short ranges (10 cm) the incident grazing angle will always be less than the Brewster angle. For grazing angle less than the Brewster angle the reflected wave is not purely circular polarised but is of same sense as the incident circular polarised wave (i.e. the RHCP will remain as RHEP after cross-polarisation due to medium). This point valid for ENP nodes as well. (The total NLOS polarisation loss for 5 cm distance (as in Table 8-9) is not conclusive as it is within one radian sphere.)

2. As the incident grazing angle decreases below the Brewster angle the Fresnel reflection coefficient become increasingly different in value (as in Fig. 8-12 and Fig. 8-13) resulting in higher polarisation loss initially (i.e. separation distances of 5-25 cm, as in Table 8-9). The cross-polarisation decreases with increasing separation distance (i.e. lower grazing angle). This is because of the parallel and perpendicular reflection coefficient

becoming increasingly equal in magnitude (see Table 8-9) for separation distances greater than 25 cm.

3. It is concluded that the cross-polarisation effect due to surface reflection can, for specknet, be neglected for separation distances greater than 25 cm as in Table. The CDF of the total polarisation loss is shown in Fig. 8-19.

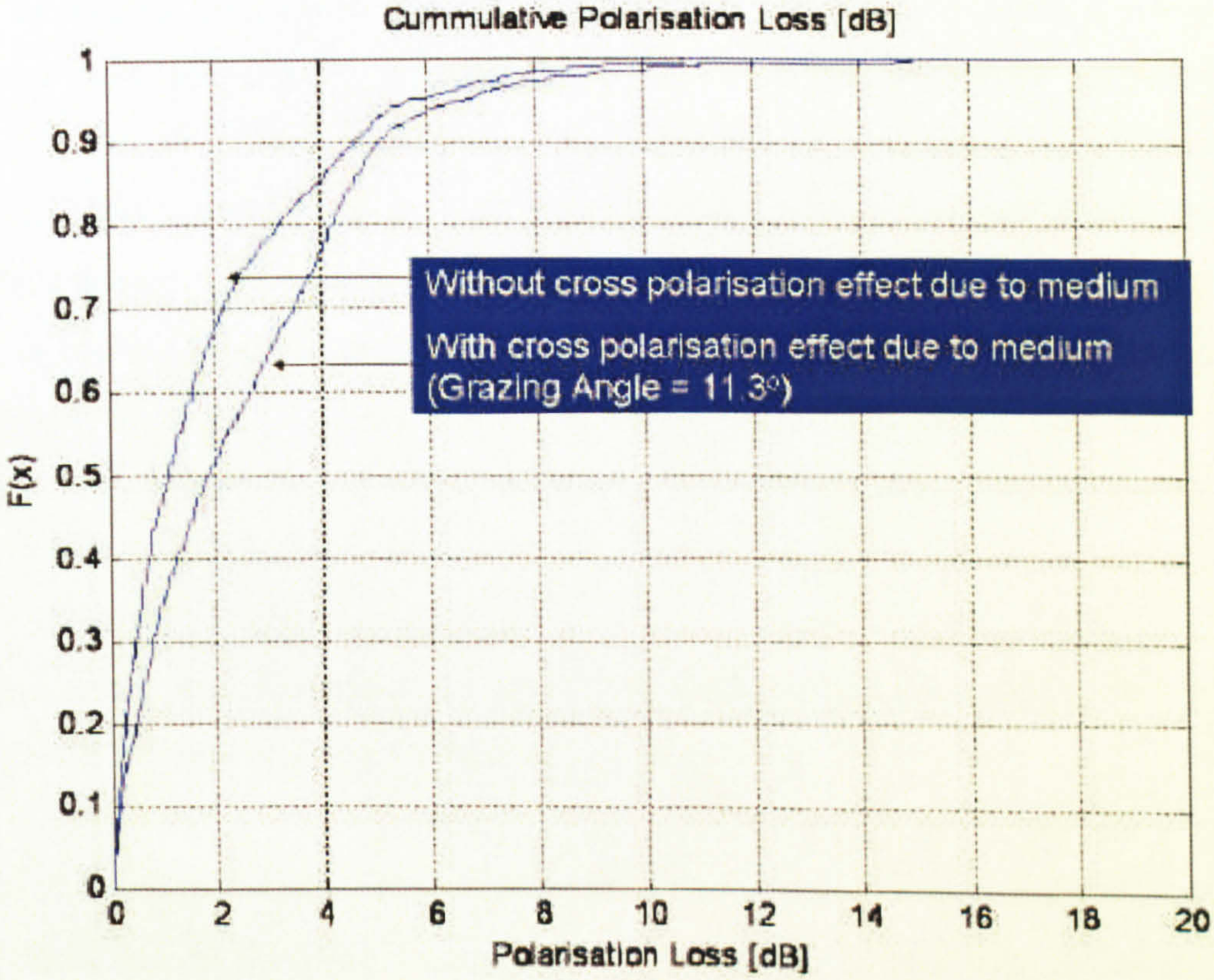

Fig. 8-19 CDF of the polarisation loss for reflected signal

4. The polarisation loss for (LOS component) can be added in the simulation model describe in Chapter 6.

8.2 Summary

The polarisation mismatch losses in a wireless sensor network depends on the design of the antenna (including its polarisation characteristics), deployment strategies, link length and physical dimensions of the device (affecting antenna height above the deployment surface). The polarisation loss due to antennas depends on the relative spatial orientation of the nodes. Since wireless sensor nodes are typically deployed randomly, both in location and in orientation, loss is likely be minimised by the adoption of circular polarisation.

Chapter 9

9. Conclusion and Further Work

The wireless channel appropriate for short wireless links has been investigated. The requirement of the Specknet consortium was to explore the wireless channel and to develop a simulation model appropriate for the design of Specknets. To the authors best knowledge no such models or measurements for short (<10 cm) wireless links were in the public domain prior to this work. The existing literature addresses loss expected due to propagation through various building materials (comprising walls, ceilings, floors, doors, etc.) and the expected transmission loss and fading statistics for propagation within room interiors. Here we are concerned with generally shorter links involving propagation over the room's bounding plane surfaces. The existing literature on indoor channel modelling deals with transmission loss due to RF penetration through indoor walls, windows, doors and across different floors in an indoor environment.

Transmission loss measurements have been made in the laboratory emulating the conditions relevant to a speck network.

Simulations have been devised to investigate interference limited networks. Aggregate interference due to neighbouring carrier-sense multiple access nodes has been calculated. The resulting dependence of signal to interference ratio on node density is presented to allow density dimensioning.

Since specks will generally be deployed close to surfaces the possibility of surface-wave propagation cannot be neglected. The significance of such surface-waves will depend on the physical dimensions of the node (affecting antenna placement), the electrical properties of the surface and antenna polarisation. The relationship between

transmission loss, antenna polarisation and heights above the surface has been explored.

Polarisation effects have been addressed in the literature mostly for long links (≈ 10 m). Likely polarisation losses for shorter links have been established using empirical, but incomplete, polarisation data for appropriate practical antennas combined with plausible assumptions.

9.1 Review

The research methodology used during the course of this research is best described by Fig. 1-1 as in Chapter 1.

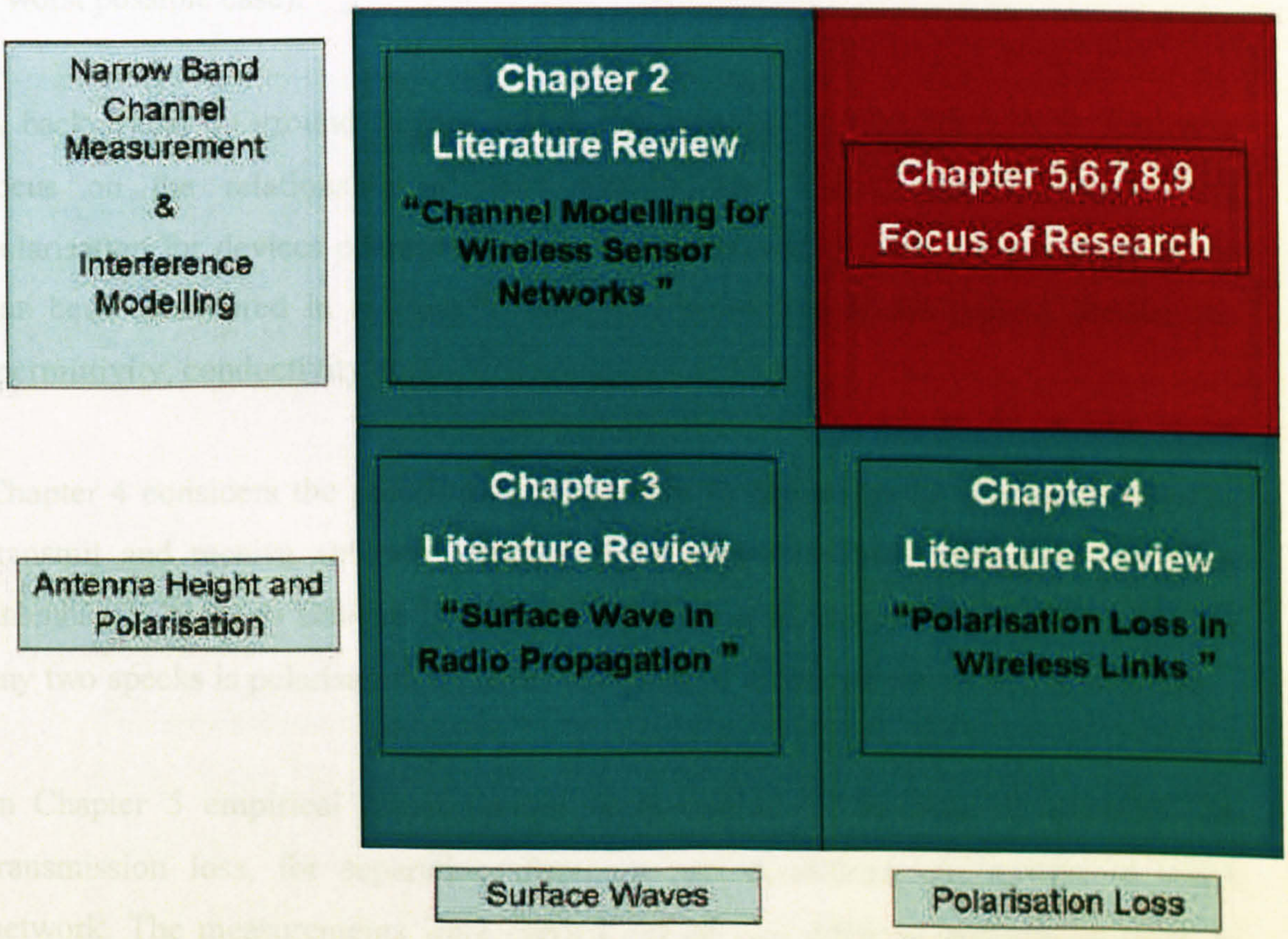

Fig. 10-1 Research methodology

Chapter 1 introduces specknet project, and its aims and objective. The motivation and setting for the subsequent work on wireless channel modelling.

In Chapter 2, the review of existing wireless channel appropriate to specknet has been considered. Since there was no existing literature on channel modelling and measurements for short wireless links it was decided to explore the propagation characteristic through empirical measurement and then using statistical approach to match the results with existing channel model (free space or two ray models etc). The factors associated with modelling a centralised or decentralised networks were explored. Since specknet is conceptualised as a decentralised randomly distributed dense network of autonomous nodes which are meant to communicate for short ranges. It was concluded to model speck network as an interference limited system in order to arrive at signal to interference likely to be experienced by a sensing node (in a worst possible case).

A background on ground surface waves was provided in Chapter 3, with particular focus on the relationship between transmission losses, antenna height and polarisation for devices operating in giga-hertz frequencies. The surface wave effect has been considered in relation to electrical properties of the ground surface i.e. (permittivity, conductivity etc).

Chapter 4 considers the polarisation loss likely to occur due to mismatch between transmit and receive antennas. Specks are designed to have circularly polarised antennas in order to achieve link diversity. This is to ensure that the link between any two specks is polarisation matched irrespective to both location and orientation.

In Chapter 5 empirical measurements were carried on in order to quantify the transmission loss, for separation distances and conditions appropriate to speck network. The measurements were carried out on two different surfaces in order to address the dependence of path loss index on antenna height.

In Chapter 6 interference limited model was developed to predict the signal to noise ratio experienced by a speck network. The model uses transmission loss measurements and fading statistics as input derived through empirical measurements.

During the initial course of measurements on short ranges it was discovered that the path loss index is affected by the antenna height possibly explained by the presence of a surface wave. In Chapter 7 detailed set of empirical measurements were carried out in order to explore the likely dependence between antenna polarisation, height and separation distances.

Finally Chapter 8 addresses polarisation loss encountered by specks. It was decided by the consortium to use circular polarised antennas at each node. During the course of antenna design it was discovered by the Glasgow University group that it is difficult to design a near ideal circular polarised antenna at each node. This has an implication of additional loss due to imperfections in antenna design. Since specks are designed to be deployed randomly this results in additional loss due to misalignment of antenna's major axis due to random spatial orientation of polarisation ellipse. Also the specks will be deployed close to the medium this results in additional loss due to cross polarisation of the reflected wave. A simulation model was developed in order to predict the polarisation loss.

9.2 Conclusion

The following conclusions are drawn.

1. The specknet wireless channel has been modelled as narrowband and subject to flat fading. For the expected data rates those paths with delay sufficient to cause ISI will result in negligible received power, i.e. there is insufficient power in that part of the channel impulse response responsible for ISI to degrade performance significantly.

2. Transmission loss is represented by a three segment piecewise-linear curve. The intermediate region is of greatest practical interest. It is suggested that

near field coupling between an electrically small antenna and the surface could results in composite radiating structure that is no bnger electrically small. Near-field coupling between antenna and surface may result in a surface-wave which dominates in the intermediate region. The nodes in future wireless sensor networks will be small. If such nodes are deployed close to surfaces then small path indices will be common.

3. An empirical fading model has been derived by making multiple, spatially displaced, measurements for each path length The result is a Ricean fading distribution with a *K*-factor between 8 and 10.

4. A simulation environment has been developed fbr a dense wireless network as envisaged by specknet. The effect of CSMA inhibition distance has been considered in relation to node density and other relevant parameters in order to predict the expected signal-to-interference ratio (SIR). The dependence of SIR on node density established allows density dimensioning. Cumulative distribution of SIR has been presented to allow the calculation of performance statistics for arbitrary modulation schemes and associated MAC-layers issues.

5. During the course of measurement it was discovered that there is a likely dependence between transmission loss and node height for both vertical and horizontal polarisations. It is concluded that vertical polarisation results in smaller transmission loss than horizontal polarisation for short wireless links when antenna height is small (< 2.65 cm). For greater antenna heights (> 2.65 cm), and smaller node separation, horizontal polarisation results in smaller transmission loss than vertical polarisation.

6. The random nature of the location and deployment mechanisms for specks suggests that speck antennas are likely to be circularly polarised. The degree to which the polarisation of a received LOS signal may differ from circular has been investigated using simple, but plausible, models of practical

antennas. The effect of the deployment surface on the cross-polarisation of a reflected wave signal has been investigated using the antenna models in conjunction with the Fresnel reflection coefficients.

9.3 Future Work

Since specks can be deployed on variety of surfaces (having different electrical properties) it is recommended to develop a rich set of data base that relates transmission loss to link length for typical applications.

The work presented here relies heavily on empirical measurements. There is significant residual uncertainty regarding the dominant physical propagation mechanisms. A careful simulation of the electromagnets using finite element software will shed light on the precise form and significance of near-field and surface-wave effects. The Multiphysical software package marketed by COMSOL could be used to address these issues.

Increased knowledge of traffic pattern and deployment strategies relating to sensor networks could improve the realism of SIR analysis.

.

References

[1] www.specknet.org, last assessed on 15 March 2008

[2] http://www.thewirelessdirectory.com/Bluetooth-Overview/Bluetooth-Standard.htm, last assessed on 15 March 2008

[3] http://www.zigbee.org/en/spec_download/download_request.asp,last assessed on 15 March 2008

[4] http://robotics.eecs.berkeley.edu/~pister/SmartDust/, last assessed on 15 March 2008.

[5] Castlia channel model, http://castalia.npc.nicta.com.au/news.php, last accessed 10 Feb 2008.

[6] Chen, G., J. Branch, M. J. Pflug, L. Zhu and B. Szymanski , "SENSE: A Sensor Network Simulator. Advances in Pervasive Computing and Networking". 2004, Springer: 249-267.

[7] Akl. R, Tummala. D, Xinrong Li, "Indoor propagation modeling at 2.4 GHz for IEEE 802.11 networks". Wireless networks and emerging technologies, July 3-5 2003, Bunff, AB, Canada.

[8] Sujak, B. Ghodgaonkar, D.K. Ali, B.M. Khatun, S, "Indoor propagation channel models for WLAN 802.11b at 2.4 GHz ISM band". Applied Electromagnetic, 2005. Asia-Pacific Conference, 20-21 Dec. 2005, Page(s):5pp 2

[9] H. Hashemi, "The Indoor Radio Propagation Channel," *Proc. IEEE*, vol. 81, pp. 943-968 (July 1993)

[10] T. S. Rappaport and S. Sandhu, "Radio-Wave Propagation for Emerging Wireless Personal-Communication Systems," *IEEE Ant. and Propag. Magazine*, October 1994, pp. 14-24.

[11] Review of channel models, http://www.ednasia.com/article-19161-estimatingtransmissionrangeforzigbeeandproprietaryshortrangewirelessdevice sin900mhzand24ghzismband-Asia.html. last assessed on 25 March 2008.

[12] Rappaport, T.S, Wireless Communication Principles and Practice, 2nd Edition, Pearson Education, Inc. 2002.

[13] Wong K J and Arvind, D K, "SpeckMAC: Low-power Decentralised MAC Protocols for Low Data-rate Transmissions in Specknets" in Proc. Int. Workshop on Multi-hop Ad-Hoc Networks, Florence, Italy, May 2006, pp. 71-78, ACM Press.

[14] Bluetooth Technical Specification, http://www.thewirelessdirectory.com /Bluetooth-Overview/Bluetooth-Specification.htm, last assessed on 15 March 2008

[15] Zig-Bee Technical Specification, http://www.zigbee.org./en/ spec_ download/download_request.asp, last assessed on 15 March 2008

[16] Darbari, F.; Glover, I. A.; Stewart, R. W.:" Narrow-Band Short-Range Channel Measurements". The XXIX General Assembly of the International Union of Radio Science (URSI), Santiago, USA 2008

[17] Zuniga, M, Krishnamachari, B.: "Analyzing the transitional region in low power wireless links". Sensor and Ad Hoc Communications and Networks, 2004. IEEE SECON 2004.Publication Date: 4-7 Oct. 2004, page(s): 517-526

[18] Chipcon. CC1000 low power radio transceiver, http://www.chipcon.com Last assessed on 10 March 2008

[19] Castlia channel model, http://castalia.npc.nicta.com.au/news.php, last accessed

[20] D. Ganesan, B. Krishnamachari, A. Woo, D. Culler, D. Estrin and S. Wicker.:"Complex Behavior at Scale: An Experimental Study of Low-Power Wireless Sensor Networks". UCLA CS Technical Report UCLA/CSD-TR 02-0013, 2002.

[21] J. Zhao and R. Govindan.: "Understanding Packet Delivery Performance in Dense Wireless Sensor Networks". Sensys '03.

[22] A. Woo, T. Tong, and D. Culler.: "Taming the Underlying Issues for Reliable Multhop Routing in Sensor Networks". SenSys '03.

[23] Darbari, F.; Glover, I. A.; Stewart, R. W.:"Channel and Interference Analysis for Wireless Sensor Networks",. ICC '07. IEEE International Conference on Communications, 2007, 24-28 June 2007 Page(s):3289 - 3294

[24] Chen, G., J. Branch, M. J. Pflug, L. Zhu and B. Szymanski .: 'SENSE: A Sensor Network Simulator. Advances in Pervasive Computing and Networking". 2004, Springer: 249-267.

[25] K. A. Norton, "The physical reality of space and surface waves in the radiation field of radio antennas," *Journal*, vol. 1, pp. 11–25, Jan. 1999.

[26] K. Bullington, "Radio Propagation Fundamentals", Bell System, Technical journal, Vol. xxxv1, Number 3, pp. 593–625. 1957.

[27] K Siwiak, 'Radio propagation and antennas for personal communication", I. Title 1995, ISBN 0-89006-755-4, pp 105-112

[28] C. R. Burrows, "Radio Propagation over Plane Earth-Field Strength Curves", Bell System, Technical journal, vol. 16, pp. 45-75, January 1937.

[29] K.A.Norton,"The propagation of radio waves over the surface of the earth and in the upper atmosphere", Pro. IRE, 24, 1967(1936):Proc.IRE,25,1203(1937; Proc. IRE, 25, 1192(1937)

[30] M. Zuniga, B. Krishnamachari, "Analyzing the Transitional Region in Low Power Wireless Links," First IEEE International Conference on Sensor and Adhoc Communications and Networks (SECON), SantaClara, CA, October 2004.

[31] F.Darbari,.:"Effect of Antenna Height and Polarisation on Short Wireless Links", Eusipco, 16th European Signal Processing Conference, Lausanne, Switzerland.

[32] Antenna Polarization Considerations in Wireless Communications Systems. www.cushcraft.com/comm/support/pdf/Antenna-Polarization-14B32.pdf, last accessed on 05 Jan 2008

[33] Warren L.Stutzman, "Polarisation in Electromagnetic Systems," *1993 ARTECH HOUSE, INC*, 1992, pp. 10-11.

[34] Ha, Tri T., "Digital Satellite Communications", 2nd Ed, McGraw-Hill, New York, 1990, Sec. 4.2.

[35] Watson, P.A., Arbabi, " Cross Polarization Isolation and Discrimination ", Electronics Letters, Vol. 9, 1973, pp. 516-517

[36] Allnutt, J.E, " Satellite-to-Ground Radio wave Propagation", Peter Pergrinus, London 1989

[37] http://castalia.npc.nicta.com.au/pdfs/Castalia%20-%20User%20Manual.pdf, lasted assessed on 15 April 2008

[38] Chen, G., J. Branch, M. J. Pflug, L. Zhu and B. Szymanski .: 'SENSE: A Sensor Network Simulator. Advances in Pervasive Computing and Networking". 2004, Springer: 249-267.

[39] MacEwen, N.C., Crockett, L.H., Pfann, E., Stewart, R.W., "Symbol Synchronisation Implementation for Low-Power RF Communication in Wireless Sensor Networks", in Conf. Rec. Thirty-ninth Asilomar Conference on Signals, Systems and Computers, November 2005.

[40] Darbari, F.; Glover, I. A.; Stewart, R. W.:" Narrow-Band Short-Range Channel Measurements". The XXIX General Assembly of the International Union of Radio Science (URSI), Santiago, USA 2008

[41] G. Whyte, N. Buchanan, I. Thayne, "An omnidirectiona,, low cost, low profile, 2.45 GHz Microstrip fed rectaxial antenna for wireless sensor network applications". IEE conference on propagation and antennas 2006, Loughborough, UK

[42] N.A. Weiss, M.J. Hassett, "Introductory Statistics" , Library of Congress Cataloguing-in-Publication Data. May, 1993. Pages 115-120

[43] Ganesan, D., Krishnamachari, B., Woo, A., Culler, D., Estrin, D., and Wicker, S. 2002. Complex Behaviour at Scale: An Experimental Study of Low-Power

Wireless Sensor Networks. Tech. rep., Technical Report UCLA/CSD-TR 02-0013.

[44] Woo, A., Tong, T., and Culler, D. 2003. Taming the Underlying Challenges of Reliable Multi-hop Routing in Sensor Networks. In ACM SenSys 2003.

[45] Zhao, J. and Govindan, R. 2003. Understanding Packet Delivery Performance in Dense Wireless Sensor Networks. In ACM SenSys 2003.

[46] Model and Solutions for radio irregularity in Wireless Sensor Networks. http://www.cs.virginia.edu/papers/Models_Soln_RIM_TOSN.pdf.Last assessed on 10 Feb 2008

[47] Ben L. Titzer. Daniel K. Lee. Jens Palsberg, "Avrora: Scalable Sensor Network Simulation Information Processing in Sensor Networks", IPSN 2005. Fourth International Symposium on 15 April 2005, pp 477 - 482 Digital Object Identifier 10.1109/IPSN.2005.

[48] T.S. Rappaport, Wireless Communication principles and practice, 2nd edition, 2002, pp. 139-141

[49] Darbari, F.; Glover, I. A.; Stewart, R. W.:" Narrow-Band Short-Range Channel Measurements". The XXIX General Assembly of the International Union of Radio Science (URSI), Santiago, USA 2008 (Paper under review).

[50] http://www.madsci.org/posts/archives/2001-05/988722218.Ph.r.html,last accessed 15 February 2008

[51] C. R. Burrows, "Radio Propagation over Plane Earth-Field Strength Curves", Bell System, Technical journal, vol. 16, pp. 45-75, January 1937.

[52] Path Antenna Data Sheet, http://www.datasheetarchive.com/C-61.htm, lasted assessed on 15 April 2008

[53] Cosine Similarity, http://en.wikipedia.org/wiki/Jaccard_index, lasted assessed on 15 April 2008

[54] Warren L.Stutzman, "Polarisation in Electromagnetic Systems," *1993 ARTECH HOUSE, INC*, 1992, pp. 25-30.

[55] http://ieeexplore.ieee.org/iel6/8233/25571/01141733.pdf?arnumber=1141733, lasted assessed on 15 April 2008

[56] Warren L.Stutzman, "Polarisation in Electromagnetic Systems," *1993 ARTECH HOUSE, INC*, 1992, pp. 183-185.

[57] Warren L.Stutzman, "Polarisation in Electromagnetic Systems," *1993 ARTECH HOUSE, INC*, 1992, pp. 190-191.

[58] Jamnejad, V. " Ground Multipath in Topex's Precision Orbit Determination Tracking System," Jet Propulsion Laboratory Interoffice Memo 3365-84-003, Jan. 1985

[59] Warren L.Stutzman, "Polarisation in Electromagnetic Systems," *1993 ARTECH HOUSE, INC*, 1992, pp. 192-193

[60] http://www.clippercontrols.com/info/dielectric_constants.html#W, last assessed on 15 August 2008.